FURTHER NUMERICAL TECHNIQUES FOR PLANAR ELASTOSTATIC ANALYSIS BY THE BOUNDARY INTEGRAL EQUATION METHOD

by

G.C. HOWELL

A thesis submitted in fulfillment of the requirements for the Degree of Doctor of Philosophy in the Faculty of Engineering, University of Cape Town.

Department of Civil Engineering
UNIVERSITY OF CAPE TOWN

December 1983

DECLARATION OF CANDIDATE

I, Graham Conrad Howell, hereby declare that this thesis is my own work and that it has not been submitted for a degree at another University.

Signed by candidate

G.C. HOWELL BSc(ENG.), MSc(ENG.)

December 1983

DEDICATION

This thesis is dedicated to my parents Mr and Mrs Howell for their unerring love and support over the years; and to my wife, Lynette, for her continuing love and devotion to my cause.

ACKNOWLEDGEMENTS

My sincere appreciation and thanks is extended to:

Assoc. Prof. W.S. Doyle*, under whose supervision this thesis and research was conducted, for his constant encouragement, enthusiasm, help, support and the vital suggestions and comments he made during the long hours of discussions he was subjected to. His interest and character has contributed greatly to this project.

My wife, Lynette and Mrs Anke Burbach for their immaculate typing of the manuscript under most trying circumstances.

The Council for Scientific and Industrial Research (CSIR) for their financial assistance during this project.

The staff of the Department of Civil Engineering, UCT for their comments and encouragement.

*Associate Professor, Department of Civil Engineering
University of Cape Town.

ABSTRACT

Prior experience of the Finite Element Method stimulated interest and led to research into the Boundary Integral Equation Method, specifically for the solution of planar elastostatic problems.

A complete exposé of the mathematical theory of the Boundary Integral Equation Method is given. The basis of the method is traced and the similarities and differences as opposed to the Finite Element Method, are highlighted. The numerical implementation of the method, using constant, linear and quadratic interpolation functions over the boundary segments is developed and then inclusion in computer programs is discussed. Attention is given to the problem of numerical integration over a singularity, for which detailed expressions are given. The verification and applicability of the technique is thoroughly investigated in five fully documented examples.

Solutions to the problem of traction discontinuities at a corner are proposed and an analysis of the inclusion of body forces, together with documented examples, are described. Also investigated is the non-symmetric form of the resulting matrices. It is proven that no direct and practical way can be found to render these matrices symmetric. By investigating the error in the numerical integration process, the suitability of segments is also discussed.

Emphasis is placed on the solution of non-homogeneous domains and domains which extend to infinity. The development of the necessary numerical techniques required in both cases is discussed and fully documented.

Finally, a method of automatically improving the accuracy of the solution of the Boundary Integral Equation Method by using p and h convergence adaptive processes is also presented.

NOTATION

Lower Case Letters

$\underline{b}$	vector of "loads"
b_i	body force component in i-direction
c_{ij}	coefficient matrix
d_{ij}	coefficient matrix
e_{ijk}	permutation tensor
$f( )$	function of ( )
g	Gauss Quadrature order, or gravitational constant
g_j	differential operator
k	constant of proportionality
n_i	component of outward normal in i-direction
$\tilde{p},\tilde{q}$	position vectors
p_i,q_i	points
r	distance or direction
t	vector of tractions
t_i	component of traction in i-direction
$\bar{t}_i$	prescribed traction in i-direction
u	vector of displacements
u_i	component of displacement in i-direction
$\bar{u}_i$	prescribed displacement in i-direction
$\tilde{u}$	displacement field
v,v^T	arbitrary weighting function (chapter 3)
v_i	general field variable, either displacement u_i or traction t_i
$\{v\}$	general field variable
w_ℓ	Gaussian Quadrature weighting factor
x_i	co-ordinate axes

$\underline{x}$	vector of unknowns
z	general cartesian co-ordinate, either x_1 or x_2

Upper Case Letters

$[A]$	BIEM systems matrix
$A(\ )$	differential operator
B	strain displacement relationships in matrix form
$B_i, \{B\}$	body force integral in vector form
$B(\ )$	differential operator
$[C]$	matrix corresponding to c_{ij}
$C(\ )$	differential operator
D_{kij}	3rd order tensor
D	symmetric elasticity matrix
$D(\ )$	differential operator
E	Young's Modulus
$E(\ )$	differential operator
$\{F\}$	boundary conditions vector
F	load vector
F_{eb}	elemental load vector
$F(\ )$	differential operator
$G = \mu = \frac{E}{2(1+\nu)}$	shear modulus
$[G], G_{ij}$	matrix of coefficients from the integration of U_{ij}
G_j	differential operator in component form
$[H], H_{ij}$	consolidated systems matrix
$[\bar{H}], \bar{H}_{ij}$	matrix of coefficients from the integration of T_{ij}
I_A^C	value of integration
K	Finite Element Stiffness matrix (chapter 3)
K_e	element stiffness matrix
N_i	shape or interpolation function

N	vector of shape functions
R	distance related to direction r
S_{kij}	3rd order tensor
S_{ij}^*	tensor
T_{ij}	fundamental traction solution
U_{ij}	fundamental displacement solution
U	Strain Energy
V_{ij}	general fundamental solution, either U_{ij} or T_{ij}
W	potential energy of the loads

Greek Letters

α	angle
β	angle
γ_k	natural co-ordinate at node k
γ	density
Γ, Γ_m	boundary, section of boundary
δ_{ij}	Kronecker Delta
δ_{ℓ}^{k}	Dirac Delta
ε	strain matrix
ε_{ij}	strain components
$\varepsilon_1, \varepsilon_2$	error or residual
ζ_i	natural co-ordinate at node i such that the shape function value is unity
η	local (natural) co-ordinate parameter $-1 \leqslant \eta \leqslant 1$
η_j	natural co-ordinate at node j
θ	angle
λ	$= \dfrac{\nu E}{(1+\nu)(1-2\nu)}$ Lamé constant or Lagrangian multiplier
μ	$= G = \dfrac{E}{2(1+\nu)}$ Lamé constant
ν	Poisson's Ratio

ξ	natural co-ordinate parameter $-1 \leqslant \xi \leqslant 1$
ξ_i	Gaussian sampling point
π	pi = 3.14159 .....
	or Potential energy of the system (chapter 3)
σ	stress matrix
σ_x, σ_y	stress
σ_{ij}	stress components
τ_{xy}	shear stress
Ω, Ω_m	domain, section of domain
Ω	mathematical sign for multiplication (chapter 8)

CONTENTS

CHAPTER 1

INTRODUCTION AND OBJECTIVES

Research into numerical structural analysis techniques by the staff of the Department of Civil Engineering at the University of Cape Town was started in the late 1960s. The first field to be investigated was that of Finite Differences, but once the Finite Element Method gained in popularity, all numerical research efforts were guided in this direction. The theme of the research has always been to concentrate on the practical or applied research aspects of the method, although some pure developments of, in particular, axisymmetric elements have previously been successfully undertaken. Methods of modelling,the use and applicability of the various finite elements and their accuracy have typically been the subjects of research. Of particular interest has been the linking of the Finite Element analysis with the various design codes in the form of automatic design packages. Two examples of these packages are first, a computer program written by the author for the optimum design of space structures [1.1] using dynamic programming techniques to facilitate the optimization and second, a thesis written by a fellow student for the automatic structural design of axisymmetric water retaining structures [1.2].

This type of applicable or practically-orientated research was continued through the 1970s. In 1978/79, papers in the technical literature stimulated an interest in the "new" numerical discipline of Boundary Element Methods (BEM) or Boundary Integral Equation Methods (BIEM). At this time, nobody in Southern Africa, to my knowledge was actively involved in research into this subject. The method promised to be a viable alternative to the Finite Element Method, and hence, if appropriate research into numerical methods was to be continued at U.C.T., the BIEM had to be thoroughly investigated. It was decided to take up the challenge and hence the reason for this thesis.

Initially a set of objectives, around which this thesis is built, were defined. It was decided at the outset, that research would be restricted to two dimensional elastostatic plane stress/strain problems.

With the lack of local experience of the method and the techniques involved, it was acknowledged that this would not be easy, but with the considerable Finite Element Method background available, research was commenced.

The broad objective of this thesis and the research that it contains, is therefore to investigate, trace, develop and verify the BIEM for 2-D elastostatic problems. However, this is a very wide definition, and it is left to the details listed below to define the objectives of this thesis clearly and the original contributions which it contains.

To begin with, the mathematical theory on which the numerical techniques of the BIEM are based, were thoroughly traced and investigated; the similarities and differences are highlighted in Chapter 3. This Chapter contains the assumptions made in the theory and details the basis on which the more practical aspects of the numerical techniques are founded.

Chapter 4 discusses, in detail, the numerical implementation of the BIEM. The integration scheme used, and the types of segment and their development are discussed. Particular importance is placed on the development of the pivot segment which successfully overcame the problem of the numerical integration over a singularity. A method is also discussed whereby displacements and stresses within the domain and particularly close to the boundary, can be found with considerable accuracy, once the boundary problem is solved. All these numerical details have been incorporated in computer programs, which were designed and programmed from scratch. To verify the applicability and performance of the BIEM, a set of well-documented examples are presented. Four of these examples have been chosen specifically because rigorous mathematical solutions are available as a benchmark, but also to highlight the advantages and disadvantages of the method. A practical engineering problem is also included to show the applicability of the method in the field.

During the course of the research, certain problems and irregularities were encountered and, naturally, these had to be overcome. Chapter 5 discusses these problems and the solutions which have been developed. Of particular importance is the existence of a traction discontinuity at a corner. Several methods to overcome this problem are discussed. The incorporation of body forces has been investigated and recommendations for their use are detailed.

One of the disadvantages of the BIEM is that the matrices are non-symmetric and hence results in considerable wastage of computer storage. If these matrices could, in some way, be made symmetric, then commensurate savings would accrue. With the present method, however, it has been catagorically proven that symmetric matrices are impossible to achieve, due to the characteristics of the fundamental solutions.

From a practical viewpoint, it is important to know how a particular segment will perform under certain conditions. Guidelines for the use of boundary segments have been developed by studying the possible errors which can arise due to the numerical integration techniques used in the method. An interesting set of error traces has been produced for this purpose.

An integral part of a numerical 2-D solution method is its ability to be able to deal with a number of connected regions of differing material properties. The basic method makes provision for only one material within the domain, but with manipulation, separate material regions can be interfaced to reflect the total stress condition of the domain. The theoretical and numerical details for this analysis are contained in Chapter 6. The traction discontinuity problem in the non-homogeneous context and its solution, are also discussed in this Chapter.

Where the solution of a problem in which the domain extends to infinity, is required, certain numerical difficulties are encountered. With finite elements, the model must be truncated artificially at a predefined boundary. "Infinite elements" have been developed to overcome this problem. For the solution of similar problems by the BIEM, an infinite segment has also been developed here. The same isoparametric

shape function formulation which is used in infinite elements, is used in the development of infinite boundary segments. Boussinesq's problem of a point load on an elastic half-space is a typical application of infinite regions; this problem is discussed in Chapter 7.

The final technical Chapter (8), addresses the problem of successively improving the solution of an analysis automatically by systematically increasing the order of the shape function over a boundary segment. This adaptive programming technique is termed the p-convergence method as compared with the h-convergence method where the size of the boundary segment is progressively decreased until the desired accuracy is achieved. The p-convergence technique requires that a unique hierarchical shape function formulation be developed so that, for example, quadratic segments could be developed directly from the basic linear segment by merely adding a few terms. This method greatly reduces the amount of recalculation required to produce an upgraded (high order) solution for a particular problem. This technique developed from the desire to ensure that solutions obtained by the BIEM are within acceptable predefined convergence limits, with the added advantage of keeping the computational costs to a minimum.

Various technical details too tedious to be included in the main text, are contained in the appendices. Also included here are the basic computer program manuals and an extensive bibliography.

A large proportion of the work contained in this thesis has been published, either in the form of papers at conferences or in international journals [1.3 to 1.8]. A considerable response to the published papers in the form of enquiries and communications, has been received from many parts of the world. It can therefore be concluded that this work has been found to be of particular interest to other researchers.

References

[1.1] G.C. HOWELL, "Dynamic Programming and Direct Iteration for the Optimum Design of Space Structures". M.Sc.(Eng.) thesis in the Faculty of Engineering, University of Cape Town, 1978.

1.2 A.R. LLOYD, "Computer Aided Design of Axisymmetric Thin Shell Concrete Structures", Ph.D. thesis in the Faculty of Engineering, University of Cape Town, 1982.

1.3 G.C. HOWELL and W.S. DOYLE, "A Resumé of Boundary Integral Methods in 2-Dimensional Elasticity", Unpublished Technical Report No. 804S, Department of Civil Engineering, U.C.T., 1980.

1.4 G.C. HOWELL and W.S. DOYLE, "Boundary Integrals - An Alternative to Finite Elements for Plane Elasticity Problems", Proceedings of the Symposium on Design Applications of the Finite Element Method, held at the University of Cape Town, 12-14 January 1981.

1.5 G.C. HOWELL and W.S. DOYLE, "Plane Stress/Strain Analysis by Boundary Integral Equation and Finite Element Methods". Proceedings of the conference of Finite Elements in South Africa (FEMSA), held at the CSIR, Pretoria, S.A., 17-18 March 1981.

1.6 G.C. HOWELL and W.S. DOYLE, "An Assessment of the Boundary Integral Equation Method for In-Plane Elastostatic Problems", Applied Math. Modelling, Vol. 6, No. 4, August 1982.

1.7 G.C. HOWELL and W.S. DOYLE, "The Plane Stress/Strain Analysis of Non-Homogeneous Continua by the Boundary Integral Equation Method", Computers and Structures, Vol. 17, No. 4, pp. 603-610, 1983.

1.8 G.C. HOWELL and W.S. DOYLE, "Infinite Domain Problems by Finite Elements and Boundary Integrals". Proceedings of FEMSA/83, International Symposium on Design and the Finite Element Method, held at the University of Cape Town, 11-12 January 1983.

CHAPTER 2

AN OUTLINE OF THE HISTORY AND APPLICATIONS OF THE BOUNDARY INTEGRAL EQUATION METHOD

2.1 Historical Outline

The origins of the numerical Boundary Integral Equation Method are clearly rooted in classical mathematics. To trace the precise point in time where the seeds of the method were sown is therefore, nigh impossible. This historical review will therefore, be a more subjective look at the method and will include only material personally read or researched by the author. The references given at the end of the chapter are arranged cronologically, and are divided into various subjects to which the Boundary Integral Equation Method has application.

Perhaps one of the earliest approaches to the BIEM as we know it today is due to Lord Kelvin, when he produces his solution to the point load on an elastic half space. This so-called Kelvin solution appeared in the late eighteen hundred's. Concurrently, the method of potentials had been derived for the solution of Laplace's and Navier's equations and became know as Potential Theory. Between 1872 and 1886, Betti applied potential methods to elasticity problems, Somigliana produced a vector reciprocal relationship which is the basis of the BIEM and Cerruti and Lauricella extended these methods. Love [2.5] in 1927 summarized the essential points in this development. Fredholm (1903) demonstrated that solutions to integral equations could be found, and developed conditions for the existence and uniqueness of such solutions in the form of the Fredholm Theorems. By the early nineteen hundred's, therefore, the theory of integral equations for the solution of both potential problems and elasticity problems [2.6, 2.7] had been established. But, the practical solution of these problems which involved the solution of systems of simultaneous equations was severely hampered by the lack of sufficient computational muscle. Only with the advent of the digital computer in the 1950's and 60's did the method become viable.

In 1963, Jaswon, Symm and Ponter [2.12, 2.13, 2.14] produced a series of papers which detailed the solutions of potential problems by the integral equation method. Of particular importance is the reference to a computer orientated method. The method is supported by a paper on the solution of the torsion problem.

Massonnett [2.15], (1965) dedicated a chapter in a book on Stress Analysis by Zienkiewicz and Holister to the numerical use of integral methods for the solution of practical problems with an example of the solution of the torsion problem. The solution of the stress field in elasticity problems is achieved by using a simple radial stress distribution as the fundamental singular stress field. This is essentially the method known as the indirect BIEM which requires the solution of a set of fictitious loads or tractions in the solution procedure.

Rizzo [2.16] saw the merits in the integral equation method and used the Betti-Somigliana vector formula to general solutions for the traction, the displacement and mixed boundary value problems for plane elastostatics. Cruse [2.20, 2.21, 2.22] developed the method further and in 1974 applied his "improved" method to the solution of 3-dimensional elastic stress analysis. By this time, the BIEM was being recognized as a possible alternative to the rapidly advancing Finite Element Method. A number of papers [2.23 to 2.27] discussed advances in the method for 3-dimensional solutions and the application to the solution of non-homogeneous bodies, which presents no problem in the FEM.

By this time (1976) the basic theory had been successfully developed. With the implementation of isoparametric concepts into the modelling [2.29] and the intense interest shown by Brebbia and colleagues in the method, a proliferation of applications was developed. Brebbia and workers at the University of Southampton coined the name, the Boundary Element Method. This has, in a way, graded the Boundary Integral Equation Method into an equivalent status to the Finite Element Method.

Four major reference works have been written on the subject. These include a theoretical discussion of the method with reference to

both potential theory and elastostatics by Jaswon and Symm [2.1] in which the detailed development is discussed. More practically orientated books have been written by Brebbia [2.2] (1978) and Brebbia and Walker [2.3] (1980) and are specifically aimed at engineers with a view to laying the ground work for further developments in the applications field. Indeed in [2.2], Brebbia has given complete listings of his computer programs in an effort to bring the method closer to the practicing engineer. Banerjee and Butterfield [2.4] (1979)edited a book in which the BIEM is applied to elastostatics, elastoplasticity fracture mechanics, thermoelasticity, plates and shells and the coupling of the FEM and BIEM, each chapter being written by acknowledged experts in their fields.

To my knowledge, 4 conferences have been held on the subject. The first was in 1975 [2.8] under the auspices of the American Society of Mechanical Engineers, Applied Mechanics Division. An ongoing series of international seminars has subsequently been organised by Brebbia [2.9, 2.10, 2.11] in respectively 1978, 1980 and 1981, and, judging from the number and quality of papers presented at these seminars, the method is becoming increasingly popular and applicable to diversity of subjects. This is no doubt inevitable and hopefully the method will continue to develop into other disciplines in the future.

2.2 Applications

Apart from the obvious application of the Boundary Integral Equation Method to potential theory and elasticity [2.12 to 2.50] in which many researchers have attacked different problems and arrived at various solutions, the method has been successfully applied to other disciplines.

The application to axisymmetric elasticity is covered by [2.51] to [2.53]. Initially, an indirect method of solution was attempted. This developed into a direct method [2,52] in which axisymmetric boundary conditions including thermal, rotational and centrifugal loading were included. Later [2.53] this work was advanced to including arbitrary loading conditions by using Fourier Series.

On the subject of thermoelasticity, Rizzo and Shippy [2.69] showed that a thermal gradient or a body force influences the stress field through the surface integrals only. Therefore, no discretization of the domain is required in the solution and the essential ingredients of a boundary solution are preserved.

Since the advent of the BIEM, Zienkiewicz has maintained that the most advantageous use of the FEM and the BIEM can be accomplished by their coupling [2.54 to 2.59]. This is particularly true in applications where a detailed stress analysis is required for a part of the structure where the solution is influenced by the surrounding domain, as is the case in mining applications. The FEM is used to model the details, while the BIEM models the remaining domain, particularly when the domain is infinite. However, with the development of infinite elements, the modus operandi of this technique seems to have become superfluous.

The singular nature of the fundamental solutions used in the BIEM, lend themselves directly to their use at the singularity encountered at the crack tip. Cruse [2.60 to 2.63], has been in the forefront of the development of the method in fracture mechanics which has obvious application in aeronautical engineering. Also, in this line, the BIEM has been applied to the solution of the problems of transient dynamics [2.65 to 2.68]. However, from the literature it appears that considerable research effort is required in this field before the BIEM will be able to compete with the FEM.

The inelastic behaviour of solids solved by the BIEM has been the subject of papers dating bach to 1971 [2.72 to 2.83] when Swedlow and Cruse published a paper on the BIEM applied to three dimensional Elasto-Plastic flow. Since this initial paper, such well know researchers as Banerjee and Brebbia have contributed to the subject and a number of papers have been read at the international seminars. This is a growing application, but particular merits seems to be in the coupling of the BIEM and the well-formulated FEM for non-linear analysis.

On the subject of transient dynamics, Cruse and Rizzo in 1968

produced two papers [2.65 and 2.66] in which the method is detailed. This method involves the solution of sets of integral equations and of numerically inverting the Laplace transform. Apparently, this method has not advanced, judging by the lack of published material [2.60 to 2.68], possibly due to the popularity of the FEM for the solution of these problems.

Another area in which the BIEM appears to have been neglected, is in the solution of the plate bending problems [2.89 to 2.95]. This could be due to the relative complexity of the resulting integral equations, but, once formulated, solution by computer is a mere formality.

Application to practical problems of Fluid-Structure interaction [2.84 to 2.88], Radiation problems [2.33] , transient heat conduction problems [2.96], [2.97], Torsion [2.98 to 2.100], and contact problems [2.101] , [2.102] have all been the subject of research into boundary integral techniques.

More mathematical application of the BIEM for the solution of 2nd order elliptical systems [2.34], parabolic differential equations [2.46] and the Laplace equation [2.41] and the use of cubic splines for the solution for integral equation [2.50] have previously been discussed.

2.3 Summary

From the foregoing commentary, it is clear that the BIEM or Boundary Element Method has been very widely used and researched, books and papers have been written on the subject and international seminars have been organized for formal discussions.

This evidence shows that further research is warranted. It is therefore, the purpose of this thesis to discuss, clarify and expand the scope of the method, by building on the foundations laid down in these references with the aim of contributing to the development of the method for everyday engineering use.

2.4 References

Books

2.1 M.A. JASWON and G.T. SYMM, Integral Equation Methods in Potential Theory and Elastostatics, Academic Press, London, (1977).

2.2 C.A. BREBBIA, The Boundary Element Method for Engineers, Pentech Press, London, (1978).

2.3 C.A. BREBBIA and S. WALKER, Boundary Element Techniques in Engineering, Newnes-Butterworths, London, (1980).

2.4 P.K. BANERJEE and R. BUTTERFIELD (eds), Developments in Boundary Element Methods - 1, Applied Science Publishers Ltd, London, (1979).

2.5 A.E.H. LOVE, A treatise on the Mathematical Theory of Elasticity, 4th edition, Cambridge University Press, (1927).

2.6 N.I. MUSKHELISVILI, Singular Integral Equations, Noordhoff, Groningen, (1953).

2.7 N.I. MUSKHELISVILI, Some basic Problems of the Mathematical Theory of Elasticity, Noordhoff, Groningen, (1953).

Conference Proceedings

2.8 T.A. CRUSE and F.J. RIZZO (eds), Boundary Integral Equation Method : Computational Applications in Applied Mechanics, ASME publication, AMD-Vol. 11, (1975).

2.9 C.A. BREBBIA (ed), Recent Advances in Boundary Element Methods, Pentech Press, London, (1978).

2.10 C.A. BREBBIA (ed), New Developments in Boundary Element Methods Butterworths, London, (1980). Proceeding of the second International Seminar Southampton, March 1980.

2.11 C.A. BREBBIA (ed), Boundary Element Methods, CML Publications, Springer-Verlang Berlin, Heidelburg (1981). Proceeding of the third International Seminar, Irvine, California, July 1981.

Papers

Potential Theory and Elastostatics

2.12 M.A. JASWON, "Intergral Equation Methods in Potential Theory. I" Proc. Royal Soc. : Series A, Vol. 275, page 23 - 32, (1963).

2.13 G.T. SYMM, "Intergral Equation Methods in Potential Thoery II" Proc. Royal Soc. : Series A, vol. 275, page 33 - 46, (1963).

2.14 M.A. JASWON and A.R. PONTER, "An integral equation solution of the Torsion Problem", Proc. Royal Soc.: Series A, Vol. 273 page 237 - 246, (1963).

2.15 C.E. MASSONNET, "Numerical use of Integral Procedures", in Stress Analysis, (eds.) O.C. Zienkiewicz and G.S. Holister, (1965).

2.16 F.J. RIZZO, "An Integral Equation Approach to Boundary Value Problems of Classical Elastostatics", Quart. Appl. Maths, Vol. 25, page 83 - 95, (1967).

2.17 M.A. JASWON, M. MAITI and G.T. SYMM, "Numerical Biharmonic Analysis and Some Applications", Int. J. Solids Structures, Vol. 3, page 309 - 332, (1967).

2.18 M.R. BARONE and A.R. ROBINSON, "Determination of Elastic Stresses at Notches and corners by Integral Equations", Int. J. Solids Structures, Vol. 8, page 1319 - 1338, (1972).

2.19 R. BENJUMEA and D.L. SIKARSKIE, "On the Solution of Plane Orthotropic Elasticity Problems by an Integral Method", JAM, Vol. 39, Series E, page 801 - 808, (1972).

2.20 T.A. CRUSE, "Some Classical Elastic Sphere Problems Solved Numerically by Integral Equations", Transactions of ASME, J of Applied Mechanics, page 272 - 274, (1972).

2.21 T.A. CRUSE, "Application of the Boundary Integral Equation Solution Method in Solid Mechanics", Proc. Int. Conference on Variational Methods in Engineering, September 25 - 29, 1972.

2.22 T.A. CRUSE, "An Improved Boundary Integral Equation Method for Three Dimensional Elastic Stress Analysis", Computers and Structures, Vol. 4, page 741 - 754, (1974).

2.23 J.C. LACHAT and J.O. WATSON, "A Second Generation Boundary Integral Equation Program for Three Dimensional Elastic Analysis", in Boundary Integral Equation Method : Computational Applications

in Applied Mechanics, (eds.) T.A. CRUSE and F.J. RIZZO, ASME publication, AMD - Vol. 11, (1975).

2.24 P.M. BESUNER and D.W. SNOW, "Application of the Two Dimensional Integral Equation Method to Engineering Problems", in the Boundary Integral Equation Method : Computational Applications in Applied Mechanics, (eds.) T.A. CURSE and F.J. RIZZO, ASME publication, AMD - Vol. 11, (1975).

2.25 P.K. BANERJEE, "Integral Equation Methods for analysis of Piecewise Non-Homogeneous Three Dimensional Elastic Solids of Arbitrary Shape", Int. J. Mechanical Science, Vol. 18, page 293 - 303, (1976).

2.26 J.C. LACHAT and J.O. WATSON," Effective Numerical Treatment of Boundary Integral Equations : A Formulation for Three Dimensional Elastostatics". Int. J. NUM METHODS ENG, Vol. 10, page 991 - 1005, (1976).

2.27 S.T. WANG and G.E. BLANDFORD, " Comparison of Boundary Integral Equation and FE Methods", J. STRUCT. DIV. ASCE, ST 9, page 1941 - 1947, (1976).

2.28 C.A. BREBBIA and J. DOMINGUEZ, "Boundary Element Methods for Potential Problems", Appl. Math. Modelling, Vol. 1, page 372 - 378, (1977).

2.29 G. JENG and A. WEXLER, "Isoparametric, Finite Element, Variational Solution of Integral Equations for Three Dimensional Fields." Int. J. NUM METHODS ENG. Vol. 11, page 1455 - 1471, (1977).

2.30 C.A. BREBBIA and R. BUTTERFIELD, "Formal Equivalence of Direct and Indirect Boundary Element Methods", Appl. Math. Modelling, Vol. 2, page 132 - 134, (1978).

2.31 T.A. CRUSE and R.B. WILSON, "Advanced Applications of Boundary Integral Equation Methods". Nuclear Eng. and Design, Vol. 46, page 223 - 234, (1978).

2.32 R.B. WILSON AND T.A. CRUSE, "Effi cient Implementation of Anisotropic Three Dimensional Boundary Integral Equation Stress Analysis", Int. J. NUM METHODS ENG., Vol. 12, page 1383 - 1397, (1978).

2.33 C.A. BREBBIA and S. WALKER, "Simplified Boundary Elements for Radiation Problems", Appl. Math. Modelling, Vol. 2 , page 135 - 137, (1978).

2.34 D.L. CLEMENTS and F.J. RIZZO, "A Method for the Numerical Solution of Boundary Value Problems Governed by Second-order Elliptic Systems". J. Inst. Maths. Applics, Vol. 22, page 197 - 202, (1978)

2.35 U. HEISE, "Numerical Properties of Integral Equations in which the given Boundary Values and the Sought Solutions are defined on Different Curves", Computers and Structures, Vol. 8, page 199 - 205, (1978).

2.36 J.L. SWEDLOW, "Singularity Computations", Int. J. NUM METHODS ENG, Vol. 12, page 1779 - 1798, (1978).

2.37 U. HEISE, "The Spectra of Some Integral Operators for Plane Elastostatical Boundary Value Problems", J. of Elasticity, Vol. 8, No. 1, page 47 - 79, (1978).

2.38 M. CHAUDONNERET, "On the Discontinuity of the Stress Vector in the Boundary Integral Equation Method for Elastic Analysis", in Recent Advances in Boundary Element Methods, ed. C.A. BREBBIA, (1978).

2.39 E. ALARCON, A. MARTIN and F. PARIS, "Boundary Elements in Potential and Elasticity Theory", Computers and Structures, Vol. 10, page 351 - 362, (1979).

2.40 N.J. ALTEIRO and S.D. GAVAZZA, "An Effective Boundary Integral Approach for the Mixed Boundary value problems of Linear Elastostatics." Appl. Math. Modelling, Vol. 3, page 99 - 104, (1979).

2.41 G. DE MEY, "The Use of Approximate Functions for the Numerical Solution of La Place Equation by an Integral Equation.", Computers and Structures, Vol. 10, page 709 - 711, (1979).

2.42 I. HERRERA, "Theory of Connectivity: Systematic Formulation of Boundary Element Methods", Appl. Math. Modelling, Vol. 3, page 151 - 156, (1979).

2.43 A. WEXLER, "Some Recent Developments in Field Calculations", paper presented at the Joint Intermag-MMM Conference, New York, July 17 - 20, 1979.

2.44 J.O. WATSON, "Advanced Implementation of the Boundary Element Method for Two-and Three-Dimensional Elastostatics" in Developments in Boundary Element Method - 1, eds. P.K. BANERJEE and R. BUTTERFIELD, (1979).

2.45 U. HEISE, "Integral Equations for the mixed Boundary value Problem

in Plane Elastostatics". Appl. Math. Modelling, Vol. 4, page 63 - 66, (1980).

2.46 D.A.S CURRAN, M. CROSS and B.A. LEWIS, "Solution of Parabolic Differential Equations by the Boundary Element Method using discretisation in Time". Appl. Math. Modelling, Vol. 4, page 398 - 400, (1980).

2.47 P. BETTESS, "Operation Counts for Boundary Integral and Finite Element Methods", Int. J. NUM. METHODS ENG. Vol. 17, page 300 - 308, (1981).

2.48 H.L.G. PINA, JLM. FERNANDES and C.A. BREBBIA, "Some Numerical Integration Formulae over Triangles and Squares with a 1/R Singularity", Appl. Math. Modelling, Vol. 5, page 209 - 211, (1981).

2.49 A. PORTELA, "Theoretical Basis of Boundary Solutions for the Linear Theory of Structures", Appl. Math. Modelling Vol. 5, page 57 - 59, (1981).

2.50 J.A. LIGGETT and J.R. SALMON, "Cubic Spline Boundary Elements", Int. J. NUM METHODS ENG., Vol. 17, page 543 - 556, (1981).

Axisymmetric Elasticity

2.51 T. KERMANIDIS, "A Numerical Solution for Axially Symmetric Elasticity Problems", Int. J. Solids Structures, Vol. 11, page 493 - 500, (1975).

2.52 T.A. CRUSE, D.W. SNOW and R.B. WILSON, "Numerical Solutions in Axisymmetric Elasticity", Computers and Structures, Vol. 7, page 445 - 451, (1977).

2.53 M. MAYR, W. DREXLER and G. KUHN, "A Semi-analytical Boundary Integral Approach for Axismmetric Elastic Bodies with Arbitrary Boundary Conditions". Int. J. Solids Structures, Vol. 16, page 863 - 871, (1980).

Coupling of FEM and BEM

2.54 O.C. ZIENKIEWICZ, D.W. KELLY and P. BETTESS, "The Coupling of the Finite Element Method and Boundary Solution Procedures",

Int J. NUM. METHODS ENG., Vol 11, page 355 - 375, (1977).

2.55 O.C.ZIENKIEWICZ, D.W. KELLY and P. BETTESS, "Marraige à la mode - The Best of Both Worlds (Finite Elements and Boundary Integrals)", Chapter 5 of Energy Methods in Finite Element Analysis, eds. R. GLOWINSKI, E.Y. RODIN and O.C. ZIENKIEWICZ.

2.56 D.W. KELLY, G.G.W. MUSTOE and O.C. ZIENKIEWICZ, "Coupling Boundary Element Methods with other Numerical Methods" in Developments in Boundary Element Methods. 1, eds., P.K. BANERJEE and R. BUTTERFIELD, (1979).

2.57 C.A. BREBBIA and P. GEORGIOU, "Combination of Boundary and Finite Elements in Elastostatics." Appl. Maths. Modelling, Vol. 3, page 212 - 230, 1979.

2.58 Various papers in New Developments in Boundary Element Methods, ed. C.A. BREBBIA, Proceeding of the 2nd Int. Seminar on Boundary Element Methods, March 1980.

2.59 Various papers in Boundary Element Methods, ed. C.A. BREBBIA, Proceeding of the 3rd Int. Seminar on Boundary Element Methods, July 1981.

Fracture Mechanics

2.60 T.A. CRUSE and W. VAN BUREN, "Three-Dimensional Elastic Stress Analysis of a Fracture Specimen with an Edge Crack", Int. J. Fracture Mech, Vol. 7, page 1 - 15, (1971).

2.61 T.A. CRUSE, "Boundary Integral Equation Fracture Mechanics Analysis" in Boundary Integral Equation Method : Computational Applications in Applied mechanics, eds, T.A. CRUSE and F.J. RIZZO, ASME publication, AMD - Vol. 11, (1975).

2.62 T.A. CRUSE, "Two-Dimensional BIE Fracture Mechanics Analysis", Appl. Math. Modelling, Vol. 2, page 287 - 293, (1978).

2.63 T.A. CRUSE, "Two- and Three Dimensional Problems of Fracture Mechanics", in Developments in Boundary Element Methods - 1, eds. P.K. BANERJEE and R. BUTTERFIELD, (1979).

2.64 J. BALAS and J. SLADEK, "Method of Boundary Integral Equations for Analysis of Three-Dimensional Crack Problems", in Boundary Element Methods, ed. C.A. BREBBIA, Proceeding of 3rd Int. Seminar on Boundary Element Methods, July 1981.

Transient Dynamics

2.65 T.A. CRUSE and F.J. RIZZO, "A Direct Formulation and Numerical Solution of the General Transient Elastodynamic Problem - 1", J. Math. Anal. and Applic. Vol. 22 page 244 - 259, (1968).

2.66 T.A. CRUSE, "A Direct Formulation and Numerical Solution of the General Transient Elastodynamic Problem - II, J. Math. Anal. and Applic., Vol. 22, page 341 -355, (1968).

2.67 D.J. SHIPPY, "Application of the Boundary Integral Equation Method to Transient Phenomena in Solids", in Boundary Integral Equation Method : Computational Applications in Applied Mechanics, eds. T.A. CRUSE and F.J. RIZZO, ASME publication, AMD - VOL. 11, (1975).

2.68 G.D. MANOLIS and D.E. BESKOS, "Dynamic Stress Concentration Studies by Boundary Integrals and La Place Transform", Int. J. NUM. METHODS ENG., Vol. 17, page 573 - 599, (1981).

Thermo Elasticity

2.69 F.G. RIZZO and D.J. SHIPPY, "An Advanced Boundary Integral Equation Method For Three-Dimensional Thermoelasticity", Int. J. NUM METHODS ENG., Vol 11, page 1753 - 1768, (1977).

Thermo Elastoplasticity

2.70 S. MUKHERJEE, "Corrected Boundary Integral Equations in Planar Thermoelastoplasticity", Int. J Solids Structures Vol. 13, page 331 - 336, (1977).

2.71 H.D. BUI, "Some Remarks about the Formulation of Three-Dimensional Thermoelastoplastic Problems by Integral Equations", Int. J. Solids Structures, Vol. 14, page 935 - 939, (1978).

Inelastic Behaviour (Plasticity)

2.72 J.L. SWEDLOW and T.A. CRUSE, "Formulation of Boundary Integral Equations for Three-Dimensional Elasto-Plastic Flow." Int. J.

Solids Structures, Vol. 7, page 1673 - 1683, (1971).

2.73 A. MENDELSON and L.U. ALBERS, "Application of Boundary Integral Equations to Elastoplastic Problems", in Boundary Integral Equation Method : Computational Applications in Applied Mechanics, eds. T.A. CRUSE and F.J. RIZZO, ASME publication, AMD - Vol. 11, (1975).

2.74 V. KUMAR and S. MUKHERJEE, "A Boundary Integral Equation Formulation for Time-dependent Inelastic Deformation in Metals". Int. J. MECH. SCI, Vol. 19, page 713 - 724, (1977).

2.75 P.K. BANERJEE, "The Boundary Element Method for Two-Dimensional Problems of Elastoplasticity", in Recent Advances in Boundary Element Methods, ed. C.A. BREBBIA, (1978).

2.76 S. MUKHERJEE and V. KUMAR, "Numerical Analysis of Time-Dependent Inelastic Deformation in Metallic Media Using the Boundary Integral Equation Method", J. of Applied Mech., Vol. 45, page 785 - 790, (1978).

2.77 J.C.F. TELLES and C.A. BREBBIA, "On the Application of the Boundary Element Method to Plasticity", Appl. Math. Modelling, Vol. 3, page 466 - 470, (1979).

2.78 P.K. BANERJEE, D.N. CATHIE and T.G. DAVIES, "Two- and Three-Dimensional Problems of Elasto-plasticity", in Developments in Boundary Element Method - 1, eds. P.K. BANERJEE and R. BUTTERFIELD, (1979).

2.79 M. MORJARIA and S. MUKHERJEE, "Improved Boundary Integral Equation Method for Time-Dependant Inelastic Deformation in Metals", Int. J. NUM. METHODS ENG., Vol. 15, page 97 - 111, (1980).

2.80 J.C.F. TELLES and C.A. BREBBIA, "The Boundary Element Method in Plasticity", in New Developments in Boundary Element Methods, ed. C.A. BREBBIA, (1980.

2.81 D.N. CATHIE, "On the Implementation of Elasto-Plastic Boundary Element Analysis", in New Developments in Boundary Element Methods, ed. C.A. BREBBIA, (1980), also Appl. Math. Modelling, Vol., 5, page 39 - 44, (1981).

2.82 J.C.F. TELLES and C.A. BREBBIA, "On New Developments in Elasto-plastic Analysis", in Boundary Element Method, ed. C.A. BREBBIA, (1981).

2.83 M. BRUNET, "Numerical Analysis of Cyclic Plasticity using the Boundary Integral Equation Method", in Boundary Element Methods, ed. C.A. BREBBIA, (1981).

Fluid-Structure Interaction

2.84 O.C. ZIENKIEWICZ and P. BETTESS, "Fluid.Structure Dynamic Interaction and wave forces. An Introduction to Numerical Treatment." Int. J. NUM. METHODS ENG., Vol. 13, page 1 - 16, (1978).

2.85 J.A. DERUNTZ and T.L. GEERS, "Added Mass Computation By the Boundary Integral Method", Int. J. NUM. METHODS ENG., Vol 12, page 531 - 549, (1978).

2.86 R. EATOCK TAYLOR and J.B. WAITE, "The Dynamics of Offshore Structures Evaluated by Boundary Integral Techniques", Int. J. NUM. METHODS ENG., Vol. 13, page 73 - 92, (1978).

2.77 S. WALKER, "Boundary elements in Fluid/Structure Interaction Problems", in New Developments in Boundary Element Methods, ed. C.A. BREBBIA, (1980).

2.88 S. WALKER, "Boundary Elements in Fluid/Structure Interaction Problems Rotational Shells", Appl. Maths. Modelling, Vol. 4, page 345 - 350, (1980).

Plate Bending

2.89 M.A. JASWON and M. MAITI, "An Integral Equation Formulation of Plate Bending Problems", J. ENG. MATHS., Vol. 2, page 83 - 93, (1968).

2.90 M. MAITI and S.K. CHAKRABARTY, "Integral Equations Solutions for Simply Supported Polygonal Plates", Int. J. Eng. Sci., Vol. 12, page 793 - 806, (1974).

2.91 E.B. HANSEN, "Numerical Solution of Integro-differential and Singular Integral Equations for Plate Bending Problems", J. of Elasticity, Vol. 6, page 39 - 56, (1976).

2.92 G.P. BEZINE and D.A. GAMBY, "A New Integral Equation Formulation for Plate Bending Problems", in Recent Advances in Boundary Element Methods, ed. C.A. BREBBIA, (1978).

2.93 N.J. ALTIERO and D.L. SIKARSKIE, "A Boundary Integral Method

applied to Plates of Arbitrary Plan Form", Computers and Structures, Vol. 9, page 163 - 168, (1978).

2.94 H. TOTTENHAM, "The Boundary Element Method for Plates and Shells", in Development in Boundary Element Methods - 1, eds. P.K. BANERJEE and R. BUTTERFIELD, (1979).

2.95 B.C. WU and N.J. ALTIERO, " A Boundary Integral Method Applied to Plates of Arbitrary Plan Form and Arbitrary Boundary Conditions", Computers and Structures, Vol. 10, page 703 - 707, (1979).

Heat Conduction/Linear Operator BV Problems

2.96 K. TANAKA and M. TANAKA, "Time-Space Boundary Elements for Transient Heat Conduction problems." Appl. Math. Modelling, Vol. 4, page 331 - 334, (1980).

2.97 K. TANAKA and M. TANAKA, "Time-Space Boundary Elements for Boundary-Value Problems", Appl. Math. Modelling, Vol. 4, page 473 - 476, (1980).

Torsion

2.98 J.P. WONG and G. AGUIRRE-RAMIREZ, "A Finite Element-Integral Equation Solution to Torsion Problem", Computers and Structures, Vol. 9, page 53 - 55, (1978).

2.99 E. ALARCON, A. MARTIN and F. PARIS, "Improved Boundary Elements in Torsion Problems", in Recent Advances in Boundary Elements, ed. C.A. BREBBIA, (1978).

2.100 D.J. WOOD, "Determination of the Torsional Properties of a Plane Section using Boundary Integral Techniques", Appl. Math. Modelling, Vol. 4, page 410 - 416, (1980).

Contact Problems

2.101 T. ANDERSSON, B. FREDRIKSSON and B.G. ALLAN PERSSON, "The Boundary Element Method applied to Two-Dimensional Contact Problems", in New Developments in Boundary Element Methods, ed. C.A. BREBBIA, (1980).

2.102 T. ANDERSSON, "The Boundary Element Method applied to Two-Dimensional Contact Problems with Friction." in Boundary Element Methods, ed. C.A. BREBBIA, (1981).

CHAPTER 3

THEORY - THE DEVELOPMENT OF THE BOUNDARY INTEGRAL EQUATION METHOD

3.1 Introduction

A successful numerical technique must be based on a sound theoretical footing. For this reason, this chapter aims to ensure that a clear representation of the fundamentals of the Boundary Integral Equation method (hereinafter the BIEM) is given, so that the discussions, improvements and problems contained in later chapters can be understood.

A summary of the complete development of the BIEM is given in this chapter. To begin, the reference axes system and the bounds on the problem are defined. Secondly, the structural parameters, such as stress, strain, displacement and traction are discussed. Their relationships to one another through the constitutive equations of the material are defined, as required in an elastostatic problem. Before stating the governing differential equation of equilibrium, the exact nature of both the effects of a gravitational field and the assumptions of plane stress and strain are summarized.

The equations of equilibrium for a particular problem, together with its boundary conditions can be solved by using a weighted residual method. This is discussed in general terms without going into details. Thereafter, a more complete treatment will be given of the BIEM and the Finite Element Method (FEM). The parallel development of the FEM and BIEM has been presented here so that the methods can be compared. Where necessary, mathematical tools, such as Green's Formula, are stated for completeness.

The BIEM will be seen to depend on a specific set of weighting functions, called the Fundamental Solutions of the Kelvin problem. These are used to produce a formula, the Betti-Somigliana formula, which relates the displacement to the values of traction and displacement

on the boundary. By manipulating this formula, an equivalent boundary formula, independant of domain integrals can be written. This is the fundamental basis of the method and it will be shown how conveniently it can be treated numerically in the following chapters.

In addition to the development of this equation, the transformation of the domain body force terms to a boundary equivalent is discussed. Finally, the calculation of displacement, strain and stress as any point within the model is presented to complete the theory.

3.2 The Governing Differential Equation

The fundamental mathematical formulation of the governing diff erential equation will be discussed in the section. The definition of the axis system used and the parameters involved are discussed before the final statement of the problem is considered. Finally, a summary of the major points embodied in this section and the projected solution strategies are discussed.

3.2.1 The axis system

The conventional right-handed cartesian co-ordinate system will be employed as shown in figure 3.1.

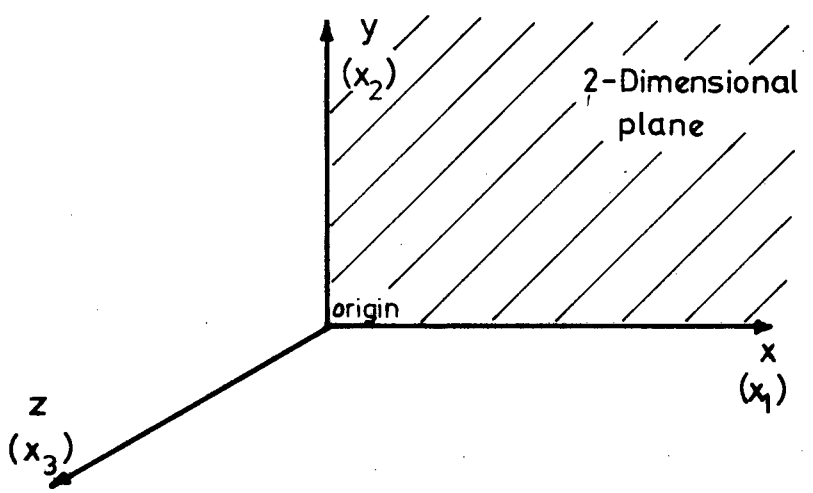

Figure 3.1 The Cartesian Co-ordinate System

The convenient labelling of the axis as x, y, z is standard practice, but for most of the mathematical formulation to follow, an indicial notation will be used where the three axis are termed x_1, x_2 and x_3. For the purpose of two-dimensional analysis, with which we shall be involved in this thesis, the x, y plane (denoted x_1, x_2) will be used. The general co-ordinate system can therefore be written as

$$x_i \text{ for } i = 1, 2 \text{ or } 3 \qquad (3.1)$$

3.2.2 Definition of Domain and Boundary regions

In order to quantify a problem in 3-dimensional space, the volume of applicability of the equations and the enclosing boundaries must be defined. Consider an element of elastic material in 3-dimensional space, - fig. 3.2.

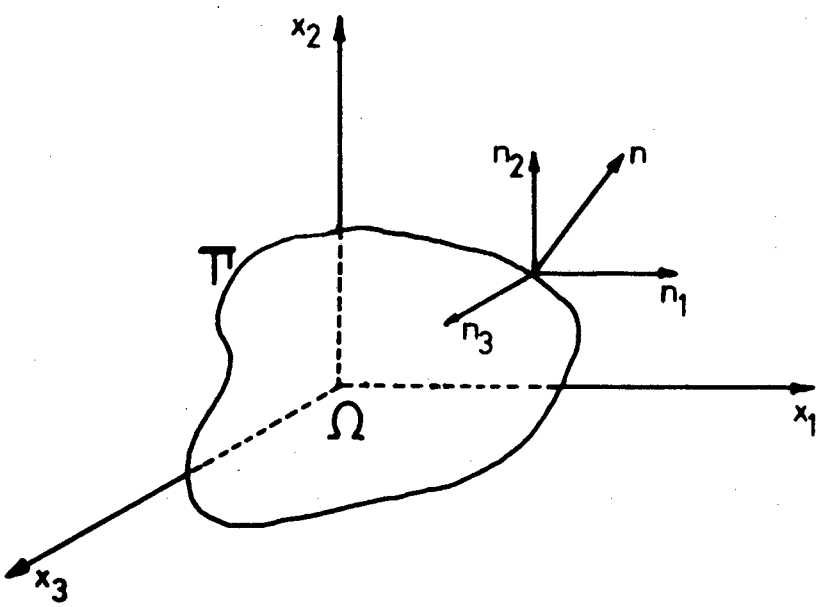

Figure 3.2 The definition of Domain and Boundary regions

The body under consideration can be divided into two separate parts namely the domain Ω enclosed within the boundary Γ. The boundary is similarily divided into sub-regions such that $\Gamma = \Gamma_1 + \Gamma_2 + \ldots$ or generally

$$\Gamma = \sum_{m=1}^{n} \Gamma_m \tag{3.2}$$

The exact significance of the boundary sub-division will be discussed later in section 3.2.11.

3.2.3 Stress

The most important parameter, and the one around which the governing diffierential equation is built, is the concept of stress [3.1]. The stress field within the domain Ω is represented by the tensor σ_{ij} where i, j = 1, 2 or 3 independently. The stress field is therefore a combination of the direct stress σ_{ii} for i = 1, 2 or 3 and the shear stresses σ_{ij} for $i \neq j$. In isotropic elasticity, the complementary shear stresses are assumed to be equal i.e., $\sigma_{ij} = \sigma_{ji}$ for $i \neq j$. The state of stress within a body can therefore be conveniently described by the matrix

$$\sigma_{ij} = \begin{bmatrix} \sigma_{11} & \sigma_{12} & \sigma_{13} \\ \sigma_{21} & \sigma_{22} & \sigma_{23} \\ \sigma_{31} & \sigma_{32} & \sigma_{33} \end{bmatrix} \tag{3.3}$$

This corresponds to the pictorial representation in fig. 3.3 where an element of material of volume $dx_1\ dx_2\ dx_3$ is shown to be subjected to the internal stress components.

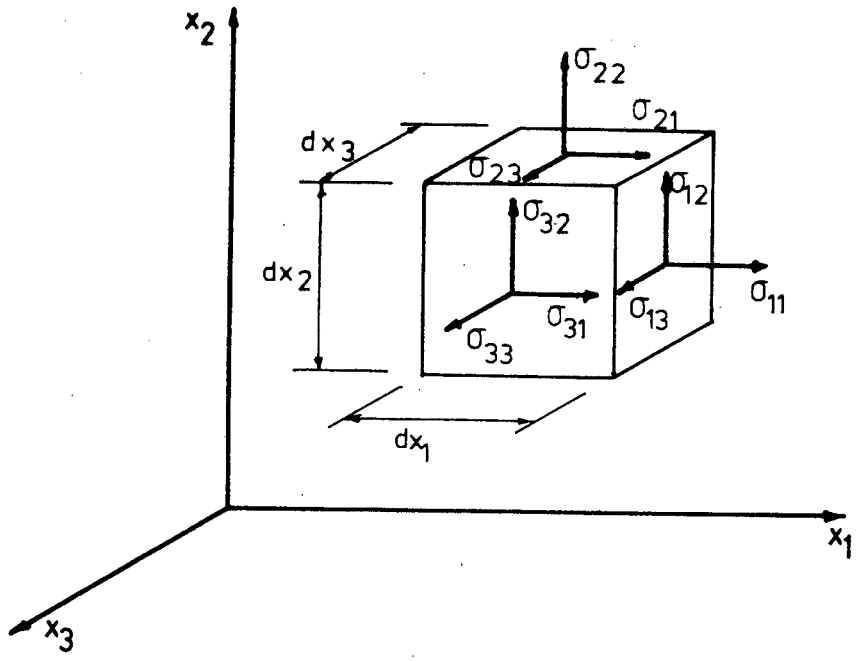

Figure 3.3 Internal Stress σ_{ij}

3.2.4 Boundary traction

Closely allied to stress is the concept of boundary traction. Each point on the boundary can be defined by the direction of an outward normal which is denoted by n_i (fig. 3.2) with respect to the axes set x_i. These direction cosines

$$n_i = \cos (n, x_i) \tag{3.4}$$

are used to define the boundary traction components t_i as

$$t_i = \sigma_{ij} n_j \tag{3.5}$$

These boundary tractions must be in equilibrium with the applied surface forces. This forms a boundary condition which must be satisfied in order to successfully solve the governing differential equation (see section 3.2.11).

3.2.5 Displacement

The deformation of a particle within the domain from its original state to its current state, with respect to the co-ordinate axes, is termed displacement and is denoted by u_i, i = 1, 2 or 3. The boundary tractions and displacements are the primary variables in the solution of an elastostatic problem by the boundary integral equation method. In the finite element method on the other hand the displacement is the primary unknown. Indeed, the finite element method seeks to approximate the displacement within the domain in order to satisfy the governing differential equation. This numerically involves the calculation of displacements at discrete points within the domain. In contrast to this method, the Boundary Integral Equation Method combines the boundary traction and the boundary displacements only in order to approximate the governing differential equation. The domain displacements are then calculated from the state of traction and displacement on the boundary.

Irrespective of the method of solution, accurate determination of displacement is crucial and hence remains the goal of most numerical methods.

3.2.6 Strain

The deformation per unit length is defined as the state of strain within material and is denoted by ε_{ij} i,j = 1, 2 or 3. In indicial notation its relationship to displacement can be written as [3.2]:

$$\varepsilon_{ij} = \frac{1}{2}\left(\frac{\partial u_i}{\partial x_j} + \frac{\partial u_j}{\partial x_i}\right) \qquad (3.6)$$

for an istropic elastic material. This is a linearization of Green's strain tensor where the second order partial derivatives have been neglected. More complicated material behaviour, for example large deformation characteristics can be accomodated by including the higher order derivatives in equation (3.6) to suit the specific application.

This is however, outside the scope of this thesis and hence will not be discussed further.

3.2.7 The Constitutive Equation [3.1]

For an isotropic elastic material, the stress, displacement and strain can be related according to Hooke's Law. In indical notation this representation can be defined as:

$$\sigma_{ij} = \lambda\delta_{ij} \frac{\partial u_k}{\partial x_k} + \mu \left[\frac{\partial u_i}{\partial x_j} + \frac{\partial u_j}{\partial x_i} \right] \tag{3.7}$$

where the Einstein summation convention on k is used. The Kronecker Delta

$$\delta_{ij} = 1 \text{ for } i = j$$
$$= 0 \text{ for } i \neq j$$

is incorporated together with the Lame Constants λ, and μ. These can be defined in terms of the Young's Modulus, E, and the Poisson's Ratio ν for the material as

$$\lambda = \frac{\nu E}{(1+\nu)(1-2\nu)} \tag{3.8a}$$

$$\mu = \frac{E}{2(1+\nu)} \tag{3.8b}$$

μ is conveniently referred to as the shear modulus of the material and is sometimes denoted by G.

The link between stress and displacement has therefore been established and will be used consistently in the following sections.

Equation (3.7) is sufficient for linear isotropic, elastic behaviour but, as in the case of the strain tensor, more elaborate

material descriptions and initial stresses can be employed for more complex materials.

3.2.8 The Body Force

The material within the domain of the body can be subjected to an environmental force such as gravitational attraction. Let this body force b_i act in the direction of the global co-ordinate axes x_i. This force is ever present and hence will be retained in the analysis wherever possible. The inclusion of the body force does not complicate the numerical method disadvantageously and it will be seen later that its effects can be simply and elegantly incorporated into the method.

3.2.9 Plane Stress and Strain

As this thesis is entirely concerned with 2 dimensional problems, it seems opportune to discuss the derivation of plane stress and strain prior to the formulation of the governing differential equations.

In the plane stress formulation, it is assumed that stress can only be developed in two dimensions, the stress in the third dimension being neglible, i.e.,

$$\sigma_{33} = \sigma_{23} = \sigma_{32} = 0 \tag{3.9}$$

and σ_{ij} for $i,j = 1,2$ are independent of x_3. In this formulation, applied tractions and the resulting displacements can only occur in the x_1 and x_2 co-ordinate directions. These simplifications require that the thickness of the body (x_3 dimension) is small when compared to the other dimensions. Similarily the body force is assumed to act only in the x_1 and x_2 co-ordinate directions. This method does not, however, preclude the development of strain in the x_3 direction; which can be derived by a combination of σ_{ij} for $i,j = 1$ and 2. This formulation is used particularly for the analysis of thin plates subjected to in plane forces. A perforated plate example of this type of analysis is given in a later chapter.

$$\frac{\partial \sigma_{ij}}{\partial x_j} + b_i = 0 \qquad \text{in } \Omega \tag{3.11}$$

It is now required to find the stress field σ_{ij} which satisfies equation (3.11) subject to the imposition of boudary conditions with respect to displacements and tractions on Γ.

3.2.11 Boundary Conditions

Two types of boundary conditions are commonly found for problems of the type being discussed here. For this purpose the boundary Γ is divided into two, namely Γ_1 and Γ_2 such that $\Gamma = \Gamma_1 + \Gamma_2$ as described in equation (3.2).

The displacement on Γ_1 can be prescribed by

$$u_i(x) = \bar{u}_i(x) \text{ for } x \in \Gamma_1 \tag{3.12}$$

This is known as the essential boundary condition required for the solution of the differential equation (3.11). The bar indicates the prescribed values.

The traction on Γ_2 relates to the application of external forces on the body. These are termed the non-essential or natural boundary conditions and are written as

$$t_i(x) = \bar{t}_i(x) \text{ for } x \in \Gamma_2 \tag{3.13}$$

Equations (3.12) and (3.13) are written in component form. At each point **x** on the boundary in a particular co-ordinate direction, only one variable (either u or t) can be prescribed, leaving the other to be found from the solution of (3.11).

3.2.12 Summary and Statement of the Problem

The parameters and variables required for the solution of an isotropic elastostatic problem in general 3 - dimensional space are defined in the preceding sections. The solution to the problem is therefore found by satisfying the equation of equilibrium (3.11). Hence the stress field σ_{ij} in the domain Ω must be calculated so that it satisfies (3.11) subject to to the boundary conditions stated in equations (3.12) and (3.13). The direct analytical solution of this problem is only possible in a very limited number of idealised problems. For the solution of general problems, numerical techniques must be employed. Typically, techniques include methods such as the Finite Difference Method, the Finite Element Method, and the subject of this thesis, the Boundary Integral Equation Method. In the following section, these basic mathematical equations will be developed in a form ideally suited to a numerical solution.

3.3 The Weighted Residual Method [3.3, 3.4, 3.5]

3.3.1 Generalized concepts

We have seen that the linear elastostatic problem requires that a solution be found for the equilibrium equation (3.11) subject to the boundary conditions imposed by equations (3.12) and (3.13). The equilibrium equation is written in terms of the stress field σ_{ij} and the body force term b_i. Through the constitutive relationship (3.7) the stress is related directly to the displacements u_i. Thus equation (3.11) can be considered as a differential equation in terms of u_i. Similarily, the boundary conditions can be written in terms of the unknown displacements or derivatives of displacements on the boundary. A general statement of the elastostatic problem can therefore be written as a partial differential equation in terms of displacements alone: it is required to find a solution for the displacement field $\tilde{u}$ such that the set of differential equations

$$A(\tilde{u}) = 0 \qquad (3.14)$$

is satisfied in the domain Ω subject to a set of boundary conditions

$$B(\tilde{u}) = 0 \tag{3.15}$$

being applied on the boundaries $\Gamma = \Gamma_1 + \Gamma_2$. In these equations A and B are interpreted as general differential operators but with special connotations when applied to the elastostatic problem.

This general approach has been adopted so that the broad basis for the Finite Element Method as well as the Boundary Integral Equation Method can be developed in parallel. The similarities and differences will then become clear and the development of a numerical solution process can be seen to be unified with currently accepted and established methods.

3.3.2 A Discrete System

The numerical approach to the solution of (3.14) and (3.15) is to find a solution which approximates to the actual solution $\tilde{u}$ by constructing an approximate solution set of the form

$$\tilde{u} \simeq u = \sum_{i=1}^{r} N_i u_i \tag{3.16}$$

N_i are a prescribed set of shape functions or interpolation functions which describe the variation between the unknowns u_i at a discrete point in the domain and on the boundary. N_i are written in terms of the independant variables governing the problem which are normally the geometric variables x_i. In other words the shape functions define the contours of variation of u_i within the physical domain of the problem.

There are two main factors which govern the choice of the shape functions:

(a) Equation (3.16) is constructed so that the variations of the

unknowns can be defined locally. This ensures that the definition is valid over a sub-domain and describes the variation of the unknowns over this latter region only. This leads to the idea of Finite "elements" as used in the Finite Element Method or "segments" as is required by the numerical Boundary Integral Equation Method.

(b) The choice of these shape functions controls the system of equations which ultimately must be solved. Here, a system of linear equations is most advantageous since their solution by Gauss reduction techniques is simple and efficient. It will be seen that the choice leads to a symmetric set of equations in the FEM case but to a non-symmetric set for BIEM. This however does not significantly effect the performance of either method.

In order for this process of approximation to remain valid, it is required that equations (3.14) and (3.15) be incorporated in an integral equation of the form [3.6]:

$$\int_{\Omega} G_j\,(u)\; d\Omega \;+\; \int_{\Gamma} g_j(u)\; d\Gamma \;=\; 0 \qquad (3.17)$$

in which G_j and g_j are prescribed differential operators corresponding to the governing equations which are described in terms of the shape function N_i. For an approximate solution of the form (3.16) to be reached, functions G_j and g_j must be piece wise integrable. Hence (3.17) must be able to be written

$$\int_{\Omega} G_j\, d\Omega \;+\; \int_{\Gamma} g_j\, d\Gamma \;=\; \sum_{k=1}^{K} \int_{\Omega_k} G_j\, d\Omega \;+\; \sum_{\ell=1}^{L} \int_{\Gamma_\ell} g_j\, d\Gamma \qquad (3.18)$$

This ensures that the piecewise integrability of the functions can be carried out over the sub-domains Ω_k or over the boundaries Γ_ℓ. The process, described above, is known as the development of a "discrete system" and forms the basis for both the FEM and the BIEM. From

this equation then, a numerical approximation to the exact solution can readily be implemented. In this case, we shall use the mathematical technique of Weighted Residuals but parallel methods, such as Variational methods, are also particularly advantageous in most cases.

3.3.3 Minimization of Errors

Let us now investigate the use of the approximate solution in equations (3.14) and (3.15).

Substitution of (3.16) into (3.14) and (3.15) does not result in the identical satisfaction of the equations but produces an error or residual:

$$A(u) = \varepsilon_1$$
$$\text{and} \quad B(u) = \varepsilon_2 \tag{3.19}$$

The weighted residual method can now be employed to distribute and minimize the errors throughout the domain. An arbitrary weighting function v is used to form an inner product with the approximating function (3.19). Hence

$$\int_{\Omega} v^T A(u)\, d\Omega = 0 \tag{3.20a}$$

$$\int_{\Gamma} v^T B(u)\, d\Gamma = 0 \tag{3.20b}$$

ensures that the distribution and minimization of the errors ε_1 and ε_2 is accomplished.

However, both (3.20a) and (3.20b) must be simultaneously satisfied, therefore

$$\int_{\Omega} v^T A(u)\, d\Omega + \int_{\Gamma} v^T B(u)\, d\Gamma = 0 \qquad (3.21)$$

can be written which is in the same form as (3.17). The definition of the unknown weighting function v determines the usefulness of (3.21). Many different methods of varying applicability have been used in this regard. All these methods will not be reviewed here, however, since only the Galerkin method is of particular relevance.

3.3.4 The Galerkin Method

The essential ingredient of the Galerkin Method is to ensure that the approximate or trial solutions (3.16) are the same as the weighting functions v [3.5]. This is simple and efficient and allows the integrals (3.21) to be piecewise integrable, a necessary requirement for a successful numerical solution.

3.3.5 The Weak form

The substitution of u and v into (3.21) does not necessarily produce the best possible basis for a numerical solution. It would be preferable to form a method where the resulting functions of u and v are of the same order. This would make it possible to produce a symmetric set of equations and consequently would result in a simplified solution. Equation (3.21) in its present form, however, does not permit this generality since v and A(u) are not of the same order. As an example, assume that A is a quadratic differential operator. For u to be continuous up to the second derivative, the function approximating u must be at least quadratic, while v could be at least constant. This is a violation of the classical Galerkin method. This state can be remedied however, by integrating equation (3.21) by parts [3.6]. Hence

$$\int_{\Omega} C(v)^T D(u)\, d\Omega + \int_{\Gamma} E(v)^T F(u)\, d\Gamma = 0 \qquad (3.22)$$

where C, D, E and F are differential operators of different orders to A and B. Now if A is quadratic, the integration leading to (3.22) will ensure that C and D are both linear. Hence, u and v can be approximated by the same function (at least linear) and symmetry of the resulting numerical equations is possible, depending on the exact definition of A. This is ensured if A is a self-adjoint quadratic operator.

Equation (3.22) is the weak form of the governing equation and is the basis of the Finite Element Method. The BIEM also relies on this equation which is integrated by parts once more to give the appropriate equations.

3.3.6 Green's Formula

The integration by parts carried out on (3.21) to form (3.22) is known as Green's formula [3.7, 3.8] when the differential operators act on vector quantities, as is the case in linear elastostatics. Green's formula can be looked upon as a decrease in the dimension of the basis and can be written as:

$$\iint_A \frac{\partial \Omega}{\partial z} \, dA = \int_S \Omega \, n_z \, dS$$

Now, if Ω is set equal to the product $\phi \, \psi$, then the formula for integration by parts can be formed:

$$\iint_A \phi \frac{\partial \psi}{\partial z} \, dA \equiv - \iint_A \frac{\partial \phi}{\partial z} \, \psi \, dA + \int_S \phi \, \psi \, n_z \, dS \qquad (3.23)$$

This formula is written for the two-dimensional domain A enclosed within the Boundary S. Z is a dummy variable which can be either x or y and ϕ and ψ are arbitrary vector potentials. n_z is the component of the boundary normal on S.

Equation (3.23) will be used extensively in the development which follows.

3.3.7 Outline of the Finite Element Method

The finite element method for a general two-dimensional solid under plane strain/stress conditions can easily be developed from the foregoing analysis. Let us now specify that the operator A is indeed the operator $\frac{\partial \sigma_{ij}}{\partial x_j}$ as found in the equation of equilibrium. Also, b_i the body force will be neglected in this instance as it tends to clutter the equations without being of any particular relevance. Also, assume that the arbitrary weighting functions are defined by the components of the displacement vector:

$$v^T = \delta u^T = \{\delta u, \delta v\} \tag{3.24}$$

Also, assume that the trial functions (3.16) satisfy the essential boundary conditions exactly. This means that the known displacements on boundary can be identically satisfied by the shape functions at the boundary nodes. Substitution of (3.24) and (3.16) into (3.21) results in the second expression in (3.21) being set identically to zero (from the trial function assumption). The first expression can then be written, for two-dimensional elasticity as:

$$\int_A \delta u^T A(u)\, dA = \int_A \left[\delta u \left\{\frac{\partial \sigma_x}{\partial x} + \frac{\partial \tau_{xy}}{\partial y}\right\} + \delta v \left\{\frac{\partial \tau_{xy}}{\partial x} + \frac{\partial \sigma_y}{\partial y}\right\}\right] dA \tag{3.25}$$

The weak form of (3.25) corresponding to (3.22) follows by integration by parts using Green's Formula (3.23):

$$-\int_A \left[\sigma_x \frac{\partial}{\partial x}(\delta u) + \tau_{xy} \left\{\frac{\partial}{\partial y}(\delta u) + \frac{\partial}{\partial x}(\delta v)\right\} + \sigma_y \frac{\partial}{\partial y}(\delta v)\right] dA$$

$$+ \int_S \left[\delta u \, (\sigma_x \, n_x + \tau_{xy} \, n_y) \; + \; \delta v \, (\tau_{xy} \, n_x + \sigma_y \, n_y) \right] \, dS = 0 \tag{3.26}$$

It will be recognised that the strain operator corresponding to (3.6) is operating on δu. Hence the set of virtual strains

$$\delta \varepsilon^T \; = \; \{ \frac{\partial}{\partial x} \, (\delta u), \; \frac{\partial}{\partial y} \, (\delta v), \; \ldots\ldots \} \tag{3.27}$$

and the boundary tractions corresponding to (3.5) can be substituted into (3.26) which then becomes the virtual work statement for two-dimensional planar elasticity.

$$\int_A \delta \varepsilon^T \sigma \, dA \; - \; \int_S \delta u^T \, t \, dS \; = \; 0 \tag{3.28}$$

The relationship between stress and strain can be written as

$$\sigma = D\varepsilon$$

where D is the symmetric elasticity matrix which is defined as:

$$D \; = \; \frac{E^*}{(1-\nu^{*2})} \begin{bmatrix} 1 & \nu^* & 0 \\ \nu^* & 1 & 0 \\ 0 & 0 & \frac{(1-\nu^*)}{2} \end{bmatrix} \tag{3.30}$$

where for plane stress $E^* = E$ and $\nu^* = \nu$, while for plane strain $E^* = \frac{E}{(1-\nu^2)}$ and $\nu^* = \frac{\nu}{(1-\nu)}$. It can be seen from this formulation, that only one method need be found for the analysis of both plane stress and plane strain problems as had been stated previously. The difference between the two analysis types depends entirely on the interpretation of the material properties E^* and ν^* (Young's Modulus and Poisson's Ratio respectively).

Substituting (3.29) into (3.28) gives

$$\int_A \delta\varepsilon^T D\varepsilon \, dA - \int_S \delta u^T t dS = 0 \tag{3.30}$$

The first term represents the strain energy of the system, U, and the second represents the potential energy of the loads W. The total potential energy of the system, π, is then

$$\pi = U - W$$

Substitution of the strain displacement relationships corresponding to (3.6)

$$\varepsilon = Bu \tag{3.32}$$

and the trial functions (3.16) into (3.31) gives

$$\int_A \delta u B^T D B u \, dA - \int \delta u^T N^T t dS = 0 \tag{3.33}$$

Since the variation of total potential energy $\delta\pi = 0$ ensures that the variation δu is arbitraty, the familiar stiffness equation

$$Ku = F \tag{3.34}$$

can be written, where

$K = \int_A B^T D B \, dA$ is the stiffness

and $F = \int_S N^T t ds$ is the surface leads

Since equation (3.34) is, by definition, piecewise integrable to conform with (3.18), it can be written as a summation of the stiffness over each sub-region or element. Hence the complete set of finite element equations can be written

$$\left[\sum_{e=1}^{E} K_e\right]\{u\} = \left\{\sum_{eb=1}^{EB} F_{eb}\right\} \tag{3.35}$$

where K_e is the element stiffness of element e and F_{eb} is the traction on a section of the external boundary eb. In numerical terms, K is a square, symmetric matrix while u and F are vectors of displacement unknowns and loads respectively. The solution of the set of linear equations gives the displacements at the discrete nodal points within the domain. The calculation of the stress and strain fields follows at element level from the definitions given.

This therefore, concludes the development of the finite element method for planar elastostatic problems. This will serve as a datum against which the development of the Boundary Integral Equation Method can be compared.

3.3.8 The Boundary Integral Equation Method

The Boundary Integral Equation Method is a further step in the mathematical expressions which preceed this section. In effect, two successive integrations by parts and a specific, unique interpretation of the weighting function is required to produce the necessary integral equation.

Before venturing further, however, let us return to the differential equation, the boundary conditions and the weighted residual formulation. Previously, we have assumed that the approximation function satisfies the essential boundary condition identically when the weighted residual expression is composed. This is sufficient and necessary in the formulation of the FEM, but this assumption will not be used in the BIEM formulation. Rather, the essential boundary condition are included by using a Lagrangian multiplier.

The augmented Weighted Residual expression for the elastostatic problem, including the body force term can be stated as:

$$\int_{\Omega}\left(\frac{\partial \sigma_{ij}}{\partial x_j}\right) v \; d\Omega + \int_{\Omega} b_i \, v \, d\Omega + \int_{\Gamma_2} (\bar{t}_i - t_i) \, v \, d\Gamma + \int_{\Gamma_1} (\bar{u}_i - u_i) \lambda \, d\Gamma = 0 \tag{3.36}$$

v is again the weighting function and λ is the Lagrangian multiplier used to include the displacement conditions.

Let us now assume that the weighting function is of the form

$$v = u_i^* \tag{3.37}$$

where u_i^* is a virtual displacement field which corresponds to the stress field σ_{ij}^* which is related to the traction on the boundary by

$$t_i^* = n_j \, \sigma_{ij}^* \tag{3.38}$$

The significance of the Lagrangian multiplier can be established by considering the variational form of equation (3.36), which will not be done here. However, from this analysis, it can be shown that [3.5]

$$\lambda = - t_i^* \tag{3.39}$$

Substitution of (3.37) and (3.38) into (3.36) gives

$$\int_{\Omega}\left(\frac{\partial \sigma_{ij}}{\partial x_j}\right) u_i^* \, d\Omega + \int_{\Omega} b_i \, u_i^* \, d\Omega - \int_{\Gamma_2} (t_i - \bar{t}_i) \, u_i^* \, d\Gamma$$

$$- \int_{\Gamma_1} (\bar{u}_i - u_i) \, t_i^* \, d\Omega = 0 \tag{3.40}$$

Integrate the first term by parts using Green's formula (3.23). The resulting weak form is:

$$- \int_{\Omega} \sigma_{ij} \frac{\partial u_i^*}{\partial x_j} \, d\Omega + \int_{\Gamma} t_i \, u_i^* \, d\Gamma - \int_{\Gamma_2} (t_i - \bar{t}_i) \, u_i^* \, d\Gamma$$

$$- \int_{\Gamma_1} (\bar{u}_i - u_i) \, t_i^* \, d\Omega + \int_{\Omega} b_i \, u_i \, d\Omega = 0 \tag{3.41}$$

The second term is produced from Green's formula where

$$\int_{\Gamma} \sigma_{ij} \, u_i^* \, n_j \, d\Gamma = \int_{\Gamma} t_i \, u_i^* \, d\Gamma \tag{3.42}$$

when equation (3.5) is used.

Now, we proceed one step further by integrating the first term of (3.41) again by parts, resulting in

$$\int_{\Omega} \frac{\partial \sigma_{ij}^*}{\partial x_j} u_i \, d\Omega - \int_{\Gamma} u_i \, t_i^* \, d\Gamma + \int_{\Gamma} t_i \, u_i^* \, d\Gamma$$

$$- \int_{\Gamma_1} (\bar{u}_i - u_i) \, t_i^* \, d\Omega + \int_{\Omega} b_i \, u_i^* \, d\Omega = 0 \tag{3.43}$$

where a similar contraction as that used in (3.42) results in the second term. The terms can be collected with the aid of equation (3.2); hence:

$$\int_{\Omega} \frac{\partial \sigma_{ij}^*}{\partial x_j} \, u_i \, d\Omega + \int_{\Gamma_1} t_i \, u_i^* \, d\Gamma + \int_{\Gamma_2} \bar{t}_i \, u_i^* \, d\Gamma$$

$$- \int_{\Gamma_1} \bar{u}_i \, t_i^* \, d\Gamma - \int_{\Gamma_2} u_i \, t_i^* \, d\Gamma + \int_{\Omega} b_i \, u_i^* \, d\Omega = 0 \tag{3.44}$$

Equation (3.44) is an inverted expression corresponding to (3.41). The differential operation has been transposed from operating on the actual stress field σ_{ij} to operating on the weighting function represented

by σ_{ij}^*. This is of special significance since, if the weighting function can be chosen so that it satisfies the domain integral (the first term) in (3.44), then the equation will involve boundary integrals only and will therefore justify the method's descriptive title. A solution to the equation

$$\frac{\partial \sigma_{ij}^*}{\partial x_j} = 0 \tag{3.45}$$

is therefore required. A general solution is not available. However, a solution of the Kelvin problem will produce a set of usable expressions.

3.3.9 The Kelvin Problem and Fundamental Solutions

Consider an infinite elastic medium subjected to a point force at a single, isolated position. A displacement and stress field is set up due to the resistance of this force. The magnitude of these fields at any point is then the solution of the Kelvin problem, and corresponds to the solution of the equation

$$\frac{\partial \sigma_{ij}^*}{\partial x_j} + \delta_\ell^k = 0 \tag{3.46}$$

δ_ℓ^k is the Dirac Delta function which represents the application of a unit point force at k in the ℓ direction. Let us now identify two points within the infinite medium; point p at which the displacement or stress is to be calculated, and point q where the unit load is applied. Also, p_i and q_i are the components of the position vectors $\tilde{p}$ and $\tilde{q}$ respectively.

Then in a two-dimensional, infinite medium, the displacement at p in the i direction due to the unit load at point q in the j direction is [3.3, 3.4, 3.9]:

$$U_{ij}\ (p,q) = \frac{(1+\nu)}{4\pi(1-\nu)}\left\{(3-4\nu)\quad \delta_{ij}\ \ln\frac{1}{r}\ +\ \frac{(p_i-q_i)\,(p_j-q_j)}{r^2}\right\} \tag{3.47}$$

where r is the distance between p and q, i.e. $r = |\tilde{p}-\tilde{q}|$ and δ_{ij} is the Kronecker Delta.

A corresponding stress field and hence a traction related to a specific unit normal can be formulated by using equations (3.6), (3.7) and (3.5). The resulting traction at point p in the i direction, due to a unit load at point q in the j direction is:

$$T_{ij}\ (p,q) = \frac{1}{4\pi(1-\nu)}\left[(1-2\nu)\left\{n_i\ \frac{(p_j-q_j)}{r}\ -\ n_j\ \frac{(p_i-q_i)}{r}\right\}\right.$$
$$\left.+\left\{(1-2\nu)\ \delta_{ij}\ +\ 2\,\frac{(p_i-q_i)\,(p_j-q_j)}{r^2}\right\}n_k\ \frac{(p_k-q_k)}{r}\right] \tag{3.48}$$

where δ_{ij} and r have the same connotations as in equation (3.47) and n_i are the components of the normal.

Equations (3.47) and (3.48) are known as the fundamental solutions of the two-dimensional Kelvin problem and can be used advantageously in the development of the BIEM.

3.3.10 Galerkin Tensor Formulation

The fundamental solution U_{ij} can be defined in terms of a Galerkin tensor. Naturally, this tensor must also satisfy the elasticity equilibrium equation and stems from the fact that a solution can be expressed in the form [3.10]

$$u_i = \phi_{,i} + e_{ijk}\,\psi_{k,j} \tag{3.49}$$

where e_{ijk} is the permutation tensor and ϕ and ψ are termed the scalar and vector potentials respectively of the displacement vector u.

3.3.11 The Betti-Somigliana Formula

Substituting (3.46) into (3.44), assuming that U_{ij} and T_{ij} are the fundamental solutions which replace the weighting functions u_i^* and t_i^*, and the two points p and q are denoted by x and y (which are associated with co-ordinate directions i and j respectively), the Betti-Somigliana formula results [3.9];

$$u_i(x) + \int_{\Gamma_1} u_j \, T_{ij}(x,y) \, d\Gamma + \int_{\Gamma_2} \bar{u}_j \, T_{ij}(x,y) \, d\Gamma = \int_{\Gamma_1} \bar{t}_j \, U_{ij}(x,y) \, d\Gamma + \int_{\Gamma_2} t_j \, U_{ij}(x,y) \, d\Gamma + \int_{\Omega} b_j(z) \, U_{ij}(x,z) \, d\Omega$$

for $x,z \in \Omega$; $y \in \Gamma$ (3.53)

Consolidating the tractions and displacement expressions, a simplified Betti-Somigliana formula can be written:

$$u_i(x) = \int_{\Gamma} U_{ij}(x,y) \, t_j(y) \, d\Gamma_y - \int_{\Gamma} T_{ij}(x,y) \, u_j(y) \, d\Gamma_y + \int_{\Omega} b_j(z) \, U_{ij}(x,y) \, d\Omega$$

for $y \in \Gamma$; $x,z \in \Omega$ (3.54)

Equations (3.53) and (3.54) relates the displacement at a field (or internal) point x to the displacements and tractions on the boundary.

3.3.12 The Boundary Formula

From equation (3.53) it can be seen that the displacement at an internal point x is related to the boundary displacements and tractions by the integral of the product of these variables and the fundamental solutions. Since $\bar{t}_i$ and $\bar{u}_i$ are the only known value (from the boundary conditions), the calculations to find the internal displacements $u_i(x)$ cannot be completed. The unknowns t_i and u_i over Γ_1 and Γ_2 respectively must first be computed. Only then can the internal displacements be found.

Consider now, the effect of moving the point x to the boundary. In so doing, equations (3.53) and (3.54) will involve only variables over the boundary and will result in the basic equation for the BIEM.

Move point x to the boundary, but enclose it within a hemisphere of "extra" material with a radius of ε and boundary Γ_ε. Hence boundary Γ_2 is made up of two sections namely

$$\Gamma_2 = \Gamma_{(2-\varepsilon)} + \Gamma_\varepsilon \tag{3.55}$$

and the fifth term in equation (3.53) can be written

$$\int_{\Gamma_2} u_j \, T_{ij} \, (x,y) d\Gamma = \int_{\Gamma_{(2-\varepsilon)}} u_j \, T_{ij} \, (x,y) d\Gamma + \int_{\Gamma_\varepsilon} u_j \, T_{ij} \, (x,y) d\Gamma \tag{3.56}$$

In the limit as $\varepsilon \longrightarrow 0$ $\Gamma_{(2-\varepsilon)}$ tends to Γ_2 and

$$\int_{\Gamma_\varepsilon} u_j \, T_{ij} \, (x,y) d\Gamma = d_{ij} \, u_j(x) \tag{3.57}$$

The exact analysis of the 2 x 2 matrix d_{ij} is shown in section (4.3.2.1) and in Appendix A. However, at this stage it is sufficient to say that if the boundary is smooth in the vicinity of point x, then $d_{ij} = -\frac{1}{2} \delta_{ij}$. Substituting equations (3.56) and (3.57) into (3.53) or (3.54) gives the boundary integral equation

$$c_{ij} \, u_j(x) + \int_\Gamma T_{ij} \, (x,y) \, u_j(y) \, d\Gamma = \int_\Gamma U_{ij} \, (x,y) \, t_j(y) \, d\Gamma_y$$
$$+ \int_\Omega b_j(z) \, U_{ij} \, (x,z) d\Omega \tag{3.58}$$

$$\text{for } x,y \varepsilon \Gamma \, , \; z \varepsilon \Omega$$

in which c_{ij} is a coefficient such that

$$(\delta_{ij} + d_{ij}) \, u_j(x) = c_{ij} \, u_j(x) \tag{3.59}$$

Since $d_{ij} = -\frac{1}{2}\delta_{ij}$ for a smooth boundary, then similarly $c_{ij} = \frac{1}{2}\delta_{ij}$ for a smooth boundary.

Equation (3.58) is the basis of the BIEM and will be used for the development of a numerical technique where the unknown variables t_i and u_i over Γ_1 and Γ_2 will be calculated. Hence, the classic boundary value problem of elasticity stated by equation (3.11), (3.12) and (3.13) can be successfully solved by consideration of the boundaries of the problem only.

3.4 The Body Force

3.4.1 General

The body force is a very important ingredient of the theory of elasticity since invariably it is found that the body is subject to some externally applied force field. In elastostatics, the usual effect encountered is when the body is placed in a constant gravitational field where every molecule is subjected to the same body load which is termed "self weight". Secondly, a body force field can be set up due to the centrifugal force encountered when a body spins about a central axis. This is conveniently described as rotational inertia and is particularly important in the analysis of axisymmetrical problems. Also the effects of a temperature gradient on a structure can be interpreted as a body force which causes thermal stresses to be set up. Since we are dealing with the static problem only, the temperature distribution is assumed to be in a steady state.

We will only be concerned here with the self weight of the body within a constant gravitational field as it is applied to problems of plane stress and strain.

3.4.2 The Integral Form

Equation (3.58) shows that the effect of the body force is included by the integral over the domain of the product of the body force and the displacement fundamental solution:

$$B_i(x) = \int_{\Omega} b_j(z)\, U_{ij}(x,z)\, d\Omega \tag{3.60}$$

If the shape of the domain Ω is simple, for example, a square, rectangle or a circle, then the body force coefficient could be calculated analytically. But for an arbitrary shaped domain this is impractical and a numerical integration scheme must be employed. This can easily be accomplished by dividing the domain into convenient sections or cells for separate integration. However, the mere fact that a domain integral is included in equation (3.58) makes the method cumbersome. A far more elegant solution would be to transform the domain integral into a boundary integral for the calculation of $B_i(x)$. Equation (3.58) would then contain only boundary integrals and an effective numerical technique, disregarding the domain could be formulated.

3.4.3 The Boundary Integral Form

The transformation of the domain integral into the boundary integral form is achieved by the use of Gauss's Theorem. However, it is first necessary to define the fundamental solution in terms of the Galerkin tensor, equation (3.52) so that the transformation can easily be facilitated.

Substituting equation (3.50) into (3.60) gives

$$B_i(x) = \int_{\Omega} \{G_{ij,kk} - \frac{G_{ik,kj}}{2(1-\nu)}\}\, b_j\, d\Omega \tag{3.61}$$

By the use of Gauss's Theorem, written in general terms as [3.7]

$$\int_V A_{jk\ell,i}\, dV = \int_S A_{jk\ell}\, n_i\, dS \tag{3.63}$$

the Body force can be written as:

$$B_i(x) = b_j(z) \int_{\Gamma} \{G_{ij,k} - \frac{G_{ik,j}}{2(1-\nu)}\}\, n_k\, d\Gamma \tag{3.63}$$

The Galerkin tensor (3.51) can now be used in (3.63) to give [3.11].

$$B_i(x) = \frac{1+\nu}{4\pi E} \int_\Gamma r\,(2\ln\frac{1}{r} - 1)\,\{b_i n_m r_{,m} - \frac{n_i b_m r_{,m}}{2(1-\nu)}\}\,d\Gamma \qquad (3.64)$$

where $r_{,m} = \frac{\partial r}{\partial x_m}$

This expression can now be used to estimate the effect of the body force at point x by the integration of the boundary only and is therefore extremely useful in the numerical method.

3.5 Internal Solutions

3.5.1 Internal Displacements

Once the unknowns t_i and u_i over Γ_1 and Γ_2 respectively have been computed, it is a simple matter to calculate the displacement at any point x in the domain (at any internal point x) from the Betti-Somigliana formula, equation (3.53). This has the advantage that the displacement, and subsequently also the stress and strain can be calculated at any designated point in the domain. For design purposes, this is ideal since the designer now has the option of specifying the precise position at which the design parameters are to be calculated. In the case of the Finite Element Method, on the other hand, these positions must be predetermined from the designers experience so that a node point can be assigned at that exact location. This positioning is extremely difficult in complex models and hence interpolation is used. In contrast, the BIEM allows the designer to "track down" the important parameters and to calculate them accurately at the relevant positions.

The strain and the stress at any designated internal point can thus similarily be accurately calculated.

3.5.2 Internal Stress and Strain

The state of strain and stress at any internal point x can now

be calculated from the Betti-Somigliana formula, equation (3.53), the strain displacement relationships, equation (3.6) and the material constitutive relationship, equation (3.7).

Performing the necessary mathematics on (3.53) using equation (3.7) results in the formula for the stress field [3.3] at point x.

$$\sigma_{ij}(x) = \int_{\Gamma} D_{kij}\ (x,y)\ t_k(y)d\Gamma_y - \int_{\Gamma} S_{kij}\ (x,y)\ u_k\ (y)d\Gamma_y + \int_{\Gamma} S_{ij}^*\ (x,y)d\Gamma_y \tag{3.65}$$

where D_{kij} and S_{kij} are 3rd order tensors which correspond to the fundamental displacement and traction solutions and S_{ij}^* is the contribution of the body force to the stress field. These expressions can be stated as:

$$D_{kij}\ (x,y) = \frac{1}{4\pi r(1-\nu)}\left[(1-2\nu)\ \{\delta_{ki}\ r_{,j} + \delta_{kj}\ r_{,i} - \delta_{ij}\ r_{,k}\} + 2r_{,i}\ r_{,j}\ r_{,k}\right] \tag{3.66}$$

$$S_{kij}\ (x,y) = \frac{E}{4\pi r^2(1+\nu)(1-\nu)}\left[2\ \frac{\partial r}{\partial n}\left\{(1-2\nu)\ \delta_{ij}\ r_{,k} + \nu\ (\delta_{ik}\ r_{,j} + \delta_{jk}\ r_{,i}) - 4r_{,i}\ r_{,j}\ r_{,k}\right\} + 2\nu\ (n_i\ r_{,j}\ r_{,k} + n_j\ r_{,i}\ r_{,k}) + (1-2\nu)(2\ n_k\ r_{,i} + \delta_{ik}\ n_j + \delta_{jk}\ n_i) - (1-4\nu)\ n_k\ \delta_{ij}\right] \tag{3.67}$$

$$S_{ij}^*\ (x,y) = \frac{1}{2\pi}\left(1-\ln\frac{1}{r}\right)\left\{n_m\ r_{,m}\ \left(b_i\ r_{,j} + b_j\ r_{,j} + \frac{\nu}{1-\nu}\ b_{,s}\ r_{,s}\ \delta_{ij}\right) - \frac{b_m r_{,m}}{2(1-\nu)}\ (n_j\ r_{,j} + n_j\ r_{,i})\right\} + \frac{1}{2(1-\nu)}\ \left(\ln\frac{1}{r} - \frac{2}{2}\right)\left(\frac{1-2\nu}{2}\ (b_i\ n_j + n_i) + n_m\ b_m\ \delta_{ij}\right) \tag{3.68}$$

In equations (3.66), (3.67) and (3.68) the index notation for the derivative is used in

$$r_{,\ell} = \frac{\partial r}{\partial x_\ell} = \frac{y_\ell - x_\ell}{r} \tag{3.69}$$

Similar expressions to the above can also be derived for the strain at point x by differentiating equation (3.53) according to the strain/displacement relationships (3.6).

3.6 Conclusion

The theoretical development of the BIEM and the FEM has been traced from the governing equilibrium equation and the boundary conditions, through the weighted residual method to a form which can readily be used as the basis for a numerical solution process for linear elastostatics.

The BIEM results in an equation which relates the variables of displacement and tractions on the boundary by using a specific weighting function which is the solution of the Kelvin problem in two dimensions. This technique results in the Betti-Somigliana formula which can be adapted so that only the boundary variables are involved. The subsequent calculations of displacement, strain and stress are easily accomplished by considering only these boundary variables. In addition the body force due to a constant gravitational field can be incorporated, and also can be written in a form dependant only upon a boundary integral.

The theoretical development has thus been completed. However, the actual calculation of the unknown boundary displacements and tractions must still be undertaken. This is the subject of the following chapter.

3.7 References

3.1 S.P. TIMOSHENKO and J.N. GOODIER, Theory of Elasticity 3rd Edition, McGraw-Hill (1970).

3.2 P.G. HODGE, Continuum Mechanics, McGraw-Hill (1970).

3.3 C.A. BREBBIA, The Boundary Element Method for Engineers, Pentech Press, London (1978).

3.4 C.A. BREBBIA, and S. WALKER, Boundary Element Techniques in Engineering, Newnes-Butterworth, London (1980).

3.5 O.C. ZIENKIEWICZ, The Finite Element Method. 3rd Edition, McGraw-Hill (1977).

3.6 G.C. HOWELL and W.S. DOYLE, "Plane Stress/Strain Analysis by Boundary Integral Equation and Finite Element Methods" Proceedings of the Conference on Finite Element Methods in South Africa held at CSIR, Pretoria, South Africa on 17 - 18 March 1981.

3.7 M.L. BOAS, Mathematical Methods in the Physical Sciences, John Wiley and Sons Inc., USA, (1965).

3.8 E. KREYSIG, Advanced Engineering Mathematics, 4th Edition John Wiley and Sons, Inc., USA (1962).

3.9 M.A. JASWON and G.T. SYMM, Integral Equation Methods in Potential Theory and Elastostatics. Academic Press, London (1977).

3.10 B.D. REDDY, Course Notes on Solid Mechanics, UCT, (1979).

3.11 D.J. DANSON, "A Boundary Element formulation of Problems in linear Isotropic Elasticity with Body Forces", Proceeding of the 3rd International Seminar on Boundary Element Methods, Irvine, California July 1981.

CHAPTER 4

THE NUMERICAL IMPLEMENTATION OF THE BOUNDARY INTEGRAL EQUATION METHOD

4.1 Introduction

The exact solution of the relevant differential equations of equilibrium is only possible for a limited number of problems. The geometry, the material properties and the boundary conditions must the simple enough, in these problems, to allow a rigorous mathematical solution to be found. If a solution of this type is not possible, then the logical alternative is to seek an approximate solution. This usually means that some simplifying assumptions must be made. For example, in the numerical representation of the boundary integral equation method, it is assumed that the boundary variables of displacement and traction vary in a predetermined manner over a segment of the boundary. The details of these variations are discussed in this chapter.

The first section of this chapter, deals with the general formulation of an approximation theory, it's significance in the BIEM, the resulting matrix equations which develop, and the method of solution.

The second section covers the details of the strategy employed in the integration of the fundamental solutions over the boundary and the importance of the coefficient c_{ij} which arises due to the singularity in the fundamental solutions.

Up to this stage, the analysis is independent of the type of interpolation used to describe the variation of the boundary variables. But, in the following section, these details are introduced. Constant, linear and quadratic interpolation methods are presented and these form the basis of all subsequent developments.

A special problem arises when the fundamental solution is required to be integrated in the region in close proximity to the singularity. To produce an accurate representation in this region, an analytical method of integration has been developed. This is

discussed in the section called 'The Pivot Segments' for the three types of interpolation used.

The calculation of the field variables within the domain once the boundary values are known, is very important, since the parameters for effective design are obtained from here. This is dealt with in the section on internal points.

To weld the foregoing details into a homogeneous unit, section 4.7 brings each part together in a macroflow chart, which clearly maps out the method from start to finish. This section also includes the techniques which were used when the computer programs were designed.

Finally, the method is put to the test in 5 specially chosen examples, which cover the major aspects of planar elastostatics. Plane stress and plane strain problems are included which accentuate certain important features. In particular, a problem where bending effects are predominant as well as a practical design problem are discussed.

To complete this chapter, a discussion of the merits and demerits of the various interpolation orders is included.

4.2 The Numerical Outline

4.2.1 Approximation Theory

To begin the discussion on the theory of approximation, let us assume that the exact solution of the particular problem is known. It is then required to calibrate an approximate solution so that it fits the exact solution in some predetermined average sense.

For this purpose, assume that the exact solution can be represented graphically by a curve in 2-dimensional space as in figure 4.1 where the horizontal axis represents the geometric variable (for example, distance from the origin, or length) and the vertical axis represents the solution or field parameter (for example, displacement or traction).

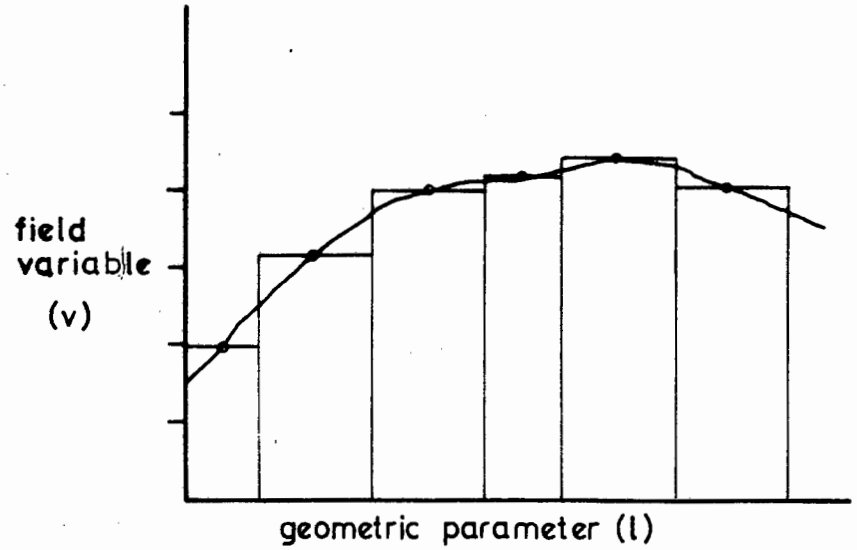

Figure 4.1 Representation of the 'Exact' and 'Approximate' Solutions

At this stage, a decision must be made as to the way in which the construction of the approximate solution is to be carried out. This decision depends upon;

(a) the positions (using the geometric parameter) at which the solution is to be found, and

(b) the assumed variation of the field variables between these points.

The sampling positions are known as nodes in the present terminology, while the variation of the field variables can be described by a set of shape functions.

In the case of the BIEM, the geometric parameter in figure 4.1 is represented by the Boundary Γ and is measured from an arbitrary fixed point somewhere on this boundary. The nodes can then be positioned at selected intervals along the boundary. A boundary segment can now

be defined which spans a prescribed number of these nodes. The number of nodes involved per segment depends on the degree of interpolation assumed. Segments with constant, linear and quadratically interpolation variations of the field variable are shown in figure 4.2. In this way, the entire boundary can be subdivided into piecewise boundary segments.

INTERPOLATION TYPE (ORDER)	DIAGRAMMATICAL REPRESENTATION	FORM OF INTERPOLATION
Constant	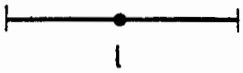	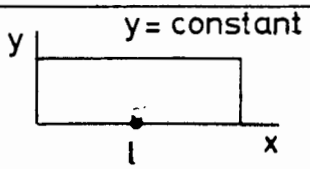
Linear	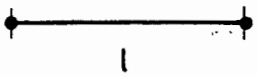	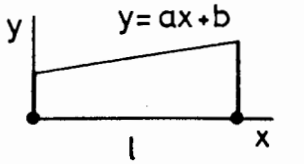
Quadratic	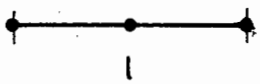	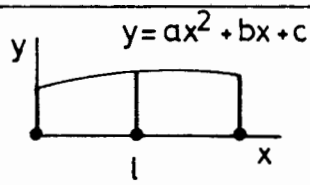

Figure 4.2 Diagrammatic representation of interpolation orders

By specifying the nodal points, the segments and the interpolation type, the exact solution can be approximated piecewise as in shown in figure 4.1, where a constant interpolation formulation has been assumed.

Let us now consider a single node i, being one of the n nodes of a segment. If the field variable is known at all n nodes, then the value at any point can be interpolated from the expression

$$v(\xi) = \sum_{q=1}^{Q} N_q \, v_q \qquad (4.1)$$

where ξ is a local geometric parameter representing the position at which the field variable is to be calculated; N_q is the shape or basis function defined in terms of ξ for node q; v_q is the value of the field variable at node q; and Q is the number of nodes per segment. The exact form of N_q depends on the interpolation order assumed and will be discussed later in section 4.4.

If we can now, in addition to the field variable, describe the geometry in terms of the same set of shape functions N_q by allowing v_q to represent the co-ordinates of node q, then we have the basis for the so-called "isoparametric" formulation. This technique has been successfully used in the Finite Element Method [4.1, 4.2, 4.3] and will also be employed here as a basis for the numerical BIEM.

The inherent errors in the assumptions made concerning the interpolation type, will not be discussed here, save to suggest that the higher the order, the more accurate the approximate solution should be. This point is discussed in detail later, by way of examples.

4.2.2 The Form of the numerical BIEM equations

It has been shown in chapter 3 that the elastostatic problem can be formulated in terms of the variables of displacement and traction over the boundaries only as depicted by equation (3.58). We can now use the foregoing approximation technique to produce a basis for the numerical BIEM.

For the purposes of generality, assume that:

(a) the boundary of the domain in question has been divided into K segments, each denoted Γ_k

(b) the interpolation order is such that the number of nodes associated with each segment is Q

(c) the total number of boundary nodes is n

The components of displacement and traction (the field variables) can now be represented in the form of equation (4.1) by

$$u_i = \left[\sum_{q=1}^{Q} N_q \, u_q \right]_i \tag{4.2a}$$

$$t_i = \left[\sum_{q=1}^{Q} N_q \, t_q \right]_i \tag{4.2b}$$

where i represents the component in terms of the global co-ordinate system.

Substitution of (4.2) into the equation (3.59) gives

$$c_{ij} \, u_j(x) + \sum_{k=1}^{K} \int_{\Gamma_k} T_{ij}(x,y) \left[\sum_{q=1}^{Q} N_q \, u_q(y) \right]_j d\Gamma_k = \sum_{k=1}^{K} \int_{\Gamma_k} U_{ij}(x,y) \left[\sum_{q=1}^{Q} N_q \, t_q(y) \right]_j d\Gamma_k + \text{body force terms} \tag{4.3}$$

Let the node at the point x be termed the pivot node and the segment over which the integration is to be performed , Γ_k, be called the focus segment. As the discussion progresses, the reasons for these names will become clear.

As $u_q(y)$ and $t_q(y)$ are constants relative to the node q, and, assuming that integration and summation are interchangeable, equation (4.3) can be rewritten as:

$$c_{ij} \, u_j(x) + \sum_{k=1}^{K} \left\{ \sum_{q=1}^{Q} \int_{\Gamma_k} T_{ij}(x,y) \, N_q \, d\Gamma_k \right\} \left[u_q(y) \right]_j = \sum_{k=1}^{K} \left\{ \sum_{q=1}^{Q} \int_{\Gamma_k} U_{ij}(x,y) \, N_q \, d\Gamma_k \right\} \left[t_q(y) \right]_j + \text{body force terms} \tag{4.4}$$

Equation (4.4) represents the differential equations of equilibrium and the boundary conditions, as discussed in chapter 3 by the piecewise descriptions of the variation of the displacement and traction over the boundaries. This therefore describes the true numerical BIEM.

4.2.3 The Matrix representation

The discrete system, (4.4), represents a set of equations by allowing each node in the boundary to become the pivot node successively. Consequently, two component equations are constructed for each pivot position, x, while the integrations are performed over every focus segment Γ_k (k = 1 to K). A total of 2n equations are therefore constructed in this way and can be represented in matrix terms as (a similar form is given in [4.4]):

$$[C]\{u\} + [\bar{H}]\{u\} = [G]\{t\} + \{B\} \qquad (4.5)$$

where

[C] is a tridiagonal matrix constructed from c_{ij} and corresponds to the pivot node x

$[\bar{H}]$ is the matrix of coefficients from the integration of the traction solution

[G] is the matrix of coefficients from the integration of the displacement solution

{u} is the vector of displacement components at the nodes

{t} is the vector of traction components at the nodes

{B} is the vector of body force terms

By consolidation of [C] and $[\bar{H}]$, the "neat" form of equation (4.5) can be presented as

matrix can easily be understood since each pivot node (i.e. each separate equation) is associated with each and every other node on the boundary through the summation over the focus segments.

Clearly, then, the method of solution must allow for these irregularities in an attempt to get as accurate an answer as possible, independant of the computer's machine accuracy.

Due to the non-symmetric form of the matrix, any in-core solution strategy would require the full matrix to be stored and manipulated. Since it was not the topic of investigation covered by the present research, it was decided, at the outset, to solve the equation by a direct in-core Gauss reduction technique with partial pivoting and back substitution.

Other methods of solution, based on the Gauss reduction method, for example, Crout reduction, can also be implemented but require a similar amount of computer storage and a number of arithmetic operations. Hence little advantage is seen in using these methods.

The iterative solution technique, Gauss-Seidel, was however, also tested. The irregularity of the coefficients in the matrix and the fully-populated form makes iteration very sensitive and large numbers of arithmetic operations are necessary. Convergence to a solution is therefore slow and consequently this method was discarded.

4.3 Boundary Integration

The governing differential equations of equilibrium have been transformed into a simple equation in which only boundary integrals are involved. Hence, a two-dimensional problem has been transformed into an integration over a line, i.e., in one dimension. The numerical method employed allows the boundary line to be subdivided into piecewise segments, over which local integration is performed.

A distinction is made, at this stage, between two differing situations which arise for integration over the boundary. Remembering that x is the pivot node and y is a point within the focus segment

over which the integration is to be performed, then due to the singularity in the Kelvin Solution when x = y, the two possible situations are [4.5, 4.6, 4.7]:

(i) $x \notin \Gamma_k$ i.e. the pivot node does not appear within the focus segment k

(ii) $x \in \Gamma_k$ i.e. the pivot node is included in the focus segment k.

For case (i) the integrations are carried out numerically by Gaussian Quadrature, while for case (ii) the integrations are performed analytically, the details being given in section 4.5 for different shape functions.

The significance of the constant c_{ij} and the proof of $c_{ij} = 0.5\ \delta_{ij}$ for smooth boundaries is given in section 4.3.2.

4.3.1 Gaussian Quadrature

The integrations to be performed are of the form

$$I = \int_{\Gamma_k} V_{ij}(x,y)\ N_q\ d\Gamma_k \tag{4.8}$$

where $V_{ij}(x,y)$ represents either the displacement fundamental solution $U_{ij}(x,y)$ or the traction fundamental solution $T_{ij}(x,y)$.

Let us now define a single segment in two dimensional space as in figure 4.3 in terms of the natural co-ordinates ξ.

The transformation between the global x-y co-ordinate system and the local ξ co-ordinate is effected by the Jacobian

$$J = \sqrt{\left(\frac{dx}{d\xi}\right)^2 + \left(\frac{dy}{d\xi}\right)^2} \tag{4.9}$$

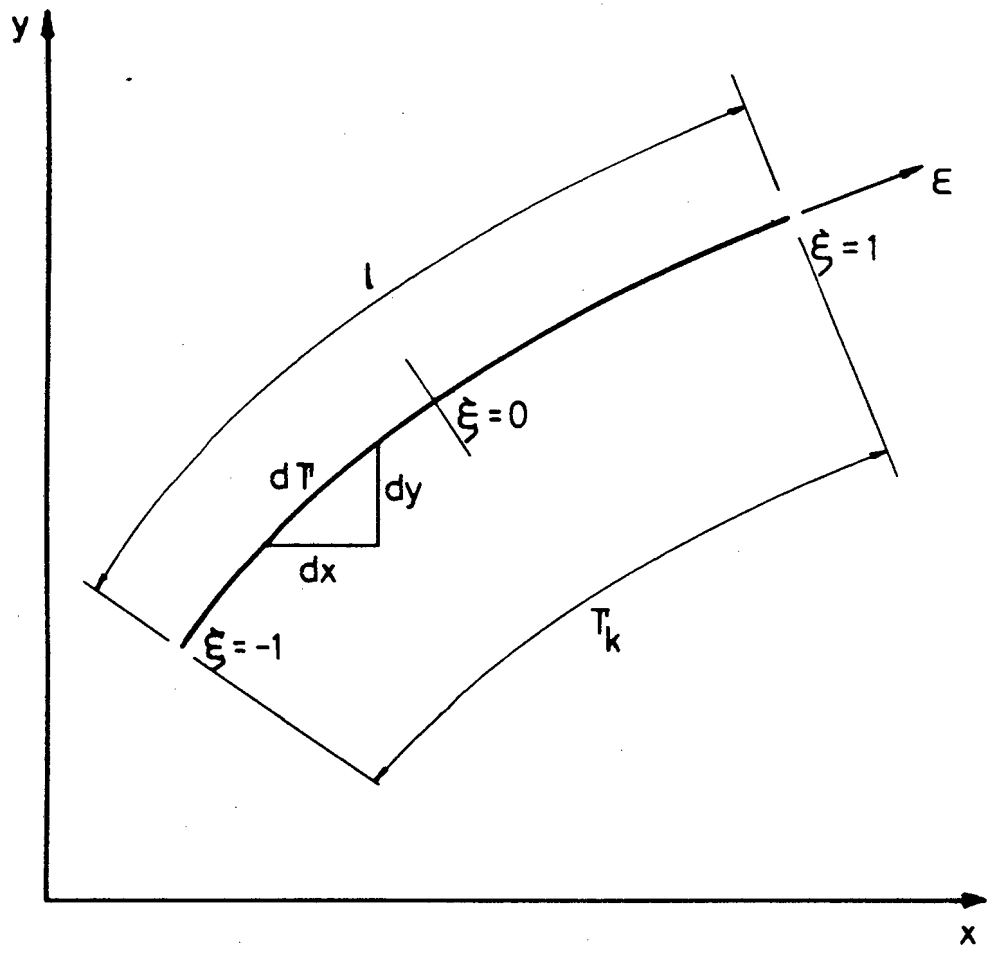

Figure 4.3 Definition of natural co-ordinate system for a single segment

which comes directly from figure 4.3 as

$$(d\Gamma)^2 = (dx)^2 + (dy)^2$$

$$= \left[\left(\frac{dx}{d\xi}\right)^2 + \left(\frac{dy}{d\xi}\right)^2\right] d\xi^2 \qquad (4.10)$$

hence $d\Gamma = J\, d\xi$ (4.11)

The integral equation can then be written in terms of the co-ordinates ξ as:

$$I = \int_{-1}^{1} V_{ij}(x,y)\ N_q(\xi)\ d\xi \qquad (4.12)$$

Here, x and y have a different connotation to that used in equation (4.9) and (4.10). In (4.12), x and y indicate the relative positions in space of the pivot node and the focus segment, while in the previous equations, x and y represent the co-ordinate system. Notice here, that the integration is to be performed over the interval [-1, 1] as required by the Gaussian Quadrature formula.

Numerical integration of (4.12) can thus be written

$$I = \sum_{\ell=1}^{g} w_\ell\ V_{ij}(x,\xi_\ell)J \qquad (4.13)$$

where ξ_ℓ is the sampling point on the segment.

w_ℓ is the Gaussian weighting factor at point ξ_ℓ.

g is the order of the Gauss integration.

and $V_{ij}(x,\xi_\ell)$ is the fundamental solution calculated at point ξ_ℓ.

In the computer program, a choice of 3 orders of Gaussian integration are catered for. The relative orders, positions of sampling points and weights are shown in table 4.1 [4.2].

GAUSS INTEGRATION ORDER g	SAMPLING POINT ξ_ℓ FOR $-1 \leqslant \xi \leqslant 1$	WEIGHT w_ℓ
2	$\pm$ 0.5773502682	1.0000000000
4	$\pm$ 0.8611363116 $\pm$ 0.3399810436	0.3478548451 0.6521451549
6	$\pm$ 0.9324695142 $\pm$ 0.6612093864 $\pm$ 0.2386191861	0.1713244924 0.3607615730 0.4679139346

Table 4.1 Gaussian Quadrature -
Sampling Points and Weights

The effectiveness of each of these orders of integration will be shown later in this chapter when specific examples are discussed.

4.3.2 The Boundary Coefficient c_{ij}

In chapter 3 it was stated that for a smooth boundary, the coefficient c_{ij} was equal to $\frac{1}{2}\,\delta_{ij}$. Let us now investigate the value of this coefficient for a general point on the boundary in order to discover the variation for non-smooth boundaries.

In most interpolation schemes, as detailed in section 4.4, it will be seen that a node is placed at the end of a segment and thus is common to two adjacent segments. If the segments are piecewise straight and the actual boundary is curved, then the idealized boundary will exhibit a "kink" at the node. Under these circumstances, c_{ij} will not

be equal to $\frac{1}{2}\,\delta_{ij}$ but, in fact assumes a value related to the external angle measured between the two adjacent segments. There are two ways in which the coefficient can be calculated, namely:

(i) Analytically, by direct integration of the fundamental solution and

(ii) Numerically, by considering the effects of a rigid body movement [4.4].

4.3.2.1 Analytical calculation of c_{ij}

To begin, we will discuss the calculation of c_{ij} by an analytical technique which requires that the fundamental solutions be integrated at the boundary point. The details of this discussion are given in Appendix A and hence only an outline will be shown here.

Equation (3.54) relates an internal point to the integration over Γ of the boundary terms. In order to form a correct boundary integral formulation, the internal point x is moved toward the boundary. Mathematically, the Boundary Integral equation (3.50) is found, in the limit, by decreasing the radius of an extra disc of material to zero i.e., $\varepsilon \to 0$ as depicted by figure 4.4.

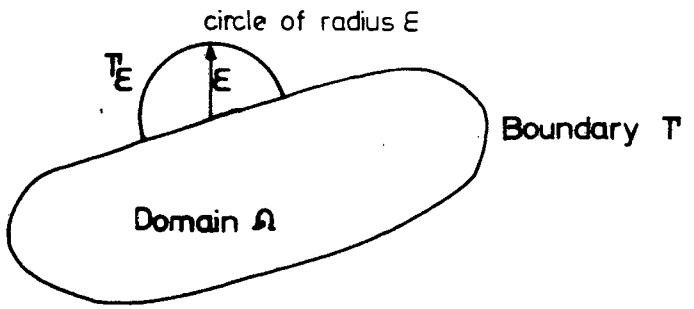

Figure 4.4 The formulation of the Boundary Coefficient

The mathematical requirement for the solution shown is the calculation of the integral

$$I = \lim_{\varepsilon \to 0} \int_{\Gamma_\varepsilon} T_{ij}(x,y)\, u_j \, d\Gamma_\varepsilon \qquad (4.14)$$

By carrying out the integration and summation to the coefficient of the u_j term (details in Appendix A) it will be found that the matrix c_{ij} for two dimensional elastostatics is in fact:

$$c_{ij} = \left[\begin{array}{c|c} 1 - \left(\frac{(\beta-\gamma)}{2\pi} + \frac{(\sin 2\beta - \sin 2\gamma)}{8\pi(1-\nu)}\right) & \frac{(\cos 2\beta - \cos 2\gamma)}{8\pi(1-\nu)} \\ \hline \frac{(\cos 2\beta - \cos 2\gamma)}{8\pi(1-\nu)} & 1 - \left(\frac{(\beta-\gamma)}{2\pi} + \frac{(\sin 2\beta - \sin 2\gamma)}{8\pi(1-\nu)}\right) \end{array}\right] \qquad (4.15)$$

where $(\beta-\gamma)$ is the external angle, in radians, between two adjacent segments and ν is Poisson's Ratio.

As a special case, a smooth boundary where $\beta-\gamma=\pi$ (i.e. $\beta-\gamma=180°$) gives the solution:

$$c_{ij} = \begin{bmatrix} \frac{1}{2} & 0 \\ 0 & \frac{1}{2} \end{bmatrix}$$

as stated previously.

4.3.2.2 Numerical calculation of c_{ij}

The second method available to calculate c_{ij} is numerically to consider the rigid body motion of the continuum in the absence of loading [4.4].

The matrix equation (4.5) relates the boundary displacements and

tractions through the square matrices C, H and G. If we now set the traction boundary condition and the body force term to zero, then this equation can be written

$$[C]\{u\} + [\bar{H}]\{u\} = \{0\}$$

or $$[C]\{u\} = -[\bar{H}]\{u\} \tag{4.16}$$

By now allowing the rigid body motion $u_i = 1.0$ for $i = 1$ or 2 the coefficients in the tridiagnal matrix c can be found for each row by:

$$c_{ij} = -\sum_{j=1}^{n} H_{ij} \quad \text{for } i = 1 \text{ or } 2 \tag{4.17}$$

The method works extremely well in all situations whether the boundary is smooth or not, since the orientation and geometery of the relevant segments are contained within the integral coefficients H_{ij}. For numerical examples, it can also be established that for the smooth boundary, c_{ij} is indeed equal to $\frac{1}{2}\delta_{ij}$.

Either method can be successfully used in the design of a computer program. However, since the numerical method is simply a summation of already calculated values, this method is preferred for programming and appears to give satisfactory results in all present analyses.

4.4 Boundary Segments

We now return to the details of the numerical formulation by considering the various types of interpolation available over a segment, as shown in figure 4.2 (see also [4.5], [4.6], [4.7]). It is assumed that the boundary displacements and tractions, u_i and t_i respectively, vary in terms of the predetermined shape function as defined by equation (4.1). For this purpose, constant, linear and quadratic interpolation orders will be discussed here, although it is possible, by using the same techniques to generate higher order interpolation formulae if necessary.

4.4.1 Constant Segments (Q = 1)

The constant segment is defined as a straight line with a single

central node and a single outward normal, as shown in figure 4.5.

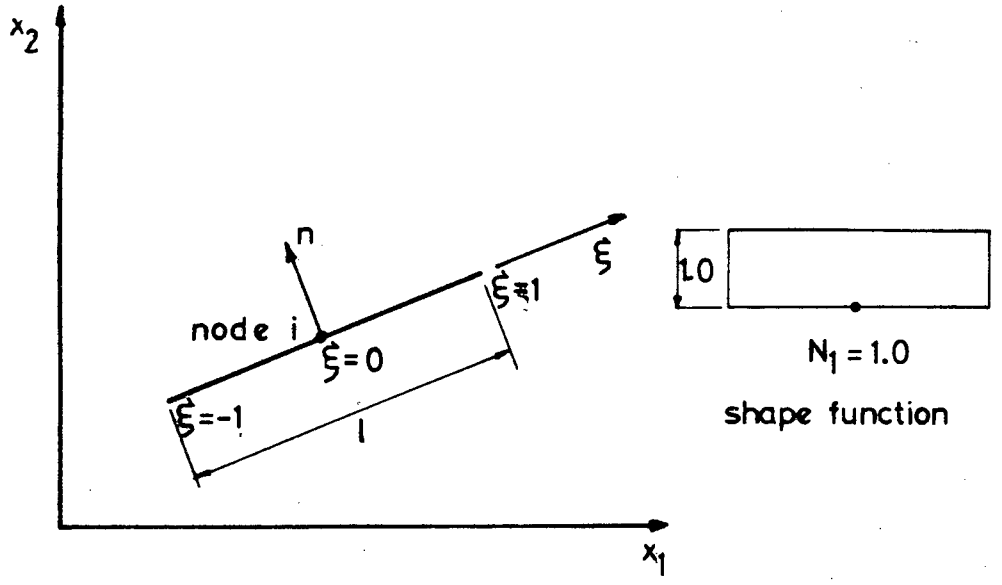

Figure 4.5 Definition of natural co-ordinate system and the constant shape function for 'constant' interpolation

The shape function N_1 is assumed to be constant across the segment and equal to unity. Hence, the displacement and traction, defined by substitution of N into (4.1) with q = 1, are uniquely and clearly specified.

The geometry of the segment is defined by the co-ordinates of the central node, the length and the direction of the outward normal to the segment.

4.4.2 Linear Segments (Q = 2)

The linear segment is defined geometrically by a straight line joining two end nodes. A single, unique normal is common to all points on the segment. It is assumed that the variables can vary linearly between nodes. The interpolation can then be defined by the shape functions:

$$N_1 = \frac{1}{2}(1-\xi)$$

$$N_2 = \frac{1}{2}(1+\xi) \qquad (4.18)$$

ξ is the natural co-ordinate as shown in figure 4.6.

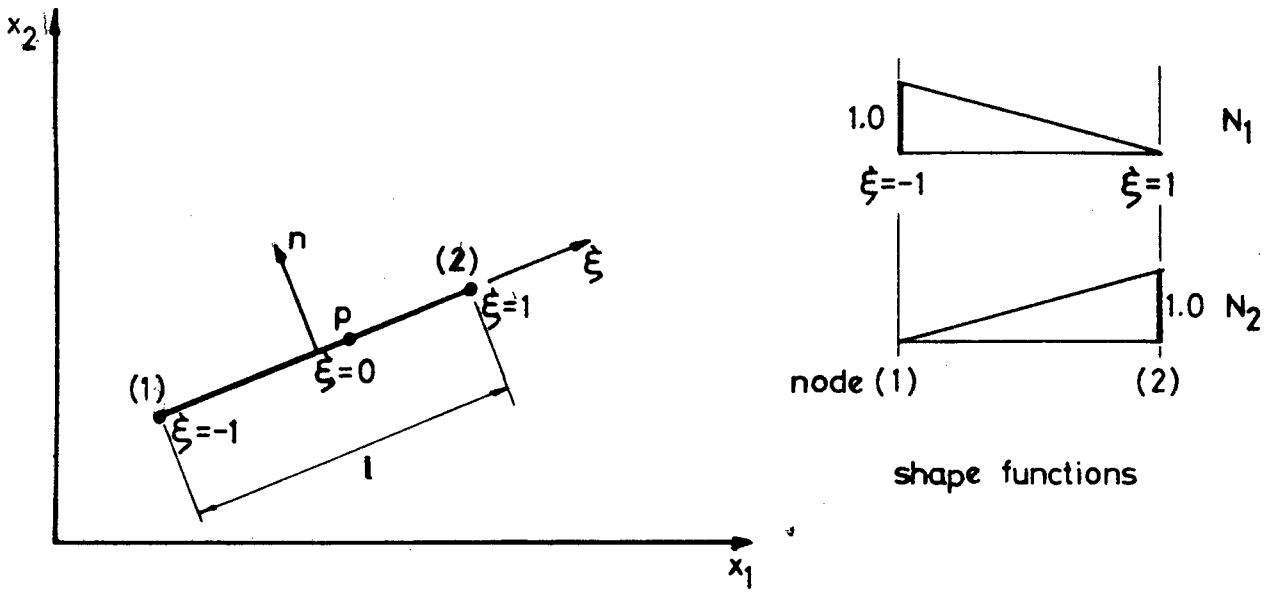

Figure 4.6 Definition of natural co-ordinate system and shape function for 'linear' interpolation

The definition of the shape functions can now also be used to describe the geometry of the segment in addition to the variation of the displacement and traction. The cartesian co-ordinates, either x_1 or x_2 (denoted by z), of a general point and within the segment are given by:

$$z(p) = \frac{1}{2}\ [\ (1-\xi(p))\, z(1) + (1+\xi(p))\ z(2)\ ] \qquad (4.19)$$

$\xi(p)$ is the value of ξ at point p and z(1) and z(2) are the co-ordinates of nodes 1 and 2 respectively. The displacements and tractions at any point within the segment is similarily given by this equation in terms of the values at the segment ends by substituting either u or t for z.

All variables are therefore uniquely defined over the segment.

4.4.3 Quadratic Segments (Q = 3)

The quadratic segment differs from the predeeding segments discussed in section 4.4.1 and 4.4.2 in that its interpolation formulations allows the segment to be curved. This means that the outward normal varies continuously over the segment, thus allowing the idealized boundary to follow the actual boundary more closely. In order to allow for this curvature, the segment is defined by the natural co-ordinates, ξ, and by the positions of 3 nodes - 2 end nodes and a central node - as shown in figure 4.7.

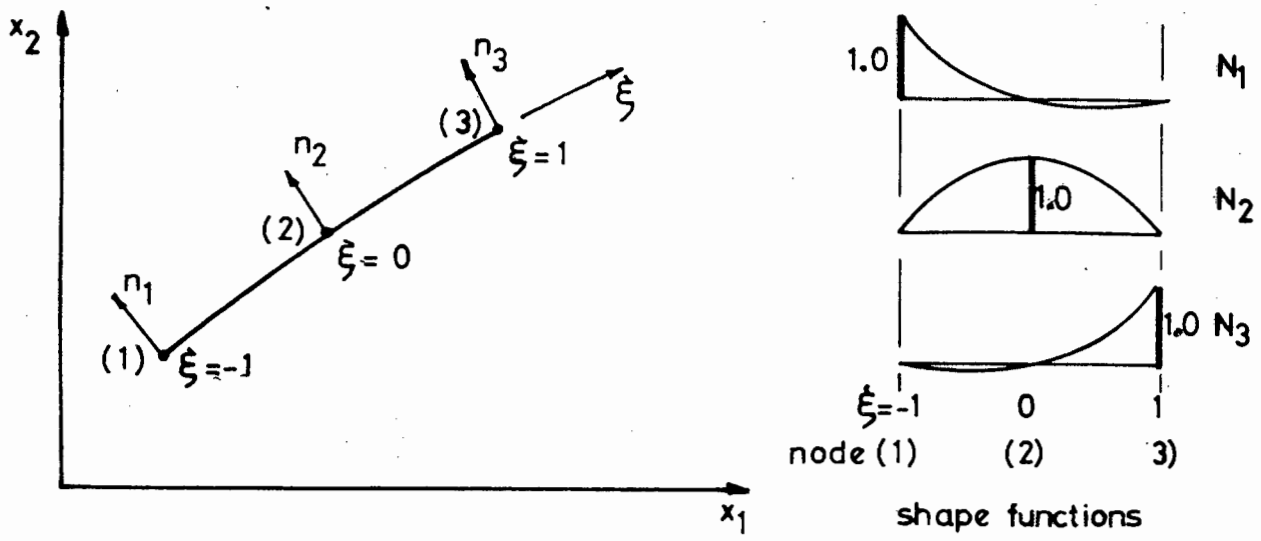

Figure 4.7 Definition of natural co-ordinate system and shape functions for 'quadratic' interpolation

The quadratic shape function N_q for the 3 nodes (q = 1, 3) are given by:

$$N_1 = \frac{1}{2}\,\xi(\xi-1)$$

$$N_2 = (1-\xi)(1+\xi)$$

$$N_3 = \frac{1}{2}\,\xi(\xi+1) \qquad (4.20)$$

The geometry (x_1, x_2 co-ordinates), the displacements (u), the tractions (t) and also the segment outward normal (n) can now be described by these shape functions in terms of the nodal values. Equation (4.1) describes this variation, where v is the relevant variable.

Since the geometry and the field variables are both described by the same interpolation functions, this formulation can be considered to be truly isoparametric.

4.4.4 Summary

The various segments have been defined in terms of their shape functions. It now remains for the relevant functions to be substituted into the numerical boundary equation (4.5), and for the Jacobian to be calculated from equation (4.9) before the numerical integration over the boundary can be completed.

For constant and linear segments, it will be seen that the Jacobian is constant and equal to half the length of the segment ($J = {}^{L}/_{2}$). For the quadratic segments, the Jacobian is calculated from equation (4.9) but simplifies directly to ${}^{L}/_{2}$ if the segment is straight.

Integration over segments in which the pivot node does not appear (i.e.: $x \notin \Gamma_k$) can thus be concluded. However, integration over segments which include the pivot node (i.e. $x \in \Gamma_k$) must still be discussed. This is the topic of section 4.5.

4.5 Pivot Segments

The fundamental solutions of displacement and traction exhibit singularities of the form $\ln\frac{1}{r}$ and $\frac{1}{r}$ respectively. As r tends to zero, as is the case when the pivot point is one of the nodes on the focus segment ($x \in \Gamma_k$), then these functions tend to infinity. The BIEM requires that these functions must now be integrated over this interval (as $r \to 0$)

and consequently a means must be found whereby this can be efficiently and accurately accomplished.

Since the integration over the boundary where $x \notin \Gamma_\varepsilon$ is being carried out numerically by using Gaussian Quadrature, it seems obvious to attempt the present integration by similar means. However, the presence of the singularity requires that a weighted Gaussian Quadrature formula be used. The accuracy of the integration is very important due to the proximity of the segment to the pivot node, therefore it was decided to integrate these functions analytically, thus avoiding any unnecessary errors that could occur in a numerical process.

The process in therefore simplified to one of direct integration over the segment. The region of integration is taken from a point an infinite distance from the pivot node (denoted ε) to the end of the segment (denoted R). The final value is obtained, in the limit as ε tends to zero.

This integration can, of course, be carried out for the three types of segments described in section 4.4; namely, constant, linear and quadratic interpolation. The method used for the integration will be shown here, with the detailed results being given in Appendix B and C.

4.5.1 Constant Segments (Q = 1)

The integration over the pivot segment for constant interpolation takes the form, for the fundamental displacement solution:

$$G_{ij} = \int_{\Gamma_k} U_{ij}(x,y)\, d\Gamma_k \tag{4.21}$$

and for the fundamental traction solution

$$H_{ij} = \int_{\Gamma_k} T_{ij}(x,y)\, d\Gamma_k \tag{4.22}$$

The integration, equation (4.22), is necessary since the 2x2 matrix H_{ij} can be found by rigid body considerations, as was discussed

in section 4.3.2. Therefore, only equation (4.21) need be evaluated. For this purpose, we define the segment geometry as in figure 4.8.

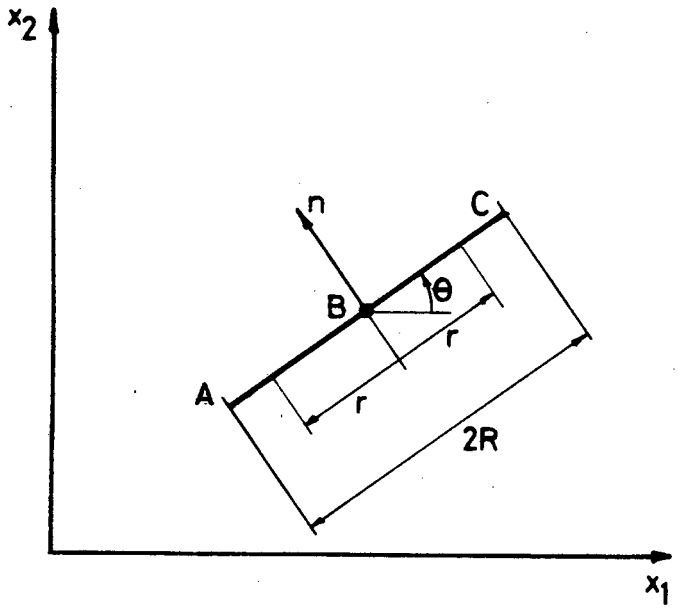

Figure 4.8 The geometry of a constant segment

Now, when the directions of r are taken into account then

$$G_{ij} = \int_A^C U_{ij}(x,y)\, d\Gamma = \int_B^A U_{ij}(x,y)\, d\Gamma + \int_B^C U_{ij}(x,y)\, d\Gamma$$

$$= 2\int_0^R U_{ij}(x,y)\, dr \qquad (4.23)$$

Since r cannot be zero, substitute $r = \varepsilon$ in the limit, hence

$$G_{ij} = \lim_{\varepsilon \to 0} 2\int_\varepsilon^R U_{ij}(x,y)\, dr \qquad (4.24)$$

Substituting the fundamental solution for U_{ij} results in

$$G_{ij} = \lim_{\varepsilon \to 0} \left[2 \int_{\varepsilon}^{R} (3-4\nu) \ln\frac{1}{r} \delta_{ij} + \frac{\partial r}{\partial x_i} \frac{\partial r}{\partial x_j} dr \right] \frac{1}{8\pi G(1-\nu)} \qquad (4.25)$$

Now, considering i = j = 1

$$G_{11} = \lim_{\varepsilon \to 0} \left[2 \left\{ \int_{\varepsilon}^{R} (3-4\nu) \ln\frac{1}{r} dr + \int_{\varepsilon}^{R} \left(\frac{\partial r}{\partial x_1}\right)^2 dr \right\} \right] \frac{1}{8\pi G(1-\nu)}$$

The term $\frac{\partial r}{\partial x_1} = \cos\theta$ by geometric definition, therefore

$$G_{11} = \lim_{\varepsilon \to 0} \left[2 \left\{ \int_{\varepsilon}^{R} (3-4\nu) \ln\frac{1}{r} dr + \int_{\varepsilon}^{R} \cos^2\theta \, dr \right\} \right] \frac{1}{8\pi G(1-\nu)}$$

$$= \lim_{\varepsilon \to 0} \left[2 \left\{ (3-4\nu) \left(r \ln\frac{1}{r} \Big|_{\varepsilon}^{R} + r \Big|_{\varepsilon}^{R} \right) + R\cos^2\theta \right\} \right] \frac{1}{8\pi G(1-\nu)}$$

In the limit

$$G_{11} = \frac{R}{4\pi G(1-\nu)} \{(3-4\nu) \ln\frac{1}{R} + \cos^2\theta\} \qquad (4.26)$$

Similarily, for i = j = 2

$$G_{22} = \frac{R}{4\pi G(1-\nu)} \{(3-4\nu) \ln\frac{1}{R} + \sin^2\theta\} \qquad (4.27)$$

and for i = 1 or 2, j = 2 or 1

$$G_{12} = G_{21} = \frac{R}{4\pi G(1-\nu)} \{\sin\theta \cos\theta\} \qquad (4.28)$$

Therefore, the 2x2 matrix G_{ij} for a pivot segment using constant interpolation has been defined.

4.5.2 Linear Segments (Q = 2)

Where the interpolation is of a linear form, then the integration over the pivot segment from either of the node points which define

the segment, is given by

(i) The displacement fundamental solution:

$$G_{ij}^{pq} = \int_{\Gamma_k} U_{ij}(x,y) N_q \, d\Gamma_k \tag{4.29}$$

(ii) The traction fundamental solution:

$$H_{ij}^{pq} = \int_{\Gamma_k} T_{ij}(x,y) N_q \, d\Gamma_k \tag{4.30}$$

where i,j are the co-ordinate directions

p is the pivot node (either 1 or 2)

q is the interpolation node (either 1 or 2) and

N_q is linear shape function for node q

The integration to find the coefficients G_{ij} is carried out in a similar fashion to that detailed in equations (4.23) to (4.28) with the addition of the shape functions which can also be written in terms of r. The resulting expressions are of the same form as in equations (4.26), (4.27) and (4.28), but now, two sets of coefficients result since the pivot node p can be at either end of the segment. The full details of these expressions are given in Appendix B where, in addition, it is seen that if the fundamental solution is defined in terms of the Galerkin Tensor, then an extra constant is added to the G_{ij} terms.

Let us now consider the details of the integral in equation (4.30). For the nodes where p = q, that is, the pivot node and the interpolation node are the same, then H_{ij} can again be found from considering the rigid body motion of the structure as was done in section 4.3.2. These can be called the "diagonal" terms of the H matrix.

However, where $p \neq q$, that is, the pivot node and the interpolation node are not the same, then the "off-diagonal" terms of the H - matrix are required. To detail these terms, consider the two possibilities.

(i) The pivot node at node 1 of the segment i.e. p = 1

(ii) The pivot node at node 2 of the segment i.e. p = 2

These two possibilities can be summarised by the statement

$$H_{ij}^{pq} = \int_{\Gamma_k} T_{ij}(x,y) N_q \, d\Gamma_k \tag{4.31}$$

for p = 1 and 2

q = 1 and 2

Let us, firstly consider the case where p = 1, q = 2 and define the geometry as in figure 4.9.

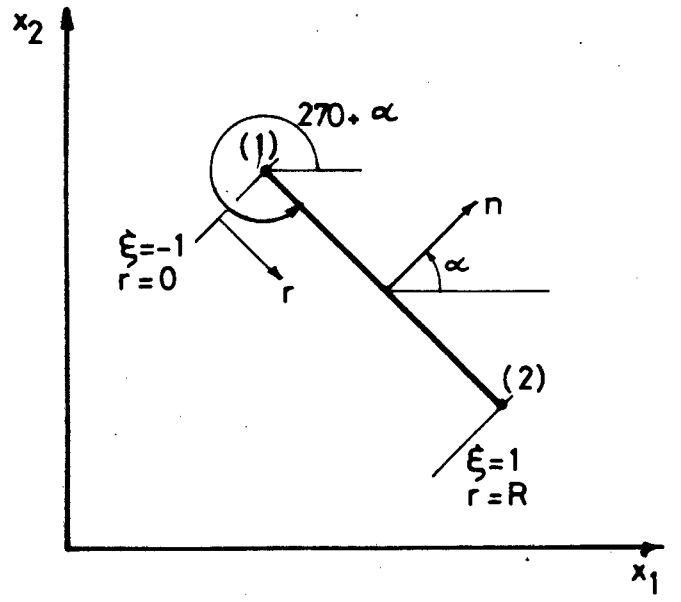

Figure 4.9 The geometry of a linear segment for p = 1

From linear interpolation of the geometry, it can be seen that the local co-ordinates ξ can be written in terms of r by

$$\xi = \frac{2r}{R} - 1 \tag{4.32a}$$

while $\frac{\partial r}{\partial x_1} = \sin \alpha$

and $\frac{\partial r}{\partial x_2} = - \cos \alpha$ (4.32b)

Considering the form of the expression

$$H_{ij}^{pq} = \int_{\Gamma_k} \{- \frac{1}{4\pi(1-\nu)r} \left[\frac{\partial r}{\partial n} \{(1-2\nu)\delta_{ij} + 2\frac{\partial r}{\partial x_i} \frac{\partial r}{\partial x_j}\} - (1-2\nu)(\frac{\partial r}{\partial x_i} n_j - \frac{\partial r}{\partial x_j} n_i) \right] \} N_q \, d\Gamma_k \tag{4.33}$$

it can be seen that the first term in the [] vanishes since $\frac{\partial r}{\partial n} = 0$ due to the n and r vectors being perpendicular. Also, when i = j, the second term vanishes, leaving the expression

$$H_{ij}^{pq} = \int_0^R - \frac{1}{4\pi(1-\nu)r} \{- (1-2\nu)(\frac{\partial r}{\partial x_i} n_j - \frac{\partial r}{\partial x_j} n_i)\} N_q \, dr \tag{4.34}$$

for p,q = 1 and 2 but $p \neq q$

and i,j = 1 and 2 but $i \neq j$

Hence, the expression for p = 1, q = 2, i = 1, j = 2, can be written

$$H_{12}^{12} = \int_0^R - \frac{1}{4\pi(1-\nu)r} [- (1-2\nu)(\sin \alpha \sin \alpha - (- \cos \alpha) \cos \alpha)] \cdot \frac{1}{2} (1 + \frac{2r}{R} - 1) \, dr$$

once the shape function and equations (4.32a) and (4.32b) have been substituted.

Performing the integration, while remembering that r cannot be zero, and hence a limit condition must be introduced, results in

$$H_{12}^{12} = \frac{(1-2\nu)}{4\pi(1-\nu)} \tag{4.35}$$

which is a constant.

Similarily for the case p = 1, q = 2, i = 2, j = 2 the expression

$$H_{21}^{12} = -\frac{(1-2\nu)}{4\pi(1-\nu)} \tag{4.36}$$

can be found.

To complete the expression for a segment, consider the application of the above analysis to the case where the pivot node is at node 2 of the segment, i.e., p = 2 and q = 1.

The geometry is now defined as in figure 4.10.

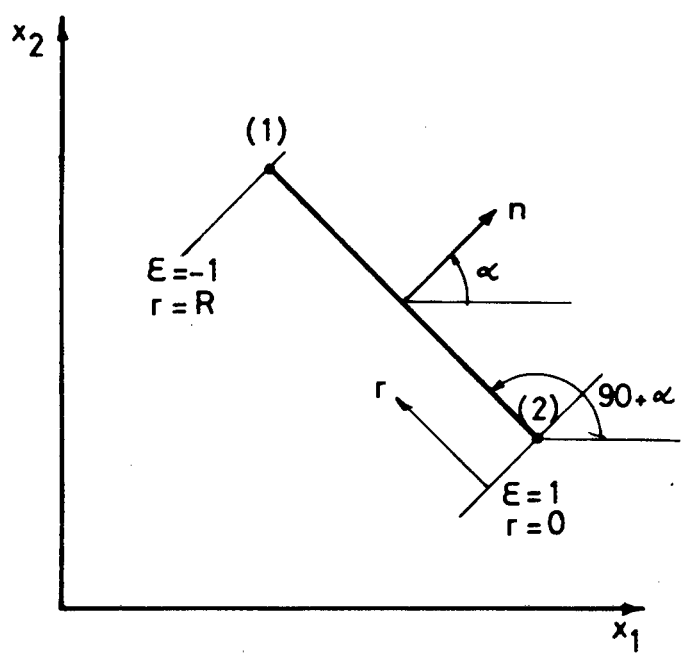

Figure 4.10 The geometry of a linear segment for p = 2

Now, the co-ordinates can be written in terms of r by

$$\xi = 1 - \frac{2r}{R} \tag{4.37a}$$

and

$$\frac{\partial r}{\partial x_1} = - \sin \alpha$$

$$\frac{\partial r}{\partial x_2} = \cos \alpha \tag{4.37b}$$

Again $\frac{\partial r}{\partial n} = 0$ and the second term vanishes when i = j, hence the expressions can be written

$$H_{ij}^{21} = \int_0^R - \frac{1}{4\pi(1-\nu)r} \left[- (1-2\nu) \left(\frac{\partial r}{\partial x_i} n_j - \frac{\partial r}{\partial x_j} n_i \right) \right] \frac{1}{2}(1-\xi)\, dr \tag{4.38}$$

After substitution of equations (4.37a) and (4.37b) the integration can be completed. For i = 1, j = 2

$$H_{12}^{21} = - \frac{(1-2\nu)}{4\pi(1-\nu)} \tag{4.39}$$

and for i = 2, j = 1

$$H_{21}^{21} = \frac{(1-2\nu)}{4\pi(1-\nu)} \tag{4.40}$$

The combination of equations (4.35), (4.36), (4.39) and (4.40) in matrix form, is as follows. Consider two linear segments (m-1) and m, joined at their common node n as in figure 4.10a. Let n be the pivot node for segments (m-1) and m. Hence for segment (m-1) at node (n-1), the H-matrix is

$$H_{ij}^{n,\, n-1} = \begin{bmatrix} 0.0 & -\omega \\ \omega & 0.0 \end{bmatrix} \tag{4.41}$$

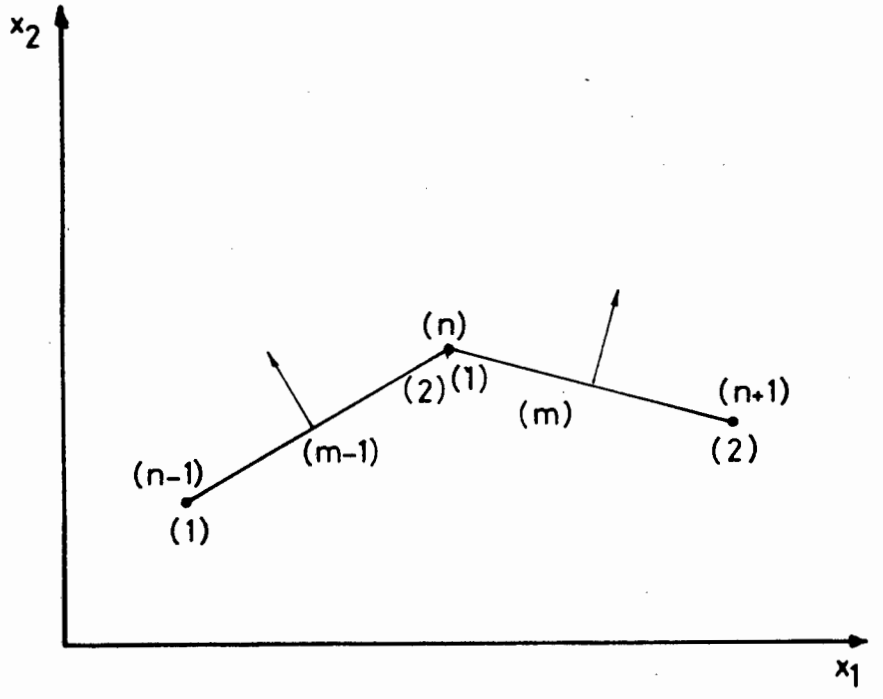

Figure 4.10a The geometry of 2 linear segments joined at a common node

where $\omega = \frac{(1-2\nu)}{4\pi(1-\nu)}$, from equations (4.39) and (4.40).

Similarily, for segment m at node n + 1, the matrix is

$$H_{ij}^{n,\,n+1} = \begin{bmatrix} 0.0 & \omega \\ -\omega & 0.0 \end{bmatrix} \tag{4.42}$$

If we now construct the equations in the systems matrix corresponding to node n, for segments m-1 and m, the following is evident:

$$[H] = \begin{array}{c} \text{node} = \\ j = \end{array} \begin{array}{ccccc} \overbrace{}^{n-1} & & \overbrace{}^{n} & & \overbrace{}^{n+1} \\ 1 \quad 2 & & 1 \quad 2 & & 1 \quad 2 \end{array}$$

$$\begin{array}{c} \text{node } n \\ \left\{ \right. \end{array} \left[\begin{array}{c|cc|cc|cc|} & & & & & & \\ & & & & & & \\ \hline & 0.0 & -\omega & & 0.0 & \omega & \\ & \omega & 0.0 & c_{ij} & -\omega & 0.0 & \\ \hline & & & & & & \\ & & & & & & \end{array} \right] \begin{array}{l} \left. \right\} 1 \\ \left. \right\} 2 \end{array} = i$$

$$\begin{array}{c} \text{segment} = \\ \end{array} \begin{array}{cc} \overbrace{}^{m-1} & \overbrace{}^{m} \end{array}$$

(4.43)

The c_{ij} submatrix is calculated from rigid body considerations as discussed earlier. Notice also that in equation (4.43) the coefficients for node n are the summation of values obtained from segments (m - 1) and m at the common node. This is true for all interpolation orders, excluding constant interpolation, and will be discussed further in section 4.6. The pivot expressions for linear segments are thus complete and the final numerical matrices can be formulated.

(ii) The pivot node is the second node (2) of the quadratic segment:

Sector A: Analytical integration by equations (4.39) and (4.40).

Sector B: Analytical integration by equations (4.35) and (4.36).

(iii) The pivot node is the third node (3) of the quadratic segment:

Sector A: Numerical integration by Gauss Quadrature.

Sector B: Analytical integration by equations (4.39) and (4.40).

These expressions allow the complete formulation of the quadratic interpolation segment to be accomplished.

4.6 The Internal Points

In the mathematical formulation of the BIEM, the weighting functions were chosen in order to reduce the equations to a form wherein only the boundary values are involved. In so doing, an equation (3.54) was formed which related the displacement at a general point x to these boundary values. It is this equation which is used, once the entire set of boundary values are known, to find the displacement at any internal point.

4.6.1 Internal Displacements

Numerically, the calculation of displacement at the general (now internal) point x is simple. By this stage the boundary value problem has been solved resulting in all the boundary tractions and displacements being known. The displacement $u_i(x)$ can be calculated by numerically integrating the fundamental solutions over the boundary segments and by substitution of the boundary values into equation (3.54). The internal point x is now the pivot node and the boundary segments are the focus segments. It is noted here that no singularities in in the fundamental solutions can arise in this case since the pivot node

will never be one of the boundary nodes, nor will it be situated on the boundary. These eventualities have already been solved by the original boundary integral process and by the positioning of the boundary segments and nodes. This being the case, no analytical integrations are necessary since r(the distance from the pivot node to the focus segment) can never be zero. Consequently, the displacement can simply be calculated by applying the Gaussian Quadrature formula over each segment in turn and by multiplying the result by the relevant boundary value. The accumulation over every segment will give the final value of the displacement at x.

4.6.2 Internal Stresses

The calculation of stress at the internal point x is also performed numerically using the equations (3.65), (3.66) and (3.67) which were generated from equation (3.54) by using the constitutive relationship for elastostatic materials, equation (3.7). A similar method, as is used for the displacement calculations in section 4.6.1, is also used in this case. The tensors D_{ijk} and S_{ijk} are integrated by using the Gauss Quadrature formula over each boundary segment in turn. Together with the boundary values of displacement and traction, the contributions are summed over all segments to produce the stresses σ_{xx}, σ_{yy}, σ_{xy}. The principal stresses σ_{max}, σ_{min} and the angle of σ_{max} to the x axis θ_p are are calculated in the classical manner by:

$$\sigma_{max} = \frac{\sigma_{xx} + \sigma_{yy}}{2} + \sqrt{\left(\frac{\sigma_{xx} - \sigma_{yy}}{2}\right)^2 + \sigma_{xy}^2} \qquad (4.44)$$

$$\sigma_{min} = \frac{\sigma_{xx} + \sigma_{yy}}{2} - \sqrt{\left(\frac{\sigma_{xx} - \sigma_{yy}}{2}\right)^2 + \sigma_{xy}^2} \qquad (4.45)$$

$$\theta_p = \frac{1}{2} \tan^{-1}\left(\frac{2\,\sigma_{xy}}{\sigma_{xx} - \sigma_{yy}}\right) \qquad (4.46)$$

4.6.3 Displacements and Stresses at Internal points close to the Boundary [4.7]

When the internal point x is within one segment length of the boundary, then the calculation of displacement and stresses by the methods detailed in section 4.6.1 and 4.6.2, become unreliable. This is caused by two facts. Firstly, the proximity of the internal point to the boundary (r) allows the sigularity of the fundamental solutions over the nearest segments, to become dominant. Secondly, the angle made by the vector r between the x_1 and x_2 axes varies considerably over the segment. The terms $\frac{\partial r}{\partial x_1}$, $\frac{\partial r}{\partial x_2}$ and $\frac{\partial r}{\partial n}$ in this case cannot be adequately represented over the segment by considering only a few Gauss points, as is used in the quadrature formulae. These two facts cause the resulting calculations to become increasingly erroneous with a decrease in the dimension r. Figure 4.12 shows, diagrammatically, the source of possible errors.

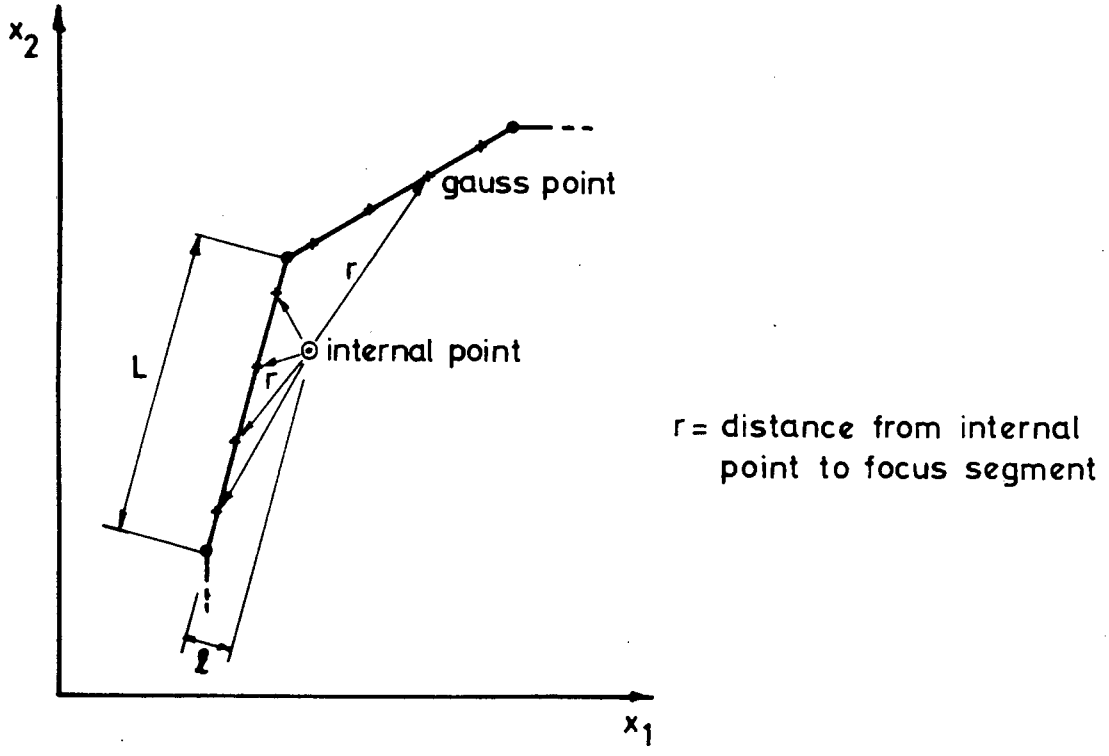

Figure 4.12 An internal point close to the boundary segments

A simple numerical technique is used to overcome these problems. The perpendicular distance from the internal point to the boundary segment is denoted by ℓ with the segment length as L. In programming, a check is performed on the value of the ratio $\ell/_L$. If the ratio is greater than one (1.0) then the internal point is assumed to be sufficiently far from the segment not to cause a spurious result in the calculation of displacement and stress. However, if the ratio is less than one, then the segment is divided into a number of subsegments, each of length less than ℓ, as shown in figure 4.13.

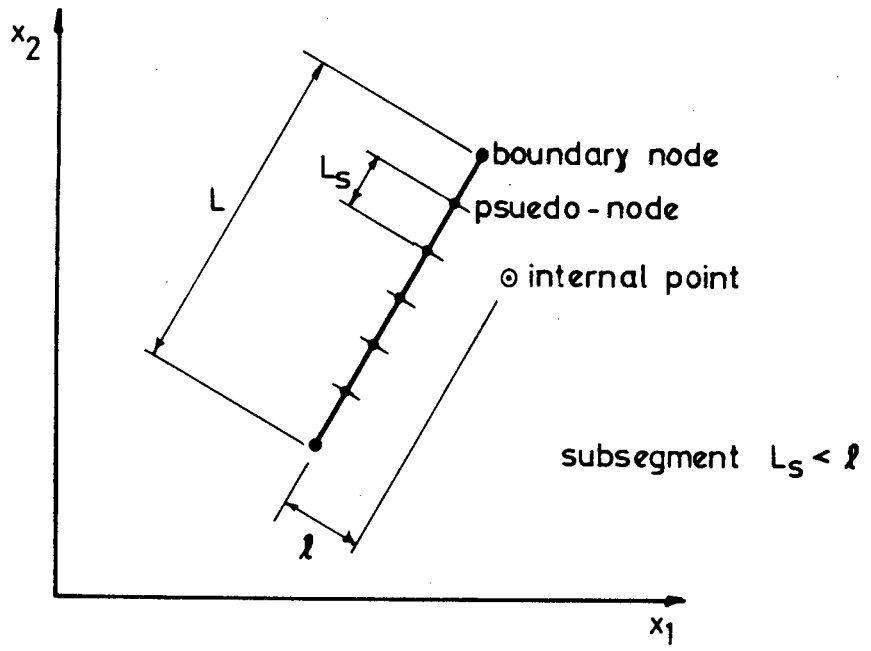

Figure 4.13 A boundary segment divided into subsegments

The displacements and tractions at the pseudo-nodes of the subsegments are interpolated from the actual boundary nodes by using the parent segment's shape functions and nodal values. Integration then takes place over each subsegment in turn, as was detailed earlier. The calculations concerning the internal point x are completed in this way.

By using this scheme, an internal point can be very close to the boundary segment. The minimum approach distance is then simply a

function of the number of subsegments used. This is a convenient method and is simply programmed. The results are accurate (see example 4.8.2) but the overheads in computer costs are considerable if the calculations are to be done for a large number of internal points, all close to the boundary. However, for most applications, this method is simple, efficient and effective.

4.7 The Combination of Details

The details which have been discussed in the preceeding sections of this chapter, can be summaried by a macro-flow chart, which contains the essential ingredients of the numerical Boundary Integral Equation Method.

4.7.1 The Macro-flow chart

The strategy which has been used to design a workable BIEM program is shown in figure 4.14. The method is categorized into a number of separate phases, each of which is subdivided into its most important aspects. The parts where details are given elsewhere in this chapter are marked with the relevant section number in the appropriate block for quick reference.

The data required to specify the geometry is:
- the total number of boundary nodes,
- the total number of boundary segments,
- the co-ordinates of the nodes,
- the directions of the normals to the segments,
- the calculation of segment lengths,
- the number of internal points,
- the co-ordinates of the internal points.

The data required under the heading "Systems Parameters" is:
- the interpolation type, either constant, linear or quadratic,
- the Gauss Quadrature order,
- the parameters to request the plotting and printing options.

The material properties required are:
- Young's Modulus; Poisson's Ratio
- the density and the gravity constants.

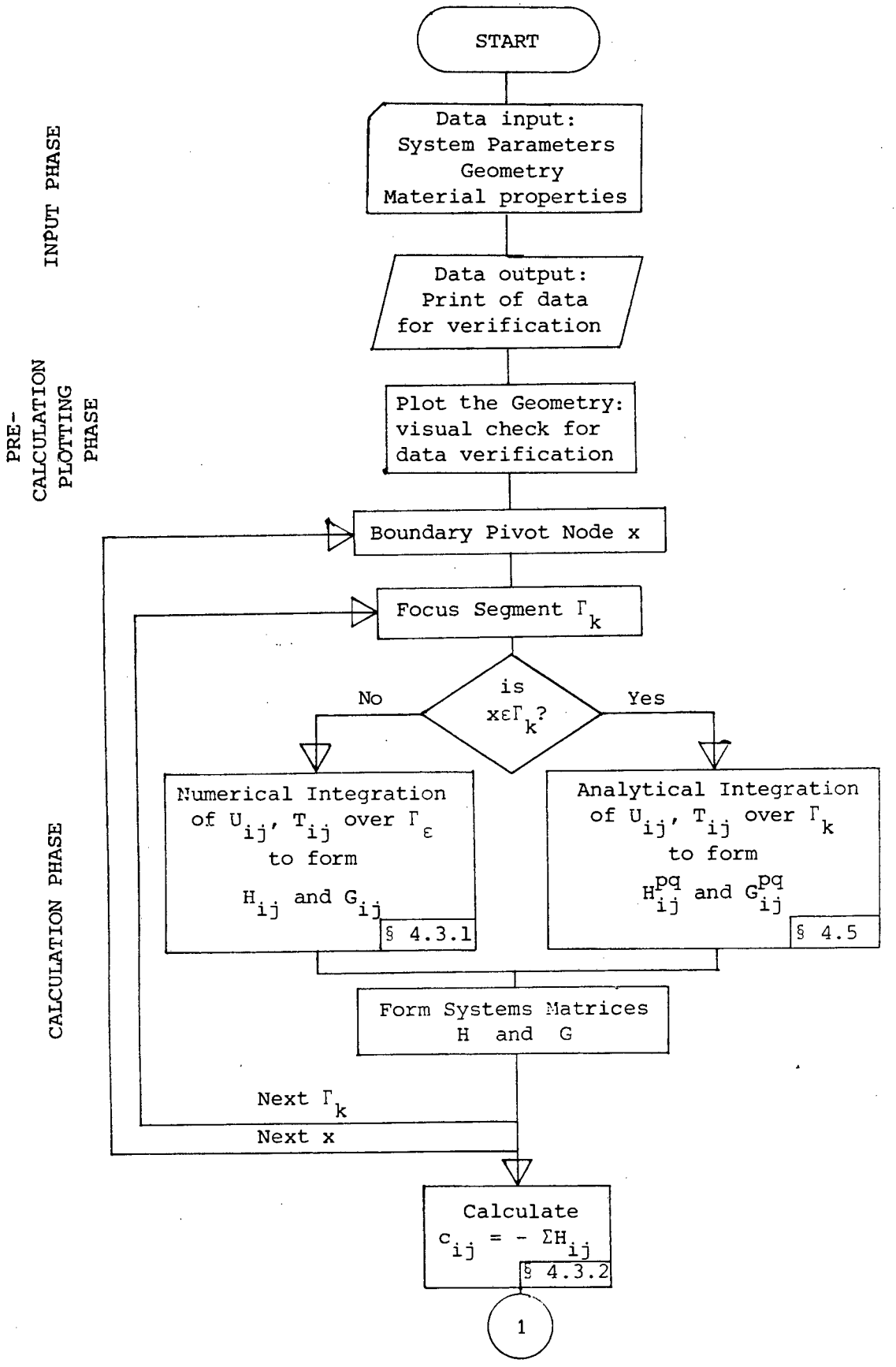
INPUT PHASE
PRE-CALCULATION PLOTTING PHASE
CALCULATION PHASE
START
Data input: System Parameters Geometry Material properties
Data output: Print of data for verification
Plot the Geometry: visual check for data verification
Boundary Pivot Node x
Focus Segment Γ_k
is $x \varepsilon \Gamma_k$?
No
Yes
Numerical Integration of U_{ij}, T_{ij} over Γ_ε to form H_{ij} and G_{ij}
§ 4.3.1
Analytical Integration of U_{ij}, T_{ij} over Γ_k to form H^{pq}_{ij} and G^{pq}_{ij}
§ 4.5
Form Systems Matrices H and G
Next Γ_k
Next x
Calculate $c_{ij} = - \Sigma H_{ij}$
§ 4.3.2
1

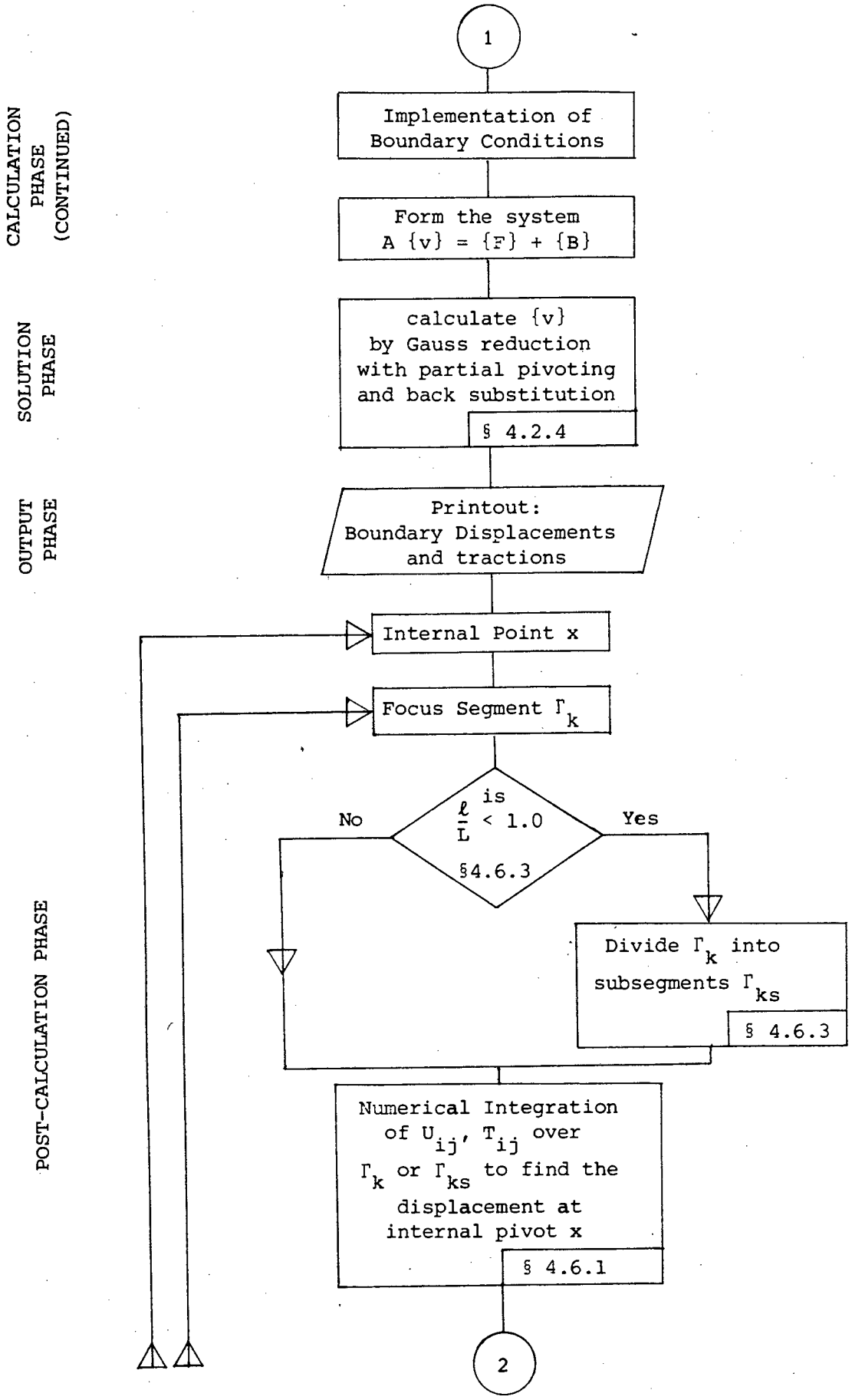
CALCULATION PHASE (CONTINUED)
SOLUTION PHASE
OUTPUT PHASE
POST-CALCULATION PHASE
1
Implementation of Boundary Conditions
Form the system A {v} = {F} + {B}
calculate {v} by Gauss reduction with partial pivoting and back substitution
§ 4.2.4
Printout: Boundary Displacements and tractions
Internal Point x
Focus Segment Γk
ℓ/L is < 1.0
§4.6.3
No
Yes
Divide Γk into subsegments Γks
§ 4.6.3
Numerical Integration of Uij, Tij over Γk or Γks to find the displacement at internal pivot x
§ 4.6.1
2

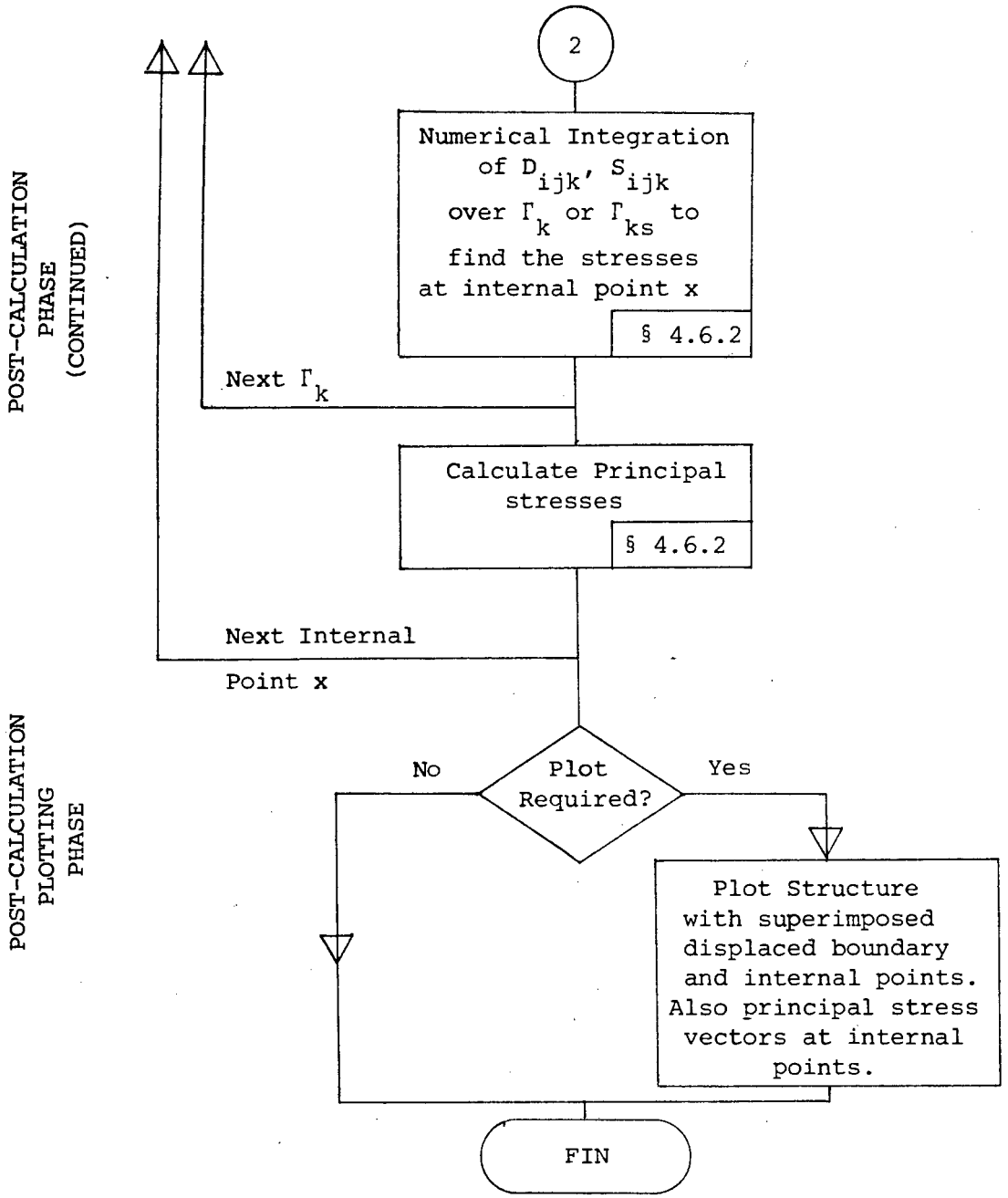

Figure 4.14 Macro Flow Chart of The BIEM Program

4.7.2 The Program Organization

As is evident from a study of the flow chart Figure 4.14, the BIEM is essentially a modular process and, as such lends itself to a modular form of computer programming. Each major section is self contained which allows the programming to be flexible for easy implementation of future developments and additions.

In addition, this modularity concept has also been incorporated within the data input phase. A data module would typically consist of a keyword followed by a set of numerical data. A number of keywords are available in each module, and each module is concluded by a terminator keyword. Typical modules are for the geometrical construction of the model, where the emphasis is put on the automatic generation of boundary data; the definition of material properties; the specification of displacement boundary conditions and applied loads; and the positioning of internal points. By arranging the data in this form, a quick and efficient method of input has been accomplished, thus decreasing the possibility of annoying and persistent data errors.

Within the geometry module, two types of automatic generation of boundary segments and nodes are available. A line of varying length segments can be generated by specifying the co-ordinates of the end nodes, the number of segments required, and the ratios of the segment lengths required. A circular curve of segments can similarily be generated with minimal data input. In addition, a general curvilinear segment generator could easily be included by employing a quadratic or cubic shape function concept.

The output from the analysis can be presented graphically, if required. The programs have the facility to produce an exaggerated displaced shape superimposed upon the original structures. An additional option available on request is the plot of the principal stress vectors at selected internal points within the domain.

Three separate programs for

(a) Constant segments

(b) linear segments and

(c) quadratic segments

have been written using the details discussed in this chapter. A sample manual for the use of these programs showing their limitations and applicability is given in Appendix G.

4.8 Examples

With the discussion of the elementary theory, numerical method and programming strategies complete, it is obvious that the next step is to put these into practice. This is done by detailing a number of examples which will best show the reliability, advantages, disadvantages and efficiency of the BIEM in the form which has been presented here.

When quoting results, an effort has been made to find accurate benchmark values, in the form of rigorous analytical solutions, where possible. Where these are unavailable for some reason, usually due to the complexity of the problem, then a refined finite element analysis using well known, commercially available package programs, has been used as a benchmark.

The comparisons made during the study of various examples, only a few of which are given here, include the effect of varying the number of boundary segments; the effect of the order of Gaussian quadrature on accuracy; the computer CPU time used for the analysis; and the accuracy of stresses and displacements at internal points.

The relevant data is given in sufficient detail, in the hope that subsequent reseachers, using this thesis, can duplicate the results given.

An important point to note here is that all examples in this section have been analysed by using the approximate traction method to deal with the discontinuous tractions at corner nodes. The details of this strategy are given in chapter 5 section 5.2.5 when this specific problem is outlined.

4.8.1 Example 1 : Thick Walled Pipe subjected to internal pressure (Plane Strain).

The objective of this example is to show: (a) the comparison of results from constant, linear and quadratic segments; (b) the convergence rate with increasing numbers of segments; and (c) the effect of the order of numerical integration on the accuracy of the results.

The model used is shown in figure 4.15. The internal radius, R_i, external radius R_e of the thick-walled pipe, are respectively, 5 and 20 units. (The units are unimportant in this example and hence have been neglected throughout). The loading is supplied by a pressure of 10 units (P_i =10.0), acting radially on the inner surface. Since only one quarter of the actual pipe is analysed, appropriate displacement boundary conditions must be supplied so that an equivalent analysis is performed. This is done by allowing displacements to occur in the x_1 direction along side c and in the x_2 direction along side a only. These conditions are identified by the word 'symmetry' in figure 4.15.

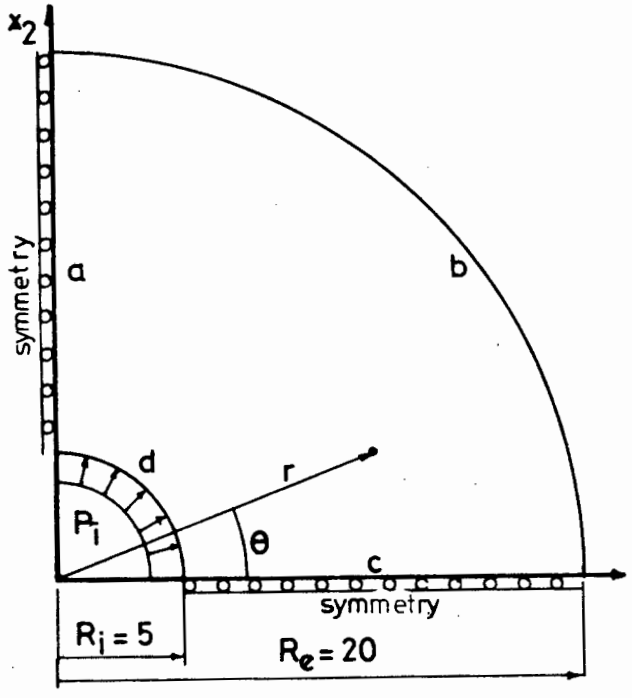

Figure 4.15 Thick walled pipe subjected to internal pressure

The material is homogeneous and gravity loading has been neglected. The material constants are;

Young's Modulus E = 1000.0

Poisson's Ratio ν = 0.3

The details of the segment modelling is given in table 4.2. The analysis was done using constant, linear and quadratic segments and comparisons are made between the models which contain the same number of boundary nodes. Consequently, the number of boundary segments used, depends on the nodes used in each analysis type. For example, a discretization using 56 nodes will have 56 constant or linear segments, but only 28 quadratic segments. On the straight faces of the model, i.e., sides a and c a graduation in segment sizes from the internal to the external radius, is used. The segment length are calculated from the ratio 1:2:3: ..... up to the number of segments used on these sides. This is denoted "4 ratio" in table 4.2. The radial boundaries b and d are divided into equal length segments and are denoted by "equal" in the table.

No. of Boundary Nodes	Constant & Linear Segments		Quadratic Segments	
	Sides a & c	Sides b & d	Sides a & c	Sides b & d
16	4 ratio	4 equal	2 ratio	2 equal
32	8 ratio	8 equal	4 ratio	4 equal
40	10 ratio	10 equal	5 ratio	5 equal
56	14 ratio	14 equal	7 ratio	7 equal
64	16 ratio	16 ratio	8 ratio	8 equal
72	-	-	9 ratio	9 equal

Table 4.2 Structural Modelling of a Thick-Walled Pipe

Figure 4.16 is an example of the subdivision used. The 56 node model, with 56 linear elements is shown.

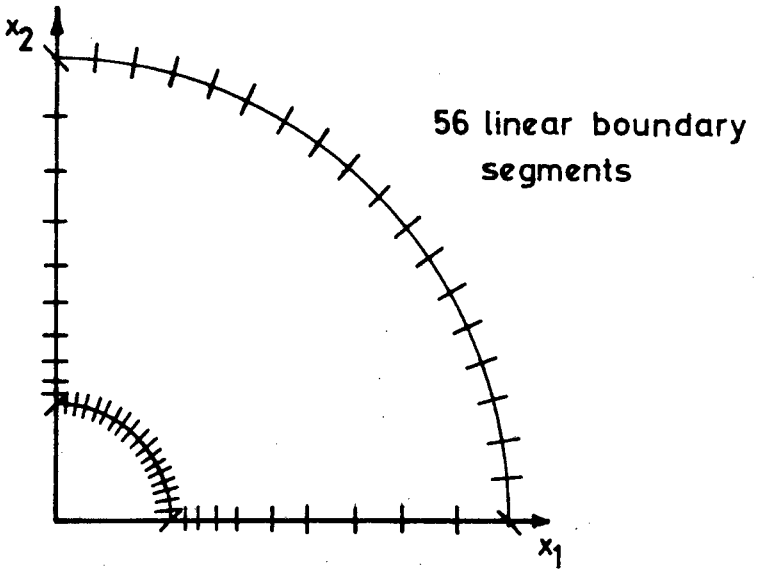

Figure 4.16 Subdivision of model - an example

In addition to the analyses using constant, linear and quadratic segments, each analysis was also performed using three orders of Gaussian Quadrature, namely, 2 point, 4 point and 6 point formulae. An analytical solution of this problem is given in Timoshenko [4.8]. This is a plane strain problem, and the resulting stress field is:

$$\sigma_r = \frac{R_i^2}{R_e^2 - R_i^2} P_i \left[1 - \frac{R_e^2}{r^2} \right] \tag{4.47}$$

$$\sigma_\theta = \frac{R_i^2}{R_e^2 - R_i^2} P_i \left[1 + \frac{R_e^2}{r^2} \right] \tag{4.48}$$

The radial displacement at r is written in terms of the stress field as:

$$u_r = (\sigma_\theta - \nu^\dagger \sigma_r) \frac{r}{E^\dagger} \tag{4.49}$$

where the material properties are:

$$E^{\dagger} = \frac{E}{1 - \nu^2} \quad ; \quad \nu^{\dagger} = \frac{\nu}{1 - \nu}$$

The value of u_r is used as the benchmark.

The results obtained from the analysis are plotted in graphical form in figure 4.17. A comparison is made, first between the three types of boundary interpolation used, and second, between the three orders of Gaussian Quadrature used. The accuracy is plotted as a percentage, using the theoretical value calculated from (4.49) and from

$$\% \text{ error} = \left\{ \frac{u_{\text{calculated}} - u_{\text{theoretical}}}{u_{\text{theoretical}}} \right\} \times 100 \qquad (4.50)$$

Consequently, a positive percentage error indicates an overestimation of the radial displacement.

The comparison of CPU times against the number of segments and the integration order is given by figure 4.18. The CPU times quoted are measured on a UNIVAC 1100/81 and includes the time taken to evaluate the displacements and stresses at 16 internal points.

The radial stress field σ_r obtained from (4.47) is compared to the stress field calculated by the numerical method at 4 internal parts. The results as shown in table 4.3 where the model used was as shown in figure 4.16, using 56 boundary notes and 6 point Gauss Quadrature in each case.

From these analyses, a number of important points have arisen. These can be summarized as follows:

(a) The analyses converge to the theoretical solution with an increase in the number of segments/nodes used.

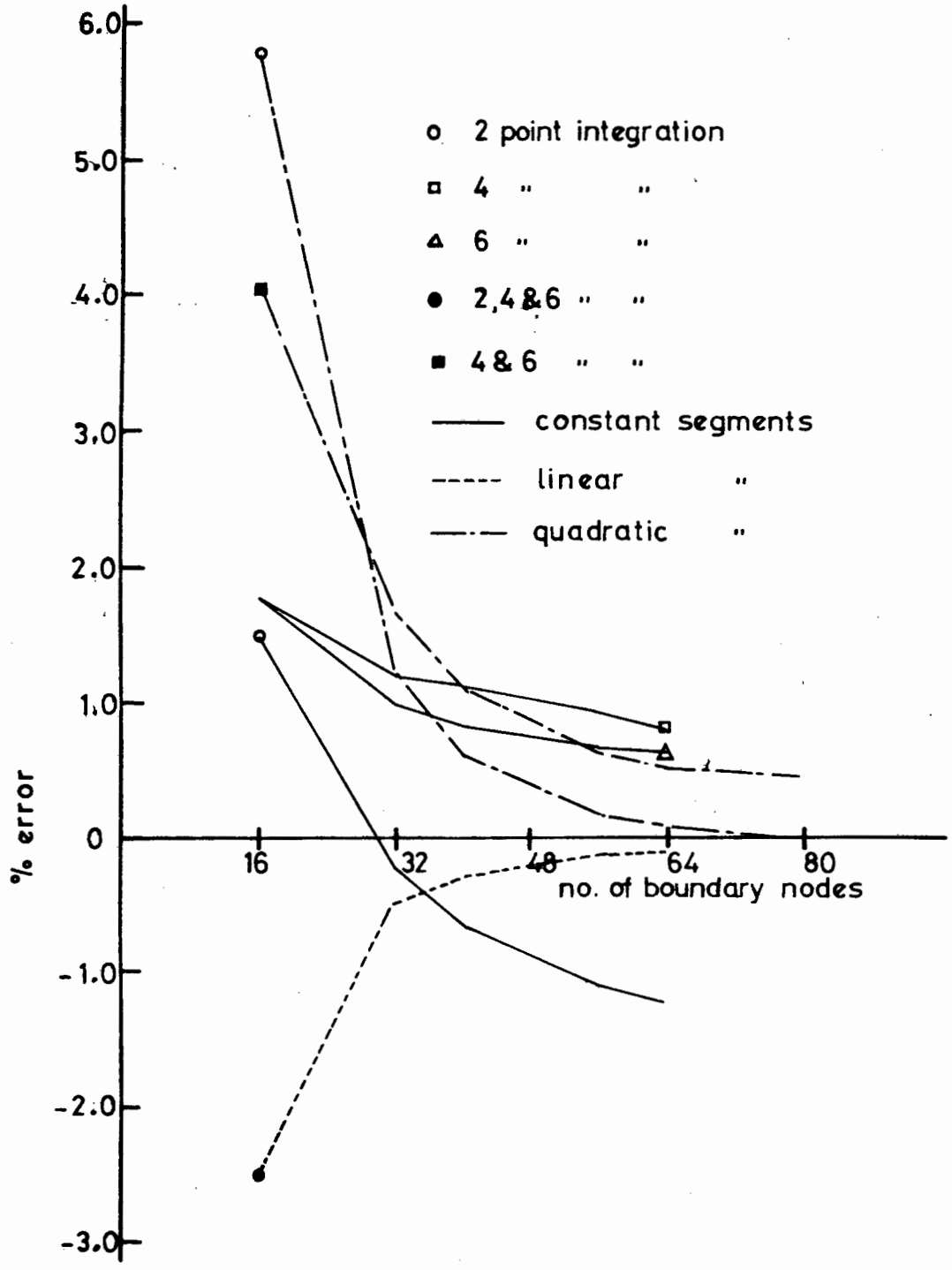

Figure 4.17 Thick Walled pipe subjected to internal pressure - plot of % error versus no. of boundary nodes

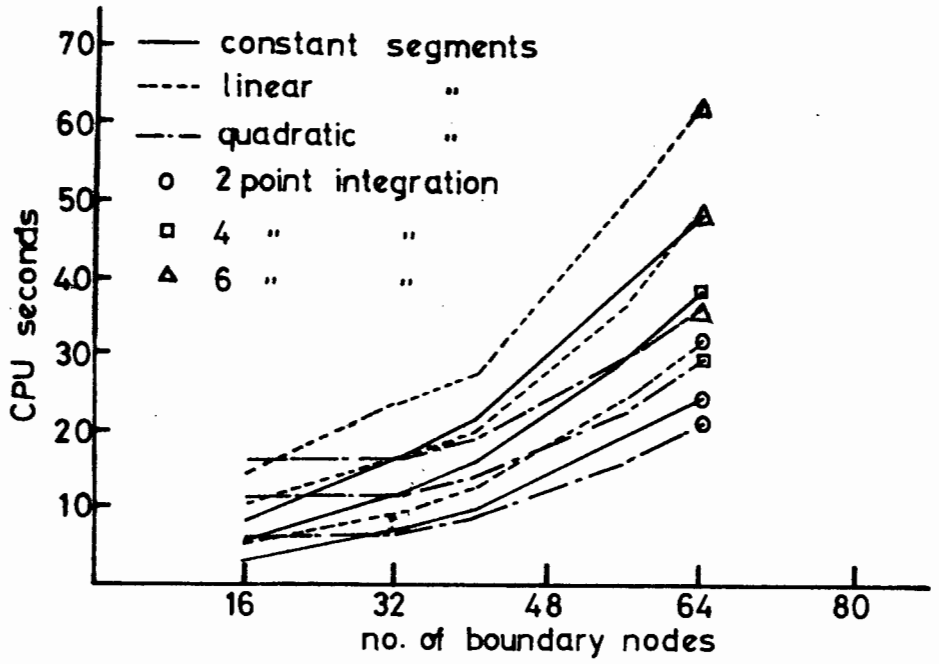

Figure 4.18 Comparison of CPU time vs number of boundary nodes for a thick walled pipe subjected to internal pressure

Position / Interpolation Order	r = 8.0	r = 11.0	r = 13.0	r = 15.0
Theoretical(4.47)	- 3.500	- 1.537	- 0.911	- 0.519
Constant	- 3.5104	- 1.542	- 0.915	- 0.523
Linear	- 3.494	- 1.536	- 0.908	- 0.516
Quadratic	- 3.501	- 1.539	- 0.915	- 0.525

Table 4.3 : Radial Stresses at Internal Points

(b) Constant and quadratic interpolation schemes converge, in general, on the correct solution "from above" while linear interpolation underestimates the displacement.

(c) The Gaussian quadrature order plays a significant role in the accuracy of constant and quadratic segments, but has no appreciable effect on the accuracy of linear segments.

(d) CPU times increase substantially with added boundary nodes. The discrepancy between constant, linear and quadratic segments is caused by the fact that a constant or linear discretization has twice as many segments as a quadratic scheme for the same number of nodal points. Hence integration takes place over only half the number of segments and consequently results in computer time savings

(e) The stresses calculated at internal points are accurate and follow the same trends as those in figure 4.17 for displacement. This is not surprising since these stresses are calculated directly from the boundary displacements and tractions by the fundamental solutions.

4.8.2 Example 2: Plate with Circular Cutout subjected to a Uniaxial Tensile In-Plane load (Plane Stress).

This example shows the application of the BIEM to a plane stress problem. The model chosen is a square plate with a circular hole at the centre. Under the influence of a uniaxial tensile force, a stress field is set up which exhibits a stress concentration around the hold. The objective of this example then, it is compare the stress and displacement field obtained from the BIEM using constant, linear and quadratic segments to the theoretical values and in particular to investigate the prediction of the stress concentration around the circular hole.

From the symmetry of the problem, it is possible to analyse only one quarter of the full plate. The geometry is shown in figure 4.19

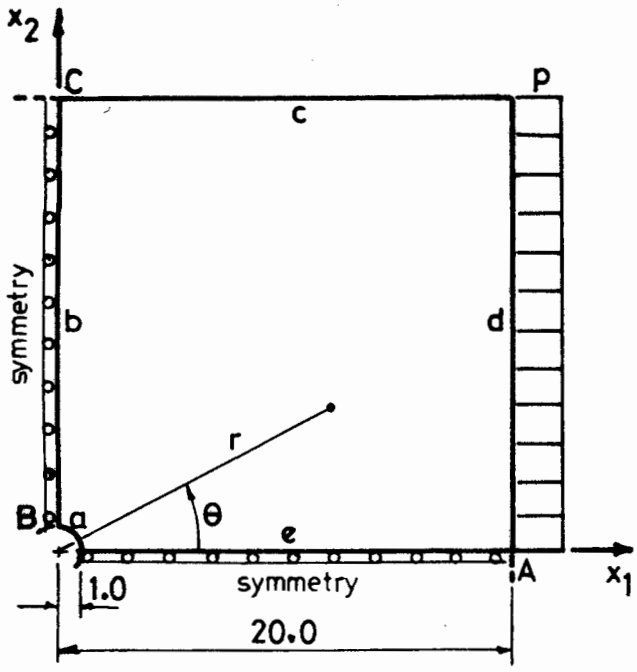

Figure 4.19 The geometry of a Plate with circular hole under a uniaxial load

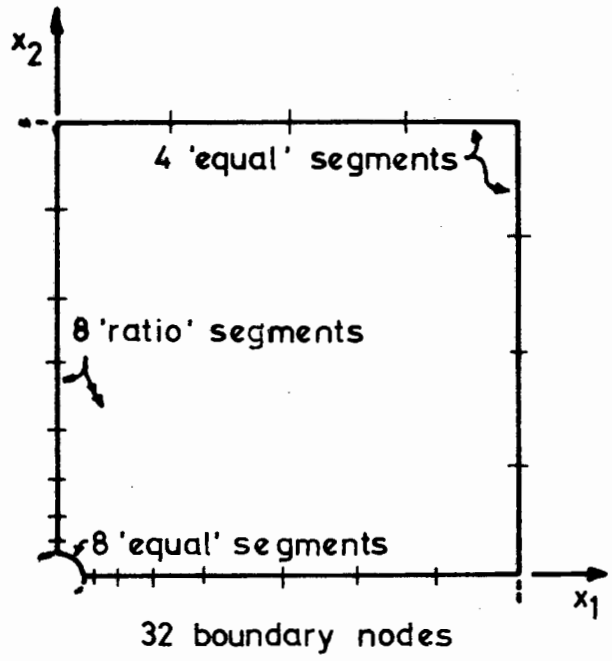

Figure 4.20 Subdivision of model - an example

The ratio of the dimensions of the plate to the diameter of the hole is 20.0. In the model used therefore, the dimension of the sides c and d are 20.0 units and the radius of side a is 1.0 units. The uniaxial loading p = 1.0/unit length is applied to side d in the positive x_1 direction. The displacement boundary conditions, taking symmetry into account are as follows:

side b u_1 = 0 (fixed) , u_2 = free

side e u_1 = free , u_2 = 0 (fixed)

The material is homogeneous, with material properties:

Youngs Modulus E = 1000.0

Poisson's Ratio ν = 0.3

In the analysis, the number of boundary nodes used forms a basis

for the comparison. The number of boundary segments therefore, is dictated by the number of nodes used, as in the previous example (4.8.1). Table 4.4 gives the subdivision details for the various models. As in (4.8.1) the word 'ratio' denotes a graduation of segment lengths by an arithmetic progression, and 'equal' denotes a number of segments of equal length.

No. Of Boundary Nodes	Constant & Linear Segments			Quadratic Segments		
	Side a	Sides b & e	Sides c & d	Side a	Sides b & e	Sides c & d
16	4 equal	4 ratio	2 equal	2 equal	2 ratio	1 equal
32	8 equal	8 ratio	4 equal	4 equal	4 ratio	2 equal
42	10 equal	10 ratio	6 equal	5 equal	5 ratio	3 equal
64	16 equal	16 ratio	8 equal	8 equal	8 ratio	4 equal
84	20 equal	20 ratio	12 equal	10 equal	10 ratio	6 equal

Table 4.4 Structural Modelling of a Plate with a circular hole.

The analysis was performed with the three interpolation orders and with 2, 4 and 6 part Gauss Quadrature rules successively.

As an example of the segment subdivision used, the model with 32 boundary nodes and 32 linear boundary segments is shown in figure 4.20.

The theoretical solution for the displacements are given by Muskhelishvili [4.9] in terms of the cylindrical co-ordinates r and θ as:

$$u_r = \frac{P}{8\mu r}\left[(\zeta-1)r^2 + 2R^2 + 2\left\{R^2(\zeta+1) + r^2 - \frac{R^4}{r^2}\right\}\cos 2\theta\right] \tag{4.51}$$

$$u_\theta = -\frac{P}{4\mu r}\left\{R^2(\zeta-1) + r^2 - \frac{R^2}{r^2}\right\}\sin 2\theta \tag{4.52}$$

where, for plane stress $\zeta = \frac{3-\nu}{1+\nu}$

$$\mu = \frac{E}{2(1+\nu)}$$

and R is the radius of the circular hole.

The stresses, also in cylindrical co-ordinates are given by Timoshenko [4.8] .

$$\sigma_r = \frac{P}{2}\left(1-\frac{R^2}{r^2}\right) + \frac{P}{2}\left(1+\frac{3R^4}{r^4}-\frac{4R^2}{r^2}\right)\cos 2\theta \tag{4.53}$$

$$\sigma_\theta = \frac{P}{2}\left(1+\frac{R^2}{r^2}\right) - \frac{P}{2}\left(1+\frac{3R^4}{r^4}\right)\cos 2\theta \tag{4.52}$$

$$\tau_{r\theta} = -\frac{P}{2}\left(1-\frac{3R^4}{r^4}+\frac{2R^2}{r^2}\right)\sin 2\theta \tag{4.55}$$

where P, R and r have the same connotations as before.

The results of the analyses with constant, linear and quadratic segments and 2, 4 and 6 point Gauss Quadrature are plotted in figure 4.21, using equation (4.50) for comparison purposes. The displacement at point A figure 4.13, is plotted i.e., r = 20, θ = 0.

The computer CPU times for the various analyses are plotted in figure 4.22. The theoretical stress profile along the line BC, figure 4.19 is plotted as a solid line in figure 4.23. It can be seen that the stress is concentrated at point B with a numerical value of 3P. The numerical values of the stress have been calculated close to the boundary BC at the positions indicated. From the figure it can be seen that there

is little difference between the numerical and theoretical values.

The theoretical values are calculated from equation (4.52) with $\theta = \pi/2$.

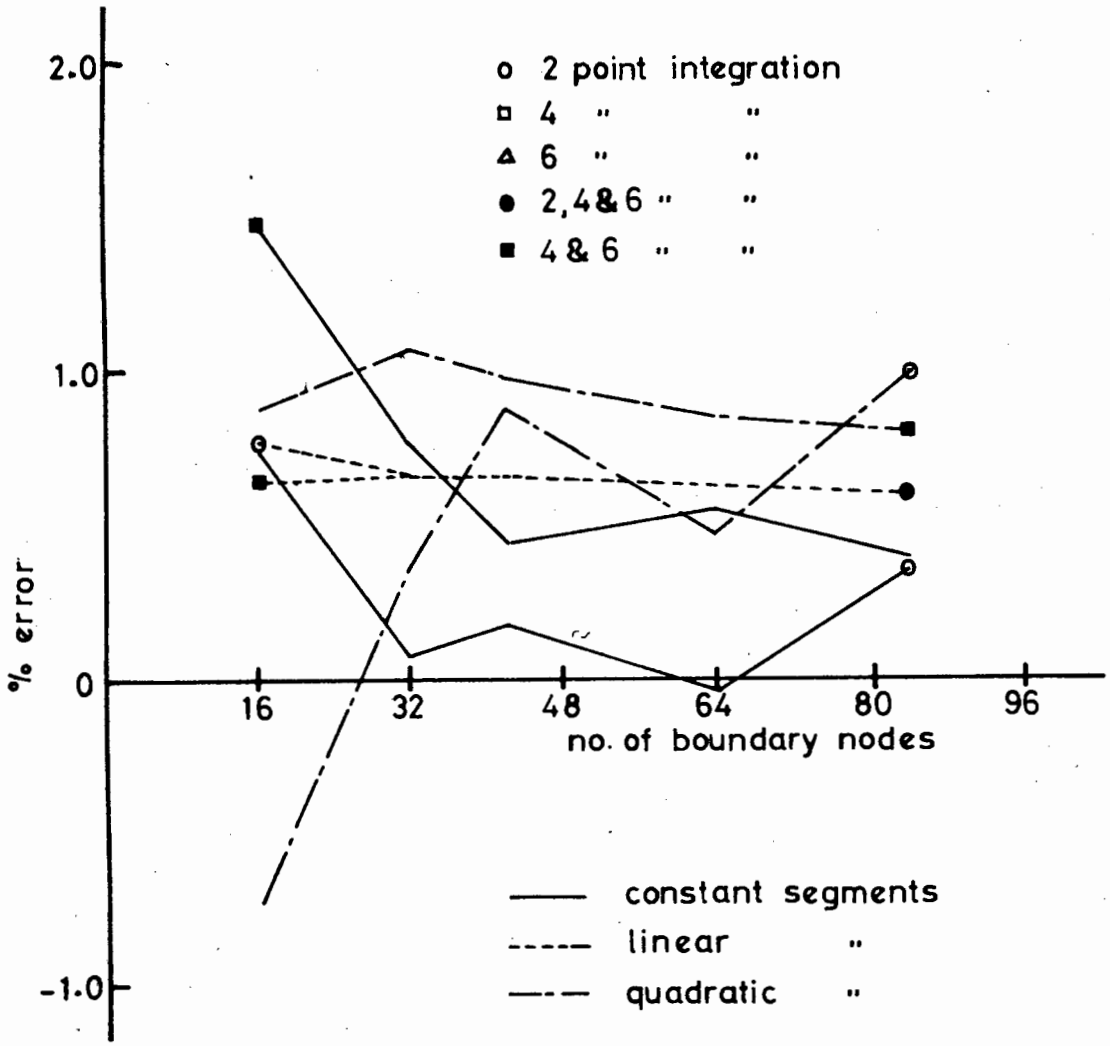

Figure 4.21 Comparison of accuracy vs number of boundary nodes for a plate with circular hole subjected to a uniaxial load

Figure 4.21 shows an erratic trend in the constant and quadratic segment calculations, particularly for 2 point integration. The higher integrations orders show a clearer convergent trend, however. The linear segments show a remarkable consistency for the three integration orders. No appreciable convergence or divergence in the accuracy with an increase in the number of segments is noticed, but, it is recognized that nowhere is the error larger than 1.5% and consequently

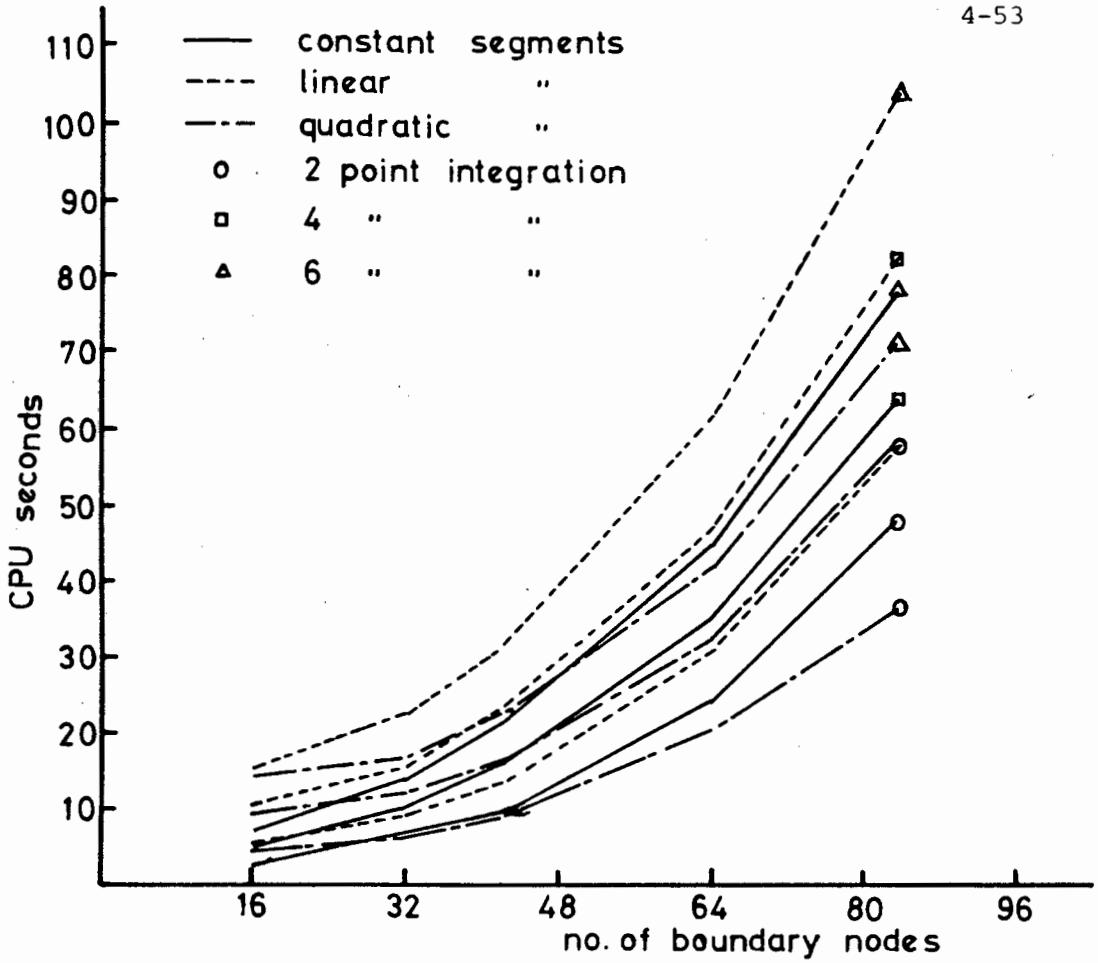

Figure 4.22 Comparison of CPU time vs number of boundary nodes for a plate with a circular hole subjected to a uniaxial load

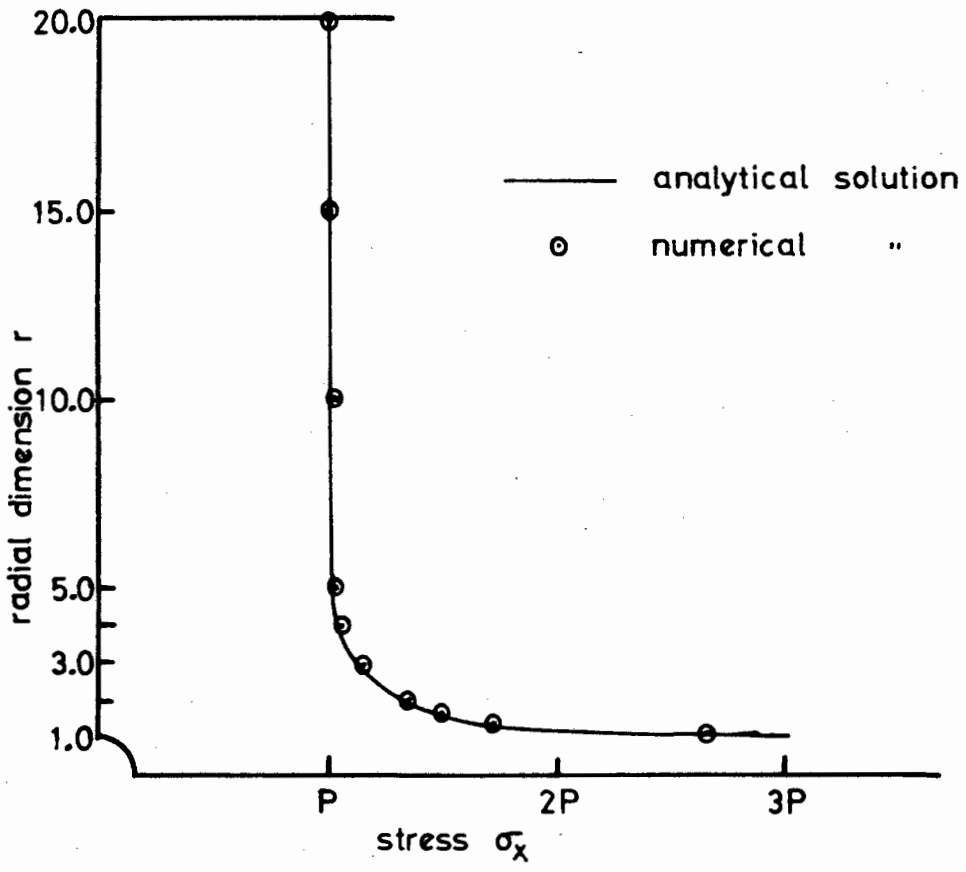

Figure 4.23 Stress concentrations around circular cavity

the slight variations in the results are of little importance.

CPU times naturally increase with the number of boundary segments and integrations order.

Although only the stresses along boundary (b) for linear elements are quoted in figure 4.23 the other schemes show similar trends. The quadratic interpolation, however, shows an oscillation about the mean value in the region r = 8 to r = 20. Here, the traction, and therefore the stress, should be approaching a constant value of P. However, the middle nodes of the quadratic segments tend to predict tractions 5 to 8% above the mean value and the end nodes are 5 to 8% below the mean. This is thought to be the result of the method employed in Appendix C.2 where the quadratic traction kernel is divided into two linear parts for the purposes of integration. A more rigorous method wherein the quadratic functions are directly involved, would cause the traction to be smoother.

4.8.3 Example 3: Horse-Shoe Beam

The accuracy of the BIEM for the problem in which bending is the major effect is investigated in this example. A U-shaped structure is subjected to loads at the ends of the "legs" of the U. Due to the symmetry of the problem, only one half was used in the model, with the necessary boundary conditions being placed on the line of symmetry. The analysis was carried out using the assumptions of plane strain.

The geometry and the boundary conditions are shown in figure 4.24 and the segment subdivisions are given in Table 4.5.

The model is prevented from movement along side BC i.e., $u_1 = 0$, $u_2 = 0$ and a load P of total value 3000 lbs is applied to side EF in the positive x_2 direction.

The material is homogeneous with material properties

Young's Modulus $E = 30 \times 10^6$ lbf/in^2

Poisson's Ratio $\nu = 0.25$

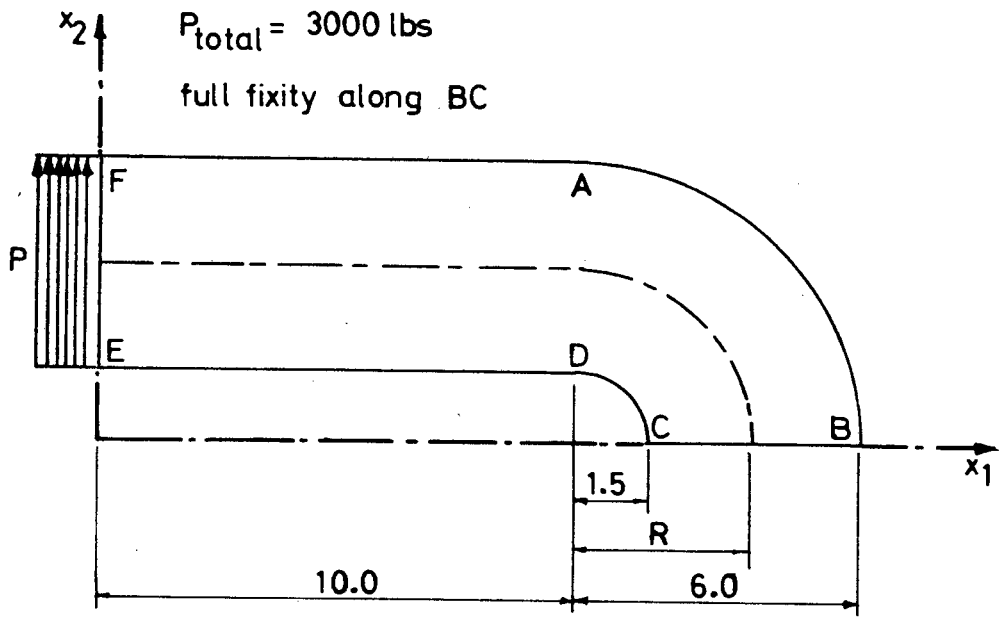

Figure 4.24 Horse-shoe beam - Geometry and Boundary conditions

No. of Boundary Nodes	Constant & Linear Segments						Quadratic Segments					
	AB	BC	CD	DE	EF	FA	AB	BC	CD	DE	EF	FA
28	6	2	6	6	2	6	2	1	2	3	1	3
40	8	4	8	8	4	8	4	2	4	4	2	4
56	10	6	12	16	6	12	5	3	6	5	3	6
68	12	8	14	12	8	14	6	4	7	6	4	7
80	14	10	16	14	10	16	7	5	8	7	5	8

Table 4.5 Structural Modelling of a Horse-Shoe Beam

Constant, linear and quadratic segments, involving either 2, 4 or 6 point Gauss Quadrature rules were used in the analysis. In addition, a finite element analysis using PAFEC 75 [4.11] was also used to verify the results. Forty eight 8-node quadrilateral elements, involving 177 nodes were used.

The theoretical solution for the displacement at point A is given by Seeley and Smith [4.10] as:

$$\delta_A = \frac{PR}{2Ea}\left\{\frac{E}{G}\frac{\pi}{2} + \frac{2d}{y_o} + \frac{R}{y_o}\frac{\pi}{2} - \frac{2d}{R} - \frac{\pi}{2}\right\} \qquad (4.56)$$

where a = area of cross section = 4.5 in^2

y_o = distance from centroidal axis to neutral axis when beam is in pure bending $4.10 = 0.1368 = 0.513$ in.

R = distance to centre of area cross-section.

Hence, once the arithmetic has been performed:

$$\delta_A = 0.001979$$

Equation (4.56) has been derived from flexural theory, and, as will be seen, is considerably inaccurate. However, for purposes of comparison, this value of displacement has been used as a benchmark.

The results obtained from the BIEM and FEM are plotted graphically in figure 4.25.

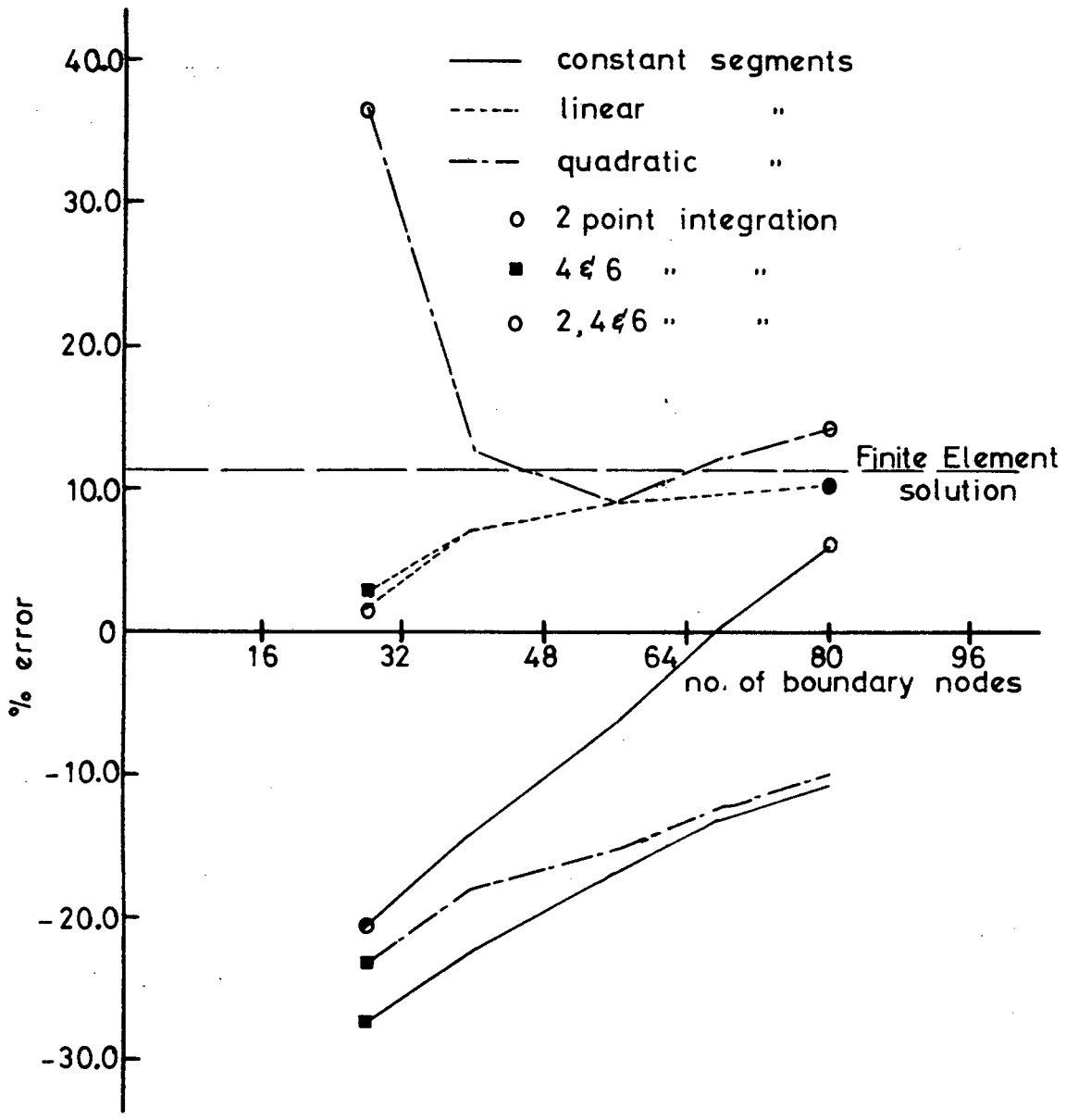

Figure 4.25 Comparison of accuracy vs number of boundary nodes for the horse-shoe beam

It is quite evident from figure 4.25 that the numerical results from the BIEM and the FEM do not converge upon the analytical solution. If the numerical results calculated by 2-point Gaussian quadrature are disregarded as being unreliable for the evaluation of the integrals involved, then the results fall into two regions. The values calculated by constant and quadratic interpolation follow the same trend and lie close to each other. On the other hand, the FE solution and the linearly interpolated BIEM are in close agreement. Assuming that the FE solution is the closest to the exact solution, then it can be seen that the constant and quadratic boundary segments underestimate the displacement by approximately 25%. This discrepancy is thought to be caused by the discontinuity of tractions at the corner and will be discussed further in chapter 5. In all three cases, the programming of the various interpolation orders follows the same lines. A check of the results quoted in figure 4.25 by using a published program [4.4] wherein constant segments and 4-point Gaussian quadrature are used shows the same wayward trends.

The order of the Gaussian quadrature can affect the results, particularly for constant and quadratic interpolation. In both cases, the solutions using a 2-point rule are substantially different from those using 4 and 6 point rules. Although it can not be said with certainty which results are more accurate, it can certainly be said that the 2-point rule gives a reasonable approximation to the analytical answer. For the constant and linear interpolation segment it is reasonable to suggest that 2-point integration is sufficient but for the quadratic segment a higher order-rule appears to be applicable.

Analyses using the traction discontinuity equation concept to be discussed in detail in chapter 5 were also performed. Here, the linear and quadratic interpolation results converge on to the finite element value shown in figure 4.25 (displacement = 0.002199). From this, it appears that the matrix formulated by the numerical technique which disregards the distinct tractions at the corners is nearly singular and hence produces slightly erroneous results. The incorporation of the traction discontinuity equations overcomes this uncertainty.

4.8.4 Example 4: Circular Disc subjected to external pressure (Plane Stress)

When a circular disc is subjected to a constant external pressure, the stress field throughout the body will be constant. This example has been chosen so that the suitability of the BIEM for the prediction of this phenomenon can be ascertained. All three types of segments discussed previously have been used for the analysis in this case. The analytical solution is given by Timoshenko [4.8].

The model used in the analysis has a radius of 10.0 units. and a Young's Modulus E of 1000.0. The pressure loading of 10.0/unit^2 is applied at the circumference. These parameters remain constant throughout the study, while a range of Poisson's Ratio (ν = 0.1, 0.2, 0.3, 0.4 and 0.45) were used for comparison purposes. The geometry and boundary conditions are shown in figure 4.26.

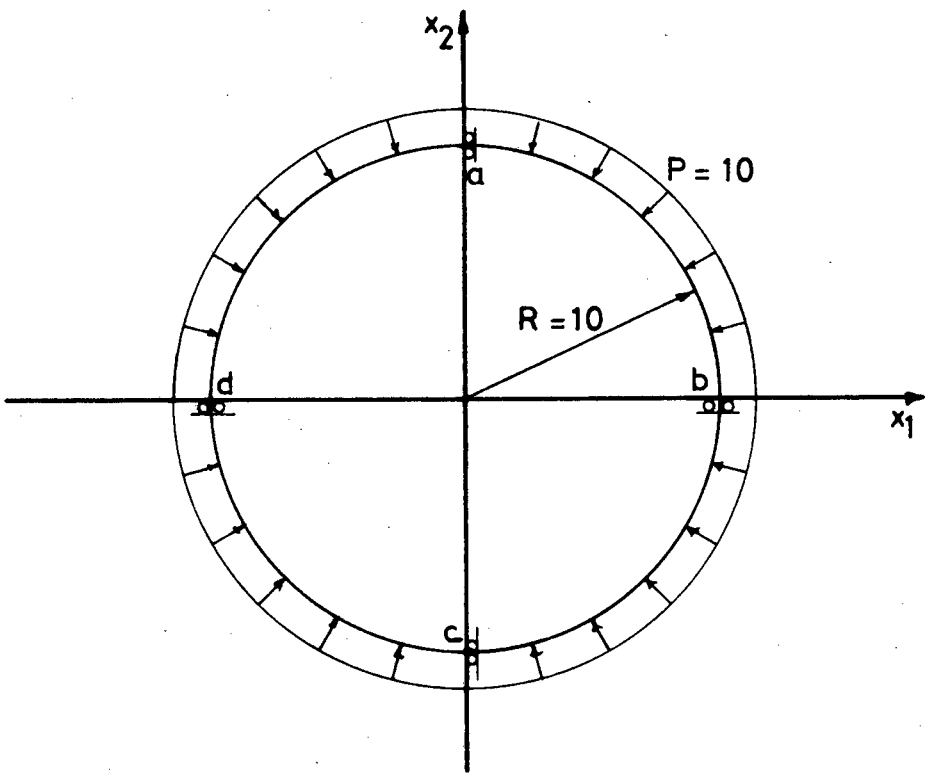

Figure 4.26 Circular Disc under Pressure

Although a infinite number of planes of symmetry are available for use as outer boundaries in the model, the complete structure was preferred in this analysis. Quadratic, linear and constant interpolation was used, where the circular boundary was divided into 3 separate models, using 24, 48 and 72 boundary nodes. The pressure load was applied to each element in the direction of the local segment normal. Displacement boundary condition were applied at points a to d. At a and c, $u_1 = o$, u_2 free and at b and d, u_1 free, $u_2 = 0.0$.

The theoretical solution is given by Timoshenko [4.8] , where the stress field for an annulus subjected to both internal and external pressures is quoted. By decreasing the internal radius and pressure to zero, the radial and circumferential stresses can be calculated.

$$\sigma_r = \sigma_\theta = - P \tag{4.57}$$

For plane stress applications, the stress-strain relationship is

$$E\varepsilon_\theta = \sigma_\theta - \nu\sigma_r$$

and strain-displacement relationship is

$$\varepsilon_\theta = \frac{u}{r}$$

Hence the radial displacement u is

$$u_r = (\sigma_\theta - \nu\sigma_r) \frac{r}{E} \tag{4.58}$$

The comparison of the radial displacements are shown in figures 4.27, 4.28 and 4.29 for the range of Poisson's Ratios. The formula (4.58) above is used as the benchmark in these comparisons.

The stress field in this structure is constant throughout. Internal points were positioned throughout the structure and an average stress intensity was calculated for comparison. Where the stress value was

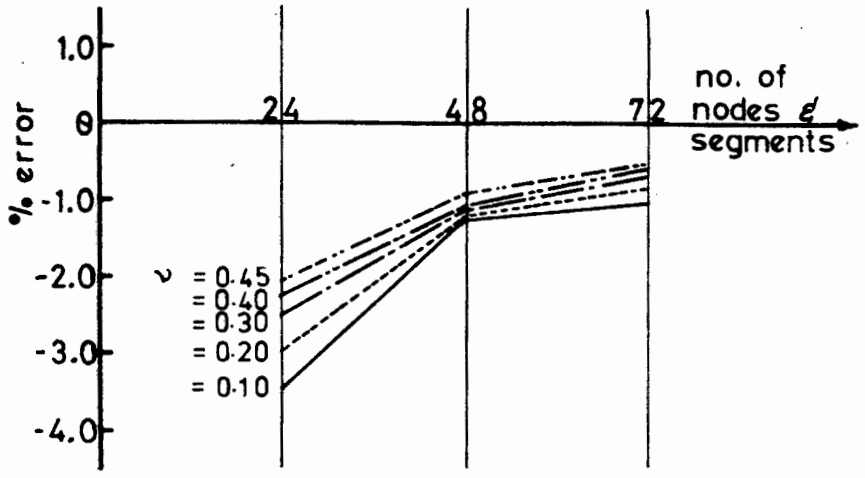

Figure 4.27 Accuracy of displacement by constant interpolation

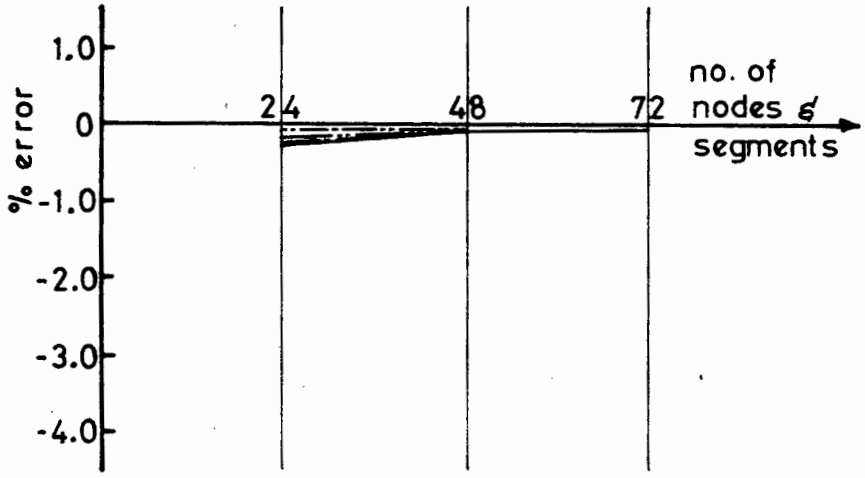

Figure 4.28 Accuracy of displacements by linear interpolation

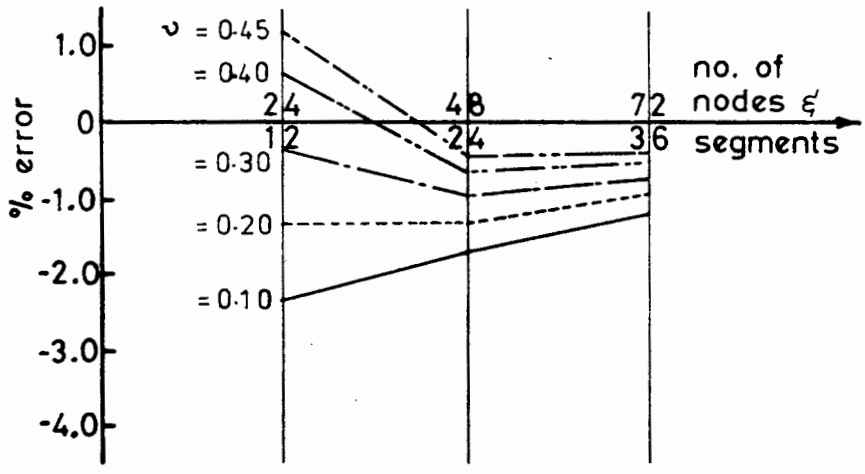

Figure 4.29 Accuracy of displacements by quadrature interpolation

clearly incorrect due to the proximity of the sampling point to the boundary, the values were neglected. Figure 4.30 shows the comparison of the calculated stress field and the stress field of equation (4.57) above.

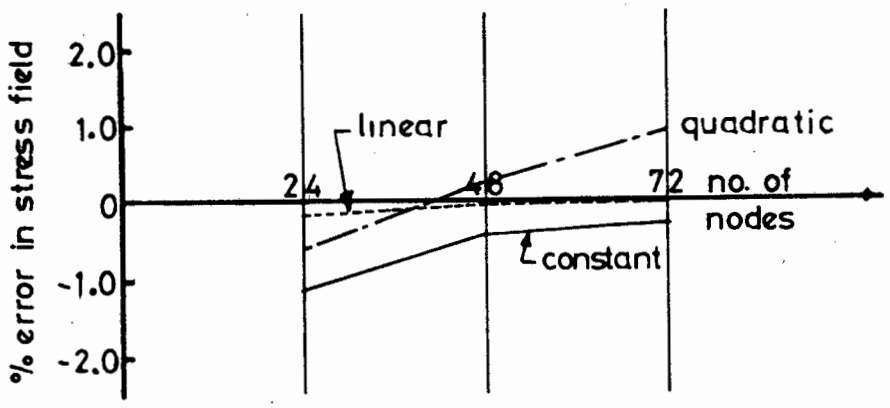

Figure 4.30 Accuracy of stress field

In these results, conclusive accuracy trends have been shown for both displacements and stress fields. It is clear that the 24 linearly interpolated boundary segments model is more accurate than the 72 constant interpolation model. The average error is displacements is:- linear : constant :: - 0.18% :- 0.75%
while the average error in stress is:-

linear : constant :: - 0.18%: - 0.29%

These comparisons show clearly that the BIEM is capable of predicting a constant stress field for problems of this type. Even with a very coarse boundary subdivision of 24 constant segments, the average error between the calculated and the analytical solutions is a mere - 2.64% for displacements, while for stress, it is only 0.29%. With as few as 12 quadratic segments, a set of values ranging from - 2.31% to + 1.18% is obtained, while for 36 quadratic segments the average error is - 0.76%.

A comparison of computer times is shown in Table 4.6 where only a few isolated times are shown, since the general trend is precisely as shown in the previous examples. A point to note here, is the close similarity between the total time and the CPU time. This shows that very little time is spent on input, output and file handling. All the computational time is being spent in the calculation of the matrix coefficients and in the solution of the system's matrix. At this stage, little can be done to overcome this problem. The method requires that each set of integrations for each pivot node be calculated separately since the orientations and distance are different in each case. For the method to become commercially competitive, therefore, some efficient integration and solution schemes will have to be designed in future.

Interpolation Type	Total No. of Boundary Segments			Time (secs)
	24	48	72	
Constant	35.219 *	71.304 *	76.703 Δ	Total
	28.306	64.161	69.486	CPU
Linear	23.311 Δ	46.189 Δ	94.252 Δ	TOTAL
	16.659	39.185	86.551	CPU
Quadratic	50.303 *	67.316 *	103.571	TOTAL
	40.283	57.149	93.296	CPU

Table 4.6 Computer Times

* 4 pt Gauss Quadrature rule

Δ 2 pt Gauss Quadrature rule

4.8.5 Example 5 - Practical Problem - Stress Analysis of Box Girder Bridge Pier

To complete this chapter, a practical problem has been chosen. In South Africa at present, a considerable number of bridges and viaducts supported by forked piers are being built. It seems opportune to choose this as an example therefore, although the geometry, loading and material properties used are hypothetical.

Consider a box-girder viaduct deck supported intermittently by reinforced concrete piers. It is required to calculate the stress distribution in the piers for various loading combinations so that an efficient, aesthetically pleasing structure can be designed. Although this is a hypothetical example as far as this analysis is concerned, it nevertheless shows the applicability of the method to practical engineering problems. For this purpose, an actual box-girder deck has been used, [4.12] from which the loading has been calculated.

The details of the structure are:

Viaduct Superstructure:
- No. of spans = 11
- Span distance = 28 m
- width of deck = 10.8 m
- Overall depth = 1.74 m
- Cross sectional area of deck = 8.8 m^2

Pier:
- Height = 6.0 m
- Base width = 1.5 m
- Crown width (overall) = 4.5 m
- Bearing area = 1.0 x 0.5 m
- Thickness (constant) = 1.0 m

Material
- Young's Modulus = 30 GPa
- Poisson's Ratio = 0.3

Analysis type : Plane Stress.

The geometry of the pier under consideration is shown in figure 4.31.

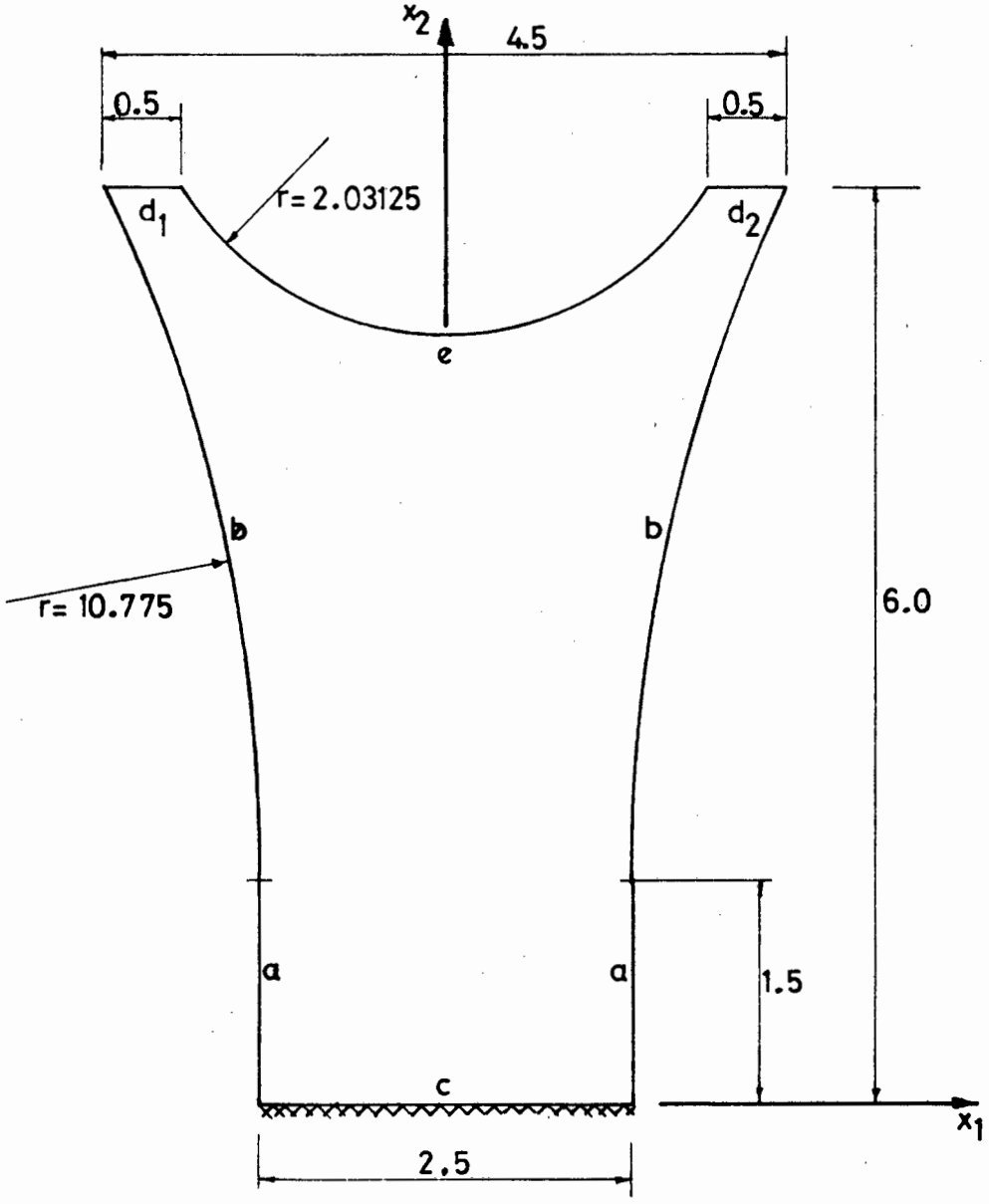

Figure 4.31 Box Girder Bridge Pier - Geometry

The computational model consists of: 76 linear interpolated segments. For ease of modelling only straight lines and arcs were incorporated in the discretization. The segments were arranged as follows:

Side (a): straight, length = 1.5 m, 6 equal segments.
Side (b): arc, radius = 10.62 m, 10 equal segments.
Side (c): straight, length = 1.5 m, 10 equal segments.
Side (d): straight, length = 0.5 m, 2 equal segments.
Side (e): arc, radius = 2.03125 m, 14 equal segments.

Displacement boundary conditions ($u_1 = u_2 = 0$) are applied to all points on side (c). Loading from the deck is transmitted to the pier through the bearing areas, side (d). Loading cases considered are:

Load Case 1: Dead load of deck only:
Traction on d_1 and d_2 = 5913.6 kN/m^2

2: Dead load plus imposed load of 10 kN/m^2 on deck:
Traction on d_1 and d_2 = 9273.6 kN/m^2

3: Dead load plus imposed load of 10 kN/m^2 on ½ of the deck:
Traction on d_1 = 9273.6 kN/m^2
Traction on d_2 = 5913.6 kN/m^2

4: Transverse loading due to wind [4.13]:
Wind speed 120 km/h
Wind pressure q = 0.650 kN/m^2
Factor = 1.5
Total transverse traction on d_1 and d_2 = 47.5 kN/m^2

Results: Figures 4.32, 4.33 and 4.34 are produced by the program and show the displaced shape and stress distribution for load cases 1 and 2, 3 and 4 respectively.

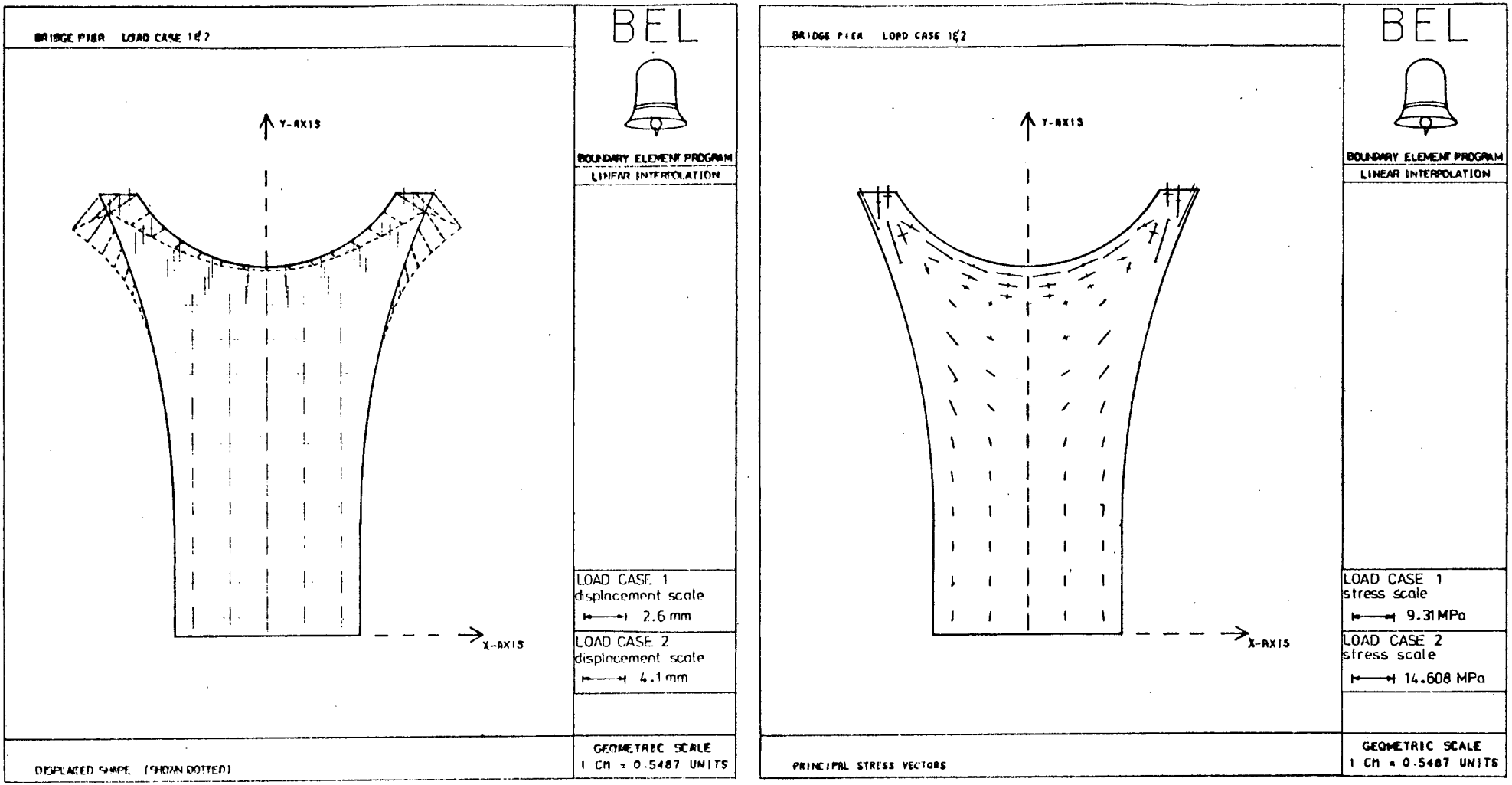

Figure 4.32 Box Girder Bridge Pier-Results for Load Case 1 & 2

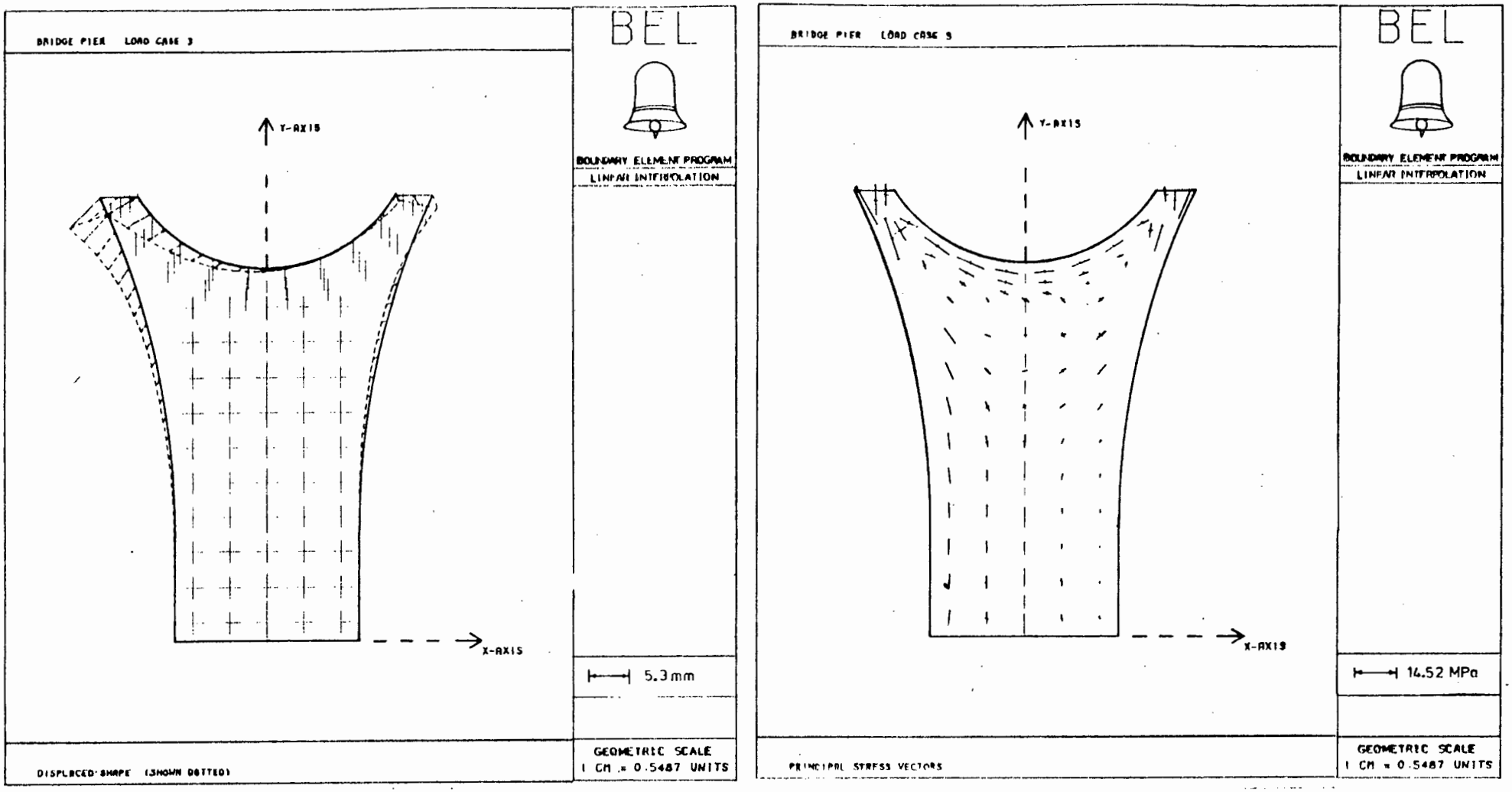

Figure 4.33 Box Girder Bridge Pier - Results for Load Case 3

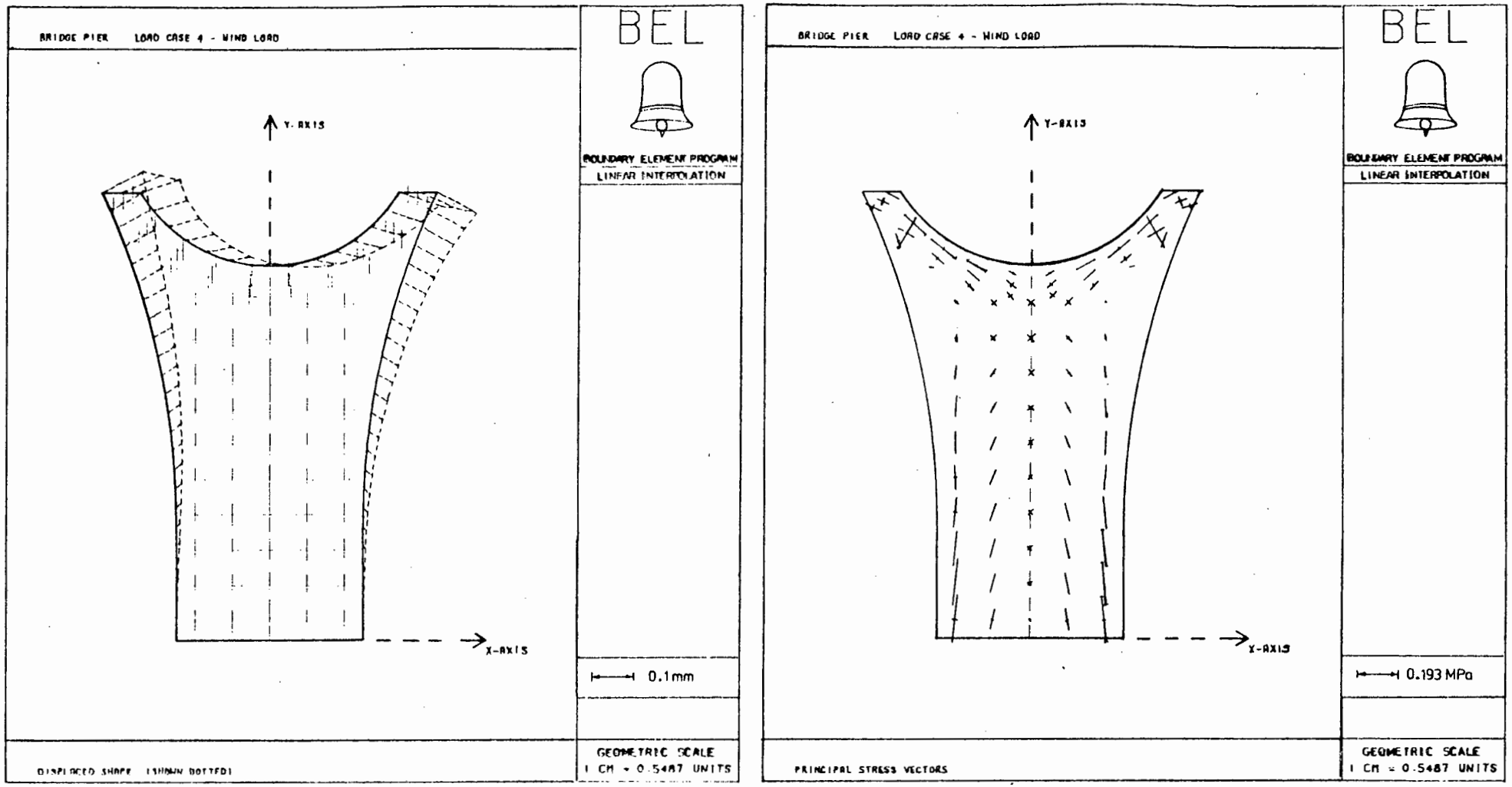

Figure 4.34 Box Girder Bridge Pier - Results for Load Case 4

A distinct advantage shown by the boundary integral method over finite element methods is its ability to predict the stress field at any internal point in the structure without mesh adjustment. Therefore, it is simple to change the internal grid to allow the calculations to be done at exactly the points at which the engineer wishes to know the stresses.

Due to the graphical output, comment on the results is superfluous and it remains only to report that the total computer time (UNIVAC 1100/81) was 1 minute 54.498 secconds of which 1 minute 41.994 seconds was CPU time. Two point Gaussian Quadrature was used in the numerical integration, and displacements and stresses were calculated at 90 internal points.

4.9 Conclusion

The discussion in this chapter has centered on the numerical implementation of the BIEM and on the applicability and accuracy of the method for the solution various problems.

The details of the use of constant, linear and quadratic interpolation schemes are included once the general numerical method, the form of the matrix equations and the solutions of the system have been covered. Integration of the boundaries by Gaussian Quadrature is also reviewed.

The exact nature of the boundary coefficient submatrix c_{ij} is investigated and results in the formulation which is dependent on the external angle between two segments at their common node. From this it can be seen that for a straight boundary the values of $c_{ij} = \frac{1}{2} \delta_{ij}$. Although this analytical method shows quite clearly the form of the submatrix, a numerical method, based on rigid body motions, is used in practice.

One of the major problems encountered, is the integration of the fundamental solutions in the vicinity of their singularities. This occurs when the distance between the pivot node and the focus segment tends to zero. This, is the case when the pivot node is one of the nodes of focus segment and occurs for all interpolation orders. In this case,

analytical integration over these segments is performed. This is covered in detail in this chapter. The resulting formulae for the integration of both the traction and displacement fundamental solutions are derived so that they can be programmed directly.

The calculation of displacements and tractions at internal points follows from the derivation of the method. However, at points close to the boundary, these calculations become inaccurate due to the existance of the singularity in the fundamental solutions. This is overcome numerically by subdividing two adjacent segments into smaller lengths. The ratio between the distance from the segment to the internal point and the length of the segment is thus kept close to one. This overcomes the inaccuracy problem to a great extent at these points.

To complete the numerical discussion ,the details are combined in an extensive flow chart of the method. Included are all the essential ingredients which have previously been discussed in the chapter.

The second major section in this chapter covers the applicability and accuracy of the BIEM for the solution of commonly encountered plane stress and plane strain problems. The examples are carefully chosen to cover specific applications. Comparisons are made between the results obtained by increasing the sophistication of the approximations over the boundary, and the analytical solutions where these are available. Where applicable, a finite element analysis using a commercially available program has also been compared.

In general, the three orders of interpolation can be summarized as follows:

(i) Constant displacement and traction segments are the simplest to implement numerically. The solutions obtained are accurate to within 1% of the analytical value in most cases even though the boundary variables are approximated by a piecewise constant function. The Gaussian integration order used to integrate the fundamental solutions has a slight effect on the accuracy. However, this simple method gives more than acceptable

results for the majority of practical problems.

(ii) Linear variations of the boundary values form a far more acceptable foundation for the numerical technique since, in particular, the displacement on the boundary can be described in a continuous manner. This makes the BIEM method amenable to a coupling with a constant strain finite element model, if required. In general, ths solutions obtained from linearly interpolated segments are more accurate than those from constant segments. Due to the extra housekeeping, however, computer CPU times are increased.

(iii) The quadratic formulation is particularly attractive since it is geometrically compatible with the general isoparametric finite elements (with 3 side nodes). The boundary geometry can be accurately approximated since the segments can be parabolically curved (unlike the constant or linear segments). It has been found that these segments give comparable results to those obtained from the other formulations. The computer times for an equivalent number of degrees of freedom are lower than the other interpolation types since the integration schemes are segment dependent. For this type of interpolation, only half the number of segments will be used for a given number of boundary variables. From this point of view, this approach is particularly attractive.

Convergence to the theoretical result is demonstrated as the number of boundary segments increases, but seldom does the error exceed a few percent. An increase in the Gaussian quadrature order increases the accuracy of both the constant and the quadratic interpolation schemes, but at the same time increases the computation time. The linear interpolation is not effected to the same degree. Consequently, acceptable results are obtained by using 2-point integration for the linear scheme while at least a 4-point quadrature formula is required when using the constant or quadratic order. By so doing, the linear (using 2-point GQ)

and the quadratic (using 4-point GQ) schemes are computationally equivalent when computer CPU times are taken into account.

Both stress concentrations and constant stress fields are competently predicted by this BIEM formulation. However, inaccurate results are obtained for problems where bending is of primary importance. This is due to the discontinuity of the traction of the corner nodes and will be dealt with in the subsequent chapter.

Finally, the method has been shown to be applicable to practical engineering problems where the geometry, model discretization and material properties are easily taken into account in the computer programs.

In conclusion, therefore, it would seem that the quadratic interpolation scheme has a slight edge over constant and linear scheme because fewer segments can be used for a comparable accuracy thus resulting in computation time efficiency, and the segments can be curved. Consequently, this interpolation order is recommended for further applications.

Since the tractions can be discontinuous at corner nodes, special account must be taken of this in the linear and quadratic formulations. A set of traction discontinuity equations can be written which interrelate the traction values at the nodes. Certain anomalies which have occurred in some of the examples quoted, can be circumvented by the incorporation of these special purpose traction discontinuity equations or by the dual-node approach discussed in the following chapter.

Data preparation is simple and although the matrices produced are unsymmetric and fully populated, the method is accurate, reliable and once the computation inefficiencies have been comprehensively reserched, will form a viable alternative to the Finite Element Method for plane elastostatic problems.

4.10 References

4.1 O.C. ZIENKIEWICZ, The Finite Element Method, 3rd Edition McGraw-Hill, New York (1977).

4.2 K.J. BATHE and E.L. WILSON, Numerical Methods in Finite Element Analysis, Prentice-Hall Inc., New Jersey (1976).

4.3 K.J. BATHE, Finite Element Procedures in Engineering Analysis, Prentice-Hall Inc., New Jersey (1982).

4.4 C.A. BREBBIA, The Boundary Element Method for Engineers, Pentech Press, London (1978).

4.5 G.C. HOWELL and W.S. DOYLE, "Boundary Integrals - An Alternative to Finite Elements for Plane Elasticity Problems", Proceeding of the Symposium on Design Applications of the Finite Element Method held at the University of Cape Town on 12 - 14 January 1981.

4.6 G.C. HOWELL and W.S. DOYLE, "Plane Stress/Strain Analysis by Boundary Integral Equation and Finite Element Methods", Proceeding of the Conference on Finite Element Methods in South Africa held at the CSIR, Pretoria, S.A. on 17 - 18 March 1981.

4.7 G.C. HOWELL and W.S. DOYLE, "An Assessment of the Boundary Integral Equation Method for In-Plane Elastostatic Problems", Applied Mathematical Modelling, Vol. 6, No. 4, August 1982.

4.8 S.P. TIMOSHENKO and G.N. GOODIER, Theory of Elasticity, 3rd Edition, McGraw-Hill (1970).

4.9 N.I. MUSKHELISHVILI, Some Basic Problems of the Mathematical Theory of Elasticity, 3rd Edition, P. Noordhoff Ltd., Gronigen, Holland (1953).

4.10 F.B. SEELEY and J.O. SMITH, Advanced Mechanics of Materials, 2nd Edition, John Wiley & Sons, Inc. (1952).

4.11 PAFEC 75, A Program for Automatic Finite Element Calculations, Pafec Ltd., Nottingham, England.

4.12 R.A. SWANN, "A Feature Survey of concrete base spine-beam Bridges", Technical Report 42.459 Cement and Concrete Association, June 1972.

4.13 South African Standard Building Regulations (1970).

CHAPTER 5

SPECIAL NUMERICAL TECHNIQUES AND INVESTIGATIONS

5.1 Introduction

Some special numerical techniques have been incorporated in the computer programs in order to overcome certain difficulties which have become evident. This chapter explores these techniques, discusses the significance of the relevent problem and makes recommendations in this regard. The chapter is divided into four separate sections. Each section deals with a specific topic and includes examples to demonstrate the application of the technique.

In the first section, the problem of the discontinuity in the traction at a corner in the continuum is reviewed. An attempt has been made to overcome the problem by designing a special segment without end nodes. This, however, is only partially successful and it leads to the specification of the dual node concept. A method whereby the tractions at a corner are inter-related by a set of discontinuity equations is also reviewed and examples are shown to substantiate the use of these methods. In particular, problems where bending is the major effect are successfully handled by these methods.

The incorporation of body forces due to gravity, is an important part of an analysis method. There are currently two methods available for the incorporation of these forces, namely, the domain integration method and the boundary integration method. In this chapter, the numerical details of both methods are given and an example which makes a critical comparison between the methods, is used.

One of the disadvantages of the Boundary Integral Equation Method currently, it its inability to produce banded, symmetric matrices without a considerable amount of time-consumming pre-processing. The non-symmetric, fully-populated matrices cannot be efficiently stored or solved in the present method. In an attempt to discover the characteristics of the matrices and the reasons for the non-symmetric behaviour, the fundamental displacement and traction solutions have been thoroughly

investigated and the method as a whole has also been critically examined. The results show that only under very rigid conditions can there be any hint of an improvement to this numerical method. This review is contained in the third major section in this chapter.

A problem which always occurs when an analysis is to be undertaken, is the question of the choice of segment lengths and structure aspect ratios. An added complication is the order of numerical integration specified and its effects on the solution. In order to give some insight into these problems, an analysis of the error between the analytical and numerical integration of the singularity expressions in the fundamental solutions has been undertaken. The effect of the integration order with respect to the segment length and the distance from the pivot node to the focus segment is investigated. From the graphs which have been drawn, recommendations regarding aspect ratios and segment lengths can be ascertained. This is the final section of this chapter.

5.2 Traction Discontinuity at a "corner"

5.2.1 The existance of the discontinuity problem

The traction at a point is defined by the stress field in the immediate vicinity and the direction of the outward normal to the continuum at the point, as stated in equation (3.5). For the traction to be uniquely defined at the point, the normal must be unique.

Consider now the situation which arises when the point is at a corner of the continuum. Two distinct normals now exist, as shown in figure 5.1 and consequently the tractions value t_i is no longer single-valued.

Writing the traction values derived from segment A and segment B gives:

$$t_i^A = \sigma_{i1}\, n_1^A + \sigma_{i2}\, n_2^A \qquad (5.1a)$$

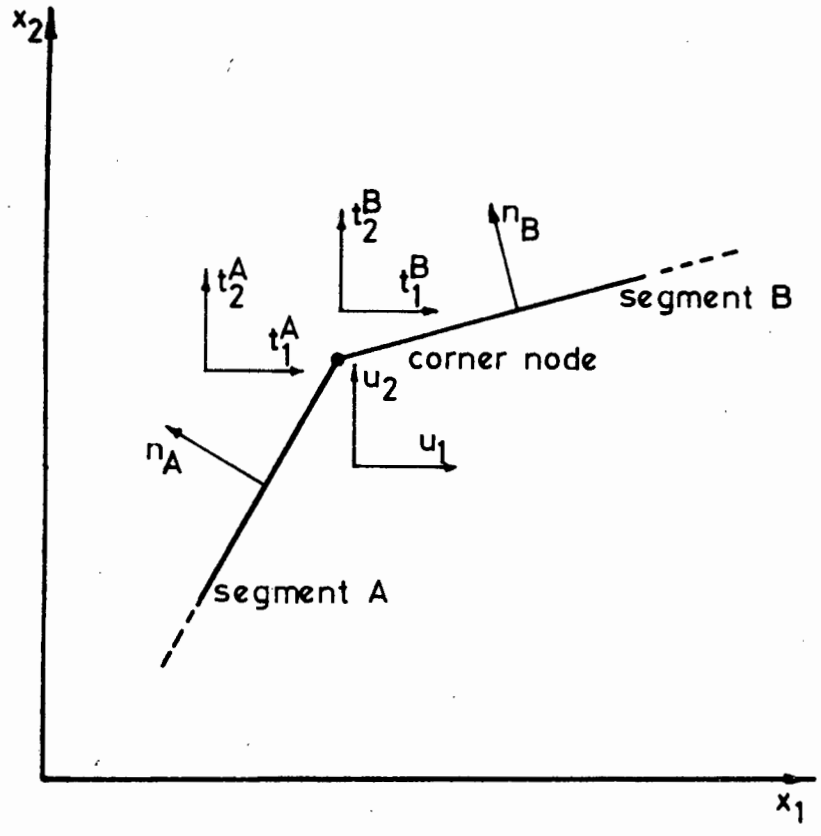

Figure 5.1 The discontinuity at a corner node

and $$t_i^B = \sigma_{i1}\, n_1^B + \sigma_{i2}\, n_2^B \qquad (5.1b)$$

Since $n_i^A \neq n_i^B$ therefore $t_i^A \neq t_i^B$. Hence, to describe the state of traction accurately in the vicinity of the corner node, 4 variables, namely t_1^A, t_2^A, t_1^B and t_2^B are required.

In the numerical procedure detailed in the previous chapter, collocation points (or knots) were necessary at the ends of the segments for linear and quadratic interpolation. Consequently, the traction discontinuity problem will arise in all cases where segments A and B do not form a straight line.

The piecewise polynomials used in the interpolation exhibit C_o continuity of the approximated variables at the common node in a conventional interpolation scheme. In the BIEM, this is ideal for the displacement variables where a continuity between segments must be ensured. However, the modelling of a traction discontinuity where essentially a jump is required, is not successfully accomplished by these interpolation techniques.

The following sub-sections describe some of the methods which can be used to overcome the traction discontinuity problem. To begin however, we show a method which was developed but which has certain shortcomings and is therefore limited in its applicability. Nevertheless, it is a viable method and as such warrants a mention in this section. The later sections show methods which are far more successful and which have been effectively introduced into the computer coding.

5.2.2 Gauss-Point Segments

Since the problem of traction discontinuity is only present for segments with nodes at their extremeties, the obvious course of action is to design a segment which does not have end nodes. By moving the nodes away from the ends of the segment, the inter-relationship between adjacent segments is circumvented. The shape functions then relate to the variables over a single segment only, thus allowing an uncoupling of segment variables.

There are many positions within the segment which can be used as collocation points. Since a Gaussian Quadrature scheme was being used for the integration, however, it was natural to suggest that the collocation points be located at positions corresponding to theGauss points in a 2 point scheme. This is shown in figure 5.2. A linear variation of both displacement and traction is assumed between the nodes and so allows a discontinuity to be present at the segment junctions.

The method has a disadvantage over the conventional linear interpolation scheme discussed in chapter 4. Extra nodes, and hence extra equations are required for a similar number of boundary segments.

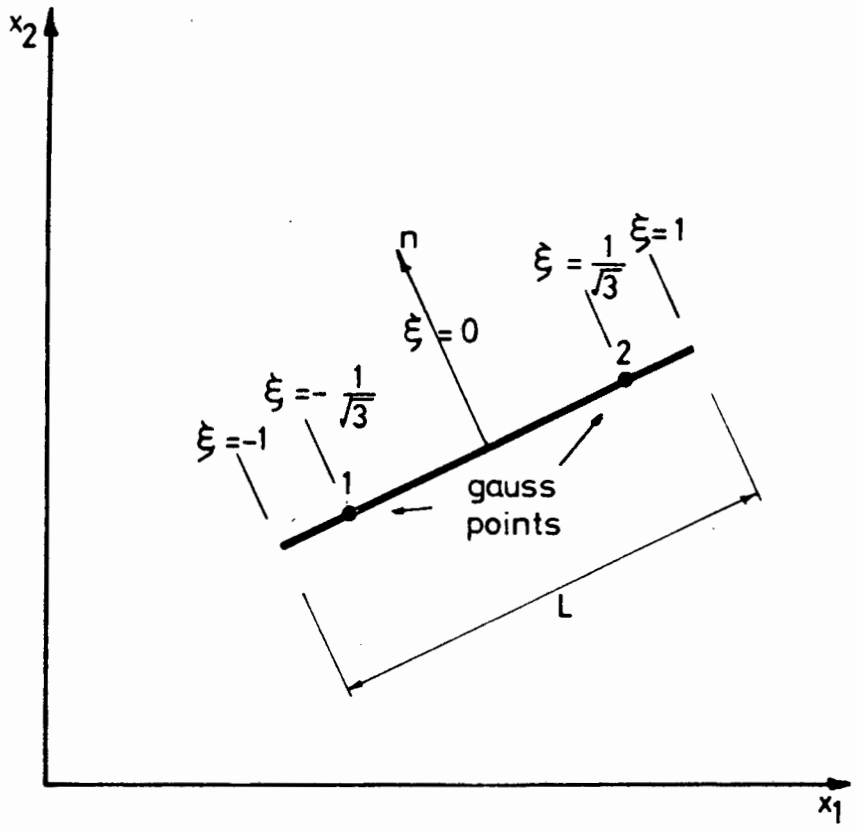

Figure 5.2 A Gauss Point Segment

Consequently, this leads to extra computation time and solution time in the computer. This is caused by the fact that the average number of nodes per segment over the whole boudary is now two, which compares with an average of one node per segment for the conventional scheme. As an example, if there are N segments placed on the boundary, then this method will require 2N nodes, whereas the latter method (linear interpolation) only requires N nodes. Although this is thought to be inefficient at this stage, it will be seen later (5.2.5) that this technique can be refined to give a most efficient and accurate analysis method.

At this stage, however, we are concerned with the fundamental concept of the Gauss-point segments.

5.2.2.1 The interpolation functions

Referring to figure 5.2, the linear shape functions N_1 and N_2 of the Gauss-point segment can be defined as follows, figure 5.3:

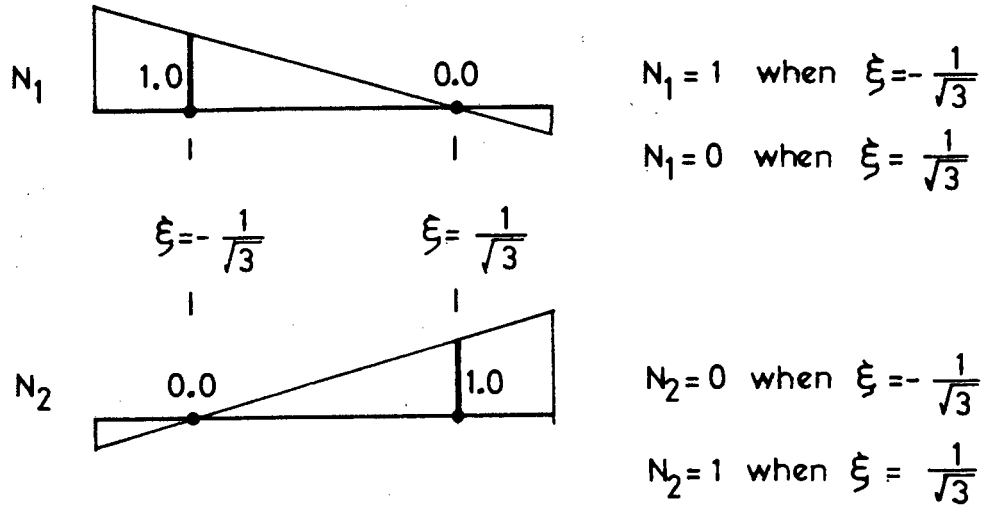

Figure 5.3 Definition of Gauss-point segment interpolation functions

The shape functions, defined in terms of the local co-ordinate ξ, are therefore:

$$N_1 = \tfrac{1}{2}(1 - \sqrt{3}\xi)$$

$$N_2 = \tfrac{1}{2}(1 + \sqrt{3}\xi) \qquad (5.2)$$

Following the traditional method, the displacement and traction at a general point within the segment, can be expressed in terms of the nodal values and the shape functions as:

$$u = \begin{Bmatrix} u_1(\xi) \\ u_2(\xi) \end{Bmatrix} = \begin{bmatrix} N_1 & 0 & N_2 & 0 \\ 0 & N_1 & 0 & N_2 \end{bmatrix} \begin{Bmatrix} u_1(1) \\ u_2(1) \\ u_1(2) \\ u_2(2) \end{Bmatrix}$$

$$t = \begin{Bmatrix} t_1(\xi) \\ t_2(\xi) \end{Bmatrix} = \begin{bmatrix} N_1 & 0 & N_2 & 0 \\ 0 & N_1 & 0 & N_2 \end{bmatrix} \begin{Bmatrix} t_1(1) \\ t_2(1) \\ t_1(2) \\ t_2(2) \end{Bmatrix} \qquad (5.3)$$

Here $u_i(1)$, $t_i(1)$ refers to the displacement and traction at node 1 respectively.

5.2.2.2 Modelling

Since it is impractical to rely on the user to position the collocation points accurately at the Gauss points, this is done automatically in the computer program. The geometry of the continuum and the length and orientation of the segments is defined by the co-ordinates of the ends of the segment. In this respect, there is little difference between the conventional methods and the present Gauss-point segments, the intricacies being transparent to the user.

5.2.2.3 Prescribed loading

In much the same way that the geometry is specified by using the ends of the segment as a datum, the loading is similarily prescribed by using the segment extremeties. The required traction values at the Gauss-point nodes can be easily calculated by using the interpolation functions (5.2). The traction at the nodes (t(1) and t(2)) is expressed in terms of the end point values (t(a) and t(b)) by:

$$\begin{matrix} t(1) \\ t(2) \end{matrix} = \frac{1}{(N_1(-1)N_2(1) - N_2(-1)N_1(1))} \begin{bmatrix} N_2(1) & -N_2(-1) \\ -N_1(1) & N_1(-1) \end{bmatrix} \begin{Bmatrix} t(a) \\ t(b) \end{Bmatrix} \tag{5.4}$$

Evaluating the shape functions leads to the numerical equations for t(1) and (2):

$$t(1) = \frac{1.3660254\ t(a) + 0.3660254\ t(b)}{\sqrt{3}}$$

$$t(2) = \frac{0.3660250\ t(a) + 1.3660254\ t(b)}{\sqrt{3}} \tag{5.5}$$

These values are now used as the prescribed values but are once again, transparent to the user.

5.2.2.4 Displacement Boundary Conditions

For the purposes of this analysis, the boundary conditions, either displacement or traction, must be specified over the entire segment, Thus different boundary conditions can not exist over the same segment. For the displacement conditions end point values can easily be related to the Gauss-point nodes by using equation (5.5), with a substitution of u for t.

5.2.2.5 The BIEM algorithm

The development of the BIEM algorithm is precisely equivalent to that detailed earlier in chapter 4, the only difference being in the definition of the shape functions. Integration performed numerically over all segments which exclude the pivot node, and analytically for the segments which include the pivot node. The analytical integration parallels the previously discussed method for linear segments detailed in Appendix B. For completeness, a summary of the resulting integrals are given here, without resorting to the numerical tedium of the calculations. The same convention, as used previously is again used, with reference to figure 5.2.

Pivot node at 1:

$$G_{11}^{11} = \frac{L}{2A}\left[(B)\ (C - \ln L) + \cos^2\theta\right] \tag{5.6}$$

$$G_{12}^{11} = G_{21}^{11} = \frac{L}{2A}\cos\theta\sin\theta \tag{5.7}$$

$$G_{22}^{11} = \frac{L}{2A}\left[(B)\ (C - \ln L) + \sin^2\theta\right] \tag{5.8}$$

$$G_{11}^{12} = \frac{L}{2A}\left[(B)\ (D - \ln L) + \cos^2\theta\right] \tag{5.9}$$

$$G_{12}^{12} = G_{21}^{12} = \frac{L}{2A}\cos\theta\sin\theta \tag{5.10}$$

$$G_{22}^{12} = \frac{L}{2A}\left[(B)\ (D - \ln L) + \sin^2\theta\right] \tag{5.11}$$

Pivot node at 2:

$$G_{11}^{21} = \frac{L}{2A}\left[B\ (D - \ln L) + \cos^2\theta\right] \tag{5.12}$$

$$G_{12}^{21} = G_{21}^{21} = \frac{L}{2A}\cos\theta\sin\theta \tag{5.13}$$

$$G_{22}^{21} = \frac{L}{2A}\left[B\ (D - \ln L) + \sin^2\theta\right] \tag{5.14}$$

$$G_{11}^{22} = \frac{L}{2A}\left[B\ (C - \ln L) + \cos^2\theta\right] \tag{5.15}$$

$$G_{12}^{22} = G_{21}^{22} = \frac{L}{2A}\cos\theta\sin\theta \tag{5.16}$$

$$G_{22}^{22} = \frac{L}{2A}\left[B\ (C - \ln L) + \sin^2\theta\right] \tag{5.17}$$

where $A = \dfrac{1}{8\pi G(1-\nu)}$

$B = (3-4\nu)$

$C = 2.3958794$

$D = 0.63553374$

Since the Gauss-Point nodes are, by definition at a point where the normal is single-valued, the coefficient matrix c_{ij} is equal to $\frac{1}{2}\delta_{ij}$.

The construction of the matrices, the inclusion of the boundary conditions, system solution and the calculation of internal displacements and stresses are identical to the foregoing discussions.

o

5.2.2.6 An Example

In order to show the use of the Gauss-point segments and the effects that they have on the solution of an elastostatic problem, an infinite plate with a central circular hole under internal pressure was chosen as an example, figure 5.4:

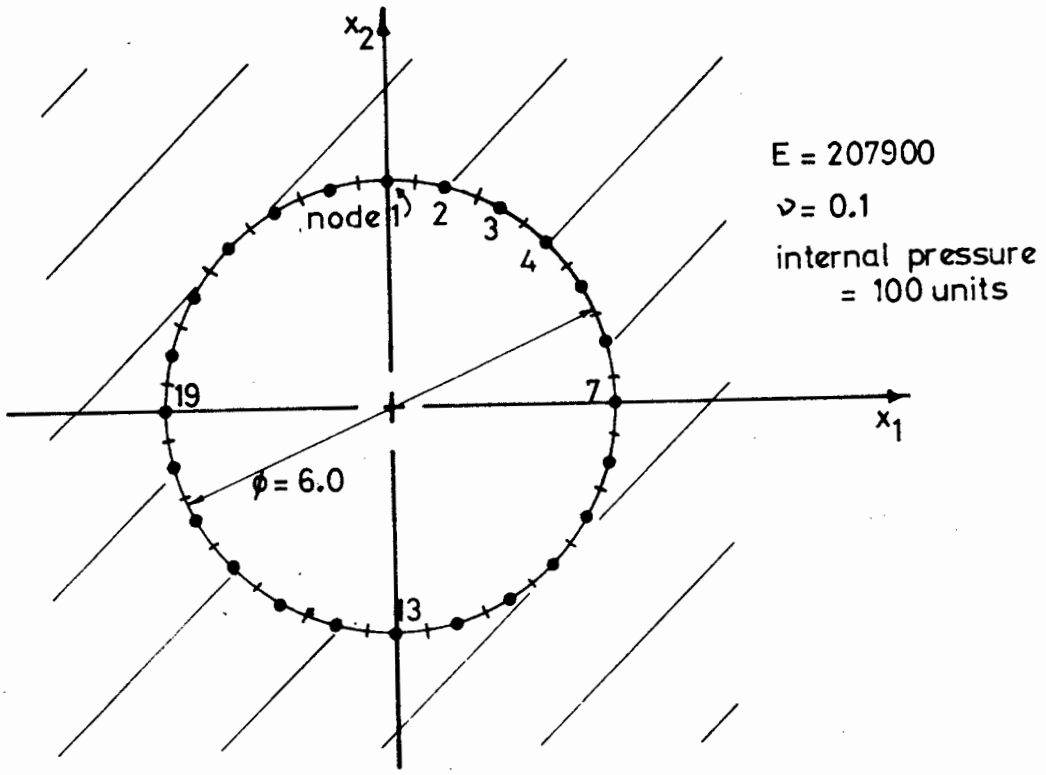

Figure 5.4 Infinite plate with circular hole under internal pressure

For comparison purposes, the boundary of the hole (diameter 6 units) was subdivided into 24 constant segments. Segments 12 and 13 are shown in figure 5.4. The results are compared to an analysis performed using 24 and 12 Gauss-point segments. The ends of these segments coincide with the node points indicated on the figure. In the case of the 24 Gauss-point segments, one segment would typically span between node 1 and node 2. For the 12 Gauss-point segments over the boundary, the end points of the first segment are nodes 1 and 3. The material properties were;

Young's Modulus E = 207900.0
Poisson's Ratio ν = 0.1

and the internal pressure was 100 units.

The calculated displacements in the x_1 and x_2 directions are plotted in figures 5.5 (24 Gauss-point segments) and 5.6 (12 Gauss-point segments).

5.2.2.7 Comment

The results obtained from the Gauss-point segment method show a marked "saw tooth" distribution which is fundamentally incorrect. The tractions are, in this case, prescribed at all the nodes but for other examples not documented here, a similar ragged distribution of both traction and displacement was noticed.

However, the average values of displacement over a Gauss-point segment compare very favourably with both the constant segment distribution and with the analytical solution, as can be seen in figures 5.5 and 5.6.

The result of this analysis, suggests that the positioning of the collocation points at the Gauss-points is not ideal, and should be adopted so that they are closer to the segment ends. This leads directly to the concept of the dual node which will be discussed in detail in section 5.2.5.

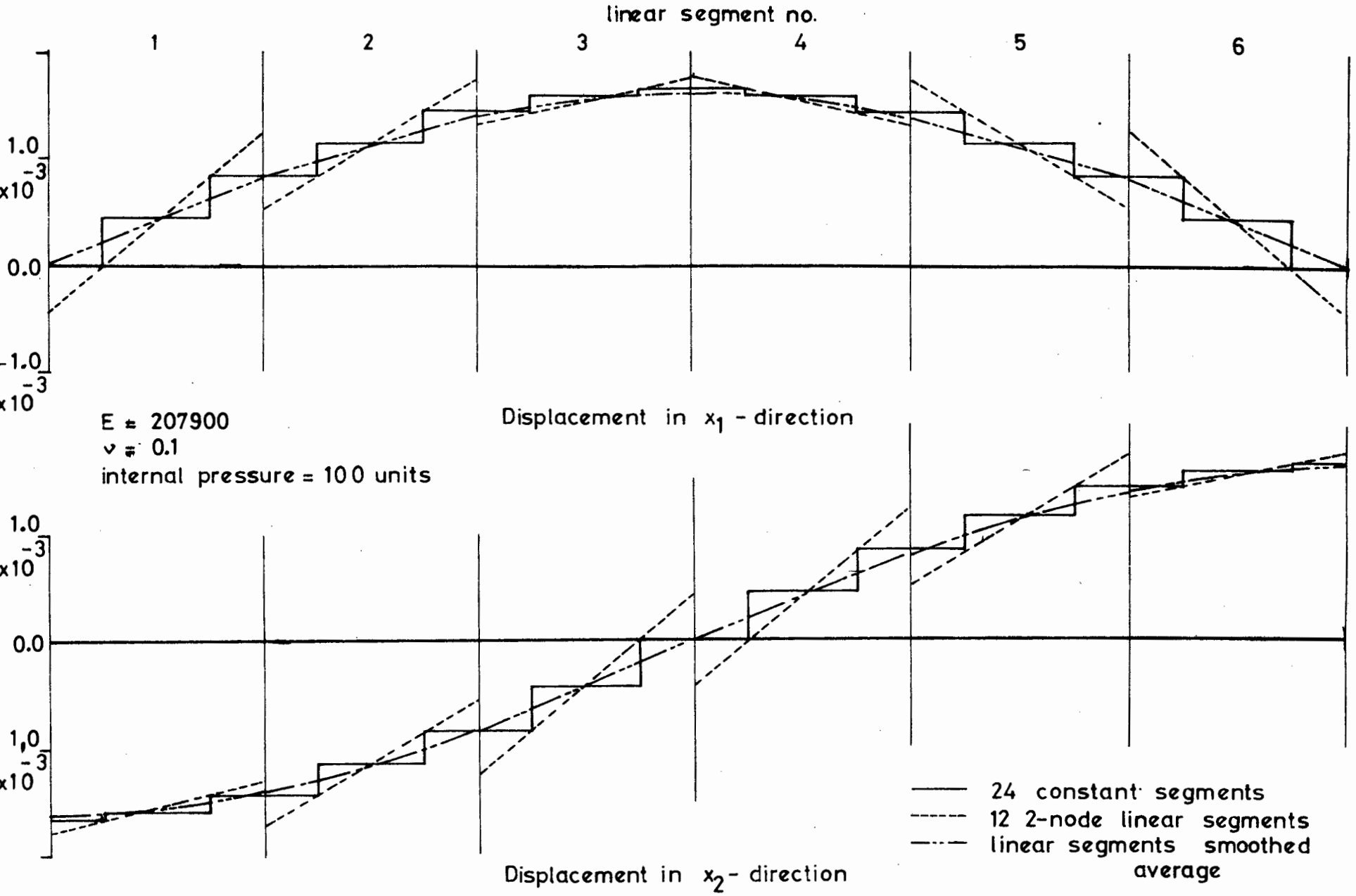

Figure 5.6 Infinite Plate with Central Circular Hole under 'Internal' Pressure

This analysis is not however superfluous since it shows that the principles of various interpolation schemes within the BIEM is possible, but in some cases, suspect. It is possible, therefore, that a more accurate and efficient method might be found in the future which ignores the shape function concepts and employs a radical, yet to be discovered, interpolation strategy.

5.2.3 The Approximate Traction Method [5.1]

In the previous section, and in the sections to follow, we recognize that the traction discontinuity problem exists. We attempt to solve it by adapting the numerical modelling procedure in order to take this into account, but, at the same time, ensuring that solution is as rigorous as possible by including all contributory variables. In this section, we also recognize the presence of the discontinuity, but attempt to solve it by introducing an approximation.

Before introducing the approximation, consider first the possible boundary conditions which can be present at, and in the vicinity of a corner node (refer figure 5.1):

(i) Tractions prescribed in 1 and 2 directions for segments A and B.

t_1^A, t_2^A, t_1^B, t_2^B, prescribed

u_1, u_2 unknown

(ii) Tractions prescribed in i-direction, displacements prescribed in j-direction for segments A and B.

t_i^A, t_i^B, u_j prescribed (i = 1 or 2, j = 2 or 1)

t_j^A, t_j^B, u_i unknown

(iii) Displacement prescribed in 1 and 2 directions.

u_1, u_2 prescribed

t_1^A, t_2^A, t_1^B, t_2^B unknown

The number of equations which are set up in the normal course of the BIEM is two for each node point, one for each co-ordinate direction. Consequently, the unique solution of only 2 unknowns per node can be accomplished. (A boundary value problem where the number of unknowns is equal to the number of known prescribed values is know as a 'well-posed' boundary value problem). Hence, for a unique, trouble free solution of the Boundary Integral equations, only two unknowns are allowed at each node.

Let us now analyse the three situations described above, and where applicable, apply an approximating assumption in order to adapt the BIEM for solution purposes.

(i) Since there are only two unknowns to be accounted for, this set of boundary conditions does not pose any particular problem. The prescribed values of traction relate directly to each individual segment and hence are taken into account separately during integration over that segment.

(ii) Three unique unknowns exist at the boundary node, two tractions and one displacement. Although the tractions are defined, classically, in terms of their separate normals, we now introduce the approximation $t_j^A = t_j^B = t_j$. Thus only two unknowns, t_j and u_i are present at the node and hence the solution can proceed. Disregarding the direction of the individual normals in this way, means, physically, that the boundary is 'rounded off' at the corner. When calculating the integrals over the segments, however, the actual normals are used. The contributions to the matrix equation from the two contiguous segments obtained from the integration, are then summed to give a single coefficient corresponding to the approximate traction t_j. Solution then continues as before, resulting in a numerical value for the conglomerate traction at the boundary node.

(iii) A more complex equivalent to (ii) is operative when only the displacements at a corner node are prescribed, but the method of procedure is precisely the same as discussed above. Now, a different approximation of tractions is used:

$$t_1^A = t_1^B = t_1 \quad \text{and} \quad t_2^A = t_2^B = t_2$$

The result and the interpretation in this case, is identical to the discussion in (ii) above and hence needs no further explanation.

This method has been used successfully for the examples given in chapter 4. As can be ascertained by a study of the quoted results, a very accurate representation compared with the exact solutions, is evident. However, in certain problems, anomalies arose when this method was used. In particular, the Horse-shoe beam gives erroneous results. This will be discussed later, after methods for the successful circumvention of these anomalies have been advanced in the following sections.

5.2.4 The Traction Discontinuity Equation Method

Considering points (ii) and (iii) of the previous section, it can be seen that if the matrix equations are derived explicitly in terms of the actual traction and displacement variables at the corner node, then a unique solution is not directly possible. If, however, a set of auxiliary equations can be found which link the independent traction variables at the node and these can be augmented into the existing matrices, then a viable unique solution method will have been found.

A set of auxiliary equations of this type is possible if the state of stress and strain in the vicinity of the node point is taken into account. The relationship between the tractions and displacements can be achieved by considering the invariance of the stress tensor and the invariance of the trace of the strain tensor. These extra equations (called Traction Discontinuity Equations) have also previously been discussed by Chaudonneret [5.2] and Wardle and Crotty [5.3].

Using the geometrical definitions of figure 5.7, the auxiliary

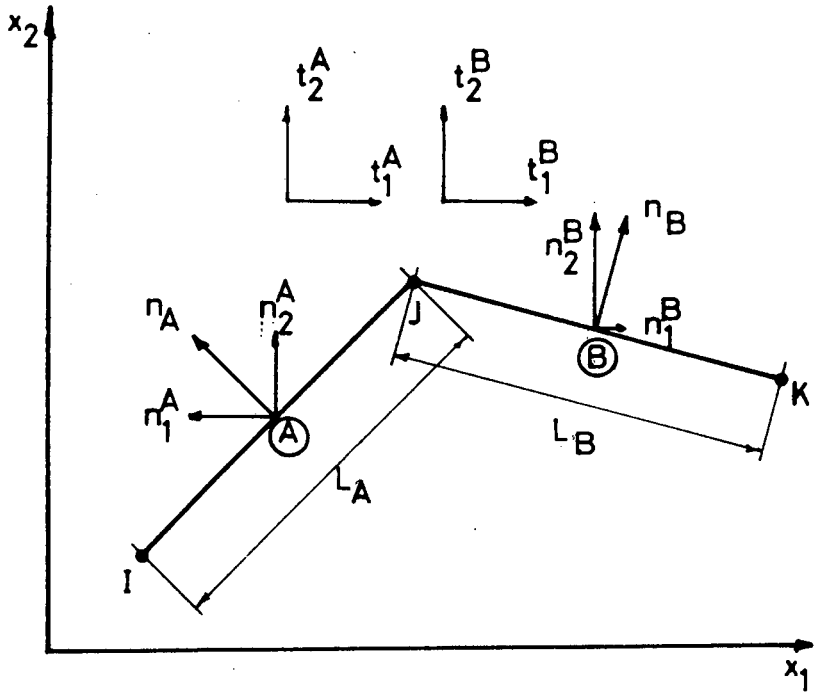

Figure 5.7 Geometric definitions at a corner node assuming linear interpolation

equations are:

(i) From the invariance of the stress tensor

$$n_1^A\, t_1^B - n_1^B\, t_1^A = n_2^B\, t_2^A - n_2^A\, t_2^B \tag{5.18}$$

(ii) From the invariance of the trace of the strain tensor

$$\begin{aligned} & t_1^B\, n_1^B + t_2^B\, n_2^B - t_1^A\, n_1^A - t_2^A\, n_2^A = \\ & 2\mu \left[\left(\frac{n_2^A}{L_A} + \frac{n_2^B}{L_B} \right) u_1(J) - \left(\frac{n_1^A}{L_A} + \frac{n_1^B}{L_B} \right) u_2(J) \right. \\ & \left. - \frac{n_2^A}{L_A}\, u_1(I) + \frac{n_1^A}{L_A}\, u_2(I) - \frac{n_2^B}{L_B}\, u_1(K) + \frac{n_1^B}{L_B}\, u_2(K) \right] \end{aligned} \tag{5.19}$$

where t and n are tractions and normals respectively

as defined by figure 5.7

L_A and L_B are the segment lengths

and $u_\ell(I)$, $u_\ell(J)$, $u_\ell(K)$ are the displacements at nodes I, J and K in the ℓ-co-ordinate direction

μ is the Lamé constant.

Equation (5.19) has been based on a linear variation of displacement between nodes I and J, and nodes J and K. This is ideal when used in conjunction with linearly interpolated segments, but represents only an approximation when used with quadratic segments. The correct procedure, in this case would be to employ the parabolic variations which uses all three nodes of the quadratic segments to define the discontinuity equation.

If the geometry for quadratic interpolation is defined as in figure 5.8, then the invariance of the trace of the strain tensor can be defined by equation (5.20). The details of the derivation are given in Appendix (D).

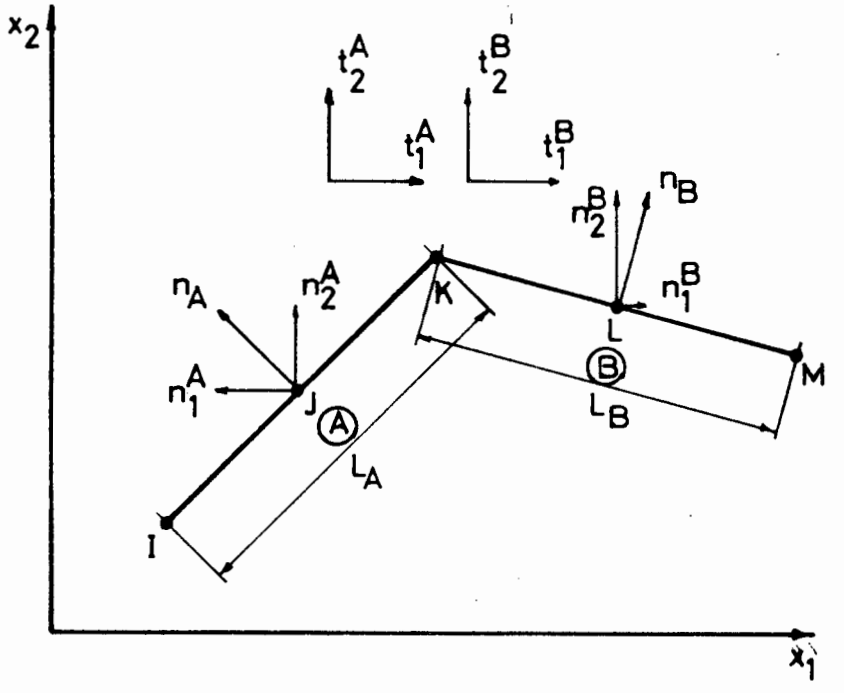

Figure 5.8 Geometric definitions at a corner node assuming quadratic interpolation

(ii) From the invariance of the trace of the strain tensor, using quadratic interpolation.

$$t_1^B n_1^B + t_2^B n_2^B - t_1^A n_1^A - t_2^A n_2^A =$$
$$2\mu \left[\frac{n_2^A}{L_A} u_1(I) - \frac{n_1^A}{L_A} u_2(I) - \frac{4n_2^A}{L_A} u_1(J) + \frac{4n_1^A}{L_A} u_2(J) \right.$$
$$+ \left(\frac{3n_2^A}{L_A} + \frac{3n_2^B}{L_B} \right) u_1(K) - \left(\frac{3n_1^A}{L_A} + \frac{3n_1^B}{L_B} \right) u_2(K)$$
$$\left. - \frac{4n_2^B}{L_B} u_1(L) + \frac{4n_1^B}{L_B} u_2(L) + \frac{n_2^B}{L_B} u_1(M) - \frac{n_1^B}{L_B} u_2(M) \right] \qquad (5.20)$$

The implementation of the auxiliary equations (5.18) and (5.19) or (5.20) is simple and they are easily slotted into the system matrices. At this stage however only the linear equation (5.19) has been programmed and used in both the linear and quadratic formulations. Consequently, a loss of accuracy can be expected when the quadratic interpolation scheme is used together with the traction discontinuity equations.

In the case of section 5.2.3 (ii), equation (5.18) is used and for section 5.2.3 (iii) both equations (5.18) and (5.19) or (5.20) are used. The equations are linearly independent of one another and thus cause no singularity effects on the matrix system.

5.2.5 The Dual-node Concept

In this section, we return to the concepts postulated for the Gauss-point segment, but, with some modifications, arrive at a method which requires nothing more than the conventional BIEM formulation.

The linear Gauss-point segment had its collocation points positioned at the Gauss points. This caused the solution to exhibit a saw tooth effect due to the discontinuity of both displacement and traction between segments. In order to eliminate this effect, the collocation points are placed at arbitrary points ε_1 and ε_2 from the ends of the

segment, as shown in figure 5.9.

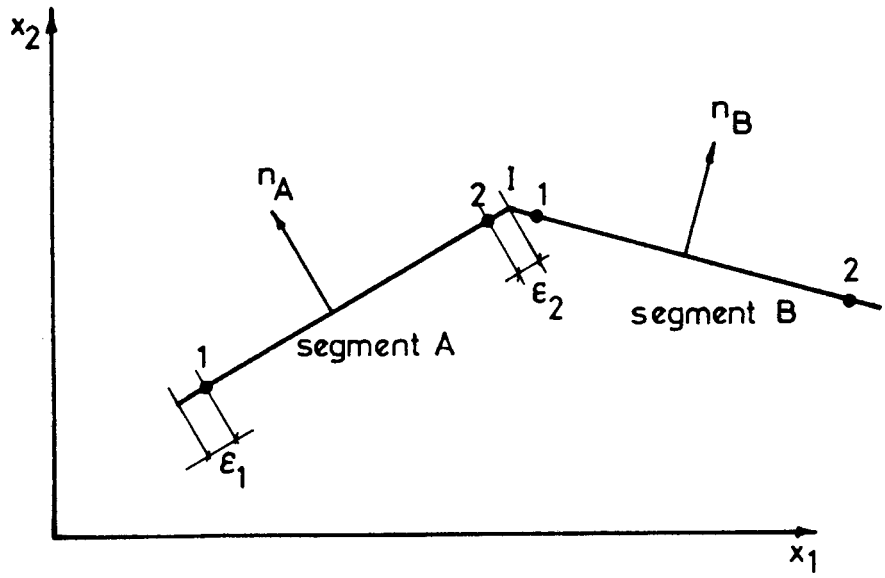

Figure 5.9 The Geometry of a variable node segment (linear interpolation)

The dimensions ε_1 and ε_2 can now be decreased progressively. In the limit, as ε_1 or ε_2 tends to zero, the original linearly interpolated element is re-established. The discussions in chapter 4 then, once again, become operative. However, the characteristic of the Gauss-point segment where the average number of nodes per segment are the whole boundary is two, is still applicable. In order to reduce this average, consider the situation at the intersection of the two segments, I (figure 5.9).

In the limit, node 2 of segment A and node 1 of segment B coincide geometrically. Provided that the normals n_A and n_B are equal, the variables of traction and displacement at the coincident position will be identical, due to the definition of the traction. Consequently, they can be coalesced to form a single node with the corresponding tractions and displacement components. The two nodes at the intersection point have been replaced by a single node.

Where n_A and n_B are not equal, the limit on ε_1 and ε_2 makes the nodes, once again, coincident at I. In this case,however, the contiguous tractions can not be combined. The nodes then remain indenpendent in terms of the solution variables but are superimposed for geometrical purposes.

This method does not lead to any confusion or singularity effects in the matrices since the normals are numerically different. The calculation of the integrals over each segment will therefore also be independent.

The advantage of this method is that a dual node is only necessary at corners. The average number of nodes per segment for linear interpolation will therefore only exceed one by a small amount. The matrices are therefore restricted and consequently computer solution times are decreased. The application of boundary conditions is also simplified, but yet more adaptable. Separate sets of boundary conditions can now be applied to each segment and each node individually in order to describe the actual state on the boundary.

The programming of this method is simple and includes all the ingredients of chapter 4. The only additional checks required are in respect of the discontinuity of the normal at the segment intersections and the consequent assignment of nodal variables. This, however, is performed internally in the computer program and is entirely transparent to the user.

The foregoing discussion has centeredon the linearly interpolated segment. The same reasoning is also applicable to the quadratic segments and leads to a similar programming conclusion.

The use and effectiveness of the dual node concept will be demonstrated in section 5.2.6 when a few pertinent examples are discussed.

5.2.6 Examples

In order to demonstrate the relative effectiveness of the

approximate traction method, the traction discontinuity method and the dual node concept, two examples have been chosen namely.

(a) The Horse-shoe beam and
(b) A simple uniaxial tension specimen.

As can be seen from the examples used in chapter 4, the majority of problems can be solved satisfactorily by using the approximate traction method in the solution algorithm. However, anomalous results have been observed in some cases, as in the horse-shoe beam analysis [5.1]. This section shows some of the anomalies which has been encountered during this research and also shows the effect of the more sophisticated traction discontinuity method and dual node concept on the results.

5.2.6.1 The Horse-shoe beam

In section 4.8.3 this example was discussed in the context of the application of the BIEM to bending problems. The approximate traction method was used to deal with the discontinuous tractions at the corners. It was found that the results which varied considerably, depend on the type of interpolation scheme employed and the quadrature order used. This example has been re-analysed using both the traction discontinuity method and the dual-node method. The results are given here.

The structure and boundary conditions are shown in figure 4.24. The modelling is identical to that used previously, with the exception that two nodes are specified at points B, C, E and F when the dual-node method is used. Both linear and quadratic segments were used in the analysis, while PAFEC 75 [5.8] provides the finite element verification of the results.

Figure 5.10 compares with results obtained from the two interpolation schemes, using 4 point quadrature, and the finite element method. The analytical result, based on flexural theory [5.9], is the datum. The graph is plotted to the same scale as figure 4.25 so that direct visual comparisons can be made.

The comparison of figure 5.10 with figure 4.25 reveals that there is little difference, in the example, between results obtained from the average traction method, the dual node method or the traction discontinuity equation method. All three solutions are well behaved and tend towards the finite element solution when the number of boundary segments is increased. It can therefore be concluded that, for this example, using the correctly formulated equations, the linear interpolation scheme is stable and reliable.

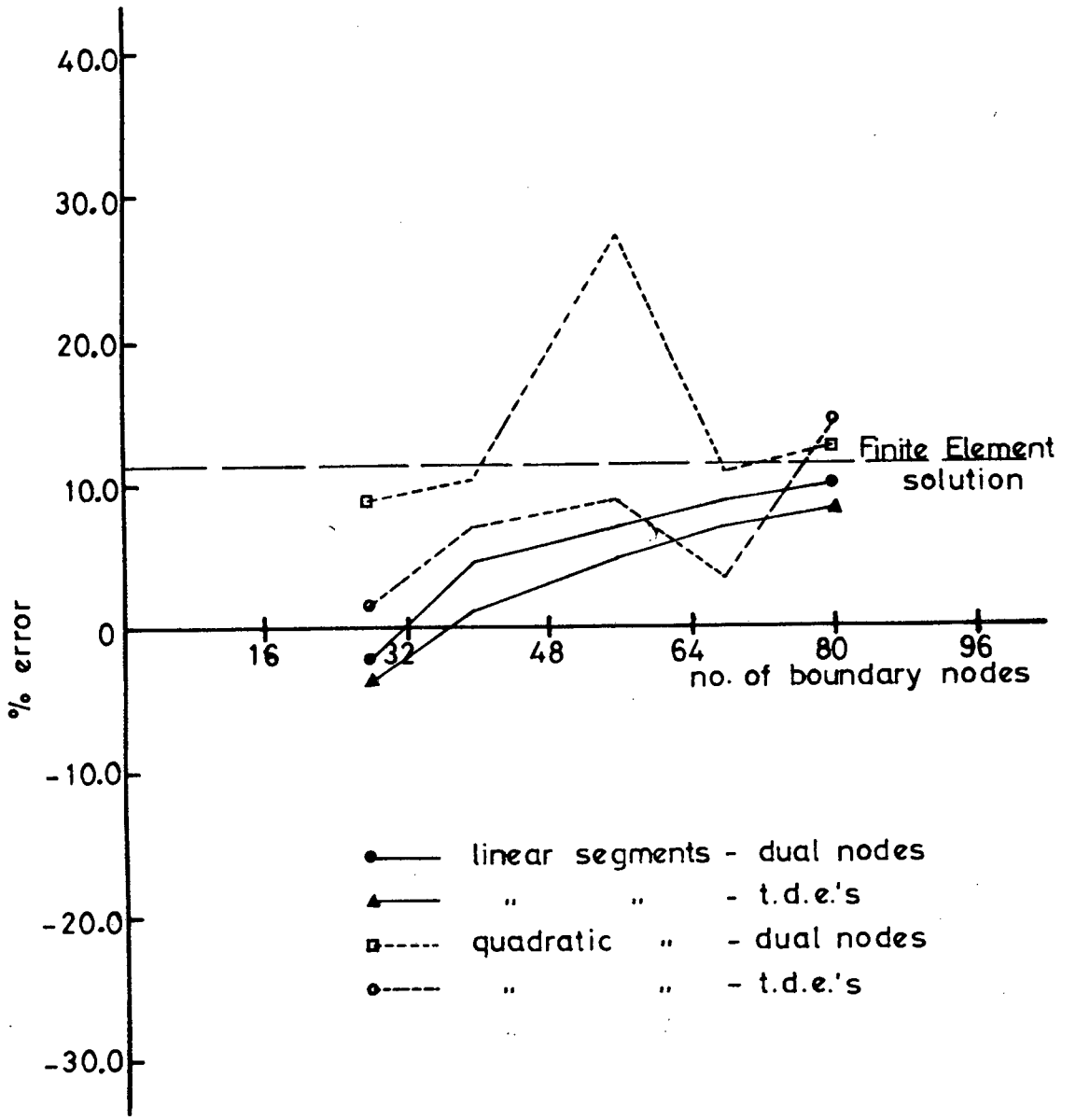

Figure 5.10 Comparison of accuracy vs number of boundary nodes for the horse-shoe beam

For the quadratic segments, the use of either the dual node method or the traction discontinuity equation method has to a large extent overcome the large inaccuraces that were present in the approximate traction formulation. However, both sets of results show an uncharacteristic kink as the number of boundary segments is increased. This is attributed to the combination of the following points;

(i) the calculation of the singular coefficients in the H_{ij} matrix for quadratic segments which involves the incorporation of the previously formulated linear equivalents;

(ii) the error in the numerical integration of the fundamental solutions over the segments. This is also discussed in section 5.5;

(iii) the use of the linear formulation of the traction discontinuity equations in the quadratic interpolation scheme.

The exact correlation between these factors and their effect on the solution method is not, at present, known. However, this topic is important and will become the subject for investigation in subsequent research projects.

Nevertheless, it is clear that both the dual node method and the traction discontinuity equation method are successful in counteracting a measure of the uncertainty in the results of problems where bending is, in particular, the major effect.

5.2.6.2 A simple uniaxial tension specimen [5.1]

The choice of this example is based on the fact that, when using the approximate traction method, large inaccuracies in the predicted displacement can occur under certain circumstances.

The model is a simple rectangular plate subjected to a uniaxial tension. One quarter of the plate is analysed, as shown in figure 5.11, where use is made of the two planes of symmetry present.

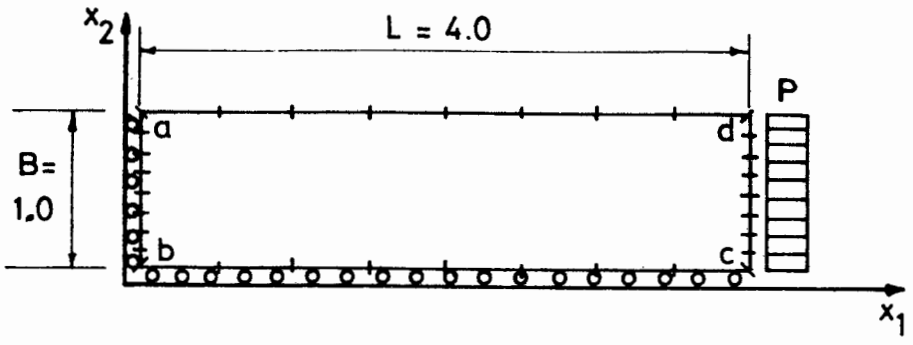

Figure 5.11 The geometry of a simple uniaxial tension specimen

The subdivision used in the model is also shown in figure 5.11. For constant and linear interpolation, 8 segments per side were used, and for quadratic interpolation, 4 segments per side were used. The actual number of segments specified, is however, of little importance since the inaccuracies are present irrespective of the boundary subdivision.

Other constants used in the analysis were:

Young's Modulus E = 400.0
Thickness t = 1.0
Uniaxial Force P = 10.0
Dimension LxB = 4.0 x 1.0 units

The displacement boundary conditions imposed where

side ab: u_1 = 0.0, u_2 free

side bc: u_1 free, u_2 = 0.0

The solution uses the approximate traction method to deal with

the traction discontinuities at the corner nodes a, b and c.

Certain factors influence the results obtained from this method. These include:

(a) the ratio of the length to the breadth of the specimen;
(b) the Poisson's Ratio assigned to the material;
(c) the numerical integration order used and
(d) the interpolation order used.

A combination of these four terms produces an instability in the system [5.1].

This instability is only present when the dimensions of the plate approach 1.0 units by 4.0 units and the Poisson's Ratio is in the range 0.25 to 0.35. Scaling the dimensions by a constant, results in stable and correct results for any value of Poisson's Ratio. The details of the analysis carried out using constant, linear and quadratic segments is given in figure 5.12 for varying Poisson's Ratios and plate dimensions 1.0 x 4.0 units. Three Gaussian integration orders were used in the analysis. The analytical solution which was used as a datum is given by

$$u_1 = \frac{PL}{AE} \tag{5.21}$$

For constant and quadratic interpolation, an increase in the Gauss integration order improves the results, but the spurious behaviour around $\nu = 0.3$ is still evident, but not as marked. However, for linear interpolation, the integration order has little effect on the results. Similar trends have also been found when using the program published by Brebbia [5.4] in which constant segments and 4 point Gaussian quadrature are used.

By contrast, the inclusion of either the dual node method or the traction discontinuity equation method substantially improves the results, although the spurious behaviour still occurs in some cases.

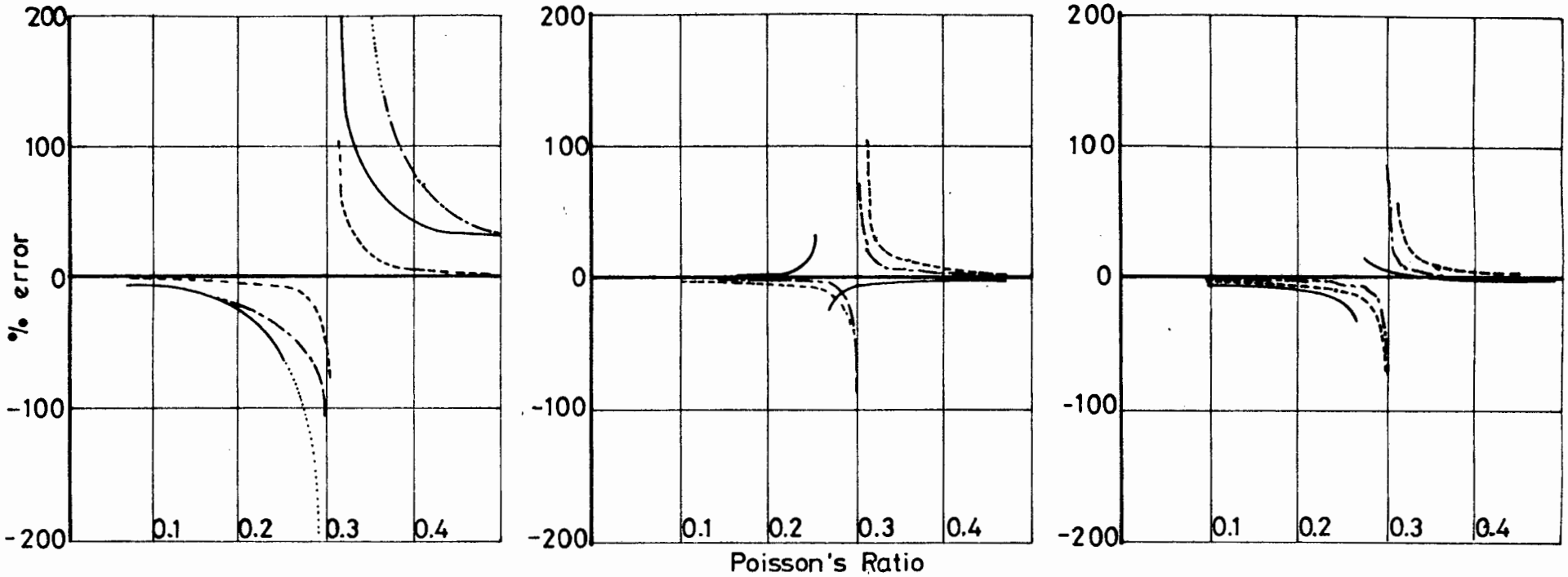

Figure 5.12 Simple uniaxial tension specimen plot of % error versus Poisson's Ratio for 2, 4 and 6 point Gauss Integration

In table 5.1 the results for a range of Poisson's Ratios using 4 point Gauss Quadrature are given. Linear and quadratic interpolation schemes were used and the results for both the dual-node method and traction discontinuity equations are presented.

Poisson's Ratio ν	Linear Segments		Quadratic Segments	
	TDE	DUAL	TDE	DUAL
0.1	0.0099932	0.0099807	0.010004	0.010014
0.3	0.009993	0.0090097	0.011149	0.016118
0.33	0.010002	0.010360	0.009649	0.0099830

Table 5.1 End displacement of a uniaxial tension specimen

From this comparison, it is clear that the traction discontinuity equations are best able to overcome the singularity problem. For linear segments, for example, only a slight perturbation in the vicinity of $\nu = 0.3$ is noticed. The quadratic segments show more variations in this region and is ascribed to the same factors as discussed in section 5.2.6.1.

Although the analysis using the dual-node method gives very accurate results in general, the perturbations are still evident when ν approaches 0.3. At this stage, no clear reason for the spurious behaviour or a true solution to the problem has been found.* Further research into this area is needed, but until an explanation to this phenomenon is found, it is suggested that for homogeneous bodies, the traction discontinuity equation method should be used. It will be seen later, however, that for non-homogeneous bodies, this method is not ideal since some of the relevant parameters are omitted. In this case, the dual node method, which is termed the multi-node method in these problems is used to give very accurate and reliable results.

* With regard to the spurious behaviour exhibited here, some light will be shed on the subject in section 5.5 where singularities in the fundamental numerical integration are found.

5.3 Body Forces

In chapter 3, it was shown theoretically that the body force can be represented by a boundary integral although it appears in the original boundary integral equation as a domain integral. The analyst now has a choice of method for the calculation of this term. Hence, the question of the effectiveness of the two methods arises. This section shows the comparison between the domain calculations and the boundary calculations and presents a numerical example for scrutiny. Firstly, however, the strategies of the two methods are discussed briefly.

5.3.1 Domain Integration

The effect of body forces at a node x in the i-co-ordinate direction is given by equation (3.60) as:

$$B_i(x) = \int_{\Omega} b_j(z)\, U_{ij}(x,z)\, d\Omega \qquad (5.22)$$

This equation represents the integration over the entire structural domain of the product of the unit weight b_j and the displacement fundamental solution, U_{ij}. Exact analytical integration is only possible, therefore, for very simple geometrical domain shapes and consequently, a numerically technique is once again used.

The domain Ω can now be divided into number of cells Ω_r so that

$$\Omega = \sum_{r=1}^{R} \Omega_r \qquad (5.23)$$

thus allowing the body force term to be written

$$B_i(x) = \sum_{r=1}^{R} \int_{\Omega_r} b_j(z)\, U_{ij}(x,z)\, d\Omega \qquad (5.24)$$

The cell shape is now chosen so that expression (5.24) can be integrated by numerical Gauss quadrature. The most convenient shape is therefore the quadrilateral which is defined in a similar way to the quadrilateral element used in the Finite Element Method [5.5, 5.6]. The Gauss points for two dimensional integration are defined in terms of the cell local co-ordinates and integration procedures as in the FEM with the term $b_j(z)\ U_{ij}(x,z)$ being evaluated at the Gauss points. At least four evaluations (2x2 integration) of the term are required in this method. For a large number of cells the calculation time would be excessive and consequently a far simpler method of integration was used.

The quadrilateral cells are divided diagonally into 2 triangular cells as in figure 5.13. The variation in the integral is assumed to be constant within the triangle and is calculated at it's centre of area. The body force integral is then:

$$B_i(x) = \sum_{r=1}^{R} A_r b_j(z)\ U_{ij}(x,z) \qquad (5.25)$$

where R is the total number of triangular cells and

A_r is the area of the triangular cell

z is the co-ordinates of the centre of area of cell r.

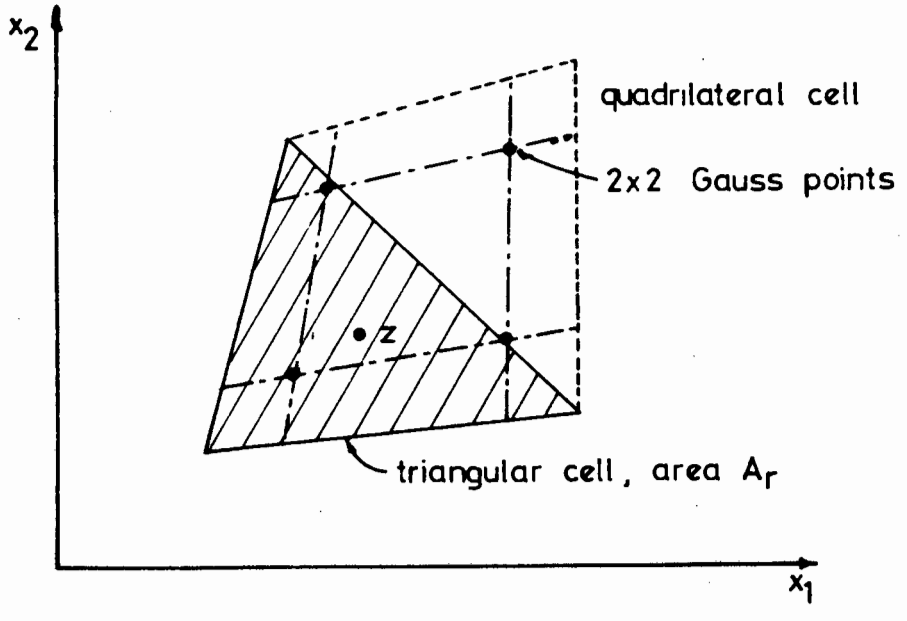

Figure 5.13 A typical internal cell

This method is simple and easy to implement in existing computer programs. Since only half the number of term evaluations are required compared with the quadrilateral scheme, but naturally the accuracy is adversely affected. Nevertheless, this simple method remains the basis of all comparisons involving the body force term.

A particular disadvantage in using this method is that the domain must now be subdivided into cells in much the same way as in the FEM. Although automatic generation of the cells is available and is used in the computer programs the original idea of a domain-free solution method is obscured. For this reason, the purely boundary related body force method was developed.

5.3.2 Boundary Integration

A method whereby only the boundaries, and hence the existing boundary subdivision, are used to evaluate the body force term has been given by [5.7] and alluded to in chapter 3. The body force term $B_i(x)$ by using the boundary integration technique of section (3.4.3), is given by reiterating equation (3.6.4).

$$B_i(x) = \frac{1+\nu}{4\pi E} \int_{\Gamma} r(2\ln\frac{1}{r} - 1)\{b_i n_m r_{,m} - \frac{n_i b_m r_{,m}}{2(1-\nu)}\} d\Gamma \qquad (5.26)$$

This formula has been based on the Galerkin tensor formulation of the fundamental solutions. As such, if equation (5.26) is to be used in the augmented BIEM statement, then the fundamental solutions used in equation (3.58) must also be formulated using this method. Hence equation (3.52) must be used in preference to (3.47) in this case. Ignorance of this fact will lead to erroneous answers when body forces are included in the analysis.

The numerical adaption of (5.26) follows the normal trends in which the boundary is subdivided into the previously assigned segments Γ_k. Unfortunately, the singularity as r approaches zero is still present in the formulation and hence integration over Γ_k takes two forms.

(i) when $x \notin \Gamma_k$, i.e. when the pivot node x is not a node on the focus segment, then the integration is performed numerical by Gaussian Quadrature as previously discussed;

(ii) when $x \in \Gamma_k$, i.e. when the pivot node x is one of the nodes on the focus segment, then the integration is performed analytically. The integration is performed in the same way as detailed previously for the pivot segments in section 4.5.1 and Appendices B and C. Geometrically, integration is performed over the region 0 to R as shown in figure 5.14.

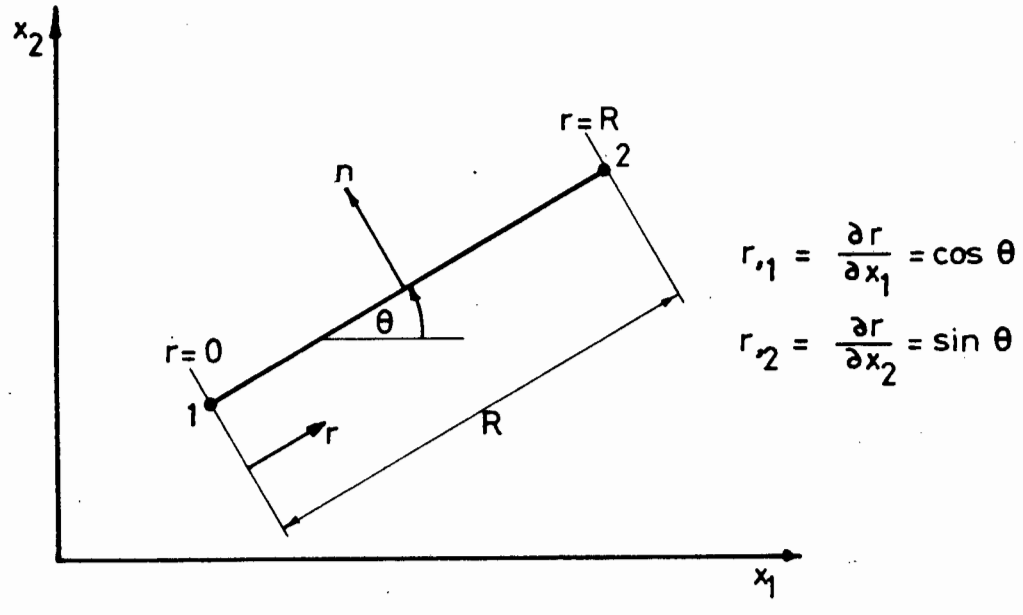

Figure 5.14 Geometrical definition for the intergration of the Body force term

The body force term is then defined by

$$B_i(x) = \frac{1+\nu}{4\pi E} \int_0^R (\text{integrand})\, dr \qquad (5.27)$$

Now b_m, n_m and $r_{,m}$ are constants since

$$r_{,1} = \frac{\partial r}{\partial x_1} = \cos\theta$$

and $$r_{,2} = \frac{\partial r}{\partial x_2} = \sin\theta$$

Therefore, in the limit,

$$B_i(x) = \lim_{\varepsilon \to 0} C \int_{\varepsilon}^{R} (2r \ln \frac{1}{r} - r)\, dr \qquad (5.28)$$

where C = the accumulated constant expressions.

Having performed the integration, in the limit:

$$B_i(x) = \frac{1+\nu}{4\pi E} R^2 \ln \frac{1}{R} \{b_i(n_1 \cos\theta + n_2 \sin\theta) - \frac{n_i}{2(1-\nu)} (b_1 \cos\theta + b_2 \sin\theta)\} \qquad (5.29)$$

The integration using node 2 as the pivot is identical to the above, with the angle θ being defined by the new direction of r (i.e. from node 2 to node 1).

It can be seen from this analysis that the single equation (5.29) can be used with all types of segments, be they constant, linear of quadratic. The dependence is only on the dimension R, and not on the shape functions which was the case in the previously discussed pivot segments.

Once again, this method is simple and easily programmed. The advantage is that no extra data, besides the unit weight of the material, is required for body force calculations. The existing boundary segments are used as a template for the evaluations. Once the integrations have been performed over the entire boundary, the two component values of the body force $B_1(x)$ and $B_2(x)$ for the pivot node x can be slotted into the matrix equation (4.5) prior to solution.

5.3.3 An example: A deep cantilever subjected to body forces only.

The analysis of deep cantilever has been chosen to illustrate the relative difference between the two methods of dealing with the body forces acting on a body. There are two major reasons for the choice of this type of problem. Firstly, the simplicity of the geometry, the boundary conditions and the material properties are such that few complications can arise which may overshadow the goals of this section. Secondly, the performance of the methods will be tested to the utmost since it has previously been found that for problems where bending is the primary function, inaccuracies can occur. For these reasons, a simple, yet testing problem has been chosed.

The geometry of the deep cantilever is shown in figure 5.15. The length and breadth dimensions are 4.0 by 2.0. The material constants used are as follows:

Young's Modulus $E = 100000.0$

Poisson's Ratio $\nu = 0.3$

Density $\gamma = 100$

Gravitation constant $g = -9.81$ in x_2 direction

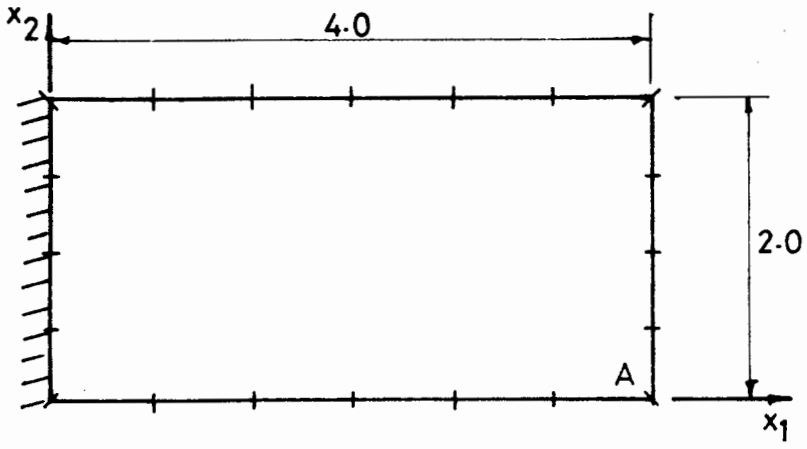

Figure 5.15 Deep Contilever subjected to body forces

In total, 20 quadratic segments were used to model the structure: 6 segments on the length-wise boundary, and 4 segments on the breadth. The dual node method was used to model the tractions in the corners. A

number of different layouts of internal cells was used in order that comparisons might be made, while the boundary integration method made use of the boundary segments as described above.

As a verification of the results, a finite element analysis using PAFEC 75 [5.8] was performed with a mesh of 6 by 4 8-noded quadrilaterals. In all cases, plane stress conditions were assumed.

The horizontal and vertical displacement of point obtained from the finite element solution are:

$$u_1 = -0.3126$$
$$u_2 = -1.1658$$

These values are used as a datum in figure 5.16, where the displacements predicted by the BIEM are presented. A comparison is made between the results from the boundary integration method and results domain integration for a number of different internal cell arrangements.

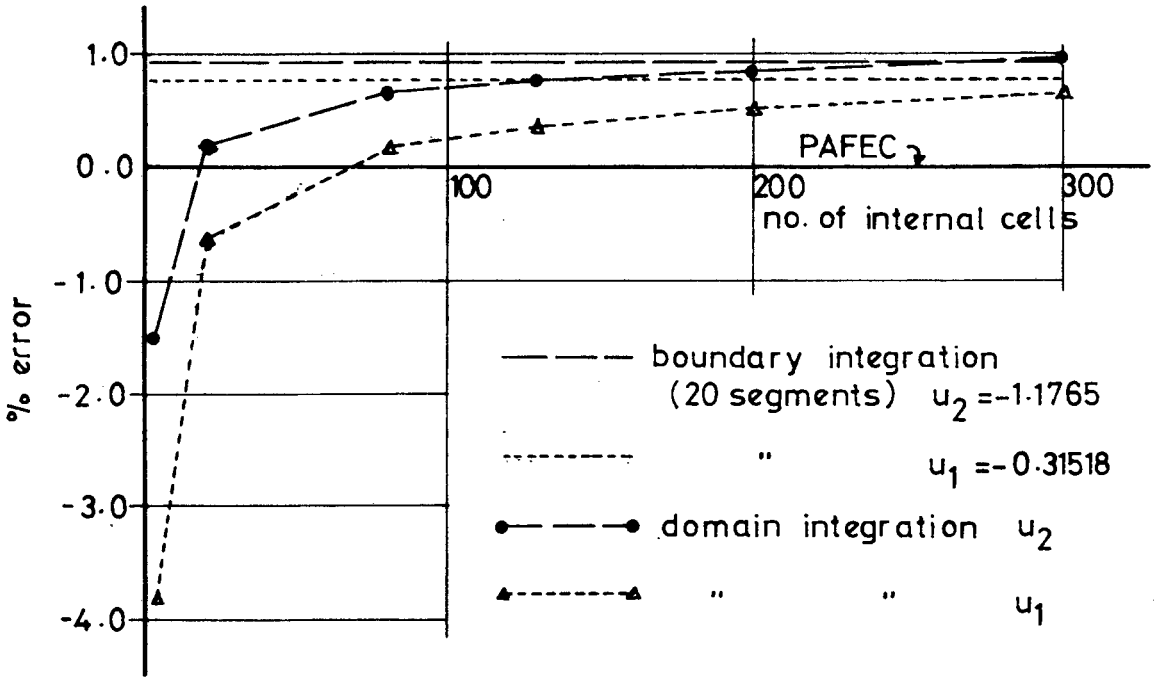

Figure 5.16 Comparison of accuracy of body force calculations by boundary integration and domain integration

The relative computer CPU times taken to perform each of these analysis given in figure 5.17.

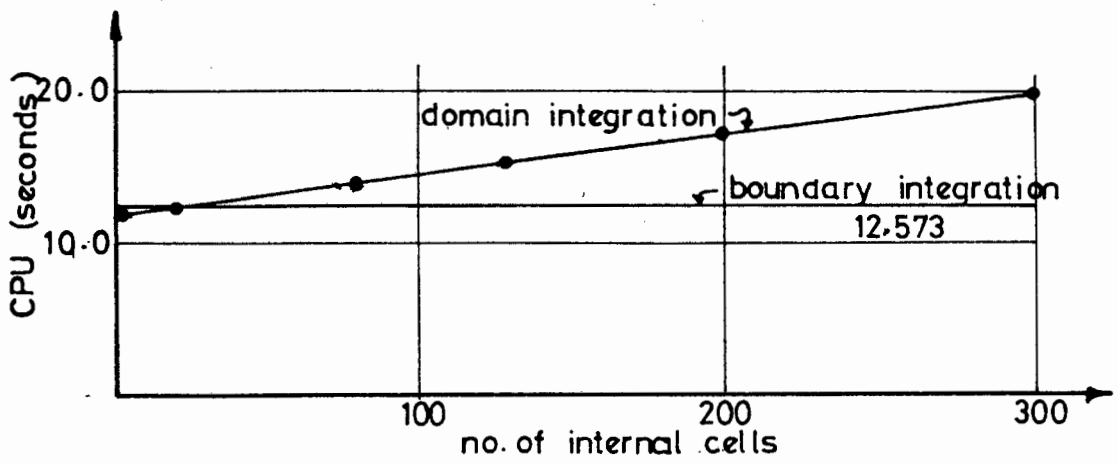

Figure 5.17 Comparison of Computer CPU time for boundary and domain integration

These results show that both the boundary integration method and the domain integration method predict very accurately the affects of gravitational loading. The results differ from an equivalent finite element analysis by less than 1.0% in all significant cases (i.e., for more than 50 internal cells). Hence, a considerable amount of confidence in the reliability of similar analyses can be assumed.

The increase in computational CPU time with an increase in the number of cells is linear for all practical purposes. This raises the question as to the number of internal cells required for an analysis. Naturally, this is virtually impossible to predict, and hence it is suggested that this method should be discarded in favour of the boundary integration method. Accuracy is then guaranteed and depends only on the boundary subdivision. Also, no extra data is required for the analysis, thus making the boundary integration method for the calculation of body forces the obvious and most practical choice.

5.4 The Asymmetrical Matrices of the BIEM

The attractiveness of the BIEM would be substantially enhanced if the matrices produced in the method were symmetric and banded. This would drastically decrease the computer cost overheads involved in calculating the coefficients in the matrices and solving the system of equations. A banded matrix can be obtained by subdividing the domain into subregions (chapter 6) and by numbering the boundary segments carefully. However, with the current formulation, a symmetric matrix is not possible. This section traces the requirements for a symmetric set of equations, as is present in the FEM, and analyses the BIEM to discover why symmetric matrices are unlikely to appear without considerable post processing.

5.4.1 The requirement for a symmetrical matrix

In section 3.3.7 the derivation of the FEM was shown so that a comparison between the methods could be undertaken. We now return to that derivation with the express purpose of specifying the ingredients for the production of a symmetric matrix.

The equation can be written in general form, since only the major trends are required in this discussion.

The general form of the equilibrium equation can be expressed as:

$$ku'' + b = 0 \quad \text{on} \quad \Omega \tag{5.30}$$

when k is constant of proportionality and b are the body forces and u'' represents the second derivative of u. Equation (5.30) is subjected to the boundary conditions

$$\bar{u} - u = 0 \text{ on } \Gamma_1 \tag{5.31a}$$

and

$$\bar{t} - t = 0 \text{ on } \Gamma_2 \tag{5.31b}$$

By combining (5.30) and the non-essential boundary conditions (5.31b) in a weighted residual statement, the necessary ingredients for the development of the FEM are provided. With v being a weighting function and with the body force b neglected, the integration by parts of the domain gives

$$- \int_{\Omega} ku'v' \, d\Omega + \int_{\Gamma} tv d\Gamma = 0 \qquad (5.32)$$

where u' denotes the derivative of u.

Operations now take place on the domain integral. Both u and v are interpolated using the same basis functions of the form:

$$u = \sum_{i=1}^{e} N_i u_i$$

$$v = \sum_{i=1}^{e} N_i v_i \qquad (5.33)$$

Since v_i is arbitrary the substitution of (5.33) into (5.32) gives

$$k\left\{\int_{\Omega_e} N_i' N_j'\right\} d\Omega \; u_i = \int_{\Gamma_e} N_j t d\Gamma \qquad (5.34)$$

where i and j represent the contributions of u and v respectively over an element Ω_e. The right hand side of (5.34) is a vector. Since N_i and N_j have been chosen to be identical, the integral on the left hand side of (5.34) ensures that the resulting matrix K_{ij} over Ω_e is symmetric. The property of the functions which satisfy the above condition is one of square-integrable first derivatives which will always result in symmetric matrices since i and j are interchangeable.

5.4.2 The BIEM equations

The BIEM can be investigated in a similar manner by including both essential and non-essential boundary conditions in the Weighted Residual statement. The essential boundary conditions are included by

using the Lagrange Multiplier technique which is proportional to the derivatives of the weighting function, i.e. v'.

After integrating the domain integral by parts twice (see section 3.3.8 for details) the following equation results:

$$\int_{\Omega} k\, v''u\, d\Omega + \int_{\Gamma_1} tv d\Gamma + \int_{\Gamma_2} \bar{t}\, v d\Gamma - \int_{\Gamma_1} \bar{u} v' d\Gamma$$

$$- \int_{\Gamma_2} uv' d = 0 \qquad (5.35)$$

The domain integral now appears as the weighted equilibrium equation, with the roles of u and v reversed. The following step in the process differ considerable from the FEM. Whereas both u and v were described by the same basis functions in the FEM, a specific meaning is given to the weighting function v in the BIEM. v must be chosen so that

$$kv'' + \delta_{\ell}^{k} = 0 \qquad (5.36)$$

thus causing the domain integral to vanish. The choice of v as the fundamental solution of the Kelvin problem, effectively limits the arbitrariness of the allowable basis functions used in the numerical procedure. This results in the form

$$-u + \int_{\Gamma_1} tv d\Gamma + \int_{\Gamma_2} \bar{t} v d\Gamma - \int_{\Gamma_1} \bar{u} v' d\Gamma - \int_{\Gamma_2} uv' d\Gamma = 0 \qquad (5.37)$$

where v and v' are prescribed.

The numerical method only allows for t and u to be interpolated using basis functions. The substitution of these functions into (5.37) results in terms such as

$$\{\int N_i\, v\, d\Gamma\}t \quad \text{and} \quad \{\int N_i\, v' d\Gamma\}u \qquad (5.38)$$

which show no square integrability of the integrands. The only hope of symmetry is in the definition of v and v' which are respectively $U_{ij}(x,y)$ and $T_{ij}(x,y)$, the fundamental displacement and traction solutions. For symmetric values therefore the integrals

$$\int_{\Gamma_y} U_{ij}(x,y)\,d\Gamma = \int_{\Gamma_x} U_{ji}(y,x)\,d\Gamma \qquad (5.39)$$

where Γ_y and Γ_x are the focus segments, with x and y respectively the pivot nodes.

A similar equation is required for symmetry of the traction values.

5.4.3 The asymmetry of the fundamental solutions

Equation (5.39) and its traction counterpart are in general not true. Only under very stringent conditions is it possible to ensure that (5.39) is true for two isolated segments. It is impossible to ensure this relationship on a one to one relationship basis between all the segments in a practical problem.

This situation can be adequately demonstrated by considering two arbitrary segments and by showing that, in general, equation (5.39) is not feasible. Consider two segments as defined in figure 5.18.

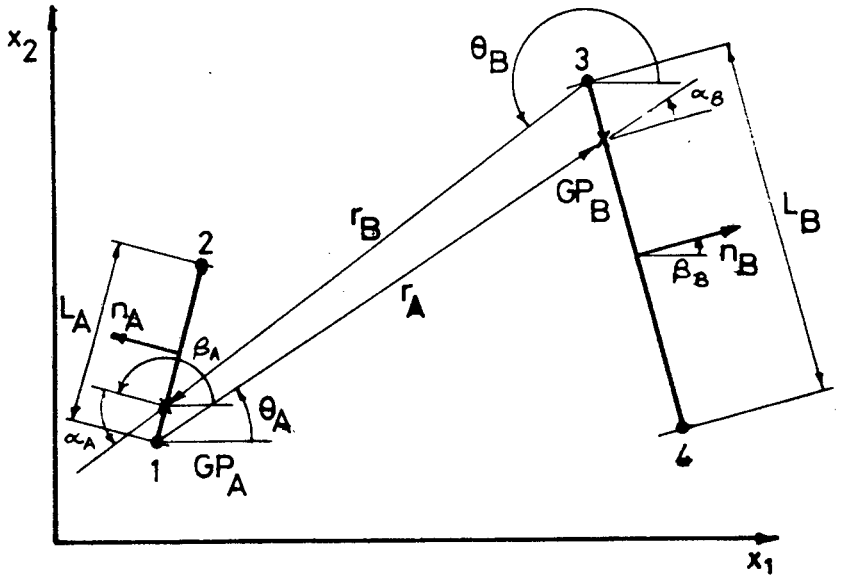

Figure 5.18 Two arbitrary segments - geometric definitions

5.4.3.1 The Displacement Fundamental Solution

The asymmetry of (5.39) is demonstrated by considering nodes 1 and 3 as the pivot nodes and segments B and A respectively as the focus segment. The integrals are then defined by a single Gauss point on each segment:

$$I_{ij}^{13} = \frac{L_B}{2}\left[\sum_{GP_B} N_3(GP_B)\ U_{ij}(1,GP_B)\right] = \text{LHS(5.39)} \qquad (5.40a)$$

and

$$I_{ji}^{31} = \frac{L_A}{2}\left[\sum_{GP_A} N_1(GP_A)\ U_{ji}(3,GP_A)\right] = \text{RHS(5.39)} \qquad (5.40b)$$

where for I_{mn}^{MN}, $N_N(GP)$ and $U_{mn}(M,GP)$,

M is the pivot node
N is the node on the focus segment
m and n are the co-ordinate directions corresponding to node M and N under consideration
and GP is the Gauss Point.

Now, consider the calculations to be performed to evaluate (5.40a) and (5.40b), assuming that GP_A and GP_B are located at the same local co-ordinate point on their respective segments. Then

$$N_3(GP_B) = N_1(GP_A)$$

but $$U_{ij}(1,GP_B) \neq U_{ji}(3,GP_A)$$

since

$$U_{mn} = \frac{1}{8\pi G(1-\nu)}\left[(3-4\nu)\ \ln\frac{1}{r}\ \delta_{mn} + \frac{\partial r}{\partial x_m}\ \frac{\partial r}{\partial x_n}\right] = f(r,\theta)$$

where $$\frac{\partial r}{\partial x_m}\ ;\ \frac{\partial r}{\partial x_n} = f(\theta) \qquad (5.41)$$

and $L_A \neq L_B$

$r_A \neq r_B$

$\theta_A \neq \theta_B$ for all values of i, j in general.

It would be noted here, that the nodal numbering system implemented, is as shown in figure 5.18 : clockwise node numbering with respect to the outward normal. By so doing, it is only possible to achieve equality between U_{mn} for segments A and B if nodes 1 and 4 coincide and nodes 2 and 3 coincide. This is impractical since it means that segments A and B are superimposed, thus in general it can be stated that, once the summation over all Gauss points has been performed:

$$\int_{\Gamma_y} U_{ij}(x,y)\, d\Gamma \neq \int_{\Gamma_x} U_{ji}(y,x)\, d\Gamma \qquad (5.42)$$

5.4.3.2 The Traction Fundamental Solution

A comparable analysis to show the asymmetry of the traction fundamental solution can also be performed. Consider T_{ij} by writing

$$T_{ij}(x,y) = C_1 \frac{1}{r}\left[\frac{\partial r}{\partial n}\{C_2\,\delta_{ij} + 2\frac{\partial r}{\partial x_i}\frac{\partial r}{\partial x_j} - C_2\left(\frac{\partial r}{\partial x_j}n_i - \frac{\partial r}{\partial x_i}n_j\right)\right]$$

$$= C_1\, a\, b\,\{C_2\,\delta_{ij} + c - C_2(d) \qquad (5.42a)$$

where locally $a = \frac{1}{r}$

$b = \frac{\partial r}{\partial n}$

$c = 2\frac{\partial r}{\partial x_i}\frac{\partial r}{\partial x_j}$

and $d = \frac{\partial r}{\partial x_j}n_i - \frac{\partial r}{\partial x_i}n_j$

These expressions can be translated geometrically as in figure 5.18 for 2 arbitrary segments.

The expressions used in (5.42a) can therefore be defined as follows:

$$a = f(r)$$
$$b = f(\alpha) = f(\theta,\beta)$$
$$c = f(\theta)$$
$$d = f(\theta,\beta)$$

Consequently,

$$T_{ij}(x,y) = f(r,\theta,\beta)$$

If the integration that must take place over the segments is now considered it will be seen, in general, that

$$L_A \neq L_B$$
$$r_A \neq r_B$$
$$\theta_A \neq \theta_B$$
and $$\beta_A \neq \beta_B \quad \text{for all values of } i,j.$$

This set of inequalities is even more stringent than those for the displacement fundamental solution. Here, in order to obtain the necessary symmetry, the direction of the normal (β) must be the same for both segments, in addition to the other parameters (L_A, r and θ) it can be stated that, once the summation over all Gauss points has been performed.

$$\int_{\Gamma_y} T_{ij}(x,y)d\Gamma \neq \int_{\Gamma_x} T_{ji}(y,x)d\Gamma \qquad (5.43)$$

5.4.3.3 Summary

The factors which influence the calculation of the integrals over the segments in which U_{ij} and T_{ij} are involved are:

(i) The distance from the pivot node to the Gauss point on the pivot segment, i.e., the distance r

(ii) The orientation of the focus segment with respect to the pivot node within the co-ordinate system, i.e., the angle θ.

(iii) The orientation of the focus segment with respect to the co-ordinate system. This is defined by the direction of the outward normal to the segment and is denoted β.

(iv) The orientation of the focus segment with respect to the vector joining the pivot node and the Gauss point, i.e., the angle α. This angle can be derived from the orientation of the focus segment normal β and the angle θ.

These 4 factors form a rigid set of conditions which are insurmountable when attempting to design a symmetrical set of matrices with the current numerical technique. In addition to these conditions, the application of the structural boundary conditions to form the matrix equation (4.7) also has a disruptive effect on the conditioning of the matrix. Having considered all these facts, it is clear that a symmetric form of the equation will not be produced without considerable theoretical and numerical changes and enhancements.

5.5 The Inherent Error in Numerical Integration

5.5.1 Background and Method of Analysis

The displacement and traction fundamental solutions contain the functions $\ln \frac{1}{r}$ and $\frac{1}{r}$ respectively which are singular as r approaches zero. In the vicinity of this singularity, numerical integration of the functions is inaccurate. This occurs over segments which contain the pivot node and hence the dimension r reaches zero during integration. Consequently, all the necessary integration has been performed analytically in these situations. This has been detailed in section 4.5 and Appendices B and C for constant, linear and quadratic interpolation schemes.

Considering this situation, the question of the applicability and suitability of numerical Gaussian quadrature for the integration

over the other boundary segments now arises. In the programming, 2, 4 and 6 point schemes have been used. It is the purpose of this section to investigate the errors which exist between the "exact" theoretical integration of the functions and the numerical integration for the three interpolation schemes.

For this purpose, the singular functions $\ln \frac{1}{r}$ and $\frac{1}{r}$ are extracted from the fundamental solutions in order to simplify the analysis. Also, the pivot node is positioned collinearly to the boundary segment, as shown in figure 5.19.

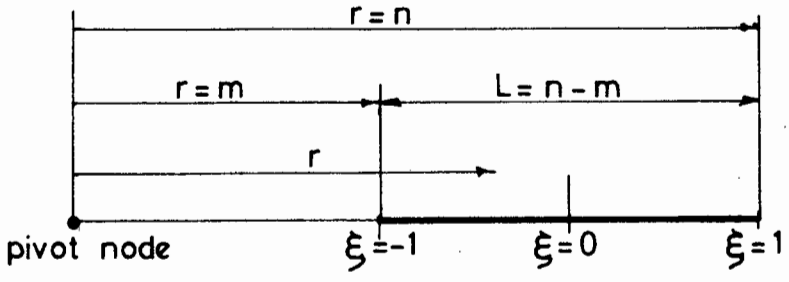

Figure 5.19 The geometry for a single boundary segment

By so doing, the range of r (i.e. from m to n) is the largest for a specified segment length L and therefore, during the numerical integration is likely to display the greatest error. For any other orientation of the boundary segment with respect to the vector $\check{r}$, the range of values will be reduced. This can easily be appreciated for a boundary segment orientation perpendicularly to $\check{r}$. An additional advantage of this assumption is that the analytical integration of the functions is simplified.

The method to be used in simple in concept. In general, the functions to be integrated are of the form

$$I = \int_m^n N \ln \frac{1}{r} \, d\Gamma \quad \text{or} \quad \int_m^n N \frac{1}{r} \, d\Gamma \qquad (5.44a) \quad (5.44b)$$

where N is a generalized shape function corresponding to the particular interpolation scheme and Γ is the boundary. For these purposes, $d\Gamma = dr$. I is now integrated both analytically, to give I_A, and numerically, using one of the 3 Gauss schemes (section 4.3.1), to give I_N. The percentage error between the two integrals is therefore

$$\% \text{ error} = \frac{I_A - I_N}{I_A} \times 100 \tag{5.45}$$

The results of this analysis are presented graphically for each integral. A number of segment lengths, L, have been chosen, with the error being plotted on a logarithmic scale for a range of values m. These graphs then provide a means of ascertaining the possible error for a general segment at an arbitrary distance from the pivot node and provide guide lines as to the aspect ratio of models and the subdivision of boundaries.

5.5.2 The Integration of $\ln \frac{1}{r}$

The numerical integration of the function has previously been discussed (section 4.3.1), therefore, only the analytical integrations will be dealt with here. Separate integrals (since the N's are different in equation (5.44)) are required for constant, linear and quadratic forms.

5.5.2.1 Constant Segments

Since N is constant, the integration over a constant segment of length L = (n - m) is:

$$I_A^C = \int_m^n \ln \frac{1}{r}\, dr$$

$$= (r - r \ln(r)) \Big|_m^n \tag{5.46}$$

Once I_A is evaluated at r = m and r = n, the integral becomes

$$I_A = (L - (n\ln(n) - m\ln(m))) \tag{5.47}$$

The final form, equation (5.47), is given here in full, but, from a computational view point, this is unnecessary since equation (5.46) can be incorporated directly. Because of this, all further integrals will be quoted in a form similar to equation (5.46).

5.5.2.2 Linear Segments

The linear shape functions are:

$$N_1 = 0.5\ (1 - \xi) \tag{5.48}$$

and

$$N_2 = 0.5\ (1 + \xi) \tag{5.49}$$

which are substituted into the equation (5.44a) to give:

$$I^L_{A1} = \int_m^n N_1 \ln \frac{1}{r}\, dr \tag{5.50}$$

and

$$I^L_{A2} = \int_m^n N_2 \ln \frac{1}{r}\, dr \tag{5.51}$$

The local co-ordinate ξ can be written in terms of the dimensions L, m, n and r in the form:

$$\xi = \frac{1}{L}\ (2r - m - n) \tag{5.52}$$

which, when substituted into the shape functions, equations (5.48) and (5.49) yields:

$$N_1 = \frac{(n - r)}{L} \tag{5.53}$$

$$N_2 = \frac{(r - m)}{L} \tag{5.54}$$

The integration is now performed with these shape function definitions to give

$$I_{A1}^{L} = \left[\frac{n}{L}(r - r\ln(r)) + \frac{r^2}{2L}\ln(r) - \frac{r^2}{4L}\right]\Bigg|_m^n \qquad (5.55)$$

and $$I_{A2}^{L} = \left[\frac{m}{L}(r\ln(r) - r) - \frac{r^2}{2L}\ln(r) + \frac{r^2}{4L}\right]\Bigg|_m^n \qquad (5.56)$$

These formulae are now used in the error equation.

5.5.2.3 Quadratic Segments

The quadratic shape functions are more complicated and therefore give a more complicated integrand. The shape functions are:

$$N_1 = 0.5\xi(\xi-1) \qquad (5.57)$$

$$N_2 = (1+\xi)(1-\xi) \qquad (5.58)$$

$$N_3 = 0.5\xi(\xi+1) \qquad (5.59)$$

The local co-ordinate is related to the geometric terms but equation (5.52) which when substituted into the above results in:

$$N_1 = \frac{1}{L^2}\{2r^2 - (m+3n)r + (mn+n^2)\} \qquad (5.60)$$

$$N_2 = \frac{4}{L^2}\{-r^2 + (m+n)r - mn\} \qquad (5.61)$$

$$N_3 = \frac{1}{L^2}\{2r^2 - (3m+n)r + (m^2+mn)\} \qquad (5.62)$$

When the integrations, equations (5.44), are performed using these shape functions, the formulae are:

$$I_{A1}^{Q} = \left[\frac{2r^3}{3L^2}(\frac{1}{2} - \ln r) - \frac{(m+3n)r^2}{2L^2} + (\frac{1}{2} - \ln r) + \frac{(mn+n^2)r}{L^2}(1 - \ln r)\right]\Bigg|_m^n \qquad (5.63)$$

$$I^{Q}_{A2} = \left[-\frac{4r^3}{3L^2}\left(\frac{1}{3} - \ln r\right) + \frac{2(m+n)}{L^2} r^2 \left(\frac{1}{2} - \ln r\right) - \frac{4mn}{L^2} r \left(1 - \ln r\right) \right] \Bigg|_m^n \qquad (5.64)$$

$$I^{Q}_{A3} = \left[\frac{2r^3}{3L^2}\left(\frac{1}{3} - \ln r\right) - \frac{(3m+n)}{2L^2} r^2 \left(\frac{1}{2} - \ln r\right) + \frac{(m^2+mn)}{L^2} r \left(1 - \ln r\right) \right] \Bigg|_m^n \qquad (5.65)$$

which are now used in the error formula.

5.5.2.4 The graphs for $I(\ln\frac{1}{r})$

The error between the analytical integration of the function $\ln\frac{1}{r}$ and the equivalent numerical integration using 2, 4 and 6 point Gauss quadrature, has been computerized and the graphs are given in Appendix E, figures E.1 to E.18.

All the graphs have the same form, with both axes subdivisions being logarithmic. The horizontal axis denotes the dimension m (figure 5.19) which is the distance from the pivot node to the closest point on the focus segment. This dimension is plotted from 0.01 units up to 1000 units.

The vertical axis denotes the percentage error in the numerical integration. The horizontal axis divides the vertical axis into two distinct sections. The upper region represents a positive error, that is, where the numerical integration scheme underestimates the integral. The range of errors allowed for, lies between 1×10^{-4} and 10 percent. In the lower region, the error is negative which represents an over estimation of the integral. The error values range from -1×10^{-4} at the horizontal axis to -10 percent at the bottom of the graph.

The trace of the error is then plotted for 6 different segment

lengths namely: L = 0.5, 1.0, 5.0, 10.0, 50.0 and 100 units. For graphical purposes, the error was calculated at 100 points within each of the logarithmic sectors. For example, between m = 1 and m = 10, the error is calculated at 1.0, 1.1, 1.2, ..., 9.9, 10.0.

The error in the integration is a relative concept, with each analyst having his own idea of what constitutes a significant error. The systems matrices are made up from a considerable number of integral coefficients, each with its own degree of error. It is quite possible then that a series of very small errors in the individual coefficients could cause a large error in the overall system. For this reason, the upper limit on the allowable error is specified arbitrarily here as 1×10^{-3} percent. For this assumption, a number of conclusions can be drawn from the graphs

(i) The trace of the error in the integration for constant segments is shown in figures E.1, E.2 and E.3 for 2, 4 and 6 quadrature respectively. The first notable fact concerning these graphs is the apparent "singularity" in the error. This is a direct consequence of the analytical integral of $\ln\frac{1}{r}$ over a finite region surrounding r = 1. A plot of this function will show that the function is positive when n is less than one and negative when r is greater than one. Consequently, for a finite interval straddling r = 1, the analytical integral will be zero. Substitution of I_A into equation (5.45) will show the singularity, and also accounts for the change in sign of the error between the shorter and longer segments. The phenomenon is clear in both the 2 and 4 point quadrature graphs but is significantly curtailed in the 6 point case. Here, the numerical and analytical integrations are sufficiently close, thus ensuring that the term $I_A - I_N$ is very nearly zero and the percentage error calculation is not affected disasterously. The position at which I_A tends to zero is still seen to be at m≅ 0.54 for a segment of length 0.5 units and at m≅ 0.78 for a 1.0 unit segment length.

For a 4 point quadrature, the error remains constant at 2×10^{-4}%

over a large interval. After this, however, the error begins to increase. For, 6 point quadrature, the error is less that 1×10^{-4}% over a large region where the practical applications are not likely to be situated.

(ii) The trace of the error characteristics for linear segments involving shape functions N_1 and N_2 for 2, 4 and 6 point quadrature are given in figures E.4 to E.9. These figures show the existance of a "cone of uncertainity" in the prediction of the integral by numerical means. The singularity point is naturally still present, but the range of stable values is considerably reduced when compared to the constant segments. Also, the error characteristics between the two shape function expressions have different signs, but are almost identical.

(iii) For quadratic segments, the error characteristics are plotted in figures E.10 to E.18. The quadratic shape functions have a considerable effect on the accuracy of the numerical integration. The 2 point integration formulae gives completely unreliable results and it is left to either 4 or 6 point schemes to produce meaningful integrals. The trace of errors for N_1 and N_3 have the same sign, while N_2 has the opposite sign.

From these comparisons, a recommendation for the use of certain quadrature orders over certain segment lengths at certain approach distances can be made. This is summarized in Table 5.2.

5.5.3 The Integration of $\frac{1}{r}$

In the same way that the error in the integration of $\ln\frac{1}{r}$ is investigated, the singularity function extracted from the traction fundamental solution, can also be analysed. Again, the formulation for the analytical integration for constant, linear and quadratic interpolation schemes must be developed.

Segment type	Gauss Quadrature order	Minimum Approach distance	Maximum Approach distance
Constant	2	2L	500L
	4	0.5L	500L
	6	0.2L	500L
Linear	2	5L	50L
	4	0.5L	60L
	6	0.3L	60L
Quadrature	2	unreliable	unreliable
	4	L	10L
	6	0.5L	10L

Table 5.2 Recommended Approach Distances for constant, linear and Quadratic Segments

5.5.3.1 Constant Segments

The integration of $\frac{1}{r}$ over the constant segment is simple and results in the formula

$$I_A^C = \int_m^n \frac{1}{r}\, dr$$

$$= \ln r \Big|_m^n \qquad (5.66)$$

5.5.3.2 Linear Segments

The shape functions and the definition of ξ are given by equations (5.48), (5.49) and (5.53) to (5.54). Once these have been substituted into equation (5.44b) and integrated, the resulting formulae are:

$$I_{A1}^{L} = \left[\frac{1}{L}(n \ln r - r)\right]\Big|_{m}^{n} \tag{5.67}$$

and

$$I_{A2}^{L} = \left[\frac{1}{L}(r - m \ln r)\right]\Big|_{m}^{n} \tag{5.68}$$

5.5.3.3 Quadratic Segments

The integration over the quadratic segments is similarily performed by substituting equation (5.60) to (5.64) into (5.44b). This yields:

$$I_{A1}^{Q} = \left[\frac{1}{L^2}(r^2 - (m+3n)r + (mn+n^2)\ln r)\right]\Big|_{m}^{n} \tag{5.69}$$

$$I_{A2}^{Q} = \left[\frac{1}{L^2}(-2r^2 + 4(m+n)r - 4mn \ln r)\right]\Big|_{m}^{n} \tag{5.70}$$

$$I_{A3}^{Q} = \left[\frac{1}{L^2}(r^2 - (3m+n)r + r(m^2+mn)\ln r)\right]\Big|_{m}^{n} \tag{5.71}$$

5.5.3.4 The graphs of $I(\frac{1}{r})$

The graphs for the comparison of the error in the integration of the function $\frac{1}{r}$ are presented in precisely the same format as in section 5.5.2.4. and are given in Appendix E, figures E.19 to E.36.

In general, these graphs show similar trends to those discussed previously, but it appears that the "cone of uncertainty" is achieved at an earlier stage.

Again, the interpretation of the degree of error is subjective

and in this case the limiting value has been taken as 1×10^{-3}%.

(i) The trace of the error in the integration for constant segments is shown in figures E.19 to E.21 for 2,4 and 6 point quadrature respectively. In all cases, the error decreases rapidly as the minimum approach distance m increases. The region where the error is less than 1×10^{-3}% extends for a distance of approximately 200 times the segment length before the error becomes random and increasing in the "cone of uncertainity". It is interesting to note that, irrespective of the order of integration used, the "cone" begins at the same point and has identical characteristics in each case. It is therefore evident that for the large approach distances, it is immaterial which quadrature order is used since all are equally erroneous.

(ii) The error trace for linear segments is given in figure E.22 to E.27. Here, 2 point quadrature is very erratic and unreliable and hence the higher order schemes should be used. For the 4 point formula, the error tends to damp out at approximately 2×10^{-3}% as in the previous case (section 5.5.2.4). The traces for N_1 and N_2 are also opposite in sign, as before.

(iii) The quadratic segment error traces were given in figures E.28 to E.36, where the 2 point quadrature is given shown to be very unreliable. The 4 point scheme has a larger region of stable and acceptable values, but it appears as if 6 point integration must be used to ensure confidence in the results. The formulae involving N_1 and N_3 have the same sign, while N_2 has the opposite sign.

In summary, the recommendations for the aspect ratios of the various segments can be stated as follows (Table 5.3):

Segment type	Gauss Quadrature order	Minimum Approach distance	Maximum Approach distance
Constant	2	5L	200L
	4	L	200L
	6	0.3L	200L
Linear	2	erratic	erratic
	4	L	30L
	6	0.3L	30L
Quadratic	2	unreliable	unreliable
	4	L	10L
	6	0.5L	10L

Table 5.3 Recommended Approach Distances for constant, linear and Quadratic Segments

5.5.4 Summary

In this section, it has been shown that the numerical integration of the expressions containing $\ln\frac{1}{r}$ and $\frac{1}{r}$ can only be integrated accurately in certain cases. The graphs showing the error between the analytical and numerical integration give an indication of the allowable aspect ratio of a problem and the limit on contiguous segment lengths.

The inclusion of the linear and quadratic shape functions in the integral significantly effects the accuracy of the numerical integration formulae. Whereas the constant segments only show an uncertainty when the approach distance reaches 200L, the linear and quadratic

segments show unreliable values at 30L and 10L respectively. Consequently, the aspect ratio of the parent problem must be adjusted to be within these bounds.

The length of contiguous segments is also of particular importance, and as can be judged from the minimum approach distance, m, it is dependent directly on quadrature order used.

To be confident in the performance of the different segments, certain conclusions and recommendations can be made. For constant segments, all quadrature orders are applicable, but for linear and quadratic interpolation schemes, at least 4 point quadrature is recommended. The lengths of adjoining segments must not, however, exceed a ratio of 2 under all normal circumstances, i.e., m must not be less than 0.5L. A more exact description of the recommended segment sizes is given in tables 5.2 and 5.3.

5.6 Conclusion

This chapter has concentrated on four major topics, namely;

(i) the discontinuity of traction at corners,
(ii) the inclusion of body forces due to gravity,
(iii) the asymmetry of the systems matrices, and
(iv) the investigation of the inherent error in numerical quadrature formula.

In chapter 4 it was found that, in certain cases, the results obtained exhibited a spurious behaviour. This was thought to be connected with the incorrect numerical modelling of discontinuous tractions at the sharp corners. In order to overcome these problesm, a special segment was designed, which, unfortunately was only partly successful. A method, using a set of discontinuity equations to link the tractions in the corners was instigated, as well as the dual node concept which allowed the tractions to be uniquely defined. Both these methods are able to overcome some of the inherent problems in the formulation, the case of problems where bending is primarily involved, these methods

give vastly superior results to those quoted previously, but nevertheless, a certain amount of uncertainity remains and hence further research is necessary to overcome these problems.

The inclusion of body forces in the methods has been demonstrated by the use of either domain integration, using a number of triangular cells, or by boundary integration, using the existing boundary segments. A comparison between the efficiency of the methods is included and from this it is recommended that the more elegant boundary integration method be used in all possible cases. This method requires a minimum amount of extra data, with the accuracy being related directly to the boundary subdivision.

The investigation of the method and the characteristics of the fundamental solutions has shown conclusively that there is little chance of the systems matrices being rendered symmetric without considerable, expensive preprocessing. In this regard, it is suggested that further research be aimed at overcoming these numerical difficulties in an effort to make the method as commercially attractive as possible.

Recommendations for the aspect ratios, the limiting lengths of adjoining segments and the required Gauss Quadrature order, are contained in this chapter. In general, it is suggested that at least 4 point quadrature be used in all cases, while the ratio of lengths between contiguous segments be restricted to a ratio of 2. The problem's aspect ratio is different for each type of interpolation scheme. Constant segments are the least affected by the size of the model but as the sophistication of the interpolation increases, the problem size becomes more dominant. For quadratic setments, it is thus recommended that model's largest dimension should not exceed 10 times the individual segment lengths. This recommendation is however subjective and problems of larger dimension can be successfully analysed with a slight deterioration in the solution accuracy.

The recommendations of this chapter will be borne in mind and where applicable will be used in the subsequent analyses contained in the following chapters.

5.7 References

5.1 G.C. HOWELL and W.S. DOYLE 'An Assessment of the Boundary Integral Equation Method for In-Plane Elastostatic Problems'. Applied Mathematical Modelling Vol. 6, No.4, August 1982.

5.2 MADELEINE CHAUDONNERET, 'On the discontinuity of the Stress Vector in the Boundary Integral Equation Method for Elastic Analysis'. Proceedings of the Conference on Recent Advances in Boundary Element Methods, Southampton, July 1978 (ed. C.A. Brebbia)

5.3 L.J. WARDLE and J.M. CROTTY, 'Two-dimensional Boundary Integral Equation Analysis for Non-homogeneous Mining Applications'. Proceedings of the conference on Recent Advances in Boundary Element Methods, Southampton, July 1978 (ed. C.A. Brebbia).

5.4 C.A. BREBBIA, 'The Boundary Element Method for Engineers', Penteck Press, London (1978).

5.5 O.C. ZIENKIEWICZ, 'The Finite Element Method', 3rd Edition McGraw-Hill (1977).

5.6 K.J. BATHE and E.L. WILSON, 'Numerical Methods in Finite Element Analysis', Prentice-Hall Inc., New Jersey (1976).

5.7 D.J. DANSON, ' A Boundary Element formulation of Problems in linear Isotropic Elasticity with Body Forces,' Proceeding of the 3rd International Seminar on Boundary Element Methods, Irvine, California, July 1981.

5.8 PAFEC 75, 'A Program for Automatic Finite Element Calculations, Pafec Ltd., Nottingham, England.

5.9 F.B. SEELEY and J.O. SMITH, 'Advanced Mechanics of Materials, 2nd Edition, John Wiley and Sons, Inc. (1952).

CHAPTER 6

THE BOUNDARY INTEGRAL EQUATION METHOD FOR NON-HOMOGENEOUS ELASTOSTATIC PROBLEMS

6.1 Introduction

In the previous chapters, the Boundary Integral Equation Method for the solution of homogeneous structures was discussed. An effective numerical method has been evolved for the analysis and the problems encountered have been examined. In this chapter, we turn to the more complex analysis of non-homogeneous bodies by the Boundary Integral Equation Method. The numerical implementation is discussed and some problems which arise are investigated [6.1].

Non-homogeneity is a characteristic which is common in practical engineering problems and is therefore worthy of a special mention. It is, of course, inevitable that the BIEM is compared with the FEM for this type of problem. In the FEM, a different set of material properties can be assigned to each element, if required and therefore allows great versatility and convenience in its usage.

In the BIEM, each region where the material properties are homogeneous must be identified. These regions are then enclosed within a boundary which can then be subdivided into segments for the purpose of a numerical solution. The weighting functions or fundamental solutions in this case, are dependent upon the appropriate regional material properties while the applied loading and displacement boundary conditions being applied externally. This is compared to the local element characteristics of the shape functions used in the FEM and so accounts for the difference in concept.

By dividing the body into a number of homogeneous regions, the BIEM method discussed previously can be implemented here. A set of boundary equations is assembled for a particular region and its interrelationship with adjoining regions is then established by means of the compatibility and equilibrium constraints at the region interfaces. In this case, as in the homogeneous case, the traction is discontinuous

at corners, both on the exterior boundary and on the region interface boundaries and hence numerical solution difficulties are encountered.

Traction discontinuity equations can be derived at each corner or alternatively, the problem can be overcome by using the multi-node concept, an advance on the dual node idea discussed in chapter 5.

The inclusion of the body force term in the analysis is also vital for practical engineering problems. Numerically, these terms can either be included by domain integration or boundary integration as previously detailed.

Finally, two examples are presented to demonstrate the methods employed. The relative performance of the BIEM is assessed by comparing the results with either a rigorous analytical solution where possible, or with a finite element solution.

Although the BIEM for non-homogeneous problems requires additional attention in the development and programming stages, it will nevertheless be shown that very satisfactory solutions can be achieved.

6.2 The Theoretical Treatment

Consider the non-homogeneous body in figure 6.1, which has been subdivided into a number of regions where the material properties are homogeneous.

The problem is now to derive an analysis method which can adequately predict the behaviour of the entire domain Ω when subjected to the action of externally applied loads. For this purpose, the domain is subdivided into its constituent regions. Taken in isolation, the behaviour of each region can be described by the BIEM equation (3.58). The theoretical development of this equation is precisely the same as that set out in chapter 3. However, to distinguish between the individual equations, for each region, a superscript R is used. Thus, for region Ω^R, the Integral Equation for a field point x is:

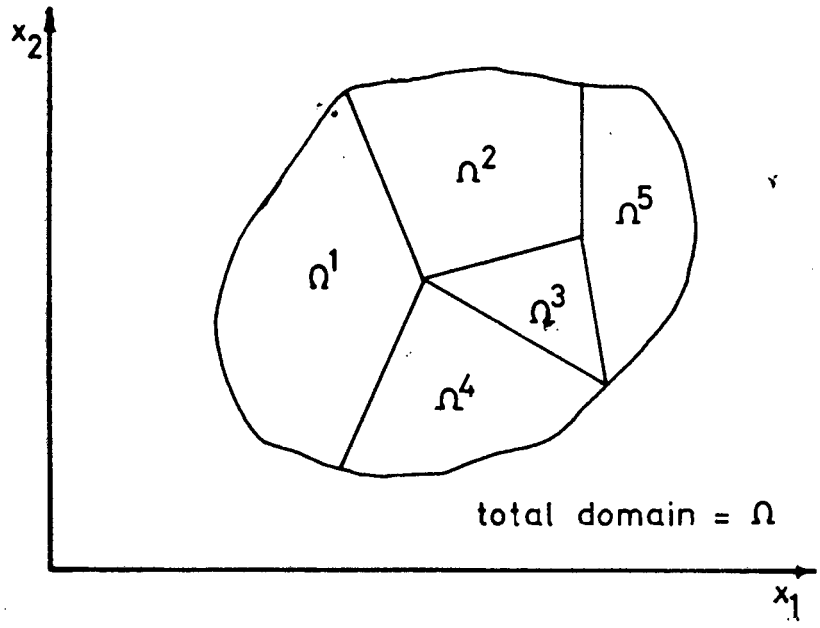

Figure 6.1 A non-homogeneous body divided into homogeneous regions

$$u_i^R(x) = \int_{\Gamma^R} U_{ij}^R(x,y)\, t_j^R(y)\, d\Gamma_y^R - \int_{\Gamma^R} T_{ij}^R(x,y)\, u_j^R(y)\, d\Gamma_y^R + \int_{\Omega^R} U_{ij}^R(x,z)\, b_j^R(z)\, d\Omega^R$$

$$\text{for } x,z \in \Omega^R \; ; \; y \in \Gamma^R \qquad (6.1)$$

where u_i^R is the displacement at point x.

$u_j^R(y)$ is the displacement on the boundary at y.

$t_j^R(y)$ is the traction on the boundary at y.

$U_{ij}^R(x,y)$, $T_{ij}^R(x,y)$ are respectively the displacement and traction fundamental solutions of the equilibrium equations in an infinite elastic space and refer to the material properties in region R.

$b_j^R(z)$ is the body force at z.

Equation (6.1) indicates that the entire domain Ω can be subdivided into many subregions Ω^R, each of which is enclosed within its own boundary Γ^R. The interaction between regions is restricted to these boundaries only, and externally applied loads and restraints can be present on the 'free' boundaries only.

The last term in equation (6.1) is the body force term which requires an integration over the domain in its present form. The introduction of the boundary integration formulation (section 5.3.2) will then be substituted in its place for numerical purposes. The integration will then be performed over each region boundary Γ^R.

Once again, the Boundary Integral Equation for a point x on the boundary Γ^R is formed by the limiting process discussed in section 3.3.12 and Appendix A. This results in the 2x2 coefficient matrix c_{ij} being prefixed to the term $u_i^R(x)$ in equation (6.1), with $x,y\varepsilon\Gamma^R$ and $z\varepsilon\Omega^R$.

$$c_{ij}\, u_i^R(x) = \text{(RHS as in equation (6.1))} \quad \text{for } x,y\varepsilon\Gamma^R \quad z\varepsilon\Omega^R \tag{6.2}$$

The value of c_{ij} is dependent upon the continuity of the outward normal to Γ^R in the vicinity of x.

The displacements at points within the region R are calculated by using equation (6.1), where it is noted that only variables relating to that particular region are involved.

By substituting equation (6.1) into the constitutive equation (3.7) for each region, a formula for stress at a point x within Ω^R is determined in terms of the respective regional variables only. This is given by equations (3.65) to (3.68) with the regional superscript R added to the terms.

If strains at the field point x are also required, these can be generated by substitution of equation (6.1) into the relevant strain/displacement relationships.

6.3 The Numerical Treatment

6.3.1 Quadratic Interpolation of the boundary variables

In this section, the numerical implementation of the boundary integral equation (6.2) is based on the quadratic variation of the displacements and tractions over a boundary segment. The method is to subdivide the boundary of each region in turn into a number of segments. On the interface boundaries, the segments will be common to two regions, but, in terms of the theoretical equations, each region will take the segment into account separately. The segments pertaining to a specific region are defined by the direction of the outward normal from that region. Here, care must be taken to ensure that the correct normal is used in the calculations. These ideas are summarized graphically in figure 6.2 , where n^1 and n^4 represent the outward normals to regions 1 and 4 respectively.

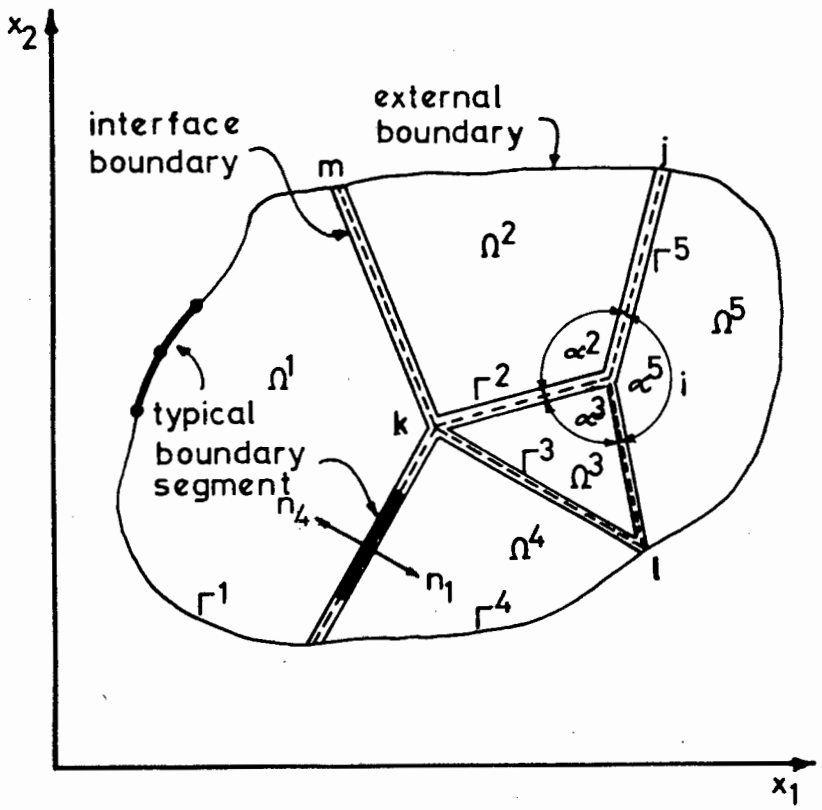

Figure 6.2 A non-homogeneous body showing material regions

The parabolic shape functions and the segment geometry used to describe the variation of boundary displacements and tractions are shown in section (4.4.3). This type of segment has been chosen for all the work carried out for non-homogeneous bodies since it has previously been proven that quadratic interpolation is accurate and that it is computationally efficient when compared to constant and linear schemes. In addition, the quadratic segment is very versatile when modelling complex shapes and curves, owing to its isoparametric formulation.

Implementation of this segment in the numerical formulation follows precisely the same form as discussed previously in chapter 4, and hence need not be reiterated here. This includes the use of Gauss Quadrature for integration over segments which do not contain the pivot node and analytical integration (Appendix C) where the pivot node is a part of the focus segment. The system equations are set up from the separate regional equation generators by allowing the pivot node to move successive from one node to the next in each region. The inter-connection of regional equations is discussed below.

6.3.2 Interfacing material regions

Where two regions abut, the variables of displacement and traction assigned to each region separately, are inter-related. Consider the situation at a typical node x on the interface boundary between regions R and R+1. Two sets of equations have been derived for the two regions, with node x as the pivot. Since no relative movement between regions in the form of a slip or a separation is allowed, the conditions of compatibility and equilibrium at the pivot node can be invoked. These conditions can be summarized as follows:

(i) Compatibility of displacements at pivot node x:

$$u_i^R(x) = u_i^{R+1}(x) \quad \text{for } i = 1, 2 \tag{6.3}$$

(ii) Equilibrium of tractions at pivot node x:

$$t_i^R(x) = - t_i^{R+1}(x) \quad \text{for } i = 1, 2 \tag{6.4}$$

At node x on a straight section of the interface boundary, there are four variables present from each region; 2 displacement components and two traction components giving a total of 8 variables. With the aid of (6.3) and (6.4), this is reduced to 4 variables. Simultaneously there are a total of four component equations generated from the two regions at x, and hence the system is soluble. However, at the multi-region interface nodes i, j, k, l and m in figure 6.2, the situation is slightly different, and further conditions are required before a solution can be found.

6.3.3 Traction Discontinuities in the non-homogeneous context

The problem of the discontinuity of tractions at a corner, as discussed for homogeneous bodies (section 5.1), is also present in this context. Now, however, the situation is exaggerated by the possible existence of more than two segments joining at a node. Examples of this are at nodes i, j and m in figure 6.2 where 3 regions are joined, and nodes k and l where 4 regions meet. In these cases, the number of normals and therefore the number of traction variables is increased. As can be seen from figure 6.2, the traction discontinuities can exist both on the external and interface boundaries.

In order to explain clearly the situation at these troublesome positions, two nodes i and j are considered. Firstly, the active variables at the internal interface node i in figure 6.2 once the compatibility and equilibrium equation have been utilised, are as follows:

number of displacements (x and y components)	=	2
number of tractions (x and y components on segments ij, ik, il)	=	6
total number of variables	=	8

Two component equations are generated from equation (6.2) for each of the three regions Ω^2, Ω^3 and Ω^5, thus giving a total of 6 independent equations. For a unique solution of the 8 variables present, two extra independent equations are required. Alternatively, the problem must be circumvented by other means.

Secondly, consider the external boundary/interface node j in figure 6.2. The number of active variables at j is:

$$N_V = 2 + 2N_{BL} \tag{6.5}$$

where N_V is the total number of active variables and N_{BL} is the number of segments joining at node j, or the number of traction surfaces in the vicinity of node j. In this case, N_{BL} is 3, hence $N_V = 8$.

The number of equations generated by the boundary integral equation (6.2) is $2N_R$ where N_R is the number of regions common to node j. Since the node is on an external boundary the system boundary conditions must be applied. Let the number of prescribed variables be N_{KBC}. Consequently, the relationship between the number of active variables and number of equations is:

$$N_{TDE} = N_V - 2N_R - N_{KBC} \tag{6.6}$$

Where the N_{TDE} is the number of extra equations required for a unique solution of the matrix system to be obtained. The following sections discuss a way of constructing these extra equations and a way of avoiding the traction discontinuities altogether.

6.3.3.1 Traction Discontinuity Equations

The method of using traction discontinuity equations to overcome the problem at external corner nodes have been discussed in detail in section 5.2.4. and in reference [6.2]. This method can also be used in the non-homogeneous context. Here, however, a choice must be made as to which region is to be used to generate the auxiliary equations. The node at which the discontinuities occur can be considered to be the corner node of any interfacing region. Hence, auxiliary equations can be constructed for one or all of these regions. For the purposes of programming, however, the region with the largest included angle α^R which is equal to or less than 180° is used. This has also been confirmed by Wardle and Crotty [6.3].

Unfortunately , this is not an ideal solution, since only one of the regions at the interface node is used to generate the extra equations. Consequently, only the tractions associated with that region will be included in the equations. The remaining tractions present at the node, but which are just as important for the correct modelling of the discontinuity, are ignored. A desirable procedure would be to include all the active variables (traction and displacement) at the interface node in the auxiliary equations. To date, however, this has not been accomplished and is thus a topic for further research.

To illustrate the effects of ignoring some of the active tractions, we consider a simple example as shown in figure 6.3.

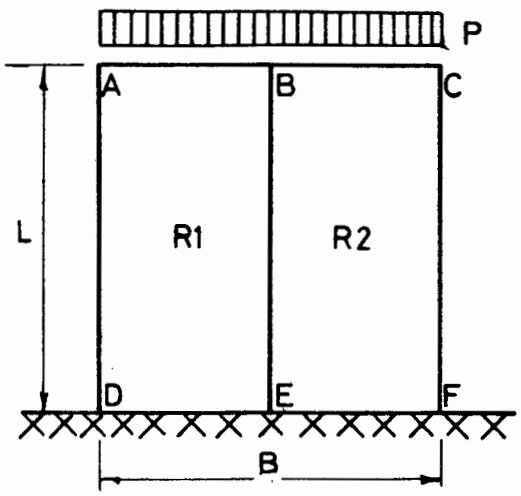

Figure 6.3 Square Plate subjected to symmetrical boundary conditions

A square plate of dimensions (L x B) 1.0 units by 1.0 units is divided centrally into 2 identical regions. Each region, R1 and R2, is assigned the same material properties, namely

Youngs Modulus E = 1000.00

Poisson's Ratio $\nu = 0.3$

and body forces are neglected. A vertical pressure P = 50 load units is applied vertically to the upper face ABC, while the lower face DEF is supported rigidly. From this set of symmetrical loads, boundary conditions and material properties, it is expected that the vertical displacements along the upper face should also be symmetrical about the line BE.

Two traction discontinuity equations are required at node E. These can either be generated from region R1 or alternatively from R2. The resulting displacements calculated at points A, B and C are given in Table 6.1.

Discontinuity Equations Written For Region	Vertical Displacement At		
	A	B	C
R1	-0.98253×10^{-1}	-0.9860×10^{-1}	-0.10246
R2	-0.10246	-0.9860×10^{-1}	-0.98253×10^{-1}

Table 6.1 Displacements of a Square Plate with Symmetrical Boundary Conditions

The traction discontinuity equations, in their present form, give non-symmetrical answers for a symmetrical problem. However, it is felt that if these equations were to involve all active tractions along segments EB, ED and EF, then the resulting displacements would be symmetrical.

6.3.3.2 The multi-node concept

An alternative to the traction disconituity equation method is to use multi-nodes at the region intersections. This is an enhance-

ment of the dual node concept examined in section 5.2.5, where auxiliary nodes were defined at the interface point, with each node being assigned a unique normal. As an example, consider the interface node i in figure 6.2. In place of a single node at i, three auxiliary nodes, denoted a, b and c in figure 6.4 are defined. Although they are considered geometrically coincidently each node is associated with a particular segment and hence has a clearly defined normal.

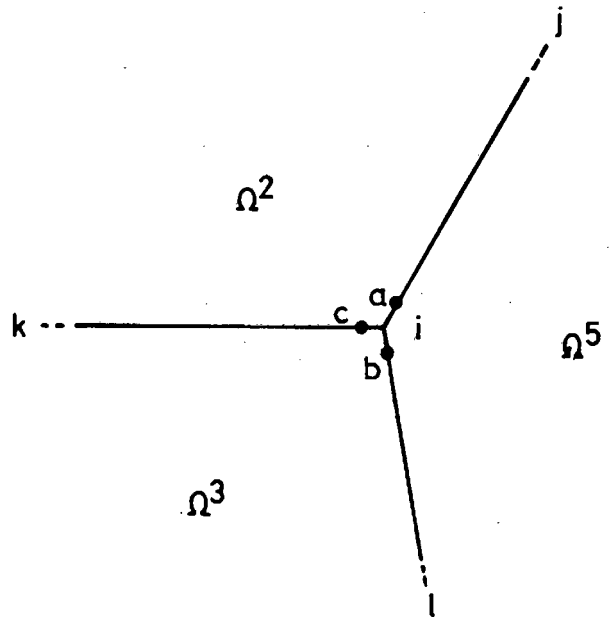

Figure 6.4 Multi-node definition at a region interface

No numerical problems are encountered when the equations are computed using equation (6.2). Auxiliary nodes are only common to two regions. Thus, two component equations are generated from each region (a total of 4 equations) which correspond with the 4 unknown active variables (2 displacement components and 2 traction components) at each node. This method is also directly applicable to external boundary interface nodes (nodes j, l, m in figure 6.2) as well as isolated corner nodes.

Although this method produces satisfactory results for problems such as that discussed here (reference figure (6.3)) it has the disadvantage of increasing the total number of system variables and hence the size of the matrix to be solved.

As an illustration, consider the number of active variables at node i. When using the traction discontinuity equation method, the number of active variables would be 8 (2 displacements and 6 tractions). With the multi-node method, on the other hand, 12 active variables are required, 2 displacements and 2 tractions for each auxiliary node.

Although this method requires more equations and a consequent increase in computational time, it is nevertheless consistent and accurate, and is recommended for use in boundary integral equation analyses. However, for large problems, where many auxiliary nodes are used, the computational overheads could become prohibitive. A more efficient method will then have to be sought.

6.3.4 The Matrices

The matrix equation which governs the foregoing discussions is akin to equation (4.6) and is written for each region as:

$$H^R \{u\} = G^R \{t\} + \{B^R\} \qquad (6.5)$$

where H^R is the matrix of coefficients from the integration of the traction fundamental solution in region R.

G^R is the matrix of coefficients from the integration of the displacement fundamental solution in region R.

B^R is the body force terms calculated for region R

$\{u\}$, $\{t\}$ are vectors of global displacements and tractions respectively.

H^R and G^R are both matrices of dimension 2nx2n in (6.5) where 2n is the total number of variables in the discretized body. Consequently

only the elements which relate directly to the active variables in region R will be non-zero. In so doing, a total of R matrix sets are formed corresponding to the R regions present. The separate matrices are then amalgamated by employing the compatibility and equilibrium conditions equations (6.3) and (6.4). The result is a matrix of the form (4.6) where H, G and B are the accumulated systems matrix. The external boundary conditions are then applied which results in a set of 2nx2n linear equations of the form (4.7). This set of equations is then solved to yield the system unknown displacements and tractions in the usual way.

The method described above for the construction of the conglomorate matrices is computationally impractical since it would require an excessive amount of computer storage space. Therefore, the above description acts only as an image to crystallize the successive steps which are required. Practically, the matrices H and G are constructed directly at calculation (integration over the boundary segments within each region) time together with the compatibility and equilibrium equations. In fact, to save further on computer storage, some of the programs written by the author, produce the final matrices A (equation 4.7) directly from the integrations, the compatibility and equilibrium equations and boundary conditions, thus circumventing the need for the two matrices H and G in store. This method has proven to be very successful in operation.

The form of the matrices H and G can be illustrated by using figure 6.1 as an example. Assuming that H^R and/or G^R have been calculated for all 5 regions, the accumulated matrices H or G are shown in figure 6.5.

Figure 6.5 shows a vaguely banded form to the matrix, but this is by no means general and depends entirely on the arrangement of the regions. An example given in [6.4] exhibits a strongly banded form. This will always occur when one region interfaces upon another in sequential form as is shown in that case.

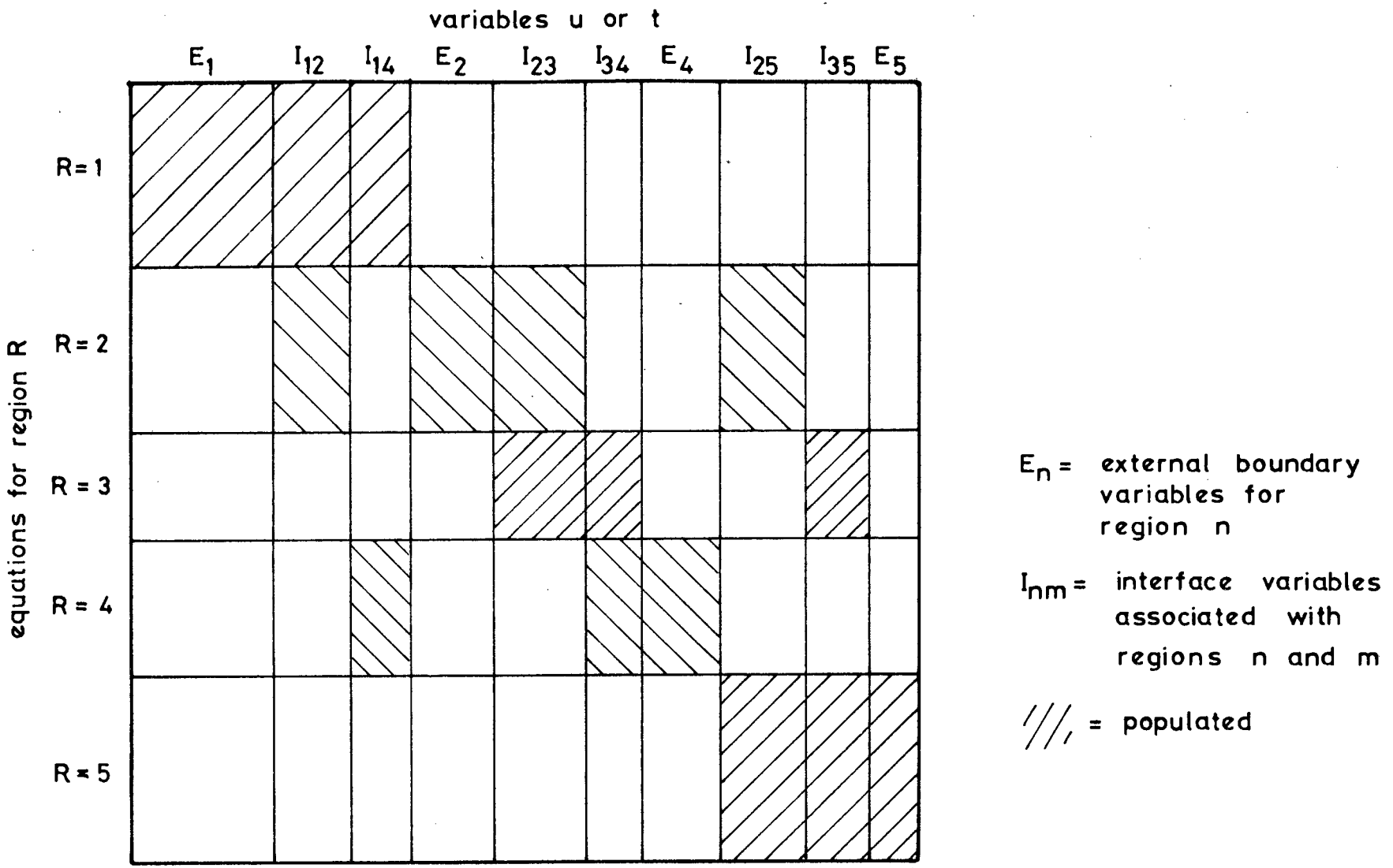

Figure 6.5 An example of the system matrices H or G

6.4 Examples

6.4.1 Thick-walled pipe subjected to internal pressure (Plane Strain).

This example has been chosen as a verification of the BIEM for non-homogeneous bodies as detailed in this chapter. In section 4.8.1, it was shown that a homogeneous thick walled pipe could be accurately analysed by using either constant, linear or quadratic interpolation over the boundary segments. In this example, two different models are described. The first model is used to analyse the structure as a homogeneous body using quadratic segments. This forms a basis for the comparison with the second model. The analysis is performed as if the model were non-homogeneous, i.e., made up of two regions, each having identical material properties. In addition, the performance of the method is also tested as the wall thickness of the pipe is reduced.

For convenience, only one quarter of the thick-walled pipe is analysed once two planes of symmetry have been identified. To begin, the internal and external radii are 5 and 20 units respectively. The internal radius is then increased progressively in increments of 1.0 units while the external radius is kept constant at 20 units.

The modelling of the pipe is shown in figure 6.6. The homogeneous model is shown in figure 6.6a where 28 quadratic boundary segments with 56 nodes were used. Figure 6.6b shows the model used for the analysis using non-homogeneous assumptions. Thirty one quadratic segments involving 61 boundary nodes were used in this case. The boundary conditions to simulate the symmetry are shown, while loading is supplied by a constant pressure of P_i = 10.0 units on the inner surface. This pressure is constant irrespective of the inner radius.

The material properties which are constant throughout regions 1 and 2, are:

Young's Modulus E = 1000 units

Poisson's Ratio ν = 0.3

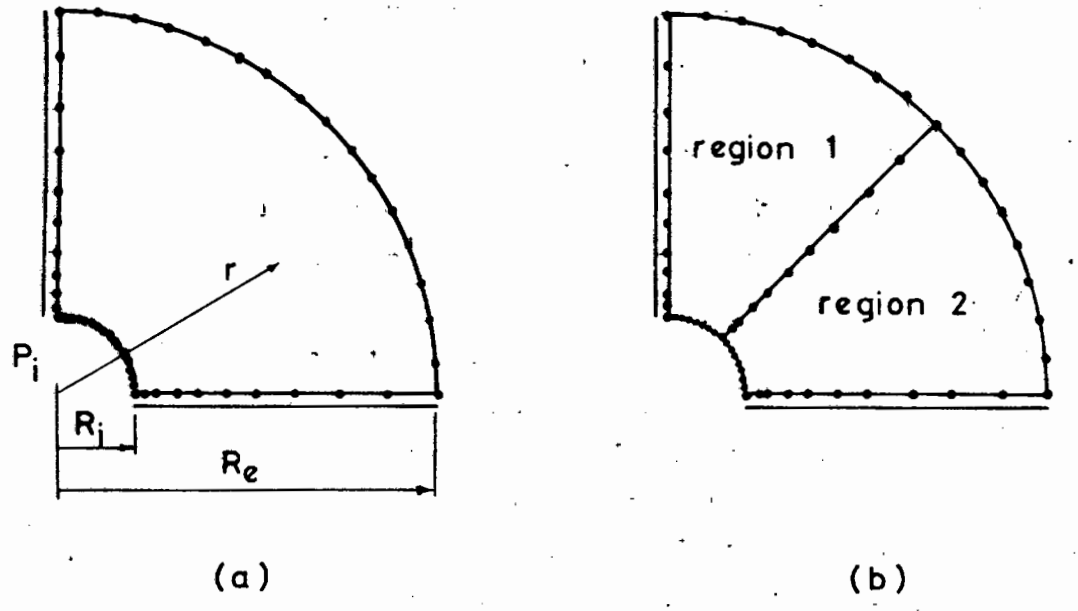

Figure 6.6 Quadrant of thick walled pipe subjected to internal pressure
(a) homogeneous (b) non-homogeneous

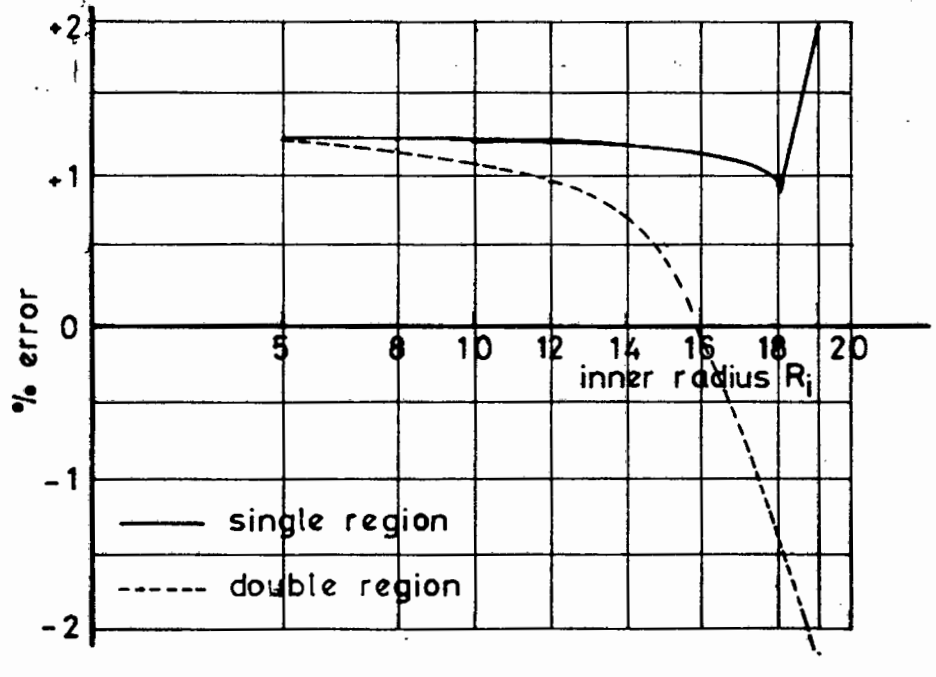

Figure 6.7 Thick-walled pipe; comparison of results

Figure 6.8a shows the geometry of the concrete gravity retaining wall and the surrounding soil backfill and foundation material. The 5 metre high wall has a sloping rear face batter with the dimensions at the top and the bottom being 0.5 metres and 2 metres respectively. This wall retains a 5 metre soil backfill, which extends a distance 6.5 metres to the artificial vertical boundary. This boundary allows vertical displacements only to a depth of 5 metres. Both the wall and the backfill are supported by a foundation material which is assumed to be rigidly fixed at it's artificial boundaries. Separate material properties are assigned to each of the material regions described above. Two load cases were considered.

(i) an imposed surcharge on the top of the retaining wall and on the horizontal surface of the backfill material; and
(ii) the self weight of the materials only.

In addition to the BIEM analysis, the structure was also analysed by the FEM using the program ADINA [6.6]. The FEM model used 57 variable node quadrilateral plane strain elements involving 104 nodes as shown in figure 6.8b.

The BIEM model is shown in figure 6.8a and consists of 40 quadratic boundary segments involving 78 nodal positions.

The data used in the analysis is as follows:

Material properties for the three regions:

	E(Young's Modulus)	ν(Poisson's Ratio)	γ(Density)
Region 1	20 GPa	0.25	2600 kg/m^3
Region 2	30 GPa	0.2	2400 kg/m^3
Region 3	1 GPa	0.35	1000 kg/m^3

Boundary conditions are shown graphically in figure 6.8. The surcharge applied along the upper horizontal surface is 10 kN/m.

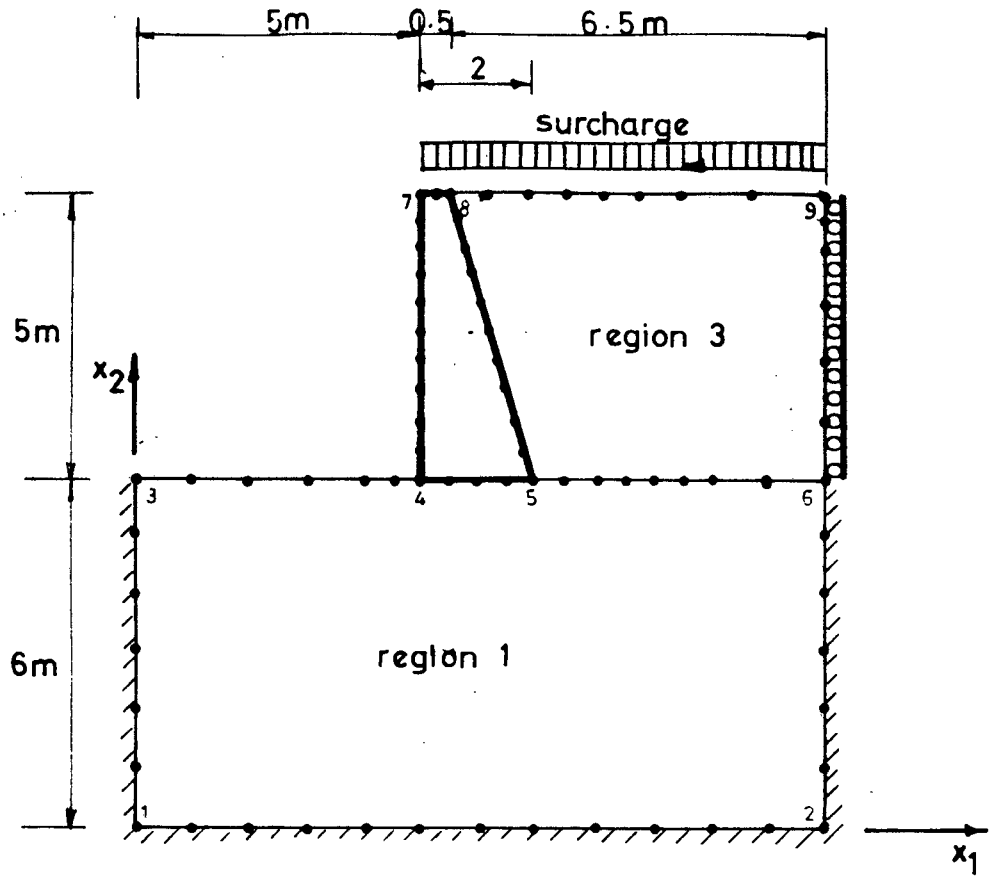

Figure 6.8a The Geometry and BIEM segments used for the gravity retaining wall analysis

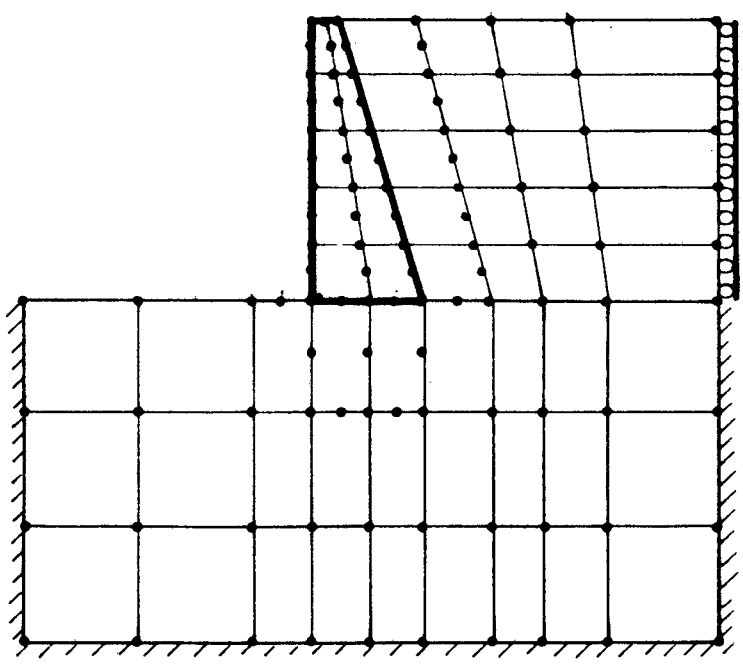

Figure 6.8b The FEM modelling of the gravity retaining wall

The displacements at points 4, 5, 7 and 9 (figure 6.8a) are used to compare the results obtained from the BIEM and the FEM. For the BIEM, two analyses were performed. The first uses the traction discontinuity equation method, while the second uses the multi-node approach in positions where the traction values are problematical. These are denoted by the abbreviations TDE and MN respectively, below.

For load case 1, the displacements at the 4 chosen points are compared in Table 6.2.

Load case 2 involves the self-weight of the material only. The contribution of the self-weight to the equations in the BIEM is calculated by the boundary integration method (section 5.3.2). These results are given in Table 6.3.

These tables show the excellent comparison between the BIEM and the FEM for this practical engineering problem. At no stage do the displacements differ by a large percentage. If the FEM is taken as a datum in this problem (it being the method most widely used in practice) then it can be seen that in general the multi-node approach used in the BIEM tends to overestimate the displacements slightly for most of the nodes. The traction discontinuity equation method on the other hand underestimates the results marginally in most cases. These differences are in no way significant, however, and competently shows the applicability of both methods. The asymmetry of results shown in section (6.3.3.1) for the traction discontinuity equations, makes the multinode approach more acceptable from a personal point of view, however.

The difference in computer CPU time for FEM and BIEM for this example are interesting. ADINA used 4.39 seconds of CPU time and this reflects the care and efficiency built into the program by Professor Bathe. In the BIEM, where calculation efficiency was not a priority, the total CPU time was 72.06 seconds. These times were measured on a UNIVAC 1100/81. This comparison emphasises the differences between the methods. The FEM, with its local element calculations can be programmed so that these localized features are enhanced. The BIEM, on the other hand, has a built-in inefficient characteristic that the equation involving one pivot node requires inte-

Node position	x_1 - Displacement (metres)			x_2 - Displacement (metres)		
	FEM (ADINA)	BIEM (TDE)	BIEM (MN)	FEM (ADINA)	BIEM (TDE)	BIEM (MN)
7	-0.910206×10^{-5}	-0.88587×10^{-5}	-0.94546×10^{-5}	-0.533617×10^{-5}	-0.52396×10^{-5}	-0.53503×10^{-5}
4	-0.88949×10^{-6}	-0.90195×10^{-6}	-0.92920×10^{-6}	-0.275142×10^{-5}	-0.29171×10^{-5}	-0.29247×10^{-5}
5	-0.111683×10^{-5}	-0.11184×10^{-5}	-0.012161×10^{-5}	-0.121285×10^{-5}	-0.11694×10^{-5}	-0.11193×10^{-5}
9	0.0	0.0	0.0	-0.350622×10^{-4}	-0.36027×10^{-4}	

Table 6.2 Load Case 1. Displacements at selected points for the gravity retaining wall structure with surcharge only.

Node position	x_1 - Displacement (metres)		x_2 - Displacement (metres)	
	FEM (ADINA)	BIEM (MN)	FEM (ADINA)	BIEM (MN)
7	-0.654997×10^{-5}	-0.64247×10^{-5}	-0.405700×10^{-4}	-0.40270×10^{-4}
4	-0.116767×10^{-5}	$-0.14423 - 10^{-5}$	-0.325557×10^{-4}	-0.33207×10^{-4}
5	-0.367999×10^{-5}	-0.38847×10^{-5}	-0.301532×10^{-4}	-0.29884×10^{-4}
9	0.0	0.0	-0.972019×10^{-4}	-1.0032×10^{-4}

Table 6.3 Load Case 2. Displacements at selected points

for the gravity retaining wall structure with self-weight only

grations to be carried out over every boundary segment in that region. Each pivot node is unique, thus requiring individual and exhaustive repetitive calculation. For the BIEM to become commercially more attractive therefore, considerable research effort will be required in this field.

6.5 Conclusion

The analysis of a non-homogeneous body can be successfully and conveniently performed by the BIEM. The method requires that the body be subdivided into its constituent parts, each with a constant set of material properties. The boundaries of each region are subdivided into segments, which, on the interface boundaries, are common to two regions. For each region, a set of equations involving the regional boundary variables, is set up. These are linked by using the compatibility and equilibrium equations at the interfaces. A set of systems equations is consequently formed. Once the externally applied boundary conditions have been taken into account, the linear equations can be solved to yield the displacements and tractions on the external and interface boundaries.

For the numerical analysis, a quadratic interpolation formulation has been used. This method, which is based on isoparametric concepts, allows accurate geometric modelling and is computationally efficient when compared with constant and linear interpolation schemes. However, due to the existance of nodes at the segment extremities, the problem of discontinuous tractions arises when the boundary is not straight. The traction discontinuity equation method and the multi-node concept have been discussed in this context. It has been found that the traction discontinuity method exhibits evidence of non-symmetric results for a symmetric problem. This is due to the omission of some of the relevant traction components at this point. Consequently, the multi-node approach, which does not show these trends, is recommended.

The matrices derived for non-homogeneous problems are in general, not banded but show a random pattern of non-zero coefficients for most problems. In certain circumstances, as in problems where one material region is interfaced sequentially with the next, the banded matrix will, however, be formed.

The numerical results from the method are extremely accurate, seldom differing from the analytical solution by more than 1%. However, as in the case of homogeneous bodies, the accuracy deteriorates when the body's aspect ratio increases. The computational time for non-homogeneous and homogeneous analyses are comparable, even so.

A practical engineering problem is also included to show that the method can be used very satisfactorily in ordinary day situations. Excellent similarity between the results from the FEM and the BIEM are contained, whether traction discontinuity equations or the multi node concept is used. For the comparison, two load cases were imposed. The first is an externally applied surcharge, while the second involves the material selfweight only, which was analysed using the boundary integration technique. A major question about the efficiency of the BIEM as regards computation time arises here. It becomes clear that if the BIEM is to become commercially more attractive than the FEM, some effort is required to reduce the computational time expended.

The advantage of the BIEM though is that it requires less data input which after all, is the most time consuming and costly part of a commercial analysis project.

6.6 References

6.1 G.C. HOWELL and W.S. DOYLE, "The Plane Stress/Strain Analysis of Non-homogeneous Continua by the Boundary Integral Equation Method", Computer and Structures, Vol.17,No.4,p.603-610 (1983).

6.2 G.C. HOWELL and W.S. DOYLE, "An Assessment of the Boundary Integral Equation Method for in-plane elastostatic problems", Applied Mathematical Modelling. Vol. 6 No. 4, August 1982.

6.3 L.J. WARDLE and J.M. CROTTY, "Two-dimensional Boundary Integral Equation Analysis for Non-homogeneous Mining Applications", Proceedings of the Conference on Recent Advances in Boundary Element Methods, Southhampton, July 1978 (ed. C.A. Brebbia).

6.4 C.A. BREBBIA and S. WALKER, Boundary Element Techniques in Engineering, Newnes-Butterworths, London (1980).

6.5 S.P. TIMOSHENKO and G.N. GOODIER, Theory of Elasticity, 3rd Edition, McGraw-Hill, (1970).

6.6 ADINA A Finite Element Program for Automatic Dynamic Incremental Non-linear Analysis, K.J. Bathe, Massachusetts Institute of Technology (1978).

CHAPTER 7

THE SOLUTION OF THE INFINITE DOMAIN PROBLEM

7.1 Introduction

The determination of displacements and stresses in structures which have boundaries which extend large distances beyond the stressed area under investigation, is the subject of this chapter. These boundaries can therefore be regarded as infinite.

Problems with boundaries which can be considered to be infinite occur frequently in practice, particularly in the mining industry and in soil/structure and fluid/structure interaction.

The conventional procedure for the stress analysis of these problems is to assume that boundaries exist at an estimated distance sufficiently remote from the stressed zone. This can lead either to inaccuracies due to the unnatural truncation of a domain, or alternatively to an excessively large domain with too many finite elements or boundary segments. The consequence of the latter procedure would be an unnecessarily large amount of data preparation and computational effort.

A far more elegant solution would, therefore, appear to be to model the infinite domain numerically, by extending the capabilities of the boundary integral equation method. This has been achieved here by using some of the concepts which have been developed in "infinite element" formulations in the finite element method.

An important consideration in this work has been to design this new technique in such a way that it can be simply slotted into already developed finite boundary integral equation computer programs, without major alterations. This would not be possible if one adopted a rigorous theoretical approach where special purpose fundamental solutions [7.12] are proposed.

At this stage, however, by only using the existing techniques

detailed in previous chapters, a special class of infinite domain problems can already be solved. This type of problem has a finite boundary but a domain which extends to infinity. An example of this is a hole in an infinite plane. Since the boundary is clearly defined and the fundamental solutions include source points at infinity, the conventional BIEM can be used.

In this chapter, we are interested in problems where both the boundary and the domain extend to infinity. Since some aspects of this special purpose BIEM are derived from the method of "infinite elements", a brief review of the major points of the latter is included here as an introduction to the formulation of the infinite boundary integral equation method.

7.2 "Infinite" Finite Elements

The majority of attempts to produce an infinite element formulation which can be used in a standard finite element program, have relied on the incorporation of a decay function of one type or another in order to satisfy the boundary conditions at infinity [7.1 to 7.7]. Some methods are based on the concept of an attenuation length which delineates the decay function. Consequently these elements require to be tuned for certain applications by varying this parameter until the best results are obtained. Other methods require an adaption of the numerical integration in order to tune the element. These are distinct disadvantages and it would therefore be desirable to use a method which obviates these difficulties.

Recently, Owen [7.8] has produced a formulation which effectively overcomes these problems by geometrically mapping the infinite element onto the standard basis element through a special set of shape functions. This has been termed a 'mapped infinite element' and will be discussed briefly here. The formulation leads to a family of infinite elements which have been developed to be compatible with an existing finite element program. The performance of these elements is then judged by comparing the numerical results obtained with the analytical results for the classical Boussinesq problem of a point load on an elastic half space.

In general terms, the method uses the existing standard quadratic shape functions to describe the variations of the field parameter, i.e., the displacements, over the parent element. In other words, the displacement derived terms of strain and stress in the finite element formulation are precisely the same as in a standard formulation. The geometry is, however, described by a set of special shape functions which maps the infinite element onto the standard parent element for the purposes of numerical integration. Standard Gaussian integration schemes can then be used to produce the element stiffness matrix.

The inclusion of infinite elements in an existing compatible finite element computer code is simple. In this section, the basic outline of the strategy involved will be discussed briefly using a one-dimensional element as a model. The resulting shape functions will then be used to generate a family of infinite elements which will be compatible with all the existing plane stress/strain and axisymmetric finite elements in the program.

7.2.1 The shape functions

The attraction of the mapped infinite element approach is that the field variables are described by the standard shape functions, while the geometry is represented, equally simply, by a set of special functions. Consider the geometric mapping, in one dimension, (defined by x) of the infinite element on to the parent basis element, as in figure 7.1.

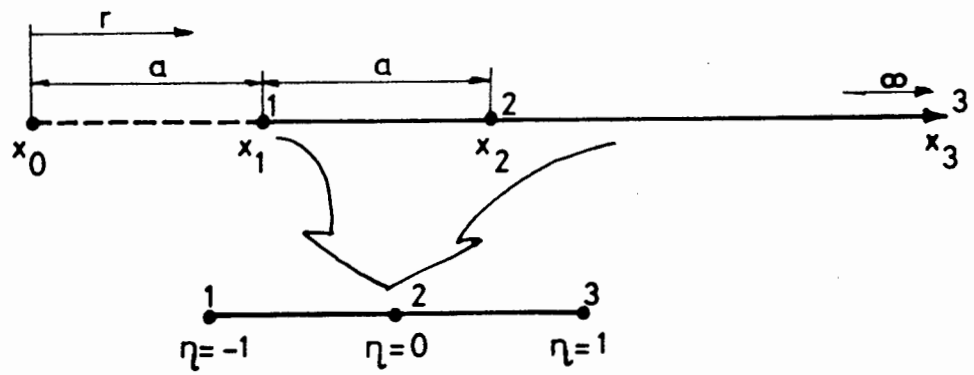

Figure 7.1 Infinite geometric mapping

In the derivation of the shape functions, it is first necessary to define an auxiliary node x_o, a distance a from node 1 as shown. This point will later be seen to represent the pole for the expression which describes the decay of the field variable as r approaches infinity.

Using nodes x_o and x_2, a general point x on the element is defined by

$$x = \hat{N}_o(\eta)x_o + \hat{N}_2(\eta)x_2 \tag{7.1}$$

where

$$\hat{N}_o(\eta) = -\frac{\eta}{(1-\eta)} \tag{7.2a}$$

$$\hat{N}_2(\eta) = 1+\frac{\eta}{(1-\eta)} \tag{7.2b}$$

According to this mapping, the following situation arises:

$$\begin{aligned} &\text{for} \quad \eta = -1 \ , \ x = (x_o + x_2)/_2 = x_1 \\ &\text{for} \quad \eta = o \ , \ x = x_2 \\ &\text{for} \quad \eta = 1 \ , \ x = \infty \end{aligned} \tag{7.3}$$

Now, by positioning x_2 to lie at a distance a from x_1 as shown in figure 7.1, the auxiliary node can be eliminated from the formulation by writing:

$$x = (2x_1 - x_2)\ \hat{N}_o(\eta) + x_2\ \hat{N}_2(\eta) \tag{7.4}$$

When this equation is rearranged by grouping the coefficients of x_1 and x_2, the following expression is derived:

$$x = 2\ \hat{N}_o(\eta)x_1 + \left\{\hat{N}_2(\eta) - \hat{N}_o(\eta)\right\}\ x_2 \tag{7.5}$$

or

$$x = \sum_{i=1}^{2} \overset{g}{N_i}(\eta)\, x_i \tag{7.6}$$

where

$$\overset{g}{N_1}(\eta) = 2\hat{N}_o(\eta) = -\frac{2\eta}{(1-\eta)}$$

and

$$\overset{g}{N_2}(\eta) = \hat{N}_2(\eta) - \hat{N}_o(\eta) = 1 + \frac{2\eta}{(1-\eta)}$$

From this it can be seen that only the finite nodes of the element are involved. Also, the condition for the uniqueness of the geometrical mapping, i.e.,

$$\sum_{i=1}^{2} \overset{g}{N_i}(\eta) = 1 \tag{7.7}$$

is satisfied by these shape functions.

The Jacobian, which facilitates the mapping, is written in terms of the shape function derivatives with respect to the natural co-ordinates η as:

$$J = \frac{\partial x}{\partial \eta} = \sum_{i=1}^{2} \frac{\partial \overset{g}{N_i}}{\partial \eta}\, x_i \tag{7.8}$$

The field variable v, on the other hand is represented by the standard quadratic shape functions N_i by the expression

$$v = \sum_{i=1}^{3} N_i(\eta) v_i \tag{7.9}$$

where

$$N_1(\eta) = \frac{1}{2}\eta(\eta-1) \tag{7.10a}$$

$$N_2(\eta) = (1-\eta)(1+\eta) \tag{7.10b}$$

$$N_3(\eta) = \frac{1}{2}\eta(\eta+1) \tag{7.10c}$$

The significance of the position of the auxiliary node now becomes evident. Substitute (7.10) into (7.9) and re-arrange the coefficient to produce

$$v = v_2 + \frac{1}{2}(v_3-v_1)\eta + \frac{1}{2}(v_1- 2v_2+v_3)\eta^2 \tag{7.11}$$

From the definition of η, a and r from figure 7.1, the following expression is valid

$$\eta = 1- \frac{2a}{r} \tag{7.12}$$

Substitution of equation (7.12) into (7.11) yields

$$v = v_3+(-v_1+4v_2-3v_3)\frac{a}{r} + 2(v_1-2v_2+v_3)\left(\frac{a}{r}\right)^2 \tag{7.13}$$

Now, considering the value of v at the various node points x_o to x_3, it is quite clear the v becomes singular at r = o. At the other nodes (i.e., at r = a, r = 2a and r = ∞), the field variable v is represented by the nodal values v_1, v_2 and v_3 respectively. This demonstrates the significance of x_o as the pole of the expansion of the expression. Since node x_3 is not included in the formulation, it is automatically assumed that v_3 = o has no contribution to the formulation.

The strain within the element is related to the displacements by the cartesian derivatives. For the one dimensional model this is written as

$$\varepsilon_x = \frac{\partial v}{\partial x} = \sum_{i=1}^{2} \frac{\partial N_i(\eta)}{\partial x} v_i \tag{7.14}$$

where

$$\frac{\partial N_i}{\partial x} = \frac{\partial N_i}{\partial \eta} \cdot \frac{\partial \eta}{\partial x} = \frac{\partial N_i(\eta)}{\partial \eta} \cdot J^{-1}$$

and J^{-1} is defined by equation (7.8).

The ingredients for a two dimensional element are therefore defined explicitly by equation (7.6), (7.8), (7.9), (7.10) and (7.14)

and it remains only for these to be combined in a coherent fashion.

7.2.2 The infinite element types

The derivation of the shape functions for two dimensional elements involves the combination of the one-dimensional functions, in the two orthogonal directions. To demonstrate the procedure, consider the grid system in figure 7.2 which represents the parent element defined for $-1 \leqslant \xi \leqslant 1$ and $-1 \leqslant \eta \leqslant 1$.

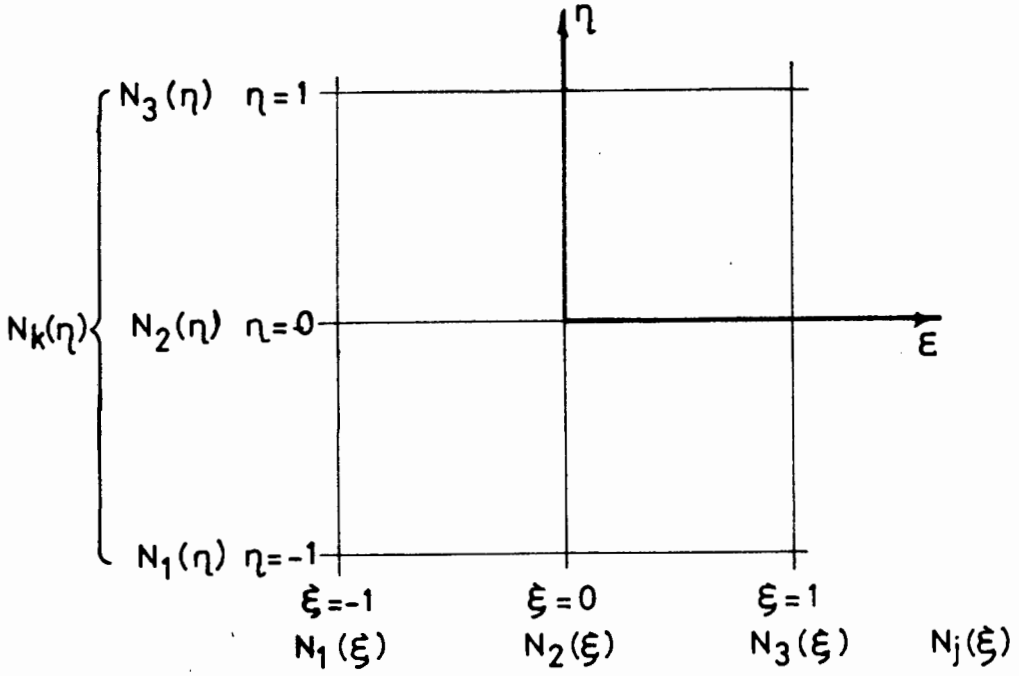

Figure 7.2 The 2-dimensional natural co-ordinate grid

The shape functions describing the geometry and corresponding to the co-ordinates j, k can be written as

$$N_{jk}(\xi,\eta) = N_j(\xi) \cdot N_k(\eta) \tag{7.15}$$

where j and k denote the grid positions.

This procedure is directly applicable when $N_j(\xi)$ and $N_k(\eta)$

are defined by Lagrange interpolation functions [7.9]. But, for the "serendipidy" elements, the shape functions are "built up" from the basic one-dimensional functions by a summation process. The details of the generation of the shape functions defining the geometry of the 4 types of infinite elements shown in Table 7.1, are given in Appendix F. It is unnecessary to present the formulation of the corresponding shape functions which describe the variation of the field variable, since these are standard and can be found in [7.9].

An important point to remember for all the infinite elements, is that the summation is performed over the 'finite' nodes only, the nodes at infinity do not contribute to the formulation. In addition, the 2-dimensional condition corresponding to equation (7.7) is always satisfied.

7.2.3 An Example: Boussinesq's problem of a point load on an elastic half space.

The family of infinite elements shown in Table 7.1 has been included by the author in an existing finite element program based on that by Owen [7.10], in which all the parent elements are present. The performance of these elements was then tested on the axisymmetric problem of a point load on an elastic half space, for which the analytical solution is known [7.11].

Two types of numerical analysis were performed. The first analysis uses only finite elements, with the mesh truncated at a radius of 5 units as shown in figure 7.3. A total of 16 elements was used. Both quadratic 8 node Serendipity and 9 node Lagrange elements were tried, with both 2x2 and 3x3 point Gauss quadrature being employed.

The second analysis uses a combined finite/infinite element mesh. 12 Finite elements extending to a radius of 4.0 units and 4 infinite elements were used. The second nodes of the infinite elements were placed at a radius of 8.0 units so that the dimension a = 4.0 units (cf equations (7.11) to (7.13)) allows the pole for the expansion of the decay function

Type	Geometry and Modal Numbering	Parent finite element	Shape Function Definition in co-ordinate direction	
			ξ	η
1	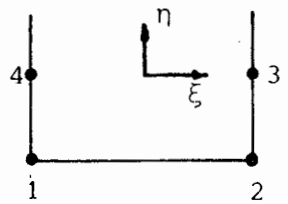	6 node element linear in ξ - direction quadratic in η - direction	linear	quadratically infinite eqn. (7.6)
2	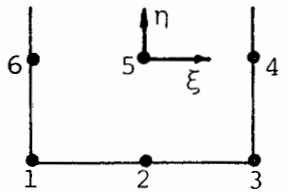	9 node Lagrange element	quadratic eqn. (7.10)	quadratically infinite eqn. (7.6)
3	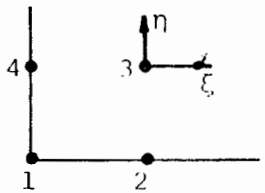	9 node Lagrange element	quadratically infinite eqn. (7.10)	quadratically infinite eqn. (7.10)
4	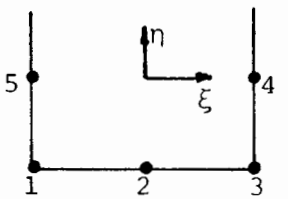	8 node Serendipity element	quadratic serendipity ref. [7.9]	quadratically infinite eqn. (7.10)

Table 7.1 Family of Infinite Elements

to fall exactly at the singularity point, i.e., the point of application of the load P. This is shown in figure 7.4.

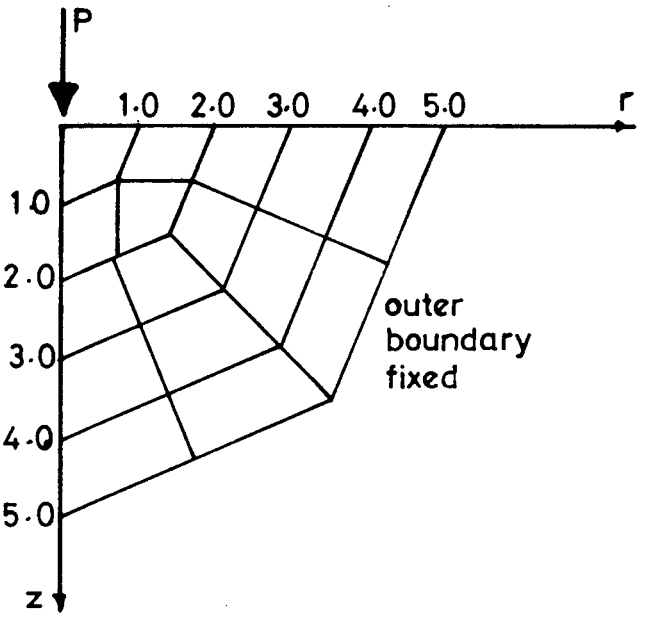

Figure 7.3 Finite element mesh for the Boussinesq problem

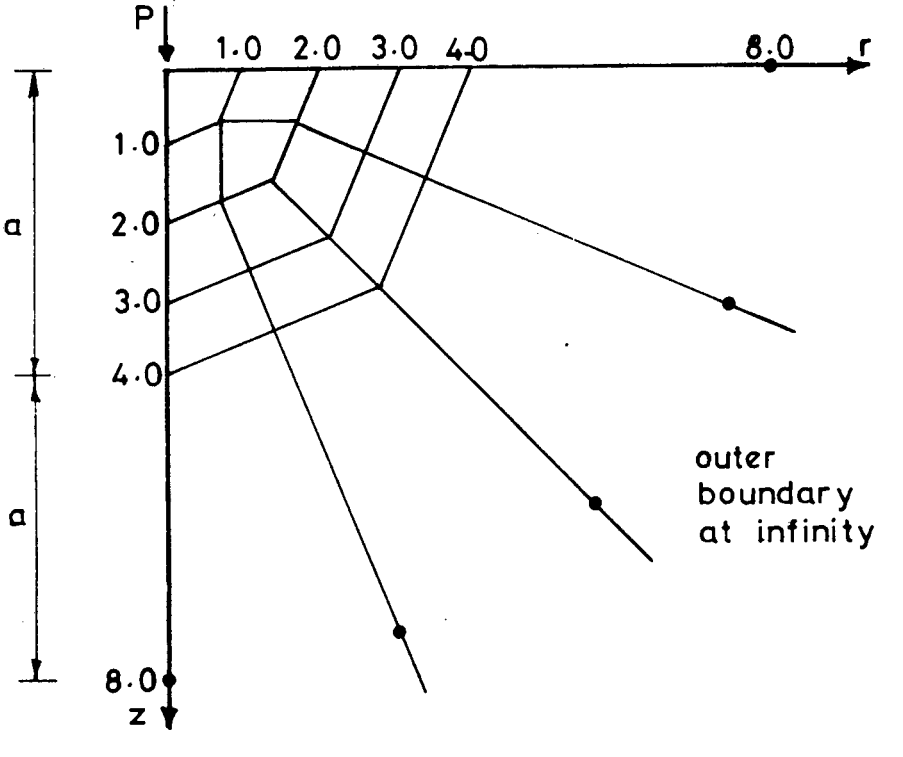

Figure 7.4 Finite/Infinite element mesh for the Boussinesq problem

Using this mesh, two separate analyses were performed. 9 Node Lagrange elements with their compatible infinite elements, Type 2 were tried using both 2x2 and 3x3 Gauss quadrature. Then the 8 node Serendipity elements with type 4 infinite elements were tried, again with both Gauss quadrature orders. In any particular analysis, however, a uniform integration order was used throughout.

The material properties used are as follows

$E = 1.0$ (Young's Modulus)
$\nu = 0.1$ (Poissons Ratio)
$P = 1.0$ (Point Load)

The results of these analyses are plotted in figure 7.5 where a comparison is made with the analytical solution given by

$$\omega = \frac{P}{2\pi E}\left\{(1+\nu)\frac{z^2}{(r^2+z^2)^{3}/2} + 2(1-\nu^2)\frac{1}{(r^2+z^2)^{1}/2}\right\} \qquad (7.16)$$

In figure 7.5 the vertical displacement along the z-axis (r = 0.0) is plotted. Consequently, the exact displacement can be calculated as

$$\omega = \frac{0.490197}{z}$$

It will be noticed that the results for the 9-node Lagrange finite or finite/infinite mesh, using 2x2 integration, have not been plotted. This is due to the severe oscillatory effect obtained when using this quadrature order and consequently it is realized that the reduced integration scheme is unsuitable for Lagrange elements. The use of 3x3 integration on the other hand, gives a perfectly smooth set of results, and, in the case of the finite/infinite mesh, exactly matches the analytical solution.

The oscillatory effect is also present in the Serendipity elements, but due to the reduced 2x2 integration order, the oscillations are effectively curtailed. An identical pattern of displacements is obtained for both the finite as well as the finite/infinite mesh, that is, the

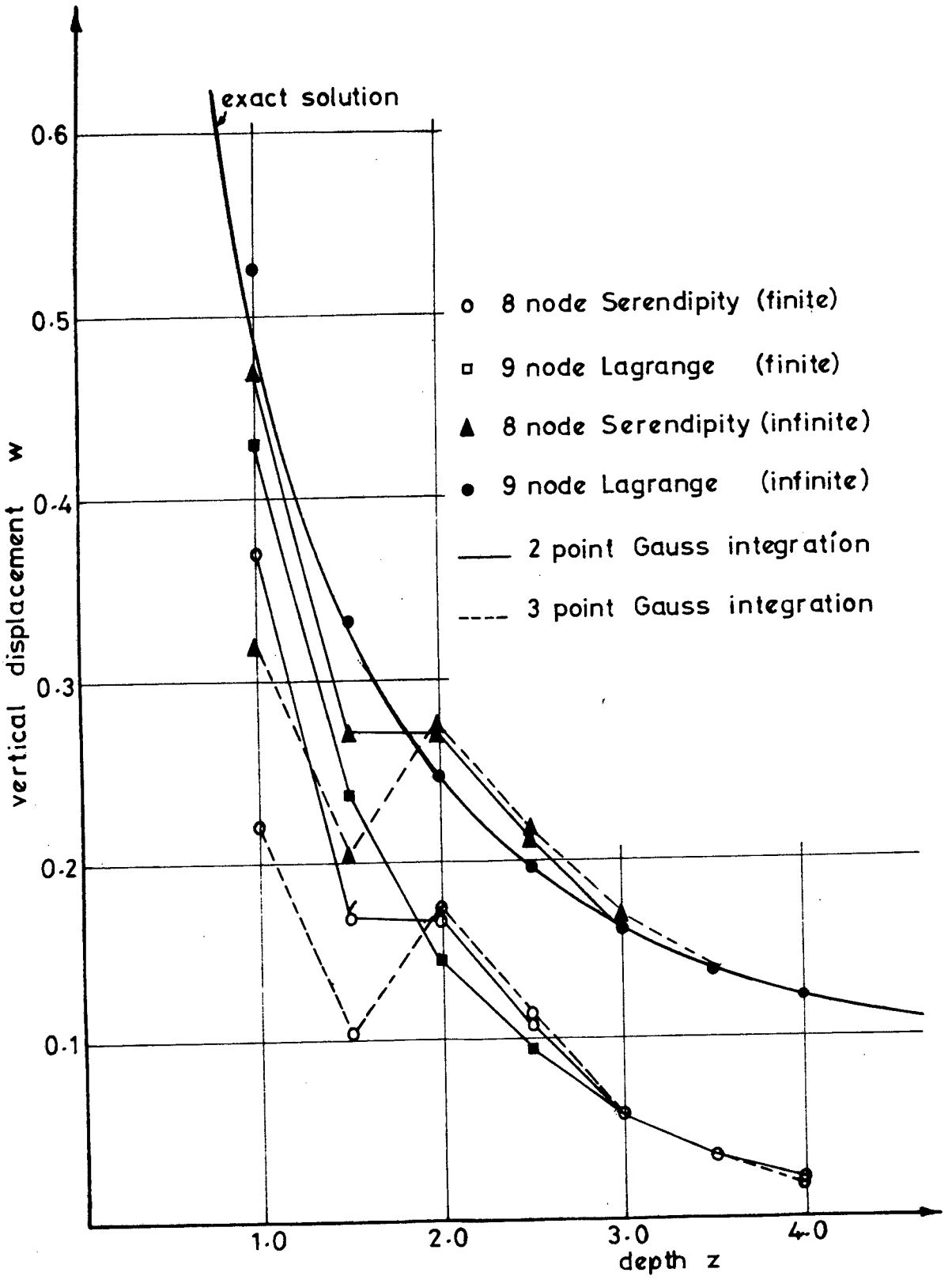

Figure 7.5 Point load on elastic half space.
Results of finite and infinite elements.

oscillations follow the same trends for both Gauss orders. An investigation shows that the most important contributory factor to the accuracy of the solution, is the order of integration over the finite elements. The infinite elements are insensitive to the integration order. Even a combination of Serendipity finite elements with Lagrange infinite elements and vice versa, produce similar results to those plotted in figure 7.5.

In summary then, the Lagrange finite/infinite elements using 3x3 integration are the most accurate. The Serendipity family requires the reduced 2x2 integration to be used to obtain a reasonable accuracy.

The advantage of infinite elements is thus clearly appreciated from the study of figure 7.5. At no extra computational cost, an accurate solution has been found. On the other hand, an extended finite element grid would be required to satisfy a reasonable accuracy criteria, but at considerable extra cost. With the incorporation of the infinite elements, the uncertainty in the solution is also diminished, provided care is taken in the positioning of the second node, that is, due regard must be placed to the pole dimension a.

7.3 The Boundary Integral Equation Method for problems to infinity

In the formulation of the infinite elements, the domain was allowed to extend to infinity in one or two directions. In the formulation of the infinite segment in the BIEM, the line segment will be allowed to extend to infinity. Similar methods to those used for finite elements will also be used here to achieve this objective. Advantages, particularly in data preparation and, to a lesser extent, in computer storage, are envisaged.

An important aspect of this formulation, is that the proposed technique must fit directly into the existing BIEM programs with a minimum of effort. This contrasts dramatically with other methods which rely on special purpose fundamental solutions [7.12] to achieve similar aims. Here, the concentration is on a numerical approach using the already established facts. For this purpose, an approach similar to

that proposed by Watson [7.13] is followed, but specific techniques learned from infinite element formulation are incorporated. Some of this work has already been presented at an international symposium [7.14].

7.3.1 The Boundary Integral Equation to infinity

To begin the analysis, it is assumed that the infinite region being investigated is, in fact, a finite area, Ω, with part of its boundary being allowed to extend to infinite in the limit. This can be represented graphically as in figure 7.6.

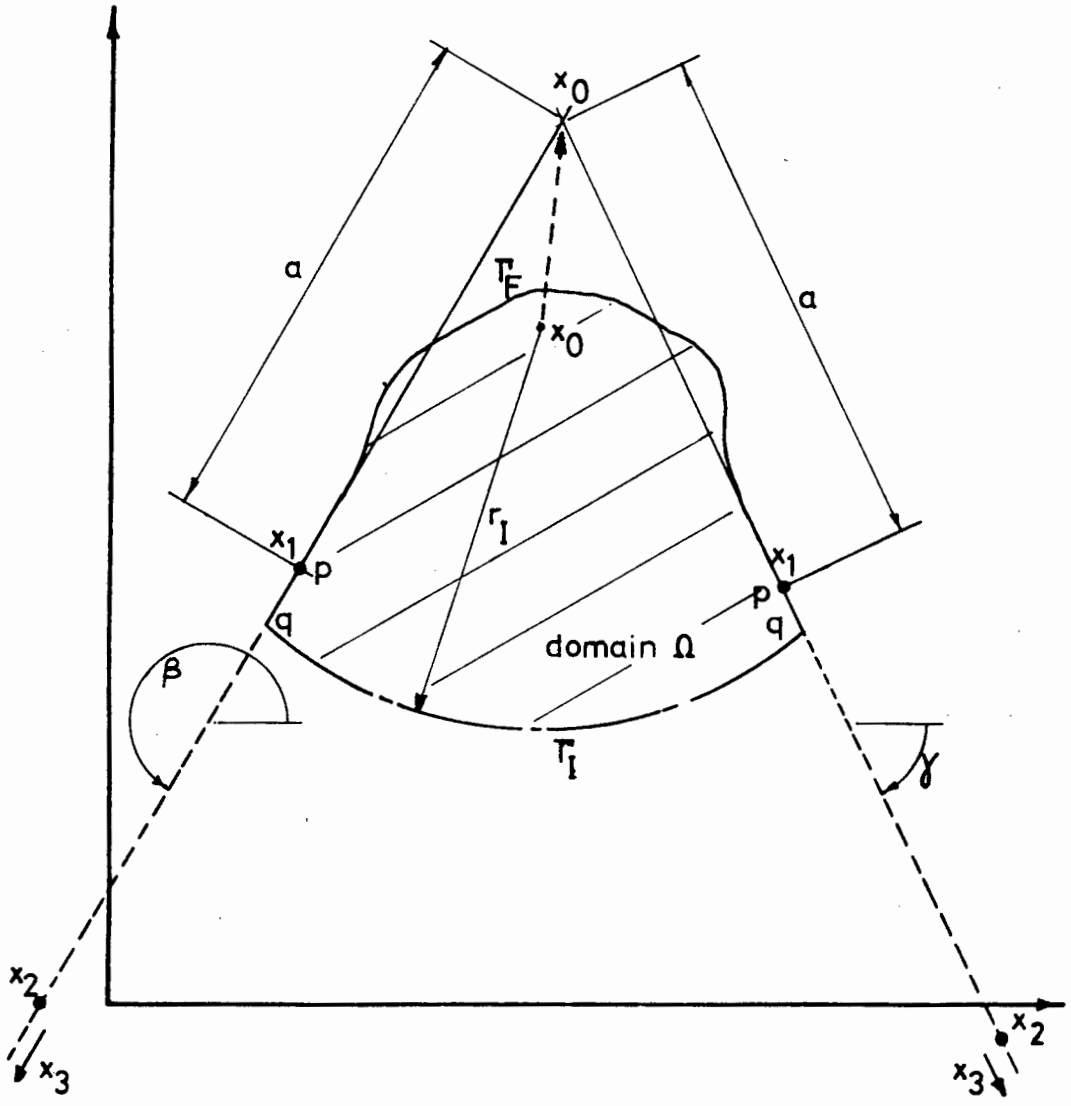

Figure 7.6 An infinite region

The finite boundary now consists of two parts so that

$$\Gamma = \Gamma_F + \Gamma_I \tag{7.17}$$

where Γ is the entire boundary (as before)

Γ_F is the finite boundary, and

Γ_I is the 'infinite' boundary

The original BIEM equation then becomes, after substitution of condition (7.17):

$$c_{ij}\, u_j(x) + \int_{\Gamma_F+\Gamma_I} T_{ij}(x,y)\, u_j(y)\, d\Gamma = \int_{\Gamma_F+\Gamma_I} U_{ij}(x,y)\, t_j(y)\, d\Gamma \tag{7.18}$$

The node x_o is an arbitrary point which is used as the pole for the variation of the displacement and traction. The distance from this point to node x is denoted by r_I, which in the limit, tends to infinity.

Now, in addition to the fundamental solutions satisfying the equations of equilibrium, two other conditions are also necessary over the boundary Γ_I [7.13], namely

$$u_i(x) \;\varepsilon\; o\left(\frac{1}{r_I}\right) \tag{7.19a}$$

$$t_i(x) \;\varepsilon\; o\left(\frac{1}{r_I^2}\right) \tag{7.19b}$$

These conditions effectively prescribe the interpolation functions required to model the displacements and tractions over sections $x_1 - x_3$ (figure 7.6), as point x_3 tends to infinity with r_I. Substitution of equation (7.19) into (7.18) ensures that the integrals over the infinite surface Γ_I tend to zero as $r \to \infty$.

In much the same way as the boundary integral equation was

produced from the Betti Somigliana formula in section 3.3.12 and Appendix A by limiting $\varepsilon \to o$, the same can be done in this case. Here, however, a limit is reached when $r_I \to \infty$. Performing this operation on equation (7.18) leads to

$$\bar{c}_{ij}\, u_j(x) + \int_{\Gamma_F} T_{ij}(x,y)\, u_i(y)\, d\Gamma = \int_{\Gamma_r} U_{ij}(x,y)\, t_j(y)\, d\Gamma \qquad (7.19)$$

where $\bar{c}_{ij} = c_{ij} + \lim_{r_I \to \infty} \int_{\Gamma_I} T_{ij}(x_o,y)\, d\Gamma$

which arises due to the limiting process.

The numerical calculation of this limiting term follows precisely the same form as described in Appendix A, with the exception that the r_I tends to infinity rather than ε tending to zero. For this purpose, the pole is postioned at the intersection of the lines drawn through $x_1 - x_2$. Γ_I then forms a segment, centred at x_o over which the integration can be performed, with a limit at infinity.

Consequently, the limiting expression can be written in terms of the angles γ and β by a 2x2 submatrix as follows

$$\bar{c}_{ij} = c_{ij} + \begin{bmatrix} -\left(\frac{\beta-\gamma}{2\pi} + \frac{\sin 2\beta - \sin 2\gamma}{8\pi(1-\nu)}\right) & \frac{(\cos 2\beta - \cos 2\gamma)}{8\pi(1-\nu)} \\ \frac{(\cos 2\beta - \cos 2\gamma)}{8\pi(1-\nu)} & -\left(\frac{\beta-\gamma}{2\pi} + \frac{\sin 2\beta - \sin 2\gamma}{8\pi(1-\nu)}\right) \end{bmatrix} \qquad (7.20)$$

From this definition it can readily be seen that if $(\beta-\gamma) = 2\pi$, i.e., a complete circle, then

$$\bar{c}_{ij} = c_{ij} - \delta_{ij} \qquad (7.21)$$

In this case, the second term is known as the azimuthal integral.

Equation (7.19) can now be used in the numerical formulation.

7.3.2 The Numerical Formulation

Over the boundary Γ_F, between the two points denoted p-q in figure 7.6, the standard boundary segments are used. In this formulation, either linear or quadratic segments can been used with equal ease. Over segments p-q as q tends to infinity however, an appropriate infinite segment must be used.

As for the finite element mapping of section 7.2.1, the geometry of an infinite boundary segment is defined by figure 7.1. x_o is the pole of the segment, x_1 is positioned at point p, a distance a from x_o, and x_2 is positioned a further distance a from x_1. The infinite shape functions defined by equation (7.6) are then applicable and results in x_3 being at infinity. The segment is defined between the natural co-ordinates $-1 \leq \eta \leq 1$ and hence the standard Gaussian integration schemes can be used. The Jacobian is easily calculated from

$$\frac{\partial x}{\partial \eta} = \frac{\partial N_1(\eta)}{\partial \eta} x_p + \frac{\partial N_2(\eta)}{\partial \eta} x_q$$

$$\frac{\partial y}{\partial \eta} = \frac{\partial N_1(\eta)}{\partial \eta} y_p + \frac{\partial N_2(\eta)}{\partial \eta} y_q$$

and $$J = \sqrt{\left(\frac{\partial x}{\partial \eta}\right)^2 + \left(\frac{\partial y}{\partial \eta}\right)^2} \qquad (7.21)$$

The numerical integration details are then given by section 4.3.1.

The interpolation of the displacement and traction variables over the infinite segment follows from conditions (7.19). The assumption is that the effects of a point load at position x (defined by equation (7.6)) decay with increased distance from the pole, as follows [7.13]:

$$u_i(\eta) = u_i(x_1)\left[\frac{r(x_o,x_1)}{r(x_o,x)}\right] \qquad (7.22a)$$

$$t_i(\eta) = t_i(x_1)\left[\frac{r(x_o,x_1)}{r(x_o,x)}\right]^2 \qquad (7.22b)$$

The only "structural" node used in this formulation is therefore the node x_1. Consequently, once the finite boundary Γ_F has been subdivided and the matrices accumulated, no extra information is required to include the infinite segments. Also, since the infinite segment is collinear with its neighbouring finite segment (by definition), both the traction and displacement are continuous at x_1.

Substitution of equation (7.20), (7.21) and (7.22) into (7.19) realized the numerical boundary integral equation method. As in the previous chapters, the integration over segments where $x \notin \Gamma_k$ is performed numerically by Gaussian Quadrature. But, for segments where $x \in \Gamma_k$, the integrals are performed analytically. For the infinite segment case, this is also true and occurs when $x=x_1$.

For this purpose, the infinite segment is defined as in figure 7.7. x_o is the pivot node, and this distance $x_o - x_1$ is denoted by a as before. r is the distance from the pivot node $x=x_1$ to an arbitrary integration point on the infinite segment, and θ is the angle between the x-axis and the vector $\tilde{r}$.

The evaluation of the integral over the infinite segment now requires the application of a double limit, as follows

$$G_{ij} = \int_o^\infty \bar{N}\, U_{ij} d\Gamma = \int_o^\infty \left(\frac{a}{a+r}\right)^2 U_{ij} d\Gamma$$

$$= \lim_{\substack{\varepsilon \to o \\ \gamma \to \infty}} \int_\varepsilon^\gamma \left(\frac{a}{a+r}\right)^2 U_{ij} d\Gamma \qquad (7.23)$$

After performing the integration and applying the limits separately the following formulae are produced:

$$G_{11} = \frac{a}{8\pi G(1-\nu)} \left[(3-4\nu)\, \ln\frac{1}{a} + \cos^2\theta \right] \qquad (7.24)$$

$$G_{12} = G_{21} = \frac{1}{8\pi G(1-\nu)} \left[a \sin\theta \cos\theta \right] \qquad (7.25)$$

$$G_{22} = \frac{a}{8\pi G(1-\nu)} \left[(3-4\nu)\ \ln\frac{1}{a} + \sin^2\theta \right] \qquad (7.26)$$

and are then accumulated into the systems matrix as before.

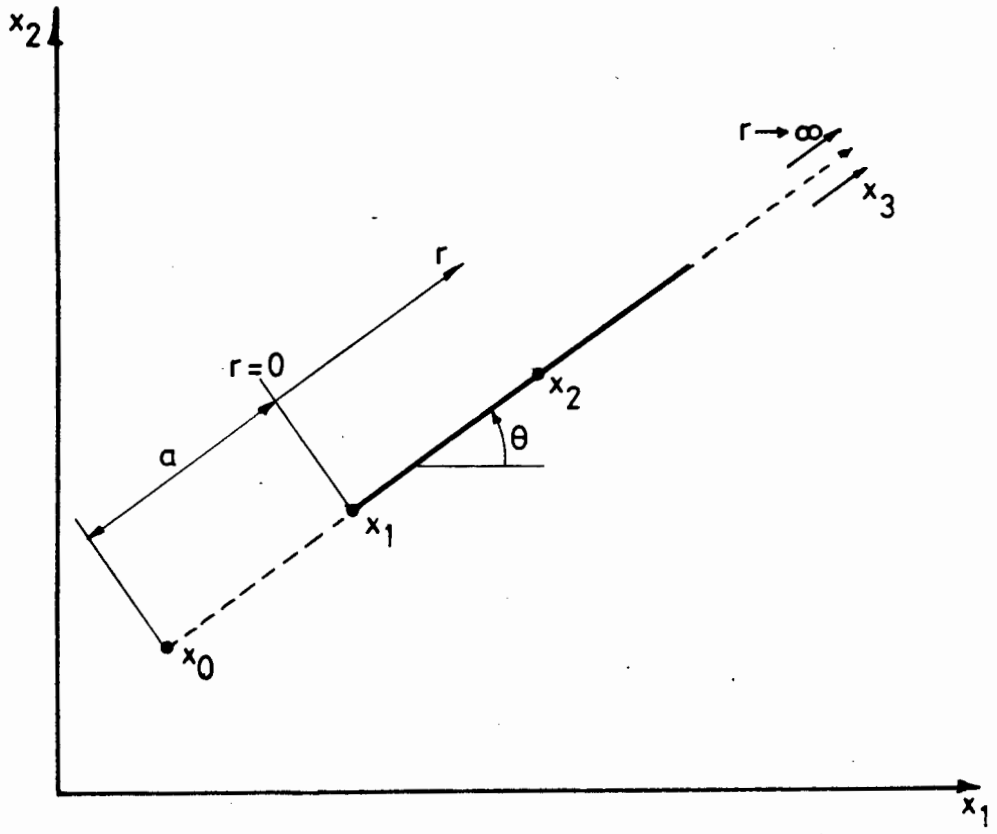

Figure 7.7 An infinite segment

These details are easily included in the existing Boundary Integral programs with only slight modifications. The accuracy of the technique when applied to an actual problem, is however the most important criterion. This is investigated, by way of an example, in the following section.

7.3.3 An Example

An elastic half space has been chosed for comparison purposes. The model is assumed to be in the condition of plane strain, with a unit

load being applied over a 1 unit length of the surface (figures 7.8, 7.9). The Youngs Modulus is E=1000 and the Poisson's Ratio ν=0.3.

In the modelling of the structure, symmetry was employed and therefore only one quadrant is used. Four models were set up, 2 finite/infinite element models and 2 BIEM models. Model 1 (figure 7.8a) consists of 12 Lagrangian 3-node finite elements and 4 compatible infinite elements. Model 2 (figure 7.8b) has 16 Lagrangian finite elements. Forced Boundary conditions are applied to at a radius of 5 units. The BIEM models consist of (figure 7.9a) a square of dimensions 3x3 units in which the right hand and lower boundaries are rigidly fixed (forced boundary conditions). In Model 4 (figure 7.9a) the infinite segments are employed on the horizontal surface and on the vertical axis of symmetry. In all models the axis of symmetry is taken to be the left hand vertical boundary on which u_1=o and u_2 is free. The line load of 1 unit is applied to a unit length on the upper surface.

The vertical surface displacement due to this load is compared in figure 7.10 for the four models. Comparison between the finite element and finite segment model is excellent. Also, the shape and the position of the BIEM results does not alter significantly when the shape of the outer boundary is changed. For instance, if the outer boundary is made into an arc, the results are virtually identical to those plotted. Therefore, although the finite element and finite segment models do not seem comparable at first glance, they are representative of the analysis method.

The comparison of the infinite element and infinite segment solutions do not show the same consistency however. Although both curves have the identical shape there is a definite discrepancy between them. The infinite element solution has been shown to be reliable (section 7.2) and it follows the displacement shape expected from a Boussenesg-type problem. The infinite segment solution also follows the expected displacement shape but seems to be misplaced by a constant amount. At present the reason for this slight discrepancy cannot be explained and remains a topic for further research. However, the results are very promising and it can be stated, without fear of contradiction, that the method proposed in this chapter will clearly be applicable to this class of

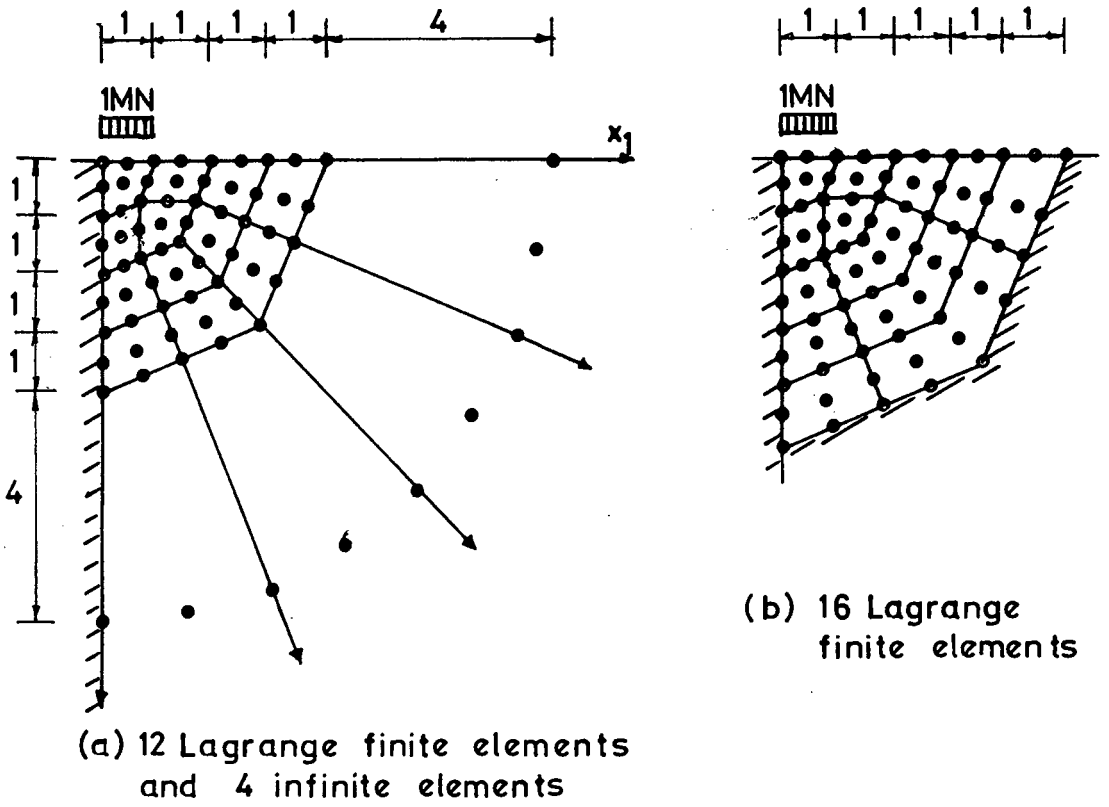

Figure 7.8 Finite/infinite element models

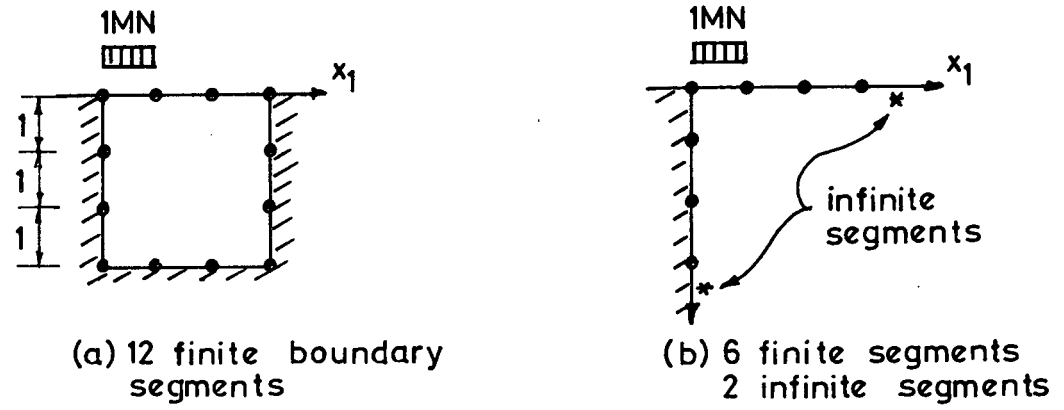

Figure 7.9 Boundary Integral Equation Method model

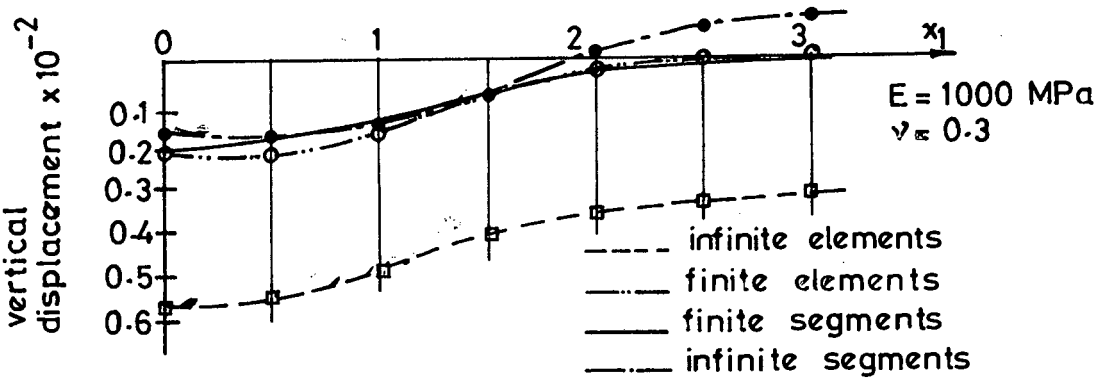

Figure 7.10 Comparison of surface displacements

problem when these minor discrepancies have been overcome.

Further analyses were also carried out in an attempt to find the cause of the inconsistency in the infinite segment solution. In these analyses 12 finite segments (6 on the horizontal boundary and 6 on the vertical boundary) and 2 infinite segments were used. This meant that the finite segments stretched from $x_1 = 0$ to $x_1 = 6$, double the distance as that used in Figure 7.9b. In addition, the Poisson's Ratio assigned to the material was varied from $\nu = 0.1$ to $\nu = 0.45$. The surface displacements of these analyses are shown in Figure 7.11.

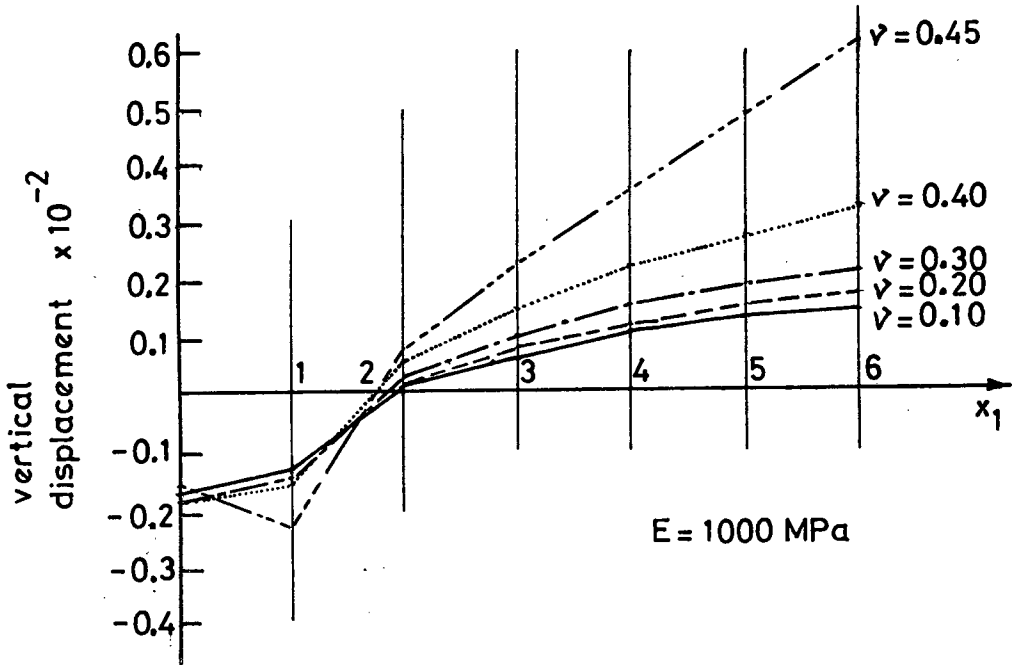

Figure 7.11 Infinite segment analyses - surface displacements

These analyses show conclusively that results from the Boundary Integral Equation Method using infinite segments are consistent, irrespective of the positioning of the infinite segment. In both cases where the infinite segment was placed at $x_1 = 3.0$ units and now at $x_1 = 6.0$ units, the shape and characteristics of the surface displacements are identical, but are still misplaced when compared to the infinite element solution.

The effect of changing the Poisson's Ratio is marked and expected. With an increase in ν , that is tending towards the incompressive material $\nu = 0.5$ results in a more prominent "bulge" of material remote from the loading points, as would be expected from an incompressible but deformable material.

Throughout these analyses it is evident that the shape of the curve described by the surface displacement in both the finite element and BIEM solutions are identical, but merely differ by a constant. This cannot be mere coincidence. The mathematical derivation of the infinite segments appears to be sound and hence it is hoped that further research will overcome this anomaly.

7.4 Conclusion

The analysis of continua which can be considered as having part of their boundary at infinity, is the subject of this chapter. Great advances have been made recently, especially by Owen [7.8], for the solution of these problems by the Finite Element Method, with the development of mapped infinite elements. Here, the inclusion of infinite segments in the standard Boundary Integral Equation Method is discussed. Both methods are designed so that they can be slotted directly into either an existing FEM or BIEM program code.

For completeness, the derivation of the mapped infinite element is included, with special reference to the shape functions employed. The shape functions for the infinite elements which join on to the common linear and quadratic 2-dimensional finite elements are also derived and discussed.

Boussinesq's problem of a point load on an infinite elastic axi-symmetric half space is used to compare the various mapped infinite elements. It has been found that the finite/infinite elements based on Lagrange-type interpolation functions are the most accurate, if a 3 x 3 integration scheme is used. A reduced 2 x 2 integration scheme must be used to obtain reasonable results from the Serendipity family of elements.

The ideas used in the mapped infinite element approach have been used to design an infinite segment for the Boundary Integral Equation Method. This segment has the advantage that the computer coding can be added directly to an existing BIEM program; indeed, this was a pre-requisite of the method. The complete definition and derivation is given.

A 2-dimensional elastic half space has been used as an example for comparison purposes. Both finite element and boundary integral models have been used in the analysis. A comparison of the results shows that, although the boundary integral infinite segment method is not entirely accurate, the shape of the displacement curves when compared to the FEM solution are identical. A constant discrepancy exists. The solutions are, however, feasible and while the exact cause of the discrepancy can not be found at this stage, it is hoped that further research will overcome the difficulty. Nevertheless, it has been shown that the method is feasible and the results are repeatable. A considerable saving on computer storage is accomplished by this method when compared with the formally used domain truncation method.

7.5 References

7.1 P. BETTESS, 'Infinite Elements', Int. J. Num. Meth. Engng., Vol. 11, page 53 - 64- (1977).

7.2 P. BETTESS, 'More on Infinite Elements'. Int. J. Num. Meth. Engng, Vol. 15, page 1613 - 1626, (1980).

7.3 P. BETTESS, O.C. ZIENKIEWICZ, 'Deffraction and refraction of surface waves using finite and infinite elements', Int. J. Num. Meth. Engng, Vol. 11, page 1271 - 1290, (1977).

7.4 G. BEER, J.L. MEEK, 'A boundary finite element for undergroung mining applications', in New Developments in Boundary Element Methods, (ed. C.A. Brebbia) Newnes-Butterworths, London (1980).

7.5 G. BEER, J.L. MEEK, 'Infinite domain elements', Int. J. Num. Meth. Engng, Vol. 17, page 43 - 51, (1981).

7.6 P.P. LYNN, H.A. HADID, 'Infinite elements with $1/r^n$ type decay', Int. J. Num. Meth. Engng., Vol. 17, page 503 - 526 (1981).

7.7 F. MEDINA, 'An axisymmetric infinite element', Int. J. Num. Meth. Engng. Vol. 17, page 1177 - 1185 (1981).

7.8 D.R.J. OWEN, private communication, February 1982.

7.9 O.C. ZIENKIEWICZ, The Finite Element Method, 3rd Edition McGraw-Hill, New York (1977).

7.10 D.R.J. OWEN, E. HINTON, Finite Elements in Plasticity: Theory and Practice, Pineridge Press Ltd., Swansea U.K. (1980).

7.11 S.P. TIMOSHENKO and G.N. GOODIER, Theory of Elasticity, 3rd Edition, McGraw-Hill (1970).

7.12 C.A. BREBBIA and S. WALKER, Boundary Element Techniques in Engineering, Newnes-Butterworths, London (1980).

7.13 J.O. WATSON, 'Advanced Implementation of the Boundary Element Method for Two- and Three-dimensional Elastostatics', in Developments in Boundary Element Methods - 1, (eds. P.K. Banerjee and R. Butterfield).

7.14 G.C. HOWELL and W.S. DOYLE, ' Infinite Domain Problems by Finite Elements and Boundary Integrals', Proceedings of the FEMSA/83 International Symposium on Design and the Finite Element Method, held on 11 - 12 January 1983 at the University of Cape Town.

CHAPTER 8

ADAPTIVE PROGRAMMING TECHNIQUES

8.1 Introduction

The choice of the boundary subdivision and the type of segment used in an analysis, has a direct bearing on the accuracy attained. The optimum choice of the parameters is not possible at a glance as can be seen from the selected examples in other chapters. It is therefore, the purpose of this chapter to investigate the possibilities of choosing the best combination of subdivisions and segment allocations automatically.

There are two main methods whereby this can be accomplished, namely:

(i) h - convergence
(ii) p - convergence

The former method, h - convergence, derives it's name from the dimension h, which represents the size of the element or segment used. Here, the convergence to the theoretically correct answer is achieved by successive analyses in which the domain is subdivided into smaller and smaller elements (Finite Element Method) or the boundary into smaller segments (Boundary Integral Equation Method), (i.e., h is decreased) but, at all times, keeping the same interpolation formulation for each element/segment. This is essentially the process of successive mesh refinement which is performed manually in a conventional numerical analysis. The h-convergence technique can be used successively in a self-adaptive sense by allowing the decision to re-analyse with a finer mesh to be made automatically, subject to some predefined convergence criteria. These criteria are, in the Finite Element Method, usually based on energy considerations or on the continuity of stresses across element boundaries [8.1 to 8.7] , but for the Boundary Integral Equation Method, a new set of criteria are required.

P-convergence, on the other hand, uses a constant geometric mesh layout for all analyses. The convergence to the theoretical result is obtained by successively increasing the order of the polynomials used to describe the variation of the variables over the elements/segments. The reassignment of higher-order polymonials is applied only to those elements/segments which do not pass the predetermined convergence tolerances. By repeated refinement, a more correct result can be obtained.

In this chapter, the p-convergence technique, as applied to the BIEM, is of particular relevance. The h-convergence technique, which is of no lesser importance, practically, is simply implemented and requires the convergence criteria only to be specified. Hence no further elaboration will be necessary.

When developing a technique of this kind, one important factor must be borne in mind throughout : economy of calculation time. With reference to h-convergence when applied to the BIEM, it will be appreciated that once the original matrices have been generated, a subdivision of a single segment would require a substantial amount of extra calculation and matrix adaption. Thus, in the design of the p-convergence technique and in the interests of economy these problems are recognised and circumvented accordingly.

It will be seen that, in this technique, the original matrices, once generated, are never changed. The refinement, due to the increased order of the interpolation polynomial, is accomplished by a simple matrix addition. In order to facilitate this however, a hierarchical formulation of the basis shape function must be derived. The details of this formulation and of the proposed convergence criteria are fully discussed.

Finally, to conclude the chapter, an example, showing the workings of the BIEM adaptive technique is presented.

8.2 The p-convergence Method

An adaptive programming technique presupposes that a series of

analyses are to be performed. The results of each analysis are subjected to a test of convergence prescribed by a set of user-defined criteria. On the strength of this test, changes to the mesh or boundary subdivision are made automatically before the following analysis is performed. By the nature of this process, it can be seen that a number of successive analyses may be necessary before an "acceptable" answer is obtained. This is naturally time-consuming and hence expensive computationally and it is imperative that all available methods be used in order to economize on computer time.

In the p-convergence method as applied to the BIEM, the boundary is subdivided into segments only once, prior to the first analysis. The geometry of the segments is then fixed and subsequent analyses merely redefine the interpolation polynomials over these segments.

From this, it is evident that the matrices derived for the first analysis must be changed to accommodate a higher order polynomial over those segments which require an adaption in later analyses. If the entire matrix were to be rederived from scratch for every analysis, this would be extremely time-consuming and prohibitively expensive. Thus, in order to economize, a method must be found whereby the existing matrices can merely be augmented with the additional data necessary for the inclusion of a higher order polynomial over a certain segment. In order to accomplish this, a special set of hierarchical shape functions are needed. Then, using this formulation, the aim of the p-convergence method to give an economical solution to a problem subjected to a set of convergence criteria, can be successfully accomplished.

8.2.1 The Hierarchical Shape Function Formulation

The basic philosophy behind the formulation of a set of hierarchical shape functions is as follows. It is required to design a recurrence formula for the shape functions so that the following conditions are met:

(i) a 2-noded segment, i.e., a linear segment is used as the basis for the formula. Hence, all the details contained

in previous chapters are valid here.

(ii) The extra nodes necessary to increase the polynomial interpolation to a higher order must be positioned so that no change in the position of the existing nodes is necessary.

(iii) The contributions, during the integration process, of the shape functions at the existing nodes must be calculated as the sum of the existing lower order contributions, plus a multiple of the shape functions for the extra node. This condition will ensure that the matrix relevant to a higher order interpolation is merely the summation of the existing matrix plus an additional matrix which is dependant on the shape functions of the added node(s) only.

These aims are easily accomplished if the established rules of geometry and geometric progressions are observed. For this purpose, consider Table 8.1 in which the complete strategy of the current p-convergence method as applied to the BIEM is presented.

There are a few accompanying notes which must be borne in mind when table 8.1 is studied. Firstly, the order of the positioning of the nodes on the segment is important and is a big factor in the design of the shape functions. Nodes 1 and 2 are at the ends of the segment, while node 3 is at the centre of the segment. These three nodes define the quadratic shape functions. The additional nodes required for the quartic shape functions are positioned at the quarter points i.e., at $\xi = -\frac{1}{2}$ and $\frac{1}{2}$. Higher order shape functions are produced by positioning nodes at the centre of each "subsegment". Hence, and octic segment, which requires 9 nodes in total, would be formed by placing nodes 6, 7, 8 and 9 at $\xi = -\frac{3}{4}, -\frac{1}{4}, \frac{1}{4}, \frac{3}{4}$ respectively. This can be seen graphically in table 8.1.

Secondly, the significance of the letter n denotes the order of the shape functions. This letter represents a simple geometric progression which starts at zero and increases by powers of two (e.g. 2^{ℓ}). The numerical order, that is, unity related to linear functions, two to quadratic functions etc., is denoted by $m = 2n$ with the exception that $m = 1$ for $n = o$.

Interpolation Order n	Node	Shape Function Diagram	Type of Node	Shape Function Formula
Linear n=o	1	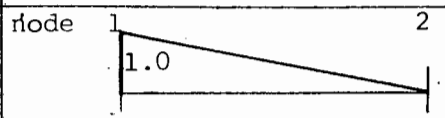	Basic	$N_1^1 = \frac{1}{2}(1 - \xi)$
	2	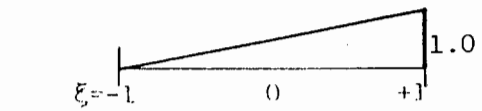	Basic	$N_2^1 = \frac{1}{2}(1 + \xi)$
Quadratic n=1	1	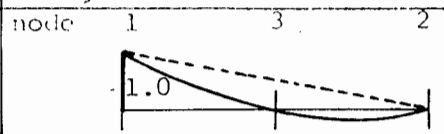	Existing	$N_1^2 = N_1^1 - \frac{1}{2} N_3^2$ $= \frac{1}{2} \xi(\xi - 1)$
	2	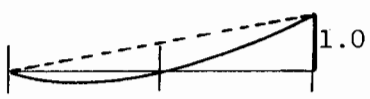	Existing	$N_2^2 = N_2^1 - \frac{1}{2} N_3^2$ $= \frac{1}{2} \xi(\xi + 1)$
	3	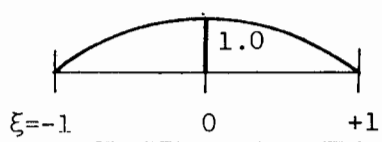	Additional	$N_3^2 = 1 - \xi^2$
Quartic n=2	1	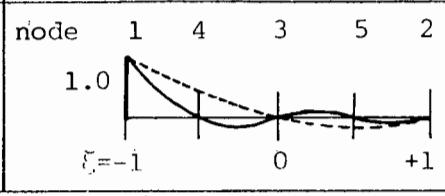	Existing	$N_1^4 = N_1^2 - N_1^2(-\frac{1}{2})\ N_4^4 - N_1^2(\frac{1}{2})\ N_5^4$

Cont./....

Interpolation Order n	Node	Shape Function Diagram	Type of Node	Shape Function Formula
Quartic n=2 continued	2	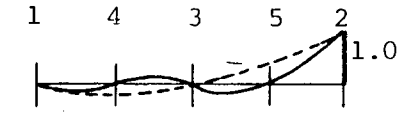	Existing	$N_2^4 = N_2^2 - N_2^2(-\frac{1}{2})\ N_4^4 - N_2^2(\frac{1}{2})\ N_5^4$
	3	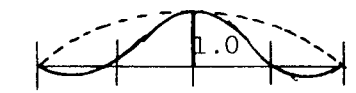	Existing	$N_3^4 = N_3^2 - N_3^2(-\frac{1}{2})\ N_4^4 - N_3^2(\frac{1}{2})\ N_5^4$
	4	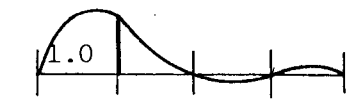	Additional	N_4^4 = new shape function
	5	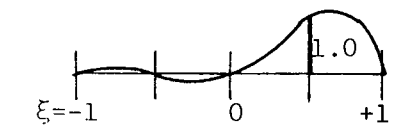	Additional	N_5^4 = new shape function
Octic n=4		node 1 6 4 7 3 8 5 9 2 ectcetera		

Key: N_i^m denotes the shape function centred at node i. The order of the interpolation functions is m where the following relationship holds

n	o	1	2	4	6	16	...
m	1	2	4	8	16	32	...

ie. m = 2n

with m = 1 for n = o

$N_i^m(\xi)$ denotes the value of the shape function for node i and of order m evaluated at a point ξ.

Table 8.1 Heirarchical shape function definitions

This nomenclature has been used so that a relatively simple and easily programmed recursive relationship can be designed to describe all possible shape functions. To reiterate, the idea is to build up the higher order shape function from

(i) the shape functions of the extra nodes introduced for that segment; and;

(ii) the previously evaluated (lower order) shape functions present at the already-defined nodes.

By so doing, the general form of the shape functions becomes:

(i) for the new nodes introduced to the segment

$$N_i^{2n}(\xi) = \prod_{\substack{k=1 \\ \gamma_k \neq \zeta_i}}^{2n+1} \frac{(\xi - \gamma_k)}{(\zeta_i - \gamma_k)} \qquad \text{for } i = j = n+2, \ldots, 2n+1 \quad (8.1)$$

(ii) for the existing nodes

$$N_i^{2n}(\xi) = N_i^n(\xi) - \sum_{j=n+2}^{2n+1} N_i^n(\eta_j) N_j^{2n}(\xi) \qquad \text{for } i = 1, \ldots, n+1$$

with n defined as above (8.2)

$$\text{where } N_i^n(\eta_j) = \prod_{\substack{k=1 \\ \gamma_k \neq \zeta_i}}^{n+1} \frac{(\eta_j - \gamma_k)}{(\zeta_i - \gamma_k)} \qquad (8.2a)$$

In both equations (8.1) and (8.2), the symbols have the following meaning :

ξ = natural co-ordinate $-1 \leqslant \xi \leqslant 1$ at which the shape function value is required.

ζ_i = natural co-ordinate at node i such that the shape function value is unity.

γ_k = natural co-ordinate at node k.

η_j = natural co-ordinate at node j.

Also

Ω denotes the multiplication of each term in the sequence, and

Σ denotes the addition of each term in the sequence.

From equations (8.1) and (8.2) it is clearly evident that the shape functions at the new nodes ($i = n + 2, \ldots, 2n + 1$) must be calculated independently. The shape function values at the old, existing nodes are then calculated from the product of the value at the new nodes and a constant, depending on the value of the shape function at the lower order ($N_i^n(\eta_j)$).

Hence the algorithm for the calculation of the shape functions at ξ can be derived as follows:

(i) Use equation (8.1) to calculate the shape function values $N_i^{2n}(\xi)$ for the new nodes, then

(ii) Evaluate the constant $N_i^n(\eta_j)$ from equation (8.2a)

(iii) Substitute $N_i^n(\eta_j)$ and $N_j^{2n}(\xi)$ into equation (8.2) together with the existing value of the shape function $N_i^n(\xi)$ node i to produce the higher order value at ξ for node i.

These formulae can easily be verified by simple numerical examples. Also, these equations are easily programmed thus resulting in efficient and automatic calculation of all the desired shape functions needed in the p-convergence algorithm.

8.2.2 The Implementation

The details of the method in which the heirarchical shape functions and their associated boundary segments are used, is most easily illustrated by the flow chart, figure 8.1. All the essential ingredients of the p-convergence, adaptive programming technique as used in the BIEM are included there. A more detailed description of each function is given in the following paragraphs ("block n" in the following refers to figure 8.1).

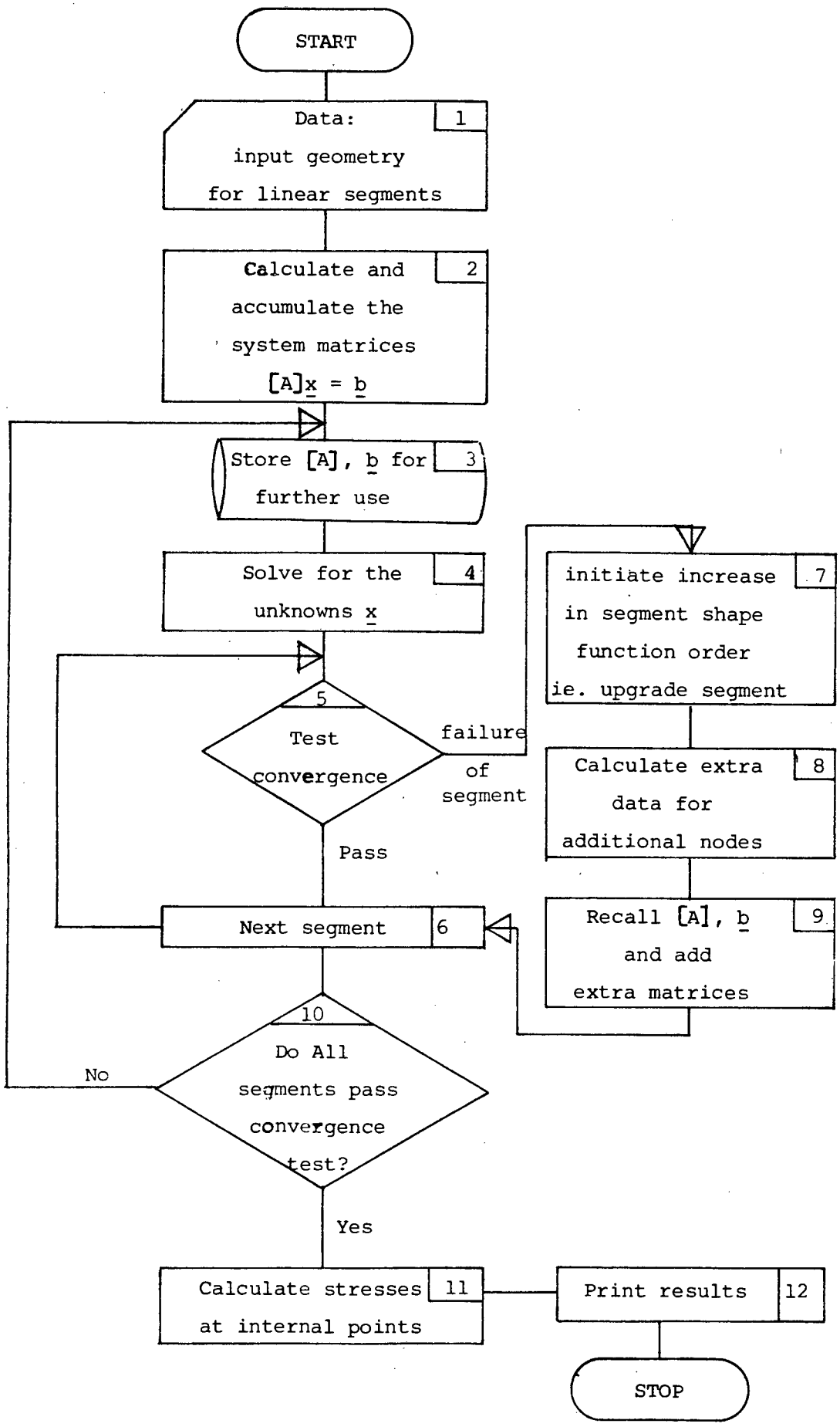

Figure 8.1 Macro flow chart of the p-convergence adaptive programming method

Block 1: Data

The whole concept of the adaptive programming technique is based on the idea that the simplest and coarsest sub-division of the boundary can be used to provide an initial solution to the problem. Thereafter, the solution is successively refined in the most critical areas, in so doing, "marching" forward to a more representative analysis. With this in mind, it is therefore, obvious that the process should start by subdividing the boundary into simple 2-noded lenear segments. This follows exactly the same form as described in chapter 4 and hence becomes the primary building block in the process.

The initial data required would be:

(a) the co-ordinates of the node points
(b) the support or essential boundary conditions
(c) the loading
(d) the material properties
(e) the location (co-ordinates) of internal points

The material properties and the co-ordinates of internal points will remain unchanged throughout the analysis. The linear segments are defined between successive node points as before, while the support conditions and the loading apply over a complete segment. In other words, if, for example, loading or support constraints are specified over segment n (which has nodes m and m+1 at its ends), then this loading or support constraint will remain applicable to all nodes subsequently included in the segment to improve the interpolation order. Loading and support data is therefore segment orientated, rather than nodally orientated.

Block 2: System Matrices

The [G] and [H] matrices are assembled in precisely the same way as was described in chapter 4, the boundary conditions are applied and the system matrix equation $[A]\underline{x} = \underline{b}$ is formed, where $\underline{x}$ is the vector of unknown degrees of freedom. At this stage, the equation represents the

analysis in terms of linear segments only. Due to the likelyhood that a very coarse boundary subdivision is used initially, matrix [A] at this stage is relatively small, but will expand when higher order interpolations are implemented.

Block 3: Storage

At the initial stage, the matrix [A] and the vector $\underline{b}$ are stored for further use. In order to save on memory space, [A] and $\underline{b}$ are written to an external file.

Block 4: Solution

The matrix equation $[A]\underline{x} = \underline{b}$ is now solved in terms of the unknown $\underline{x}$. A solution is now available and can therefore, be checked for consistency.

Blocks 5 and 6: Convergence test for each segment

Each segment is now taken in turn and subjected to the test for convergence. At this stage, it is enough to say that the displacements and tractions over the segment must conform to some predefined criteria. The details of these criteria are given in section 8.2.3.

Block 7: Increase interpolation order of segment

In the event that a segment fails the convergence test, it means that the shape function (i.e., the segment type) used was unable to interpolate the field variable in this region with sufficient accuracy. Hence, the interpolation order n for this segment (see Table 8.1) is increased by one, that is, a linear segment (n=o) is upgraded to a quadratic segment (n=1), and so on.

Block 8: Additional data

Increasing the interpolation order of a segment requires that additional nodes be introduced. The co-ordinates of these nodes are

calculated to lie on a straight line between the end nodes. Hence, the normal to the segment and the segment length remain unchanged. It should be noted here that no attempt is made in this analysis to successively reduce the possible error occuring due to the initial modelling of the geometry of the structure. It is assumed that the initial layout of linear segments is sufficiently fine to ensure that this possible error is negligble. Consequently, a curve modelled with a number of facets of linear segment, will not be more accurately modelled by the successive use of quadratic, quartic, etc, segments assigned to overlay the original segments. Only the accuracy of the field variables are affected by this process.

Block 9: Additional terms from upgraded shape functions

Once the matrix [A] has been set up initially, any upgrading of the interpolation functions over a segment merely requires the addition of the extra terms to the matrix.

The terms in the matrix are of the form:

$$\int_{\Gamma_k} N_i^{2n} V_{ij} d\Gamma \, v_j = A_{ij} \qquad (8.3)$$

where N_i^{2n} is defined as in (8.1) or (8.2)

V_{ij} is either the fundamental traction solution T_{ij}
or the fundamental displacement solution U_{ij}

and v_j is the traction variable t_j
or the displacement variable u_j

The integration is performed by Gauss Integration as usual.

Diagrammatically, the accumulation process can be laid out as in figure 8.2. For the purposes of clarity, let the numerical value obtained for A_{ij} from (8.3) be denoted by the lower case alphabet for the nodes i = 1, 2, ... Also, let the letters denoted by primes be the additional contributions to existing nodes calculated from the second term in (8.2). The unprimed letters denote the contribution from

Node		1	2	3	4	5	6	7	8	9	....	Row
Linear n = o		a	b									1
Quadratic n = 1	+ -	a'	b'	c								2
	=	a+a'	b+b'	c								3
Quartic n = 2	+	a"	b"	c'	d	e						4
	=	a+a'+a"	b+b'+b"	c+c'	d	e						5
Octic n = 3	+	a"'	b"'	c"	d'	e'	f	g	h	i		6
	=	etc.										

Figure 8.2 Diagrammatic representation of the successive accumulation process

new nodes in the segment.

As an example of the actual accumulation process, assume that the matrix [A] has been set up using only linear segments. Also assume that only one linear segment (with end nodes i and j) is to be upgraded to a quadratic segment (the additional node being k). Then, for an arbitrary pivot node n, the existing elements of matrix [A] for nodes i and j are respectively a and b, using the nomemclature of figure 8.2. The additional contributions due to the upgrading of the segment to quadratic are denoted a', b' and c. This is depicted in figure 8.3.

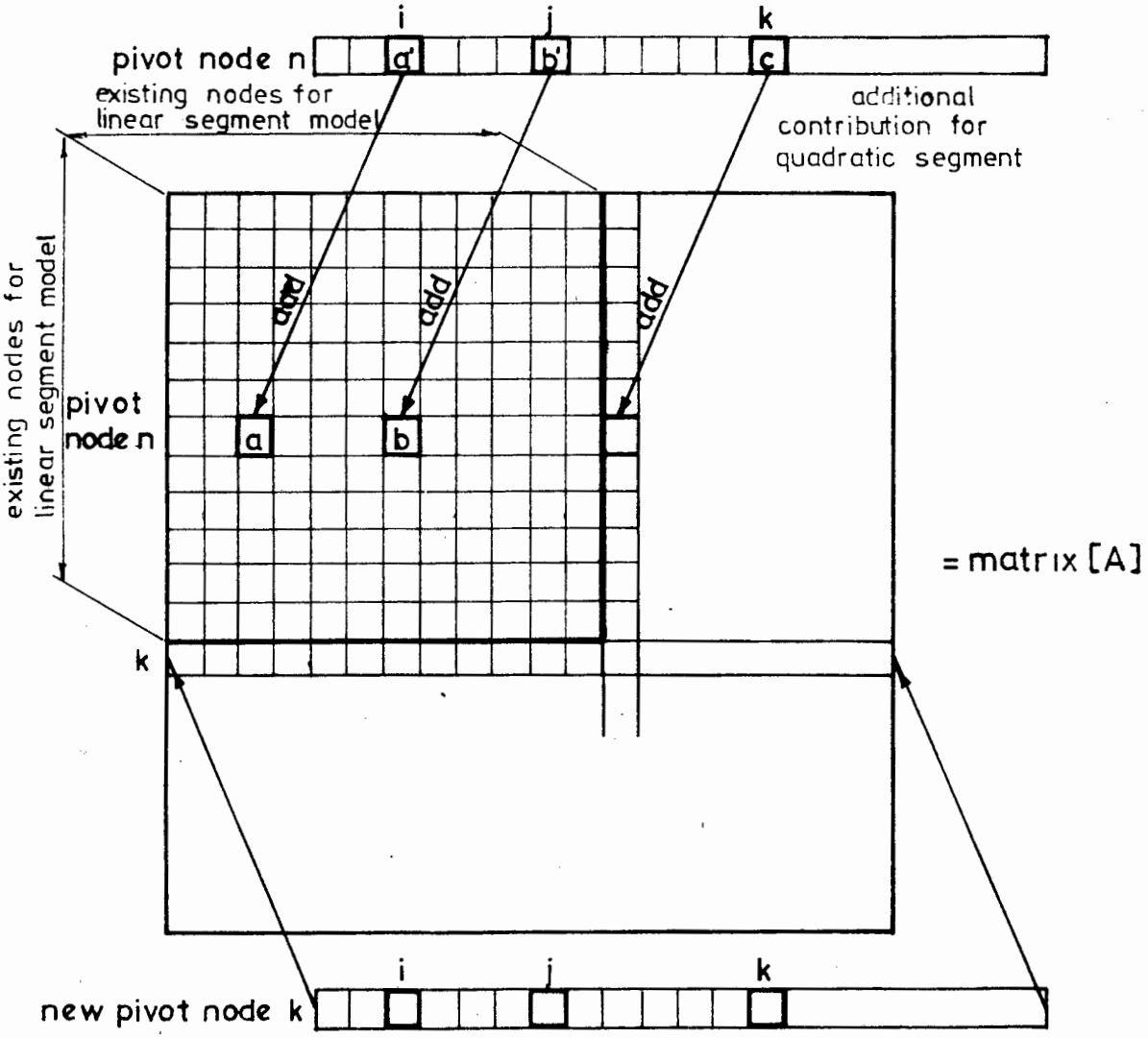

Figure 8.3 Diagrammatic accumulation of a quadratic segment into an existing linear segment matrix

The process shown in figure 8.3 is repeated for each successive pivot node n(n = 1, ..., N) in the structure. Of course, since an additional node k has been added, an additional row is needed for the pivot at node k.

This process is carried out for each upgraded segment in turn.

Block 10: Completion check

In the event that any of the segments failed the convergence check, a reanalysis is necessary. Control is therefore, transferred back to Block 3 so that a resolution can be performed.

Once all segments have passed the convergence check, the solution is accurate enough and post processing of the results can begin.

Block 11: Calculation of stresses and displacements at internal points

Using the upgraded boundary subdivision and the additional nodes, the displacements and stresses at the predefined internal points are calculated as in Chapter 4.

Block 12: Output

Finally, a comprehensive set of results, including the displacements and tractions at the boundary nodes as well as the displacements and stresses at the internal nodes are printed.

Summary

The details discussed above are written directly into a computer program which includes all the experience gained from the earlier chapters. Programming is relatively simple although a very precise housekeeping scheme is required to keep track of order of interpolation applied to each segment, the node numbers assigned to each segment and their relative positions in the matrix [A].

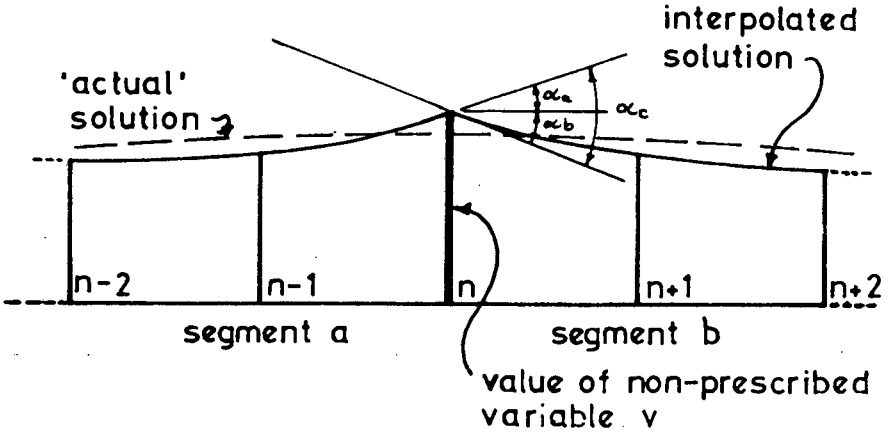

Figure 8.4 Convergence criterion

If the segments are linear, then the gradients are calculated directly from the linear shape functions:

$$\alpha_a = \frac{\partial v}{\partial x} = \frac{v_n - v_{n-1}}{/n-(n-1)/}$$

$$\alpha_b = \frac{\partial v}{\partial x} = \frac{v_{n+1} - v_n}{/(n+1)-n/} \qquad (8.4)$$

where $/n-(n-1)/$ = distance between node n-1 and node n

Where the segments are quadratic, the gradients are calculated from the quadratic shape functions

$$\alpha_a = \frac{v_{n-2} - 4v_{n-1} + 3v_n}{/n-(n-2)/}$$

$$\alpha_b = \frac{-3v_n + 4v_{n+1} - v_{n+2}}{/(n+2)-n/} \qquad (8.5)$$

For segments where the interpolation functions are more complex than quadratic, i.e., quartic etc., the derivatives of the functions in equations (8.1) and (8.2) are too complicated to be worked out practically. In these cases, the gradients are approximated by using the quadratic interpolation shown in equation (8.5) taken over the three nodes closest to the segment intersection. This approximation does not seem to effect the analysis adversely.

From experience, it has been found that the criterion for an accurate solution is $\alpha_c \cong 10°$ ($\alpha_c = 0.1745$ rads) which is verified in the following example.

8.3 Examples

8.3.1 Square Plate under Uniaxial Tension (plane stress)

One quarter of a square plate in tension is shown in Figure 8.5, where each of the four sides is initially modelled by 2 quadratic segments. The boundary conditions applied to the model are as follows :

side a : $u_1 = 0$, u_2 = free
c : $t_1 = 10.0$, $t_2 = 0$
d : u_1 = free, $u_2 = 0$.

Young's Modulus $E = 1000.0$; Poisson's Ratio $\nu = 0.1$.

This example has been chosen as it shows the difference between the h-convergence and the p-convergence techniques very clearly. It also gives an idea of the savings in computer calculation time which can be achieved when p-convergence, using the hierarchical shape functions is used.

Figures 8.5 and 8.6 show, graphically, the results from the h-convergence and p-convergence methods respectively.

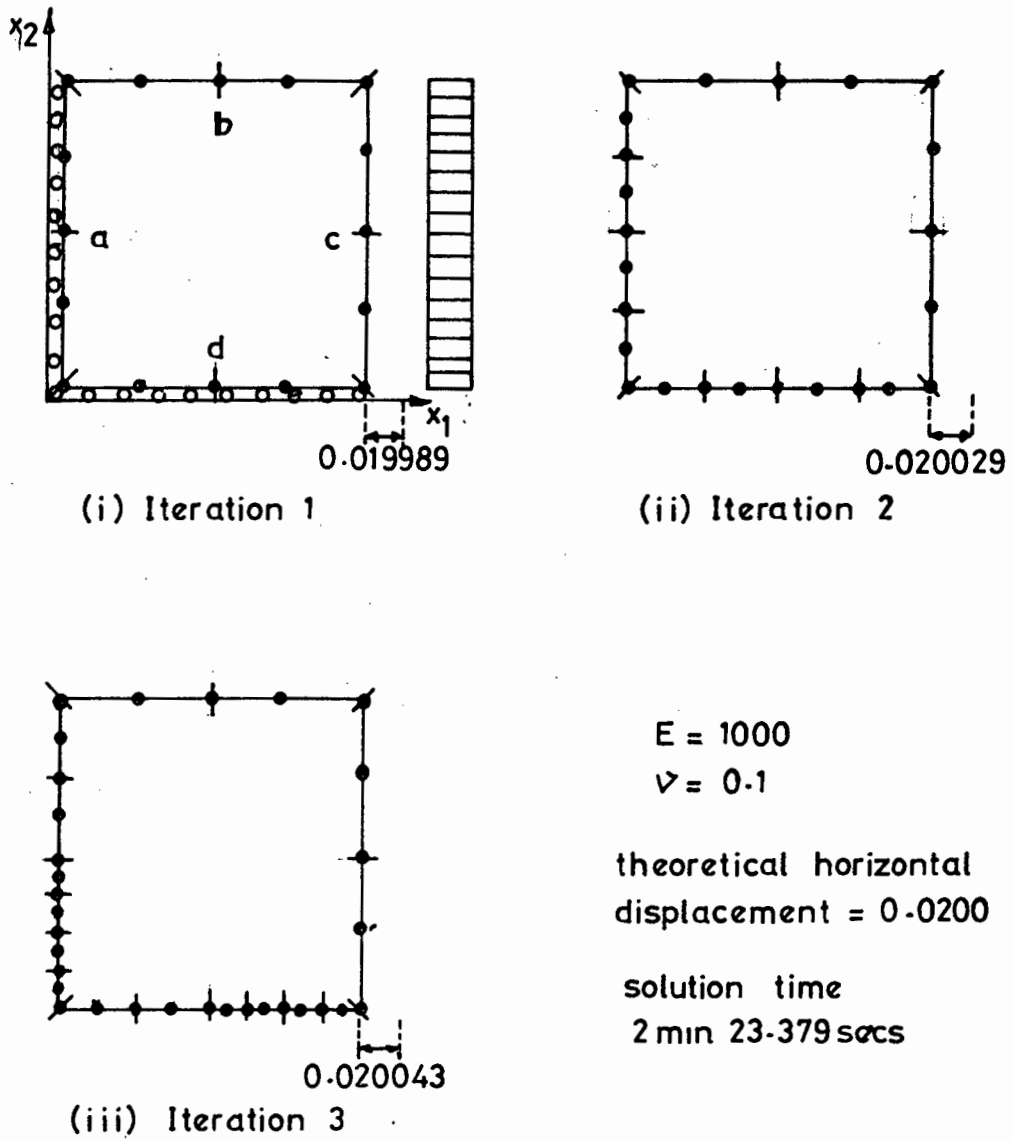

Figure 8.5 Square plate under uniaxial tension - h-convergence solution

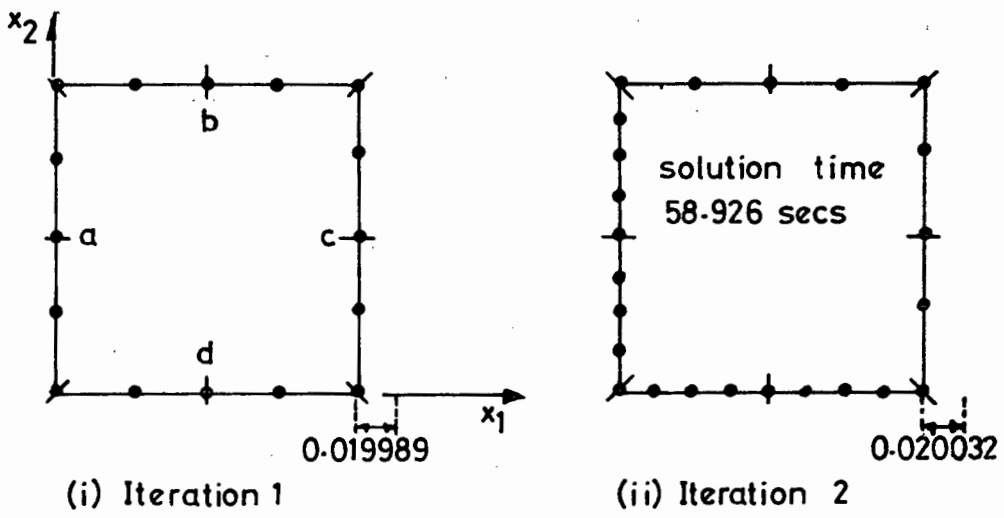

Figure 8.6 Square plate under uniaxial tension - p-convergence solution

The h-convergence method required 3 iterations to achieve convergence. The model for the first iteration consists of 2 quadratic segments per side. When the smoothness of the interpolation was checked, it was found that the interpolation of the tractions (i.e. reactions) along sides a and d were not acceptable. Hence, for the second iteration, 4 quadratic segments were used on sides a and d, while 2 segments remained on sides b and c.

The convergence check revealed that the traction (i.e. reactions) on side a between x_2 = 0 to x_2 = 1.0 units was still not acceptable. Similarly, over side d tractions were unacceptable between x_1 = 1.0 and x_1 = 2.0. The resulting model is shown in Figure 8.5 (iii) which then passed the convergence test.

The theoretical displacement of side c in the x_1-direction is 0.02000. Successive iterations produce x_1-displacements of 0.019989, 0,020029, and 0.020043. Total computer solution time was 2 minutes 23.379 seconds on a UNIVAC 1100/81.

Figure 8.6 shows the iterations required for the p-convergence solution. Iteration one is identical to the h-convergence model. Again, the traction along sides a and d do not conform to the convergence criteria. Hence quartic segments replaced the quadratic segments on these sides. Convergence checks on iteration 2 were successful and hence the solution is acceptable. The x_1 - displacements are 0.019989 and 0.020032 respectively. The total solution time was 58.926 seconds.

This model clearly shows the economy of the p-convergence technique, and the accuracy that can be achieved. The selective re-allocation of the interpolation functions over specific areas is clearly demonstrated and the accuracy of the resulting solutions shown.

8.3.2 Thick walled pipe under internal pressure

Previously, in chapter 4, this example was used to discuss the virtues of constant, linear and quadratic segments. In this chapter, a very coarse initial boundary subdivision, using linear segments, is used to begin the p-convergence method. 5 segments are used on each of the

curved sides a and c, and 3 segments on the straight boundaries b and d. This is shown in Figure 8.7 (i).

The boundary conditions applied to the model are as follows :

side a : pressure 10.0 units

b : $u_1 = 0.0$, u_2 = free

d : u_1 = free, $u_2 = 0.0$.

The model is analysed under plane strain conditions with Young's Modulus E = 1000.0 and Poisson's Ratio $\nu = 0.3$.

The successive solution iterations are shown diagrammatically in Figure 8.7

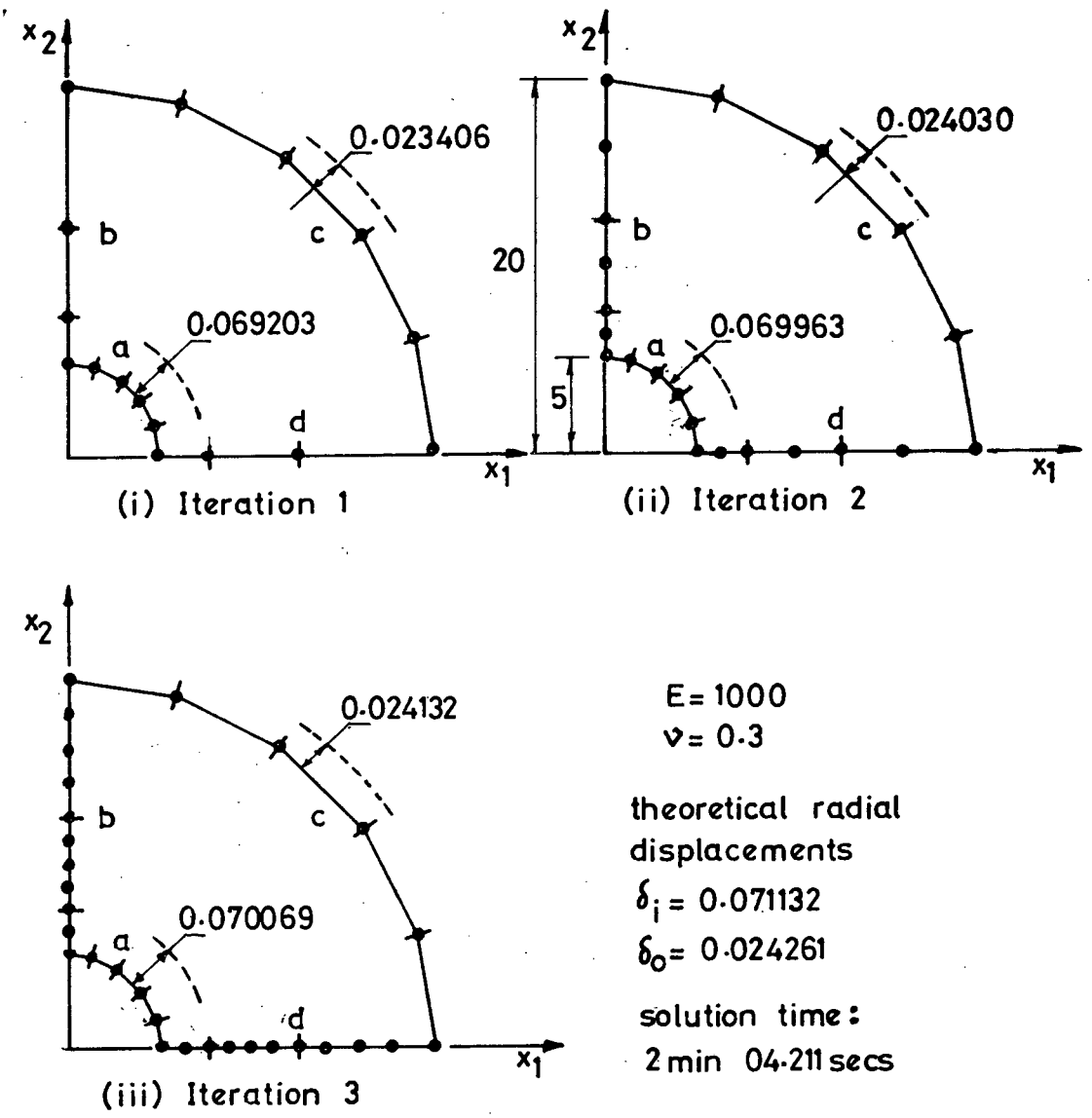

Figure 8.7 Thick walled pipe under internal pressure-solution by the p-convergence method

On the curved boundaries, sides a and c, the initial subdivision of 5 linear segments is retained throughout, since the interpolation of traction and displacement over these boundaries satisfies the convergence criteria. However, the straight boundaries, sides b and d, are significantly adapted during the analysis.

The tractions along sides b and d were not accurately predicted in iteration 1. The failure to pass the convergence test applied to all 3 segments. Hence, the segments were upgraded to quadratic segments, by including extra nodes at the centres. On checking the convergence of iteration 2, only the outer two segments did not conform to the criteria, and were thus upgraded to quartic segments. This model passed the test. The total computer time was 2 minutes 04.211 seconds on a UNIVAC 1100/81.

The accuracy of the inner and outer radial displacements are excellent. The theoretical inner and outer radial displacements are respectively 0.071132 and 0.024261 (see equation 4.49). The maximum error is 3.5%.

It is interesting to note that in Figure 8.7 (iii). linear, quadratic and quartic segments are present in the same model, without any ill-effects.

8.4 Conclusion

One of the major problems encountered by the analyst is the uncertainty of the accuracy of his solution. Conventionally, the analyst re-analyses the model with a finer boundary grid, and by comparing the difference in the results, a measure of the accuracy can be obtained.

In this chapter, however, a method has been investigated to automatically reanalyse with finer boundary sub-divisions by submitting the solution to a convergence check. This convergence check ascertains whether the interpolation of the boundary displacements and tractions is within acceptable bounds, and so makes a decision as to whether to re-analyse or not.

Two methods exist whereby the boundary subdivision can be refined. The first method is called the h-convergence method. Here, a single segment type (be it linear or quadratic or a higher interpolation) is used. For reanalysis, the boundary is subdivided into a larger number (and hence smaller) of segments. The h denotes the segment size. This is essentially a method of successive refinement. The disadvantage of this method is that each reanalysis, with a revised boundary subdivision, requires that the entire systems matrix be re-calculated. This can be prohibitively expensive in most cases.

A more interesting method is the p-convergence technique in which the order of the interpolation functions (p) over a segment of the boundary is successively increased in order to satisfy the convergence criteria. For this purpose, a special set of hierarchical shape function formulae has been designed. These formulae enable higher order interpolation functions over a segment to be successively built up automatically by simple matrix addition. This method is extremely versatile and shows a large economic advantage over the h-convergence method in comparative tests. Savings on computer time of the order of 60% are achieved.

The computer program written includes both the p- and h-convergence method. The decision to employ either p- or h-convergence is defined by the user at the beginning of the data entry. The convergence criteria in each case are identical and hence comparisons can be made.

Complete details of this method and the convergence criteria are given in this chapter. The two examples presented show clearly the methods employed and the advantages that accrue by using the p-convergence method. The method, as tested, is highly successful and it is recommended that research be continued in this field, particularly into, possibly, more pertinent convergence criteria and its application to a wide variety of practical problems.

8.5 References

8.1 A.G. PEANO, "Hierarchies of conforming Finite Elements for Plane Elasticity and Plate Bending", Computers and Maths. with Applic., Vol. 2, page 211 - 224, (1976).

8.2 A.G. PEANO, A. PASINI, R. RICCIONI, L. SARDELLA, "Self-Adaptive Finite Element Analysis", Paper presented at the 6th International Finite Element Conference, Baden-Baden, Germany, November, 1977.

8.3 G. PETRUSKA, "Finite Element convergence on a fixed grid", Computers and Maths. with Applic., Vol. 4, page 67 - 71, (1978).

8.4 I. KATZ, A.G. PEANO, M.P. ROSSOW, "Nodal Variables for complete conforming Finite Elements of arbitrary polynomial order", Computers and Maths, with Applic., Vol. 4, page 85 - 112, (1978).

8.5 A.G. PEANO, M. FANELLI, R. RICCIONI, L. SARDELLA, "Self-adaptive convergence at the crack tip of a dam buttress", paper presented at the International Conference on Numerical Methods in Fracture Mechanics, Swansea, January 9 - 13, (1978).

8.6 A.G. PEANO, R. RICCIONI, A. PASINI, L. SARDELLA, "Adaptive Approximation in Finite Element Structural Analysis", research publication of the Mathematical Models Dept., ISMES, Bergamo, Italy and MCS, Centre for Computational Mechanics, Polytecnico di Milano.

8.7 A.G. PEANO, R. RICCIONI, "Automated Discretization Error Control in Finite Element Analysis", research publication of the Mathematical Models Dept., ISMES, Bergamo, Italy and MCS, Centre for Computational Mechanics, Polytecnico di Milano.

CHAPTER 9

CONCLUSION AND TOPICS FOR FURTHER RESEARCH

The numerical method of Boundary Integral Equations is firmly founded on classical mathematical theory developed mainly near the end of the nineteenth century. Without high powered numerical computational means, however, these methods remained untried and untested until the advent of the digital computer. Since then, a number of numerical techniques, of which the Finite Element Method and the Boundary Integral Equation Method are the most important, have been developed. For a numerical method to be successful, it must have evolved from a viable mathematical basis. The approach adopted in this thesis is therefore one of "back to basics" in order to accomplish the objectives set out at the start of it. These were to trace, develop and expand the Boundary Integral Equation Method for planar elastostatic problems by concentrating on problem areas arising during the research, while remembering that prior background experience lies in the Finite Element Method.

To this end, the theory has been thoroughly researched, beginning with the basic differential equations. The development of both the FEM and BIEM is traced, with particular reference to the similarities and differences between the methods. This has been done so that the mathematics could be put into perspective prior to continuing with the numerical analyses of the BIEM.

The numerical implementation of the BIEM is based on standard isoparametric interpolation functions for the definition of both the geometry and the field variables (displacement and traction) over the boundaries. Constant, linear and quadratic variations are included and their applications tested. From the nature of the fundamental solutions used, the matrix formulation involves fully populated, non-symmetric matrices. The system is solved by standard Gauss reduction with partial pivoting.

Integration over the boundary to produce these matrices takes two forms. The first involves integration over a segment remote from the pivot node. This is dealt with quite adequately by Gauss quadrature for which 2, 4 and 6 point schemes have been employed. However, when the pivot node is within the focus segment, then a singularity exists in the fundamental solution and numerical integration is unreliable. For this purpose, special analytical expressions have been developed for all segments.

Summation techniques for the evaluation of the diagonal terms have been found to give satisfactory results. For quadratic segments, special cognisance is attached to the contributions of the contiguous nodes. These contributions are included analytically.

The calculations of displacements and stresses at points within the boundary present no problem once the boundary solution has been found. However, for internal points within one segment length of the boundary, the results are erratic. A simple method of subdividing the boundary segment at this point has provided greatly improved results in these cases.

Computer programs have been written to test the methods developed. Data input to these programs is in modular form (a data input manual is given in the appendix). However, further research efforts could focus on more enhanced auto-generation facilities which could dramatically decrease the data volume and thus increase the viability of the method.

The constant segment formulation generally produces acceptable results for most practical problems, but requires a refined boundary subdivision for accuracy. Due to the improved interpolation functions, the linear segments are more accurate. With the quadratic segments, fewer segments are required to give compatible results. in fact, 2 linear segments are generally equivalent to 1 quadratic segment. However, linear segments require only a 2-point Gauss quadrature scheme for accuracy, while constant and quadratic segments require at least a 4-point scheme. All things considered, linear (2-point integration scheme) and quadratic (4-point integration scheme) are computationally equivalent. The advantage of the quadratic segments is that they can be curved in practice.

Stress concentrations in the models tested, were predicted accurately, but due to the discontinuity of tractions at corners, models where bending predominates, were not accurately analysed. On development, these inaccuracies were eliminated.

The present computer solutions are, however, uneconomical when compared with the FEM for equivalent models. Although not the subject of this thesis, research is required into economical methods of generating the systems matrices before the BIEM will realistically rival the FEM.

For bending problems in particular, traction discontinuities at corners have resulted in inaccuracies. Several methods have been proposed to overcome these problems. The partially successful Gauss point segment, a segment without end nodes, was designed. This segment suffered from spurious behaviour at the segment ends and this led to the development of the dual node concept. Here, two nodes are placed at a corner. This overcomes the uncertainties at these points and produces good results. A mathematical method, called the traction discontinuity equation method, also successfully overcame these problems.

Research should be continued into these aspects, and especially into the effects of the linear segment assumptions which are included in the evaluation of the quadratic integrals when the pivot node and focus segment coincide.

The inclusion of gravity loads (self weight) is substantially simplified by using the Galerkin tensor to reduce the contributions to a mere boundary integration. No extra domain data is required in this method.

It has been categorically proven that with the present method, rendering of the systems matrices into a symmetric form is nigh impossible and certainly impractical. From a trace of the theory and a comprehensive investigation of the fundamental solutions, a set of very stringent requirements for symmetry are obtained, which cannot be achieved in practice. Nevertheless, intensive research should concentrate on this problem, in order to enhance the economy and viability of the method.

An extensive investigation of the error characteristics of the numerical integration over various segments has produced graphs of the differences between analytical and numerical methods. These graphs have allowed guidelines for the practical use of the various segments to be defined.

The theory and the numerical solution of a non-homogeneous domain has been discussed in depth. Again, problems were encountered with traction discontinuities at corner nodes. The inclusion of multi-nodes at these points overcomes the problems, but tends to increase the size of the systems matrix. Traction discontinuity equations were also included, but involve variables from only one of the interfacing regions. Research should be continued to include the contributions of all the traction components from all interfacing regions in the equation. Substantially better results will then be obtained.

Some mining, soil/structure and fluid/structure interaction problems require that the solution be found within a domain which stretches to infinity. Instead of artificially truncating the domain at a convenient distance, the numerical modelling to the infinite domain by BIEM is attempted here. "Infinite Elements" have been successfully used in the FEM and some of these techniques have been used in the present development. The method has been designed to slot directly into existing BIEM programs with a minimum of adaption. The advantage of the method is that no extra structural nodes are needed to extend the solution over the infinite domain. Also no special fundamental solutions are incorporated in the method. Only standard, previously defined techniques are used. The numerical solutions show minor discrepancies when compared with accepted solutions. However, the basic procedure seems acceptable. Further research is required here, with a view to investigating and adapting, in particular, the form of equations 7.19a and b which define the interpolation used to infinity.

The practising engineer who uses a numerical technique as a tool, seldom knows how accurate his solution is. The generally accepted method is to refine the mesh, reanalyse and compare results. This is a long-winded approach. Instead, an automatic method was sought. Hence, h- and

p-convergence techniques were designed. In the h-convergence method, the initial boundary sub-division is refined automatically over regions where the solution is unacceptable, but the interpolation order of the segments is kept constant. The p-convergence method involves increasing the interpolation order over a boundary segment by adding nodes, but by keeping the original boundary sub-division unchanged. The decision to redefine, either by h- or p-convergence, is performed automatically by a convergence check which compares the gradient of the displacement and/or tractions between segments. If this is within the defined tolerances, the solution is accepted and calculation stops.

The design of the p-convergence method involved the development of unique recurrence formulae for the hierarchical shape functions used. These were specially designed so that a minimum amount of extra calculation would be required for a re-analysis. An economic matrix method has been produced which successively builds up the matrices as the complexity of the shape functions is increased. Research is required in this section into the general acceptability of the methods. An interesting project could be designed where practical engineering problems could be investigated in order to produce guidelines for the use and the optimum number of segments required in various situations, for example, in bending or plane strain/stress or pressure vessel problems, etcetera. A practically orientated project is envisaged here.

In conclusion, this work conforms to the policy adopted by my research group which is to concentrate on the practical user orientated aspects of numerical structural analysis methods.

Throughout, a delicate balance has been maintained between theory and practice. The topics covered have been aimed at improving, developing and implementing the method for the benefit of the practical user, but they hopefully also provide sufficient fuel to initiate and inspire further research into Boundary Integral Equation Methods in the future.

APPENDIX A

AN INVESTIGATION OF THE SIGNIFICANCE OF THE COEFFICIENT c_{ij} FOR A GENERAL POINT ON THE BOUNDARY

The boundaries of the continuum are defined by Γ_1 and Γ_2 such that $\Gamma = \Gamma_1 + \Gamma_2$. The boundary conditions are specified on these boundaries by

$$u_k = \bar{u}_k \quad \text{for} \quad k = 1,2 \quad \text{on} \quad \Gamma_1$$

and $$t_k = \bar{t}_k \quad \text{for} \quad k = 1,2 \quad \text{on} \quad \Gamma_2 \tag{A.1}$$

Therefore, to solve the elastostatic problem, it is required to find u_k or Γ_2 and t_k on Γ_1.

The general equation which relates the boundary values to a point in the continuum is given by :

$$\delta_{ij}u_j(x) + \int_{\Gamma_2} T_{ij}(x,y)u_j d\Gamma + \int_{\Gamma_1} T_{ij}(x,y)\bar{u}_j d\Gamma = \int_{\Gamma_1} U_{ij}(x,y)t_j d\Gamma + \int_{\Gamma_2} U_{ij}(x,y)\bar{t}_j d\Gamma + \text{body terms} \tag{A.2}$$

where the usual notation, as in chapter 3, is used.

As the internal point x is brought towards the boundary, equation (A.2) will be valid until x becomes part of the boundary. In order to validate equation (A.2) at the boundary, it is assumed that point x is at the centre of a disc of "extra" material, where ε is the radius. This is shown in figure (A.1)

We denote the boundary of the disc as Γ_ε and note that the boundary Γ_2 , over which the displacement is unknown can be written as

$$\Gamma_2 = \Gamma_{(2-\varepsilon)} + \Gamma_\varepsilon \tag{A.3}$$

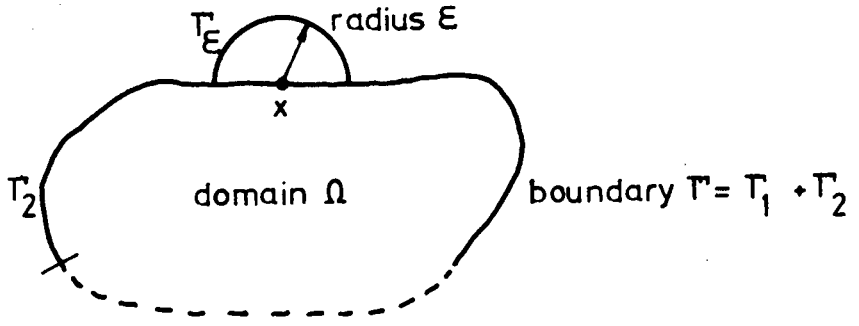

Fig. A.1 Point x at the boundary

By using this fact, the second term in equation (A.2) can be transformed to :

$$\int_{\Gamma_2} T_{ij}(x,y)\, u_j d\Gamma = \int_{\Gamma_{(2-\varepsilon)}} T_{ij}(x,y)\, u_j d\Gamma + \int_{\Gamma_\varepsilon} T_{ij}(x,y)\, u_j d\Gamma \qquad (A.4)$$

Then, in the limit, i.e. as $\varepsilon \to 0$, the original boundary will be restored. Hence :

$$\int_{\Gamma_2} T_{ij}(x,y)u_j d\Gamma = \lim_{\varepsilon\to 0} \int_{\Gamma_\varepsilon} T_{ij}(x,y)u_j d + \lim_{\varepsilon\to 0} \int_{\Gamma_\varepsilon} T_{ij}(x,y)u_j d\Gamma$$

$$= \int_{\Gamma_2} T_{ij}(x,y)u_j d\Gamma + d_{ij}u_{ij} \qquad (A.5)$$

where d_{ij} is the coefficient accumulated from the integral over Γ_ε. On the left-hand side of (A.5), point x is an internal point ($x\varepsilon\Omega$), while on the right-hand side, point x is on the boundary ($x\varepsilon\Gamma$).

Substitution of (A.5) back into (A.2) results in

$$c_{ij}u_j(x) + \int_{\Gamma_2} T_{ij}(x,y)\, u_j d\Gamma + \int_{\Gamma_1} T_{ij}(x,y)\, \bar{u}_j d\Gamma =$$

$$\int_{\Gamma_1} U_{ij}(x,y)t_j d\Gamma + \int_{\Gamma_2} U_{ij}(x,y)\bar{t}_j d\Gamma + \text{body terms} \qquad (A.6)$$

where $c_{ij} = \delta_{ij} + d_{ij}$

Let us now consider the calculation of the coefficient d_{ij} from

$$\lim_{\varepsilon \to o} \int_{\Gamma_3} T_{ij}(x,y) u_j d\Gamma = d_{ij} u_j = I \qquad (A.7)$$

where $$d_{ij} = \lim_{\varepsilon \to o} \int_{\Gamma_\varepsilon} T_{ij}(x,y) d\Gamma$$

The fundamental traction solution, as given in chapter 3 is :

$$T_{ij}(x,y) = -\frac{1}{4\pi(1-\nu)r}\left[\frac{\partial r}{\partial n}\left\{(1-2\nu)\delta_{ij} + \frac{2\partial r}{\partial x_j}\frac{\partial r}{\partial x_i}\right\} - (1-2\nu)\left(\frac{\partial r}{\partial x_i} n_j - \frac{\partial r}{\partial x_j} n_i\right)\right] \qquad (A.8)$$

Hence, the integral I from equation (A.7) can be written :

$$I = \lim_{\varepsilon \to o}\left\{-\int_{\Gamma_\varepsilon}\left[\frac{\partial r}{\partial n}\left\{(1-2\nu)\delta_{ij} + \frac{2\partial r}{\partial x_j}\frac{\partial r}{\partial x_i}\right\} - (1-2\nu)\left\{\frac{\partial r}{\partial x_i} n_j - \frac{\partial r}{\partial x_j} n_i\right\}\right] \frac{1}{4\pi(1-\nu)r}\right\} u_j \, d\Gamma \qquad (A.9)$$

In detail, Γ_ε can be defined as shown in figure A.2. The local coordinates x_1, x_2 are used as a template in space and are defined so that x_1 is in the direction of segment 1 and β is the external angle measured between 2 adjacent segments 1 and 2 at their common node point x.

Since $r = \varepsilon$ is the radius of the circle, the vector $\tilde{r}$ and the normal vector n at the surface, coincide. Hence

$$n_i = \frac{\partial n}{\partial x_i} = \frac{\partial r}{\partial x_i} \quad ; \quad n_j = \frac{\partial r}{\partial x_j}$$

Also

$$\frac{\partial r}{\partial n} = 1.0 \qquad (A.10)$$

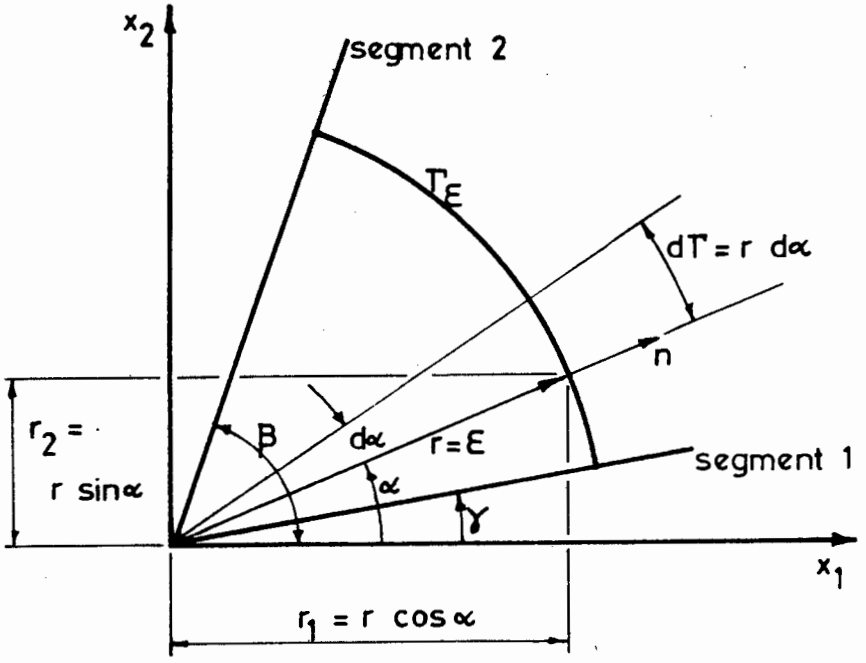

Fig. A.2 Definition at a boundary node

Consequently, the last term in equation (A.9) can be disregarded since

$$\frac{\partial r}{\partial x_i} n_j - \frac{\partial r}{\partial x_j} n_i = \frac{\partial r}{\partial x_i} \frac{\partial r}{\partial x_j} - \frac{\partial r}{\partial x_j} \frac{\partial r}{\partial x_i} = 0 \qquad (A.11)$$

Using (A.10) and (A.11), equation (A.9) is written :

$$I = \lim_{\varepsilon \to 0} \left\{ - \int_{\Gamma_\varepsilon} \left\{ (1-2\nu)\delta_{ij} + \frac{2\partial r}{\partial x_i} \frac{\partial r}{\partial x_j} \right\} \frac{1}{4\pi(1-\nu)r} \dot{u}_j \, d\Gamma \right\} \qquad (A.12)$$

Now, from Fig. A.2, it can be seen that

$$\frac{\partial r}{\partial x_i} = \frac{r_i}{r} \quad \text{and} \quad d\Gamma = r d\alpha \qquad (A.13)$$

Hence, for i = 1 and j = 1,2 :

$$I = \lim_{\varepsilon \to o} \left\{ - \int_{\Gamma} \left\{ u_1 (1-2\nu) + 2 \frac{r_1}{r} \frac{r_1}{r} u_1 + 2u_2 \frac{r_1}{r} \frac{r_2}{r} \right\} \frac{r d\alpha}{4\pi(1-\nu) r} \right.$$

$$= \lim_{\varepsilon \to o} \left\{ \int_{\gamma}^{\beta} - \left\{ u_1 (1-2\nu) + 2 \cos^2 \alpha u_1 + 2 \cos\alpha \sin\alpha \, u_2 \right\} \frac{1}{4\pi(1-\nu)} d\alpha \right.$$

which is now independent of $\varepsilon = r$. Now, integration of α between γ and β(radians)gives :

$$I = - \left[u_1 (1-2\nu)\alpha + 2 u_1 \left(\frac{\alpha}{2} + \frac{\sin 2\alpha}{4} \right) - u_2 \frac{\cos 2\alpha}{2} \right]_{\gamma}^{\beta} \frac{1}{4\pi(1-\nu)}$$

$$= - \left(\frac{(\beta-\gamma)}{2\pi} + \frac{(\sin 2\beta - \sin 2\gamma)}{8\pi(1-\nu)} \right) u_1 + \frac{(\cos 2\beta - \cos 2\gamma)}{8\pi(1-\nu)} u_2 \qquad \text{(A.14)}$$

Similarly, for $i = 2$ and $j = 1,2$

$$I = + \frac{(\cos 2\beta - \cos 2\gamma)}{8\pi(1-\nu)} u_1 - \left(\frac{(\beta-\gamma)}{2\pi} + \frac{(\sin 2\beta - \sin 2\gamma)}{8\pi(1-\nu)} \right) u_2 \qquad \text{(A.15)}$$

The numerical value of $\sin 2\alpha$ and $\cos 2\alpha$ evaluated between γ and β depends on the magnitude of angles γ and β for a specific case. Hence, no definite value can be given for these expressions. It can, however, be seen that if $\beta - \gamma = \pi$, then both $\sin 2\alpha$ and $\cos 2\alpha$ evaluate over this interval will be zero.

Using (A.5) and substituting back into (A.2) leads to the formula for C_{ij}, which, in matrix form, is :

$$\begin{bmatrix} 1 & 0 \\ 0 & 1 \end{bmatrix} \begin{Bmatrix} u_1 \\ u_2 \end{Bmatrix} + \begin{bmatrix} d_{ij} \end{bmatrix} \begin{Bmatrix} u_1 \\ u_2 \end{Bmatrix} = \begin{bmatrix} c_{ij} \end{bmatrix} \begin{Bmatrix} u_1 \\ u_2 \end{Bmatrix} \text{ for point x} \qquad \text{(A.16)}$$

$$\text{where } \begin{bmatrix} d_{ij} \end{bmatrix} = \left[\begin{array}{c|c} - \left(\frac{(\beta-\gamma)}{2\pi} + \frac{(\sin 2\beta - \sin 2\gamma)}{8\pi(1-\nu)} \right) & + \frac{(\cos 2\beta - \cos 2\gamma)}{8\pi(1-\nu)} \\ \hline + \frac{(\cos 2\beta - \cos 2\gamma)}{8\pi(1-\nu)} & - \left(\frac{(\beta-\gamma)}{2\pi} + \frac{(\sin 2\beta - \sin 2\gamma)}{8\pi(1-\nu)} \right) \end{array} \right]$$

Hence, the coefficient matrix c_{ij} can be rewritten as

$$[c_{ij}] = \begin{bmatrix} 1 - \left(\frac{(\beta-\gamma)}{2\pi} + \frac{(\sin 2\beta - \sin 2\gamma)}{8\pi(1-\nu)}\right) & + \frac{(\cos 2\beta - \cos 2\gamma)}{8\pi(1-\nu)} \\ + \frac{(\cos 2\beta - \cos 2\gamma)}{8\pi(1-\nu)} & 1 - \left(\frac{(\beta-\gamma)}{2\pi} + \frac{(\sin 2\beta - \sin 2\gamma)}{8\pi(1-\nu)}\right) \end{bmatrix} \tag{A.17}$$

This formula therefore completes the boundary integral equation for a point on a boundary of general shape. It is interesting to note that for a smooth boundary, where $(\beta-\gamma) = \pi (\beta = 180°)$ then

$$[c_{ij}] = \begin{Bmatrix} \frac{1}{2} & 0 \\ 0 & \frac{1}{2} \end{Bmatrix}$$

APPENDIX B

INTEGRATION OF THE SINGULAR KERNELS FOR LINEAR INTERPOLATION

The following integrals occur when the pivot node x is one of the nodes of the segment over which the integral is to be performed. This is defined as :

$$G_{ij}^{pq} = \left[\int_{\Gamma_k} U_{ij}(x,y)\ N_q\ d\Gamma_k \right] \qquad \text{(B.1)}$$

where i, j are the coordinate directions

p is the pivot node (p = 1 or 2)

q is the interpolation node (q = 1 or 2)

and N_q is the linear shape function for node q.

NOTE : The terms enclosed within the box in the following expression arise when the fundamental solution is defined by the Galerkin tensor formulation.

B.1 Pivot node at node 1 (p = 1)

The geometry of the segment is defined as in Fig. B.1

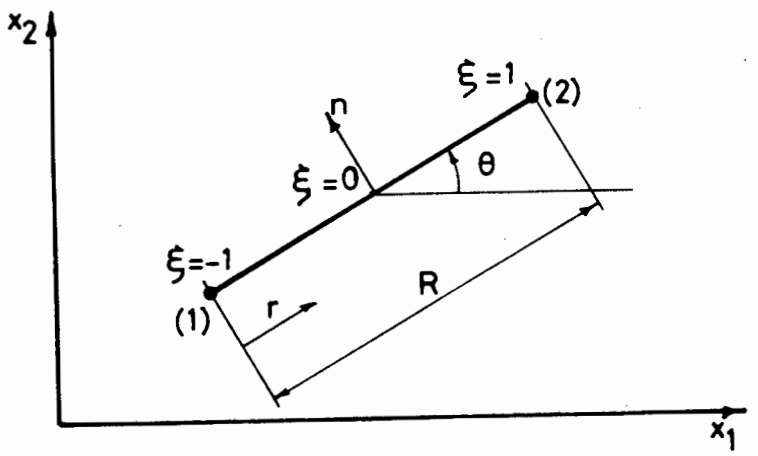

Fig. B.1 Geometry of a linear segment for pivot node p = 1

The coordinates are defined by

$$\xi = \frac{2r}{R} - 1 \tag{B.2a}$$

while $$\frac{\partial r}{\partial x_1} = \cos\theta = \frac{x_1(2)-x_1(1)}{R} \tag{B.2b}$$

$$\frac{\partial r}{\partial x_2} = \sin\theta = \frac{x_2(2)-x_2(1)}{R}$$

and the linear shape functions are

$$N_1 = \tfrac{1}{2}(1-\xi) \tag{B.2c}$$
$$N_2 = \tfrac{1}{2}(1+\xi)$$

For p = 1, q = 1, i = 1 and j = 1, the expression is :

$$G_{11}^{11} = \int_{(1)}^{(2)} U_{ij}(x,y)\, N_1 d\Gamma$$

$$= \lim_{\varepsilon\to 0}\left[\frac{1}{8\pi G(1-\nu)}\left\{\int_{\varepsilon}^{R}(3-4\nu)\ln\frac{1}{r}N_1 dr + \int_{\varepsilon}^{R}\left(\frac{\partial r}{\partial x_1}\right)^2 N_1 dr\right\}\right] \tag{B.3}$$

Substituting (B.2a, b and c) into (B.3) and integrating, results in

$$G_{11}^{11} = \frac{R}{16\pi G(1-\nu)}\left\{(3-4\nu)\left(\frac{3}{2} - \ln R\right) + \cos^2\theta\left[-\left(\frac{7-8\nu}{2}\right)\right]\right\} \tag{B.4}$$

Similarly :

$$G_{12}^{11} = G_{21}^{11} = \frac{R}{16\pi G(1-\nu)}\left\{\sin\theta\cos\theta\right\} \tag{B.5}$$

$$G_{22}^{11} = \frac{R}{16\pi G(1-\nu)}\left\{(3-4\nu)\left(\frac{3}{2} - \ln R\right) + \sin^2\theta\left[-\left(\frac{7-8\nu}{2}\right)\right]\right\} \tag{B.6}$$

$$G_{11}^{12} = \frac{R}{16\pi G(1-\nu)}\left\{(3-4\nu)\left(\frac{1}{2} - \ln R\right) + \cos^2\theta\left[-\left(\frac{7-8\nu}{2}\right)\right]\right\} \tag{B.7}$$

$$G_{12}^{12} = G_{21}^{12} = \frac{R}{16\pi G(1-\nu)}\left\{\sin\theta\ \cos\theta\right\} \tag{B.8}$$

$$G_{22}^{12} = \frac{R}{16\pi G(1-\nu)}\left\{(3-4\nu)\ (\tfrac{1}{2}-\ln R) + \sin^2\theta\ \boxed{-\left(\frac{7-8\nu}{2}\right)}\right\} \tag{B.9}$$

B.2 Pivot node at node 2 (p=2)

The geometry of the segment is defined as in Fig. B.2

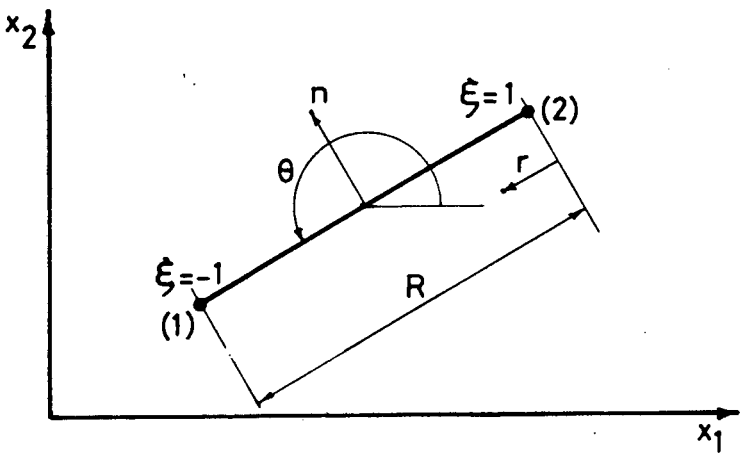

Fig. B.2 Geometry of a linear segment for pivot node p=2

The coordinates are defined by

$$\xi = 1 - \frac{2r}{R} \tag{B.10a}$$

while

$$\frac{\partial r}{\partial x_1} = \cos\theta = \frac{x_1(1)-x_1(2)}{R} \tag{B.10b}$$

$$\frac{\partial r}{\partial x_2} = \sin\theta = \frac{x_2(1)-x_2(2)}{R}$$

Substituting (B.10a), (B.10b), (B.2c) into B.1 for p=2 and integrating the resulting expressions in the limit, results in

$$G_{ij}^{21} = G_{ij}^{12} \tag{B.11}$$

and $$G_{ij}^{22} = G_{ij}^{11} \qquad (B.12)$$

where G_{ij}^{12} and G_{ij}^{11} are identical to equation (B.4) to (B.9), with the trigonometrical functions of angle θ being defined by equations(B.10b).

APPENDIX C

INTEGRATION OF THE SINGULAR KERNELS FOR QUADRATIC INTERPOLATION

C.1 The displacement kernel

The following integrals occur when the pivot node x is one of the nodes of the segment over which the integral is to be performed. The integration is defined by :

$$G_{ij}^{pq} = \left[\int_{\Gamma_k} U_{ij}(x,y) N_q d\Gamma_k \right] \qquad (C.1)$$

where ij are the coordinate directions

p is the pivot node

q is the interpolation node

N_q is the quadratic shape function for node q

NOTE : The terms enclosed within the box in the following expressions arise when the fundamental solution is defined by the Galerkin tensor formulation.

C.1.1 Pivot node at node 1 (p=1)

The geometry of the segment is defined as in Fig. C.1, where it is assumed for the purpose of this analysis that the segment is straight.

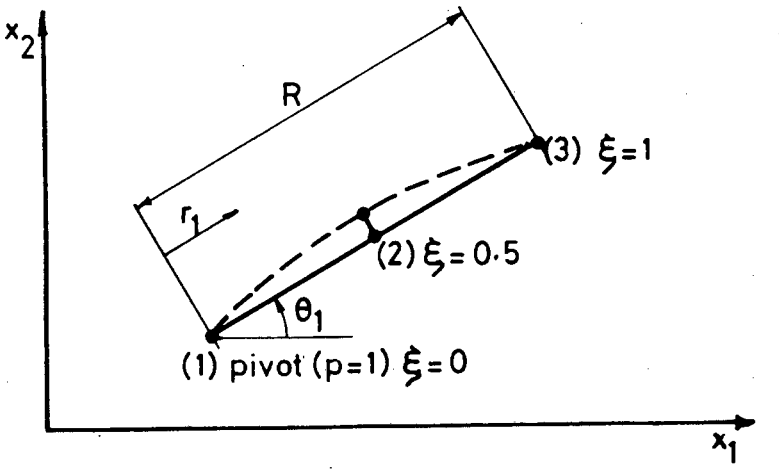

Fig. C.1
The geometry of a quadratic segment for pivot node p=1

The natural coordinates ξ are redefined as in figure C.1 so that a convenient relationship between ξ and r can be formed. Consequently

$$\xi = \frac{r}{R} \tag{C.2a}$$

while
$$\frac{\partial r}{\partial x_1} = \cos\theta = \frac{x_1(3)-x_1(1)}{R} \tag{C.2b}$$

$$\frac{\partial r}{\partial x_2} = \sin\theta = \frac{x_2(3)-x_2(1)}{R}$$

The quadratic shape function, defined in terms of the revised natural coordinate system ξ is

$$\begin{aligned} N_1 &= 2\xi^2 - 3\xi + 1 \\ N_2 &= -4\xi^2 + 4\xi \\ N_3 &= 2\xi^2 - \xi \ . \end{aligned} \tag{C.2c}$$

For p=1, q=1, i=1, j=1, the resulting expression becomes :

$$G_{11}^{11} = \int_0^R U_{11} N_1 dr_1 = \lim_{\varepsilon\to 0} \int_\varepsilon^R U_{11} N_1 dr_1 \tag{C.3}$$

With $\theta = \theta_1$,

$F = \pi G(1-\nu)$

and N defined in terms of r and R, then

$$G_{11}^{11} = \frac{R}{48F} \left\{ (3-4\nu) \left[\frac{17}{6} - \ln R\right] + \cos^2\theta_1 \boxed{-\left[\frac{7-8\nu}{2}\right]} \right\} \tag{C.4}$$

Similarly :

$$G_{12}^{11} = G_{21}^{11} = \frac{R}{48F} \{\sin\theta\cos\theta\} \tag{C.5}$$

$$G_{22}^{11} = \frac{R}{48F} \left\{ (3-4\nu) \left[\frac{17}{6} - \ln R\right] + \sin^2\theta \boxed{-\left[\frac{7-8\nu}{2}\right]} \right\} \tag{C.6}$$

$$G_{11}^{12} = \frac{R}{24F}\left\{(3-4\nu)\left(\frac{5}{3} - 2\ln\right) + 2\cos^2\theta\left|-(7-8\nu)\right|\right\} \quad (C.7)$$

$$G_{12}^{12} = G_{21}^{12} = \frac{R}{12F}\{\sin\theta\cos\theta\} \quad (C.8)$$

$$G_{22}^{12} = \frac{R}{24F}\left\{(3-4\nu)\left(\frac{5}{3} - 2\ln R\right) + 2\sin^2\theta\left|-(7-8\nu)\right|\right\} \quad (C.9)$$

$$G_{11}^{13} = \frac{R}{48F}\left\{(3-4\nu)\left(-\frac{1}{6} - \ln R\right) + \cos^2\theta\left|-\left[\frac{7-8\nu}{2}\right]\right|\right\} \quad (C.10)$$

$$G_{12}^{13} = G_{21}^{13} = \frac{R}{48F}\{\sin\theta\cos\theta\} \quad (C.11)$$

$$G_{22}^{13} = \frac{R}{48F}\left\{(3-4\nu)\left(-\frac{1}{6} - \ln R\right) + \sin^2\theta\left|-\left[\frac{7-8\nu}{2}\right]\right|\right\} \quad (C.12)$$

C.1.2 Pivot Node at node 3 (p=3)

By redefining the meaning of the angles and distances a set of integrals similar to C.4 to C.12 can be found. Figure C.2 defines the geometry of the segment.

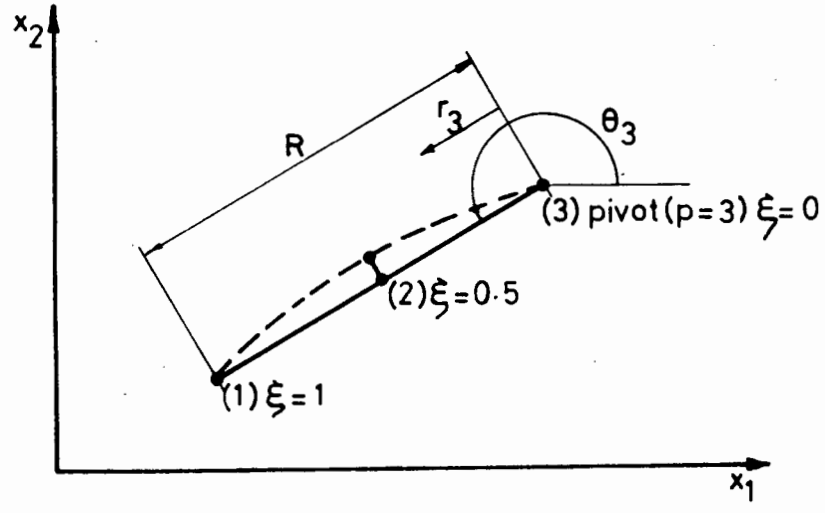

Fig. C.2
The geometry of a quadratic segment for pivot node p=3

The natural coordinates ξ are written in terms of r and R

$$\xi = \frac{r}{R} \tag{C.13a}$$

while
$$\cos\theta = (x_1(1) - x_1(3))/R$$
$$\sin\theta = (x_2(1) - x_2(3))/R \tag{C.13b}$$

and the shape functions are

$$N_1 = 2\xi^2 - \xi$$
$$N_2 = -4\xi^2 + 4\xi \tag{C.13c}$$
$$N_3 = 2\xi^2 - 3\xi + 1$$

For p=3, q=1, i=1, j=1

with $\theta=\theta_3$ and $r = r_3$

$$G_{11}^{31} = \int_0^R U_{11} N_1 \, dr_3 = \lim_{\varepsilon\to 0} U_{11} N_1 \, dr_3$$
$$= \frac{R}{48F}\left\{(3-4\nu)\left(-\frac{1}{6} - \ln R\right) + \cos^2\theta \left[-\frac{7-8\nu}{2}\right]\right\} \tag{C.14}$$

Similarly, the remaining integrals are defined as

$$G_{ij}^{3k} = G_{ij}^{1\ell} \tag{C.15}$$

where $G_{ij}^{1\ell}$ are the integrals in C.1 with the trigonometrical values defined by (C.13b) and

$\ell = 3$ when $k = 1$
$\ell = 2$ " $k = 2$
$\ell = 1$ " $k = 3$

C.1.3 Pivot node at node 2 (p=2)

The geometry of the segment for the pivot at node 2 is defined as in Fig. C.3.

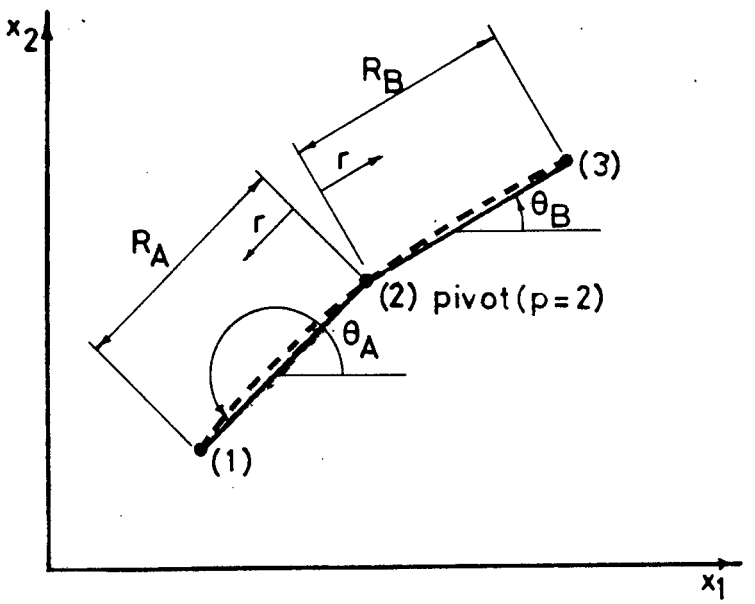

Fig. C.3
The geometry of a quadratic segment for pivot node p=2

Using the same convention as above, the integrals for p=2, q=1, i=1, j=1 are as follows :

$$G_{11}^{21} = \int_{(1)}^{(3)} U_{11} N_1 \, d\Gamma = \int_{(1)}^{(2)} U_{11} N_1 \, d\Gamma + \int_{(2)}^{(3)} U_{11} N_1 \, d\Gamma$$

$$= \lim_{\varepsilon \to 0} \left(\int_{\varepsilon}^{R_A} U_{11} N_1 \, dr + \int_{\varepsilon}^{R_B} U_{11} N_1 \, dr \right) \qquad \text{(C.16)}$$

For sector (1) - (2), the natural coordinates are defined by

$$\xi = -\frac{r}{R_A} \qquad \text{(C.17a)}$$

and $$\cos\theta_A = (x_1(1) - x_1(2))/R_A$$

$$\sin\theta_A = (x_2(1) - x_2(2))/R_A \qquad \text{(C.17b)}$$

The shape functions are

$$N_1 = \frac{1}{2}\xi^2 - \frac{1}{2}\xi$$

$$N_2 = 1 - \xi^2 \qquad \text{(C.17c)}$$

$$N_3 = \frac{1}{2}\xi^2 + \frac{1}{2}\xi$$

For sector (2) - (3), the natural coordinates are defined by

$$\xi = \frac{r}{R_B} \qquad \text{(C.18a)}$$

and $$\cos\theta_B = (x_1(3) - x_1(2))/R_B \qquad \text{(C.18b)}$$

$$\sin\theta_B = (x_2(3) - x_2(2))/R_B$$

The shape functions are given by (C.17c).

Hence, for p=2, q=1, i=j=1 ,

$$G_{11}^{21} = \frac{1}{96F}\left[(3-4\nu)\left\{R_A\left(\frac{13}{8} - 5\ln R_A\right) - R_B\left(\frac{5}{8} - \ln R_B\right)\right\} + 5R_A\cos^2\theta_A - R_B\cos^2\theta_B\left|-\left(\frac{7-8\nu}{2}\right)5R_A + \left(\frac{7-8\nu}{2}\right)R_B\right|\right] \qquad \text{(C.19)}$$

Similarly :

$$G_{12}^{21} = G_{21}^{21} = \frac{1}{96F}\left[5R_A\sin\theta_A\cos\theta_A - R_B\sin\theta_B\cos\theta_B\right] \qquad \text{(C.20)}$$

$$G_{22}^{21} = \frac{1}{96F}\left[(3-4\nu)\left\{R_A\left(\frac{13}{8} - 5\ln R_A\right) - R_B\left(\frac{5}{8} - \ln R_B\right)\right\} + 5R_A\sin^2\theta_A - R_B\sin^2\theta_B\left|-\left(\frac{7-8\nu}{2}\right)5R_A + \left(\frac{7-8\nu}{2}\right)R_B\right|\right] \qquad \text{(C.21)}$$

$$G_{11}^{22} = \frac{1}{12F}\left[(3-4\nu)\left\{R_A\left(\frac{4}{3} - \ln R_A\right) + R_B\left(\frac{4}{3} - \ln R_B\right)\right\} + R_A\cos^2\theta_A + R_B\cos^2\theta_B\left|-\left(\frac{7-8\nu}{2}\right)R_A - \left(\frac{7-8\nu}{2}\right)R_B\right|\right] \qquad \text{(C.22)}$$

$$G_{12}^{22} = G_{21}^{22} = \frac{1}{12F}\left[R_A\sin\theta_A\cos\theta_A + R_B\sin\theta_B\cos\theta_B\right] \qquad \text{(C.23)}$$

$$G_{22}^{22} = \frac{1}{12F}\left[(3-4\nu)\left\{R_A\left(\frac{4}{3} - \ln R_A\right) + R_B\left(\frac{4}{3} - \ln R_B\right)\right\} + R_A\sin^2\theta_A + R_B\sin^2\theta_B\left|\overline{-\left(\frac{7-8\nu}{2}\right)R_A - \left(\frac{7-8\nu}{2}\right)R_B}\right|\right] \quad (C.24)$$

$$G_{11}^{23} = \frac{1}{96F}\left[(3-4\nu)\left\{R_A\left(\ln R_A - \frac{5}{8}\right) + R_B\left(\frac{13}{8} - 5\ln R_B\right)\right\} - R_A\cos^2\theta_A + 5R_B\cos^2\theta_B\left|\overline{+\left(\frac{7-8\nu}{2}\right)R_A - \left(\frac{7-8\nu}{2}\right)5R_B}\right|\right] \quad (C.25)$$

$$G_{12}^{23} = G_{21}^{23} = \frac{1}{96F}\left[-R_A\sin\theta_A\cos\theta_A + 5R_B\sin\theta_B\cos\theta_B\right] \quad (C.26)$$

$$G_{22}^{23} = \frac{1}{96F}\left[(3-4\nu)\left\{R_A\left(\ln R_A - \frac{5}{8}\right) + R_B\left(\frac{13}{8} - 5\ln R_B\right)\right\} - R_A\sin^2\theta_A + 5R_B\sin^2\theta_B\left|\overline{+\left(\frac{7-8\nu}{2}\right)R_A - \left(\frac{7-8\nu}{2}\right)5R_B}\right|\right] \quad (C.27)$$

C.2 The traction kernel

The following expression for H_{ij}^{pq} occurs when the pivot node x is one of the nodes of the segment over which the integral is to be performed.

The integration is defined by :

$$H_{ij}^{pq} = \int_{\Gamma_k}^{R} T_{ij}(x,y)\, N_q\, d\Gamma_k \quad (C.28)$$

where i, j, p, q, N_q are as defined in section C.1.

C.2.1 Pivot node at node 1 (p=1)

The geometry of the quadratic segment is defined by two linear segments as shown in Fig. C.4. For the pivot at node 1, the integral over section (2) - (3) can simply be calculated by using the Gaussian quadrature with N defined as linear shape functions. Integration of section (1) - (2) takes place in two parts :

(i) H^{11}_{ij} is calculated by rigid body considerations once the complete equation for node n has been assembled

(ii) H^{12}_{ij} can be calculated by explicit integration.

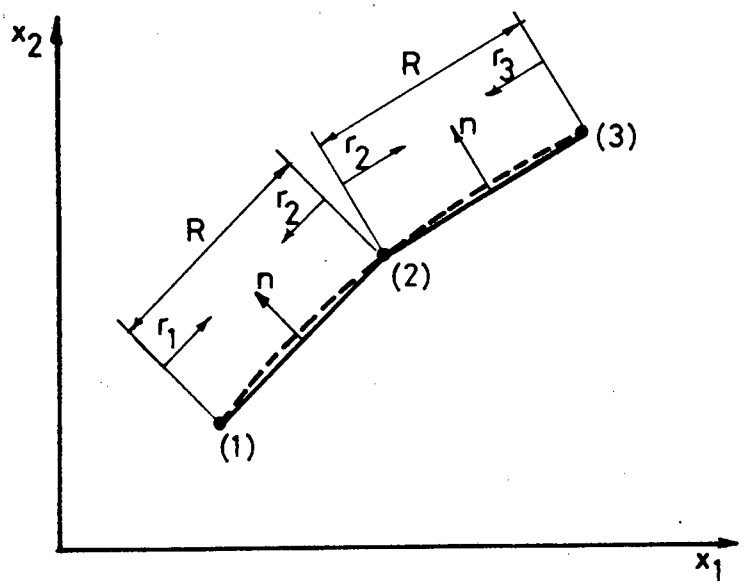

Fig. C.4
The geometry of a quadratic segment
for the integration of the traction kernel

By consideration of the fundamental solution $T_{ij}(x,y)$ and noting that $\frac{\partial r}{\partial n} = 0$ over (1) - (2), the integral becomes :

$$H^{12}_{ij} = \int_0^R -\frac{1}{4\pi(1-\nu)r}\left[-(1-2\,)\left(\frac{\partial r}{\partial x_i}n_j - \frac{\partial r}{\partial x_j}n_i\right)\right] N_2\,dr \qquad (C.29)$$

where N_2 is a linear shape function over (1) - (2) and is defined in terms of r and R. Thus, summarizing the integral :

$$H^{12}_{ij} = \lambda\left\{\frac{1-2\nu}{4\pi(1-\nu)}\right\} \qquad (C.30)$$

where $\lambda = 1$ for $i = 1,\ j = 2$

$= -1$ for $i = 2,\ j = 1$

$= 0$ for $i = j$.

It is interesting to note that (C.30) is dependent solely on the value of Poisson's Ratio and is zero for $\nu = 0.5$.

C.2.2 Pivot node at node 3 (p=3)

Gaussian quadrature is used to integrate over section (1) - (2) while integration over (2) - (3) takes the same form as before:

H_{ij}^{33} calculated from rigid body considerations

$$H_{ij}^{32} = \lambda \left\{ \frac{1-2\nu}{4\pi(1-\nu)} \right\} \qquad (C.31)$$

where $\lambda = -1$ for $i = 1, j = 2$

$= 1$ for $i = 2, j = 1$

$= 0$ for $i = j$

C.2.3 Pivot node at node 2 (p=2)

Integration over the section (1) - (2) and (2) - (3) follows directly

$$H_{ij}^{21} = \lambda_1 \left\{ \frac{1-2\nu}{4\pi(1-\nu)} \right\} \qquad (C.32)$$

$$H_{ij}^{22} = \text{calculated from rigid body considerations} \qquad (C.33)$$

$$H_{ij}^{23} = \lambda_2 \left\{ \frac{1-2\nu}{4\pi(1-\nu)} \right\} \qquad (C.34)$$

where $\lambda_1 = -1$, $\lambda_2 = 1$ for $i = 1$, $j = 2$

$= 1$, $= -1$ for $i = 2$, $j = 1$

$= 0$, $= 0$ for $i = j$.

APPENDIX D

DERIVATION OF THE TRACTION DISCONTINUITY EQUATION FROM THE INVARIANCE OF THE TRACE OF THE STRAIN TENSOR USING QUADRATIC INTERPOLATION

The geometry of the corner node for two quadratic segments is shown in figure D.1 and supplemented by figure 5.5.

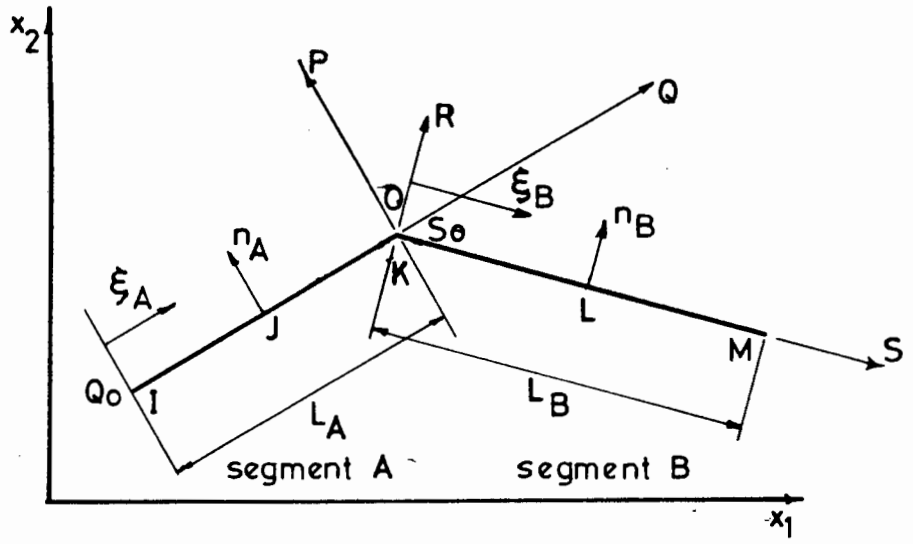

Fig. D.1 Geometric definitions at a corner node assuming quadratic interpolation

In order to derive an equation which relates the discontinuous tractions in the vicinity of node k, the displacement functions for segments A and B must first be derived.

Segment A :

$$u_i(\xi_A) = N_1 u_i(I) + N_2 u_i(J) + N_3 u_i(K) \qquad (D.1)$$

Segment B :

$$u_i(\xi_B) = N_1 u_i(K) + N_2 u_i(L) + N_3 u_i(M) \qquad (D.2)$$

where the quadratic shape functions are, in terms of $\xi = \xi_A$ or ξ_B and $0 \leqslant \xi \leqslant L$ with $L = L_A$ or L_B

$$N_1 = \frac{2\xi^2}{L} - \frac{3\xi}{L} + 1$$

$$N_2 = \frac{-4\xi^2}{L^2} + \frac{4\xi}{L}$$

$$N_3 = \frac{2\xi^2}{L^2} - \frac{\xi}{L}$$

The displacement along each segment is defined by the directions of the normals as :

for segment A in the direction oQ

$$u_Q = u_1 \cos(\eta_A - 90) + u_2 \sin(\eta_A - 90)$$

$$= u_1 \eta_2^A - u_2 \eta_1^A \qquad (D.3)$$

similarly for segment B in the OS direction

$$u_Q = u_1 \eta_2^B - u_2 \eta_1^B \qquad (D.4)$$

The strain in the two directions OQ for segment A and OS for segment B is calculated from :

for segment A, $\varepsilon_{QQ} = \frac{\partial u_Q}{\partial Q}$ (D.5)

and for segment B, $\varepsilon_{SS} = \frac{\partial u_S}{\partial S}$ (D.6)

The Z-coordinate value is related to ξ_A by

$$\xi_A = Q - Q_o \qquad (D.7)$$

and the coordinate value to ξ_B by

$$\xi_B = S - S_o \tag{D.8}$$

Consequently, by the chain rule

$$\varepsilon_{QQ} = \frac{\partial u_Q}{\partial Q} = \frac{\partial u_Q}{\partial \xi_A} \frac{\partial \xi_A}{\partial Q} \tag{D.9}$$

and

$$\varepsilon_{SS} = \frac{\partial u_S}{\partial S} = \frac{\partial u_S}{\partial \xi_B} \frac{\partial \xi_B}{\partial S} \tag{D.10}$$

Substituting (D.1) and (D.2) into (D.3) and (D.4) respectively, performing the differentiation according to (D.9) and (D.10) and evaluating the strain at point K i.e. $\xi_A = L_A$ and $\xi_B = 0$, leads to :

$$\varepsilon_{QQ} = \left| \frac{1}{L_A} u_1(I) - \frac{4}{L_A} u_1(J) + \frac{3}{L_B} u_1(K) \right| n_2^A - \left| \frac{1}{L_A} u_2(I) - \frac{4}{L_A} u_2(J) + \frac{3}{L_B} u_2(K) \right| n_1^A \tag{D.11}$$

and

$$\varepsilon_{SS} = \left| -\frac{3}{L_B} u_1(K) + \frac{4}{L_B} u_1(L) - \frac{1}{L_B} u_1(M) \right| n_2^A - \left| -\frac{3}{L_B} u_2(K) + \frac{4}{L_B} u_2(L) - \frac{1}{L_B} u_2(M) \right| n_1^B \tag{D.12}$$

The traction and stress at K for segments A and B can be expressed by

$$t_P = t_1 \cos n_A + t_2 \sin n_A = t_1^A n_1^A + t_2^A n_2^A = \sigma_{PP} \tag{D.13}$$

$$t_R = t_1 \cos n_B + t_2 \sin n_B = t_1^B n_1^B + t_2^B n_2^B = \sigma_{RR} \tag{D.14}$$

Also, from Hooke's Law :

$$\sigma_{PP} = (\zeta + \mu)\varepsilon_{PP} + (\zeta - \mu)\varepsilon_{QQ} \tag{D.15}$$

$$\sigma_{RR} = (\zeta + \mu)\varepsilon_{RR} + (\zeta - \mu)\varepsilon_{SS} \tag{D.16}$$

where $\zeta = \lambda + \mu$ and λ, μ are Lamé constants.

Substituting (D.13) and (D.14) into (D.15) and (D.16) respectively and subtracting the one resulting equation from the others, gives

$$(\zeta+\mu)\ (\varepsilon_{RR}-\varepsilon_{PP}) + (\zeta-\mu)\ (\varepsilon_{SS}-\varepsilon_{QQ}) = t_1^B n_1^B + t_2^B n_2^B - t_1^A n_1^A - t_2^A n_2^A \tag{D.17}$$

But, the invariance of the strain tensor can be written as

$$\varepsilon_{SS} + \varepsilon_{RR} = \varepsilon_{PP} + \varepsilon_{QQ} \tag{D.18}$$

and hence

$$\varepsilon_{RR} - \varepsilon_{PP} = \varepsilon_{QQ} - \varepsilon_{SS} \tag{D.19}$$

By substituting (D.19) into (D.17) and using the expression for ε_{QQ} and ε_{SS} from (D.11) and (D.12), gives the final equation in terms of the nodal displacements and tractions

$$\begin{aligned} t_1^B n_1^B + t_2^B n_2^B - t_1^A n_1^A - t_2^A n_2^A = \\ 2\mu \Bigg[& \frac{n_2^A}{L_A} u_1(I) - \frac{n_1^A}{L_A} u_2(I) - \frac{4n_2^A}{L_A} u_1(J) + \frac{4n_1^A}{L_A} u_2(J) \\ & + \left(\frac{3n_2^A}{L_A} + \frac{3n_2^B}{L_B} \right) u_1(K) - \left(\frac{3n_1^A}{L_A} + \frac{3n_1^B}{L_B} \right) u_2(K) \\ & - \frac{4n_2^B}{L_B} u_1(L) + \frac{4n_1^B}{L_B} u_2(L) + \frac{n_2^B}{L_B} u_1(M) - \frac{n_1^B}{L_B} u_2(M) \Bigg] \end{aligned} \tag{D.20}$$

APPENDIX E

GRAPHS OF ERROR IN NUMERICAL INTEGRATION OF $\ln\frac{1}{r}$ and $\frac{1}{r}$

The error between the numerical integration (Gauss Quadrature) and the analytical integration of the expressions $\ln\frac{1}{r}$ and $\frac{1}{r}$ is given in this appendix.

All graphs shown are of the same form. The essential properties of the graph can be summarized as follows:

(i) The horizontal axis is the dimension m which is the distance from the pivot node to the closest point on the focus segment (figure 5.19).

(ii) The vertical axis is the percentage difference (either positive or negative) between the numercal and analytical integration (equation 5.45).

(iii) Each graph contains the trace of the error for 6 segment lengths, L = 0.5, 1.0, 5.0, 10.0, 50.0 and 100.0 units. The graphs are plotted for various m values, ie., various distances between pivot node and the closest point of the focus segment.

The trace of the errors in integration are as follows:

Figure	Numerical Integration of	Interpolation/ segment type	Gauss Quadrature order
E.1 E.2 E.3	$\ln\frac{1}{r}$	constant	2 4 6
E.4 E.5 E.6	$N_1 \ln\frac{1}{r}$	linear	2 4 6
E.7 E.8 E.9	$N_2 \ln\frac{1}{r}$	linear	2 4 6
E.10 E.11 E.12	$N_1 \ln\frac{1}{r}$	quadratic	2 4 6
E.13 E.14 E.15	$N_2 \ln\frac{1}{r}$	quadratic	2 4 6
E.16 E.17 E.18	$N_3 \ln\frac{1}{r}$	quadratic	2 4 6
E.19 E.20 E.21	$\frac{1}{r}$	constant	2 4 6
E.22 E.23 E.24	$N_1 \frac{1}{r}$	linear	2 4 6
E.25 E.26 E.27	$N_2 \frac{1}{r}$	linear	2 4 6

Figure	Numerical Integration of	Interpolation/ segment type	Gauss Quadrature order
E.28 E.29 E.30	$N_1 \frac{1}{r}$	quadratic	2 4 6
E.31 E.32 E.33	$N_2 \frac{1}{r}$	quadratic	2 4 6
E.34 E.35 E.36	$N_3 \frac{1}{r}$	quadratic	2 4 6

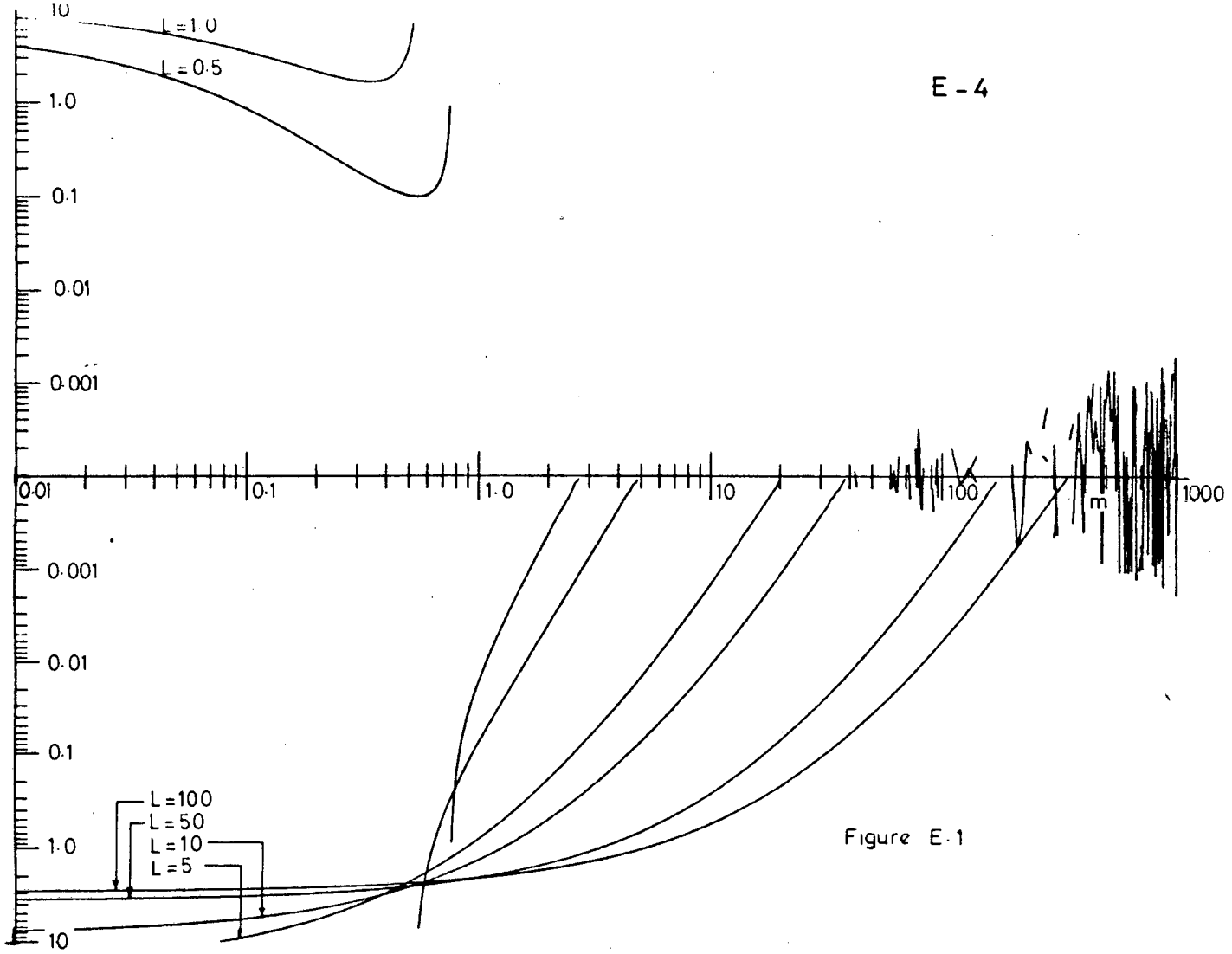

Figure E.1

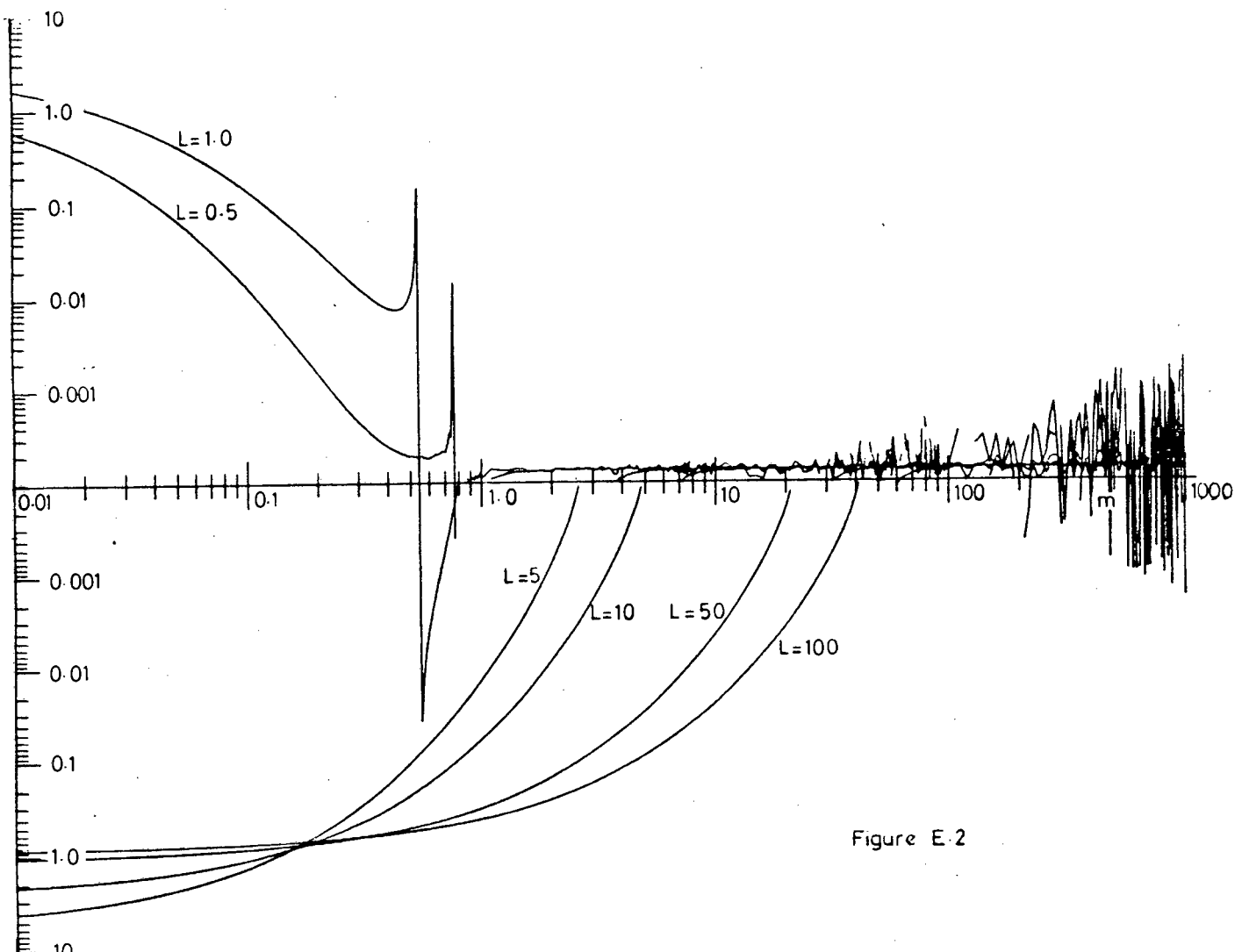

Figure E.2

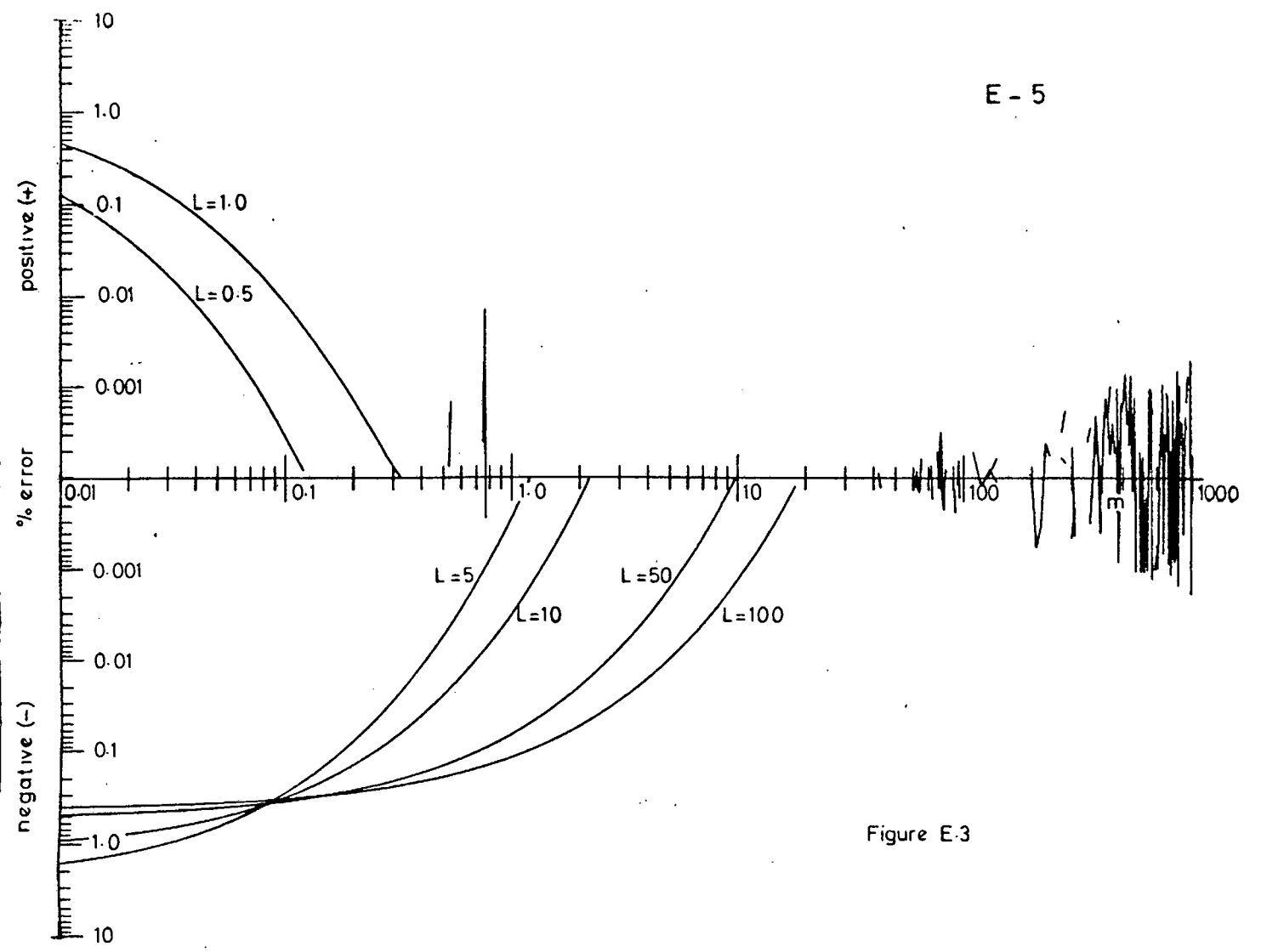

Figure E·3

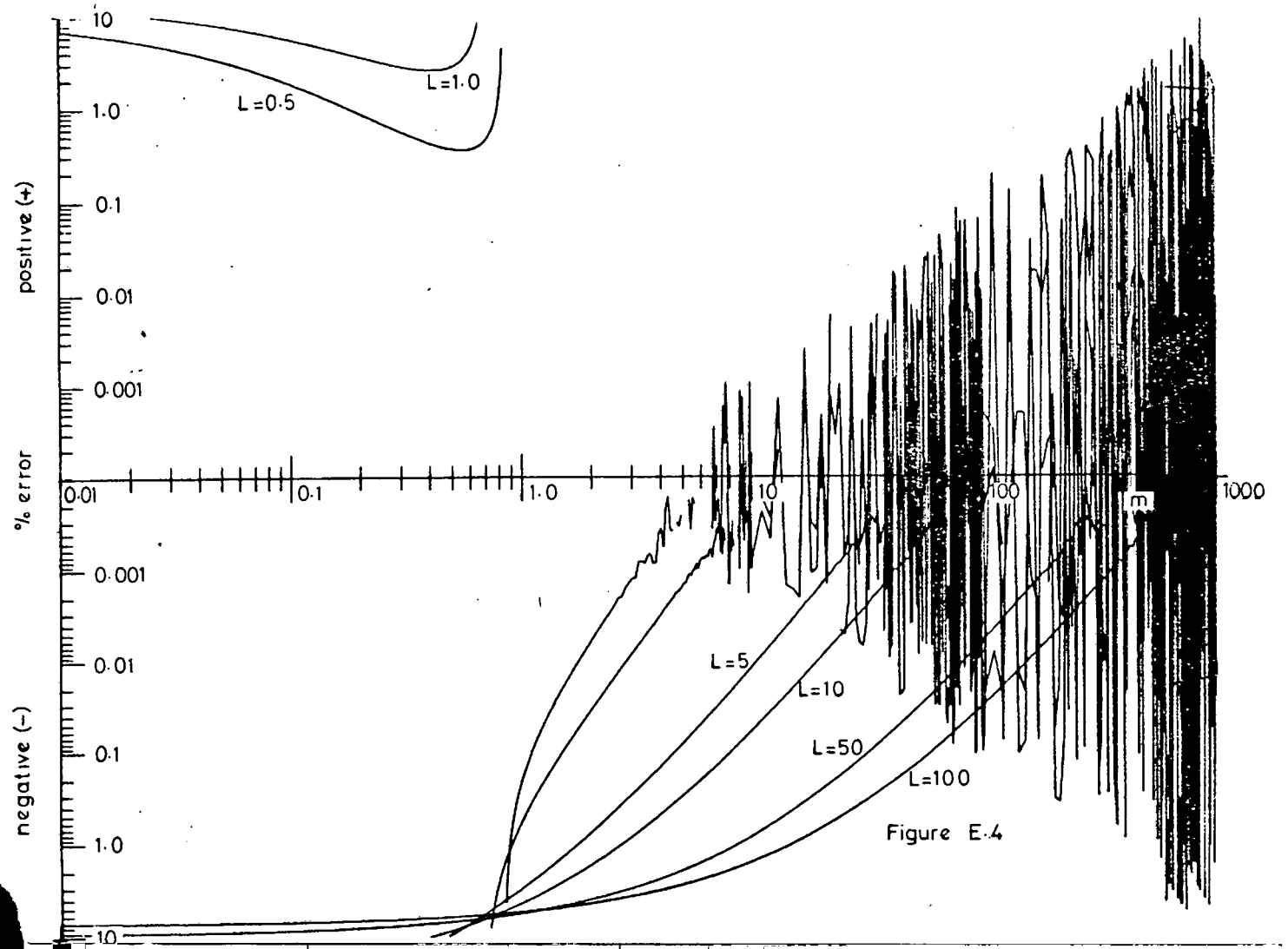

Figure E·4

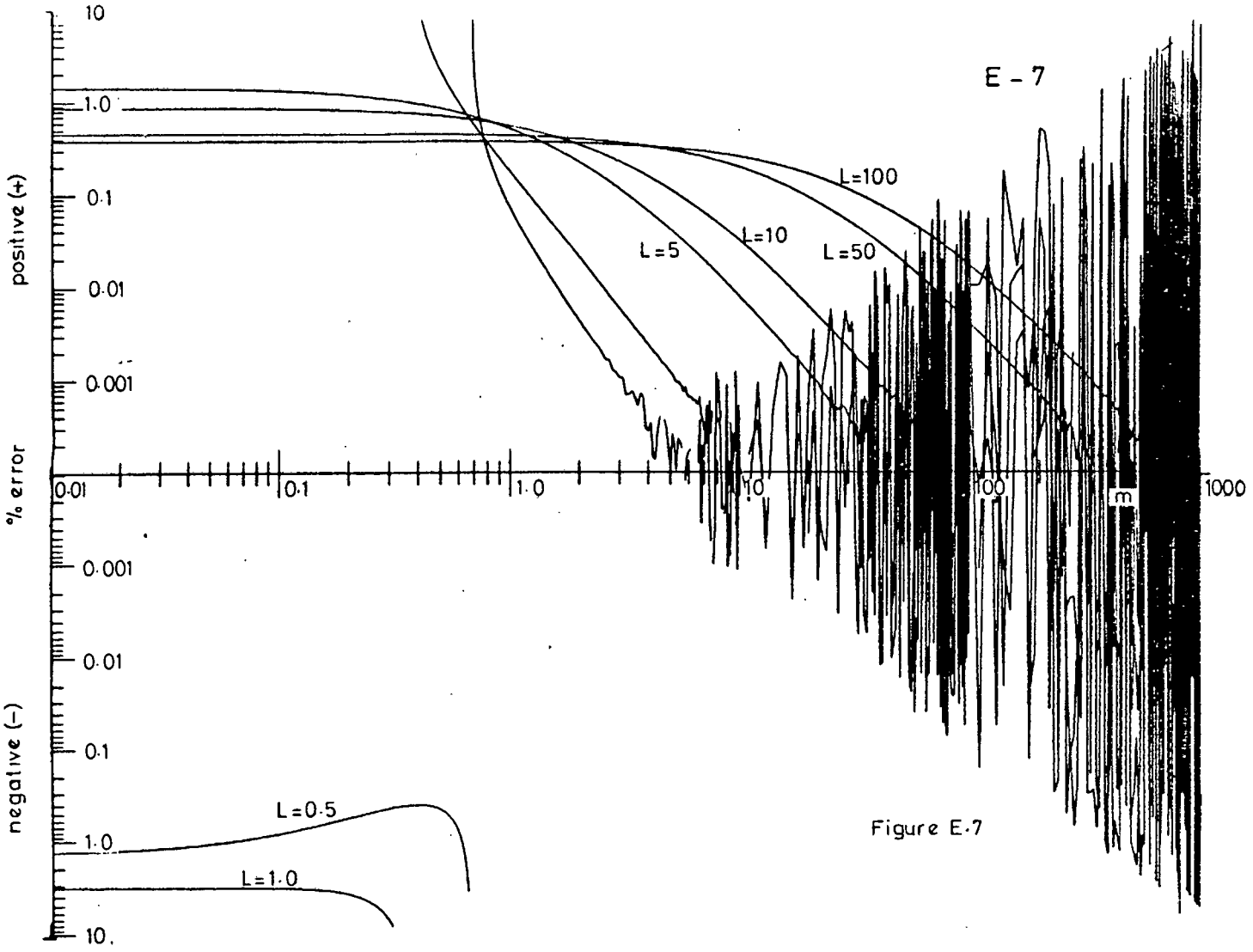

Figure E.7

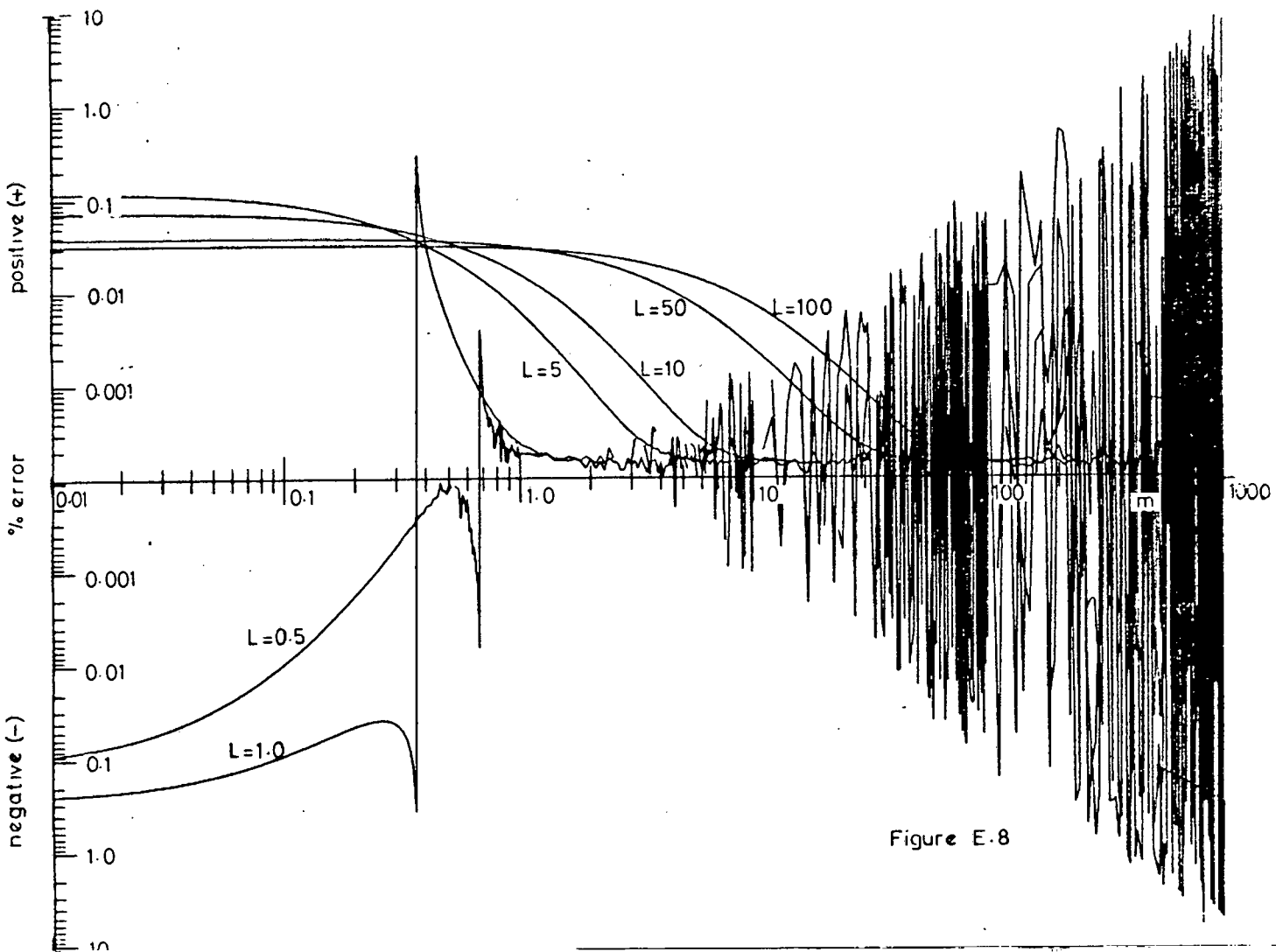

Figure E.8

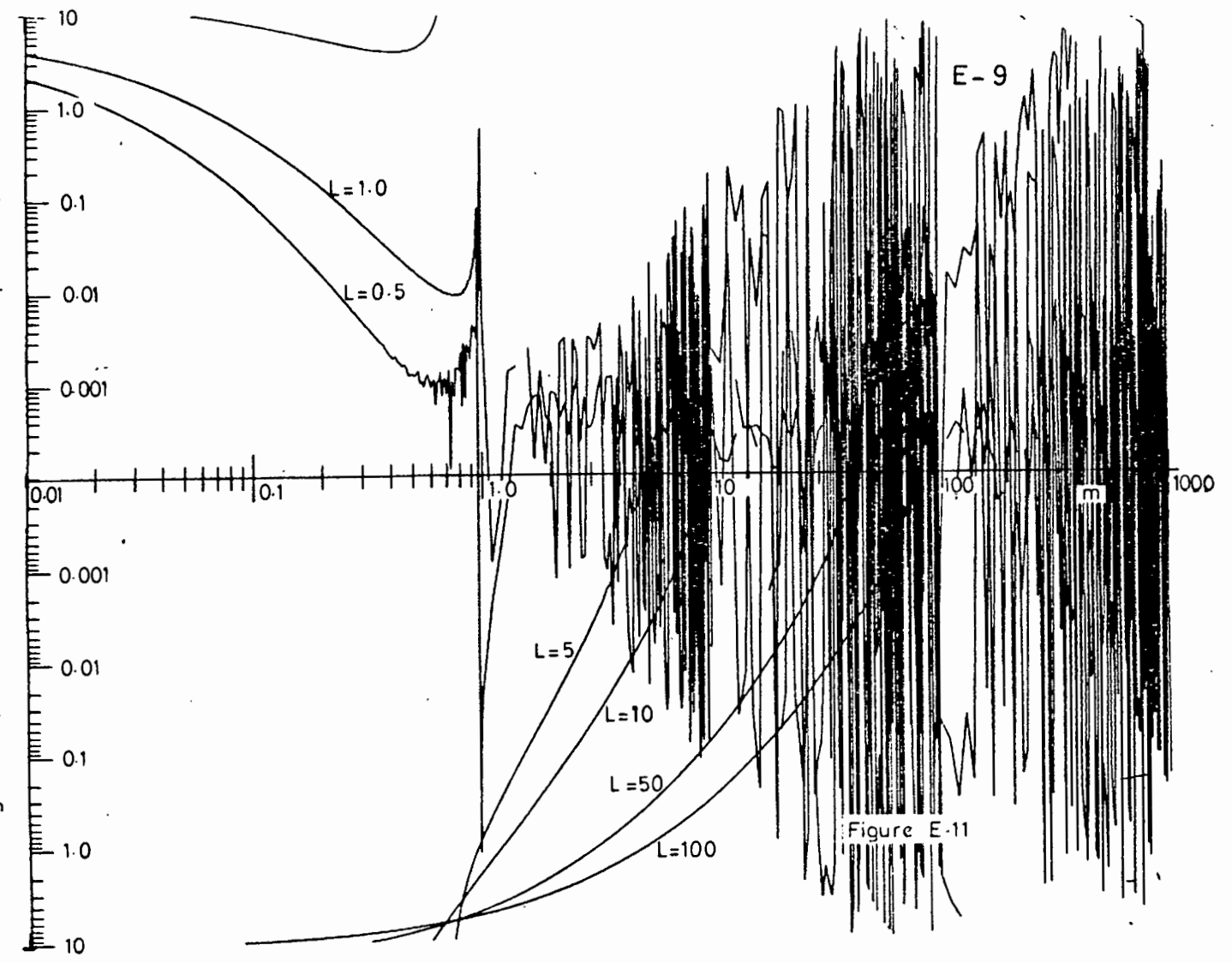

Figure E-11

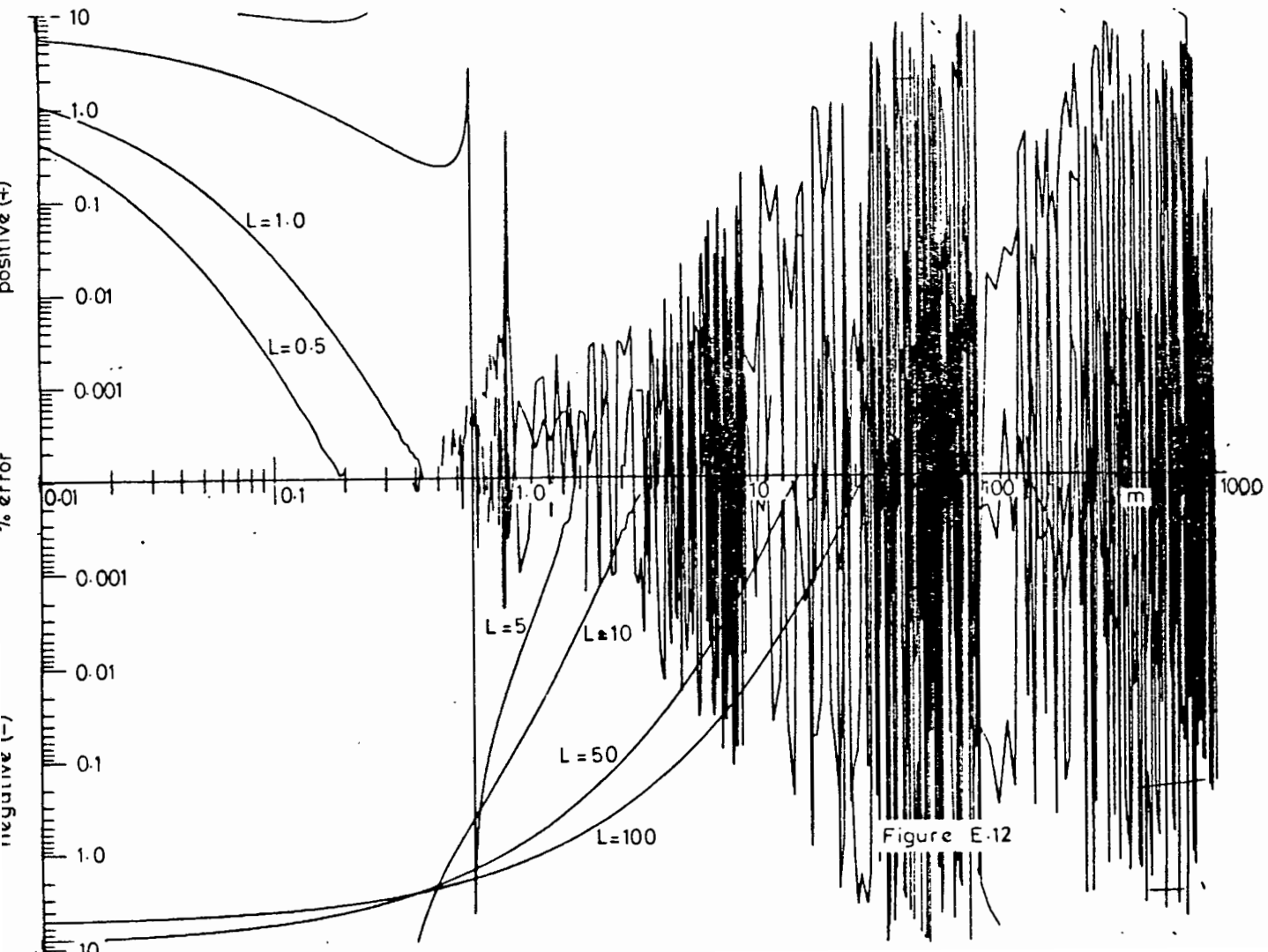

Figure E-12

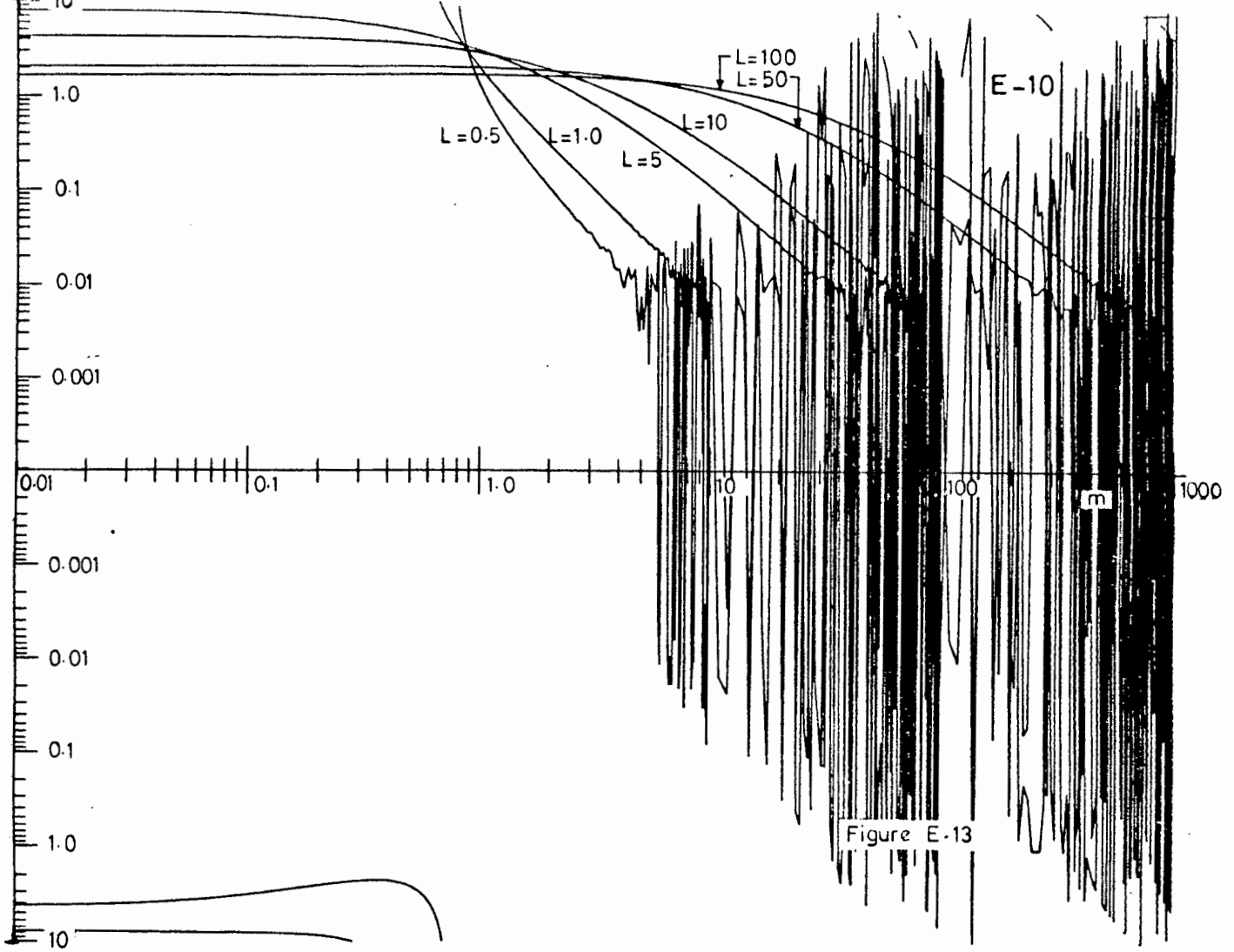

Figure E-13

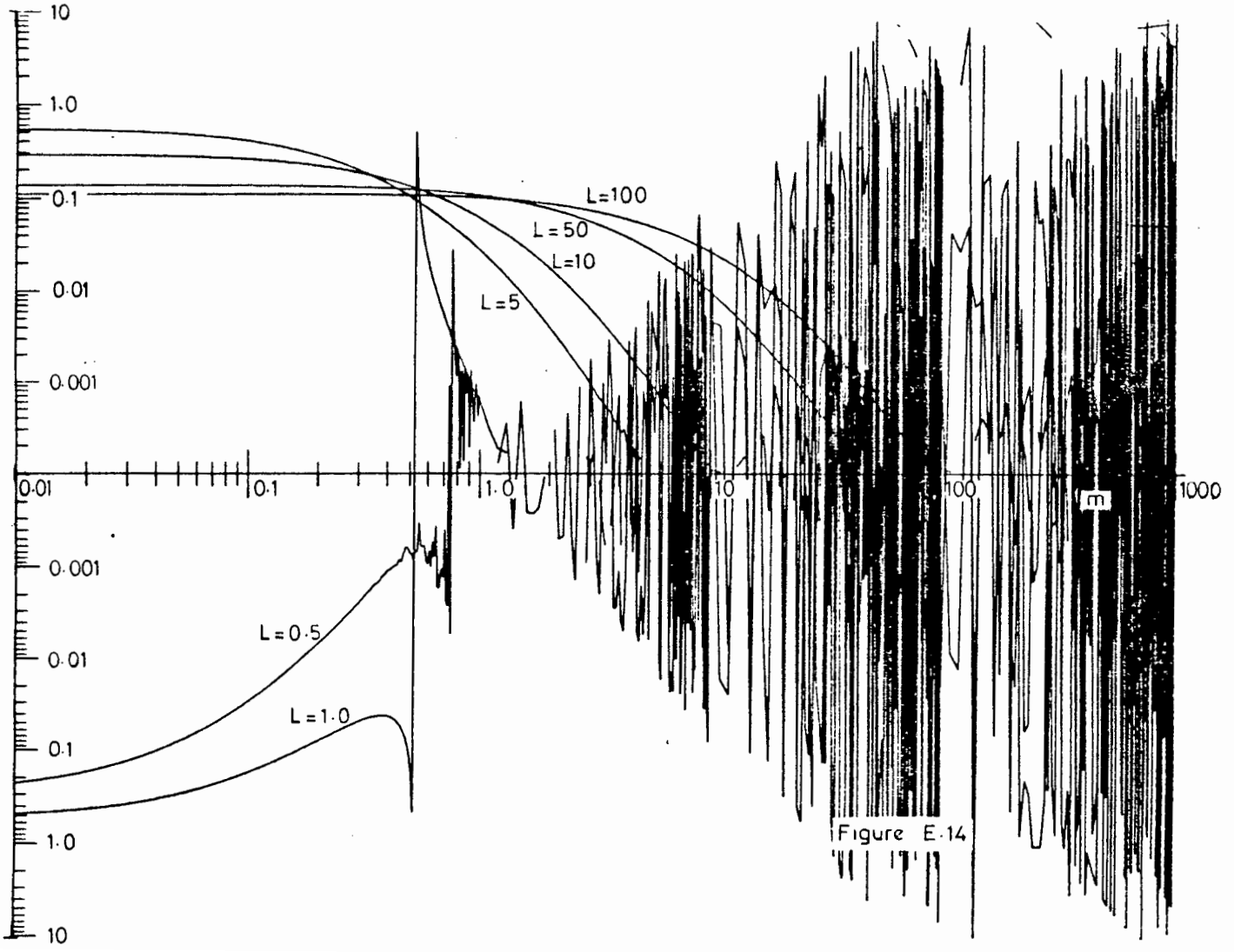

Figure E-14

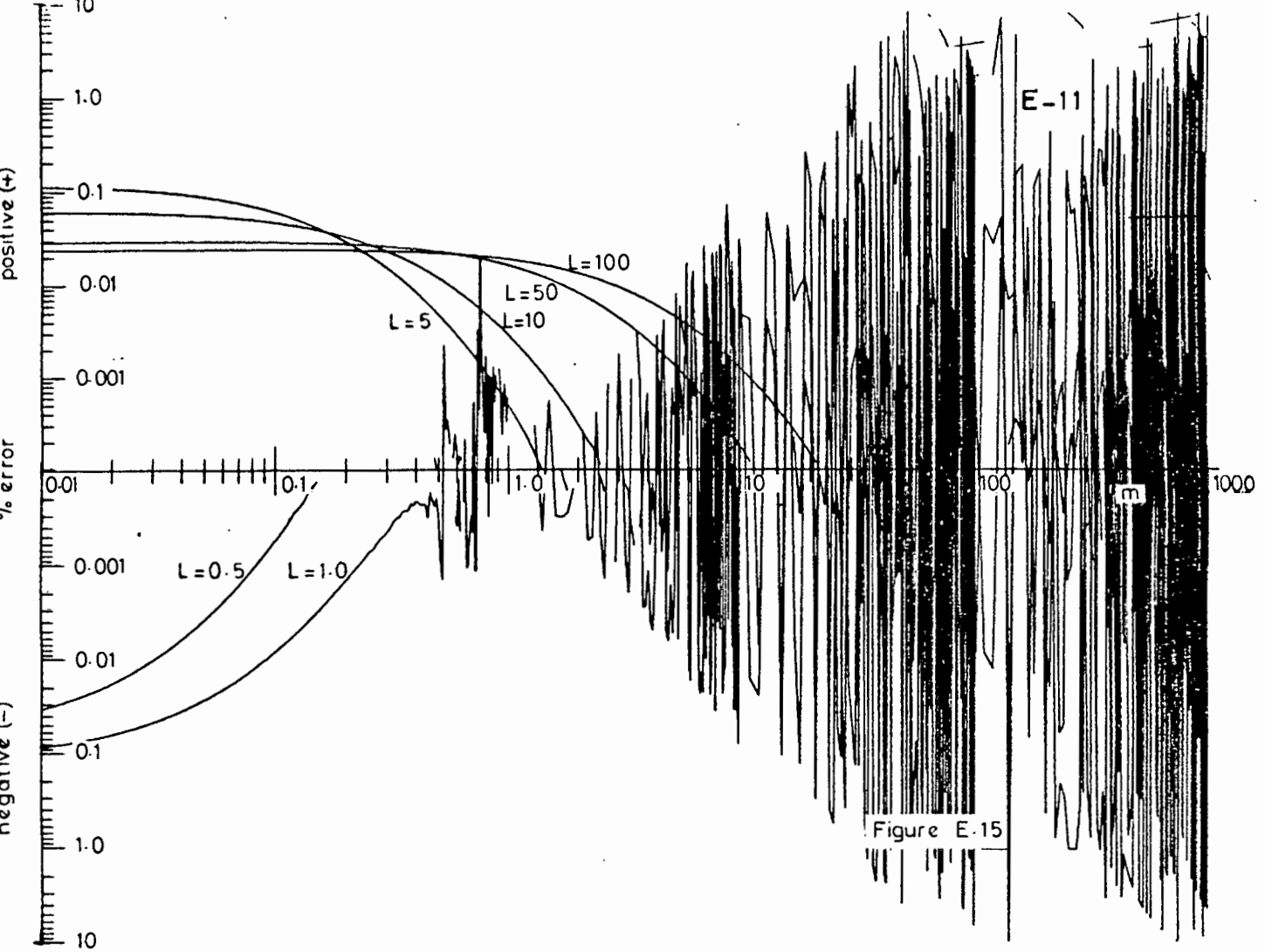

Figure E·15

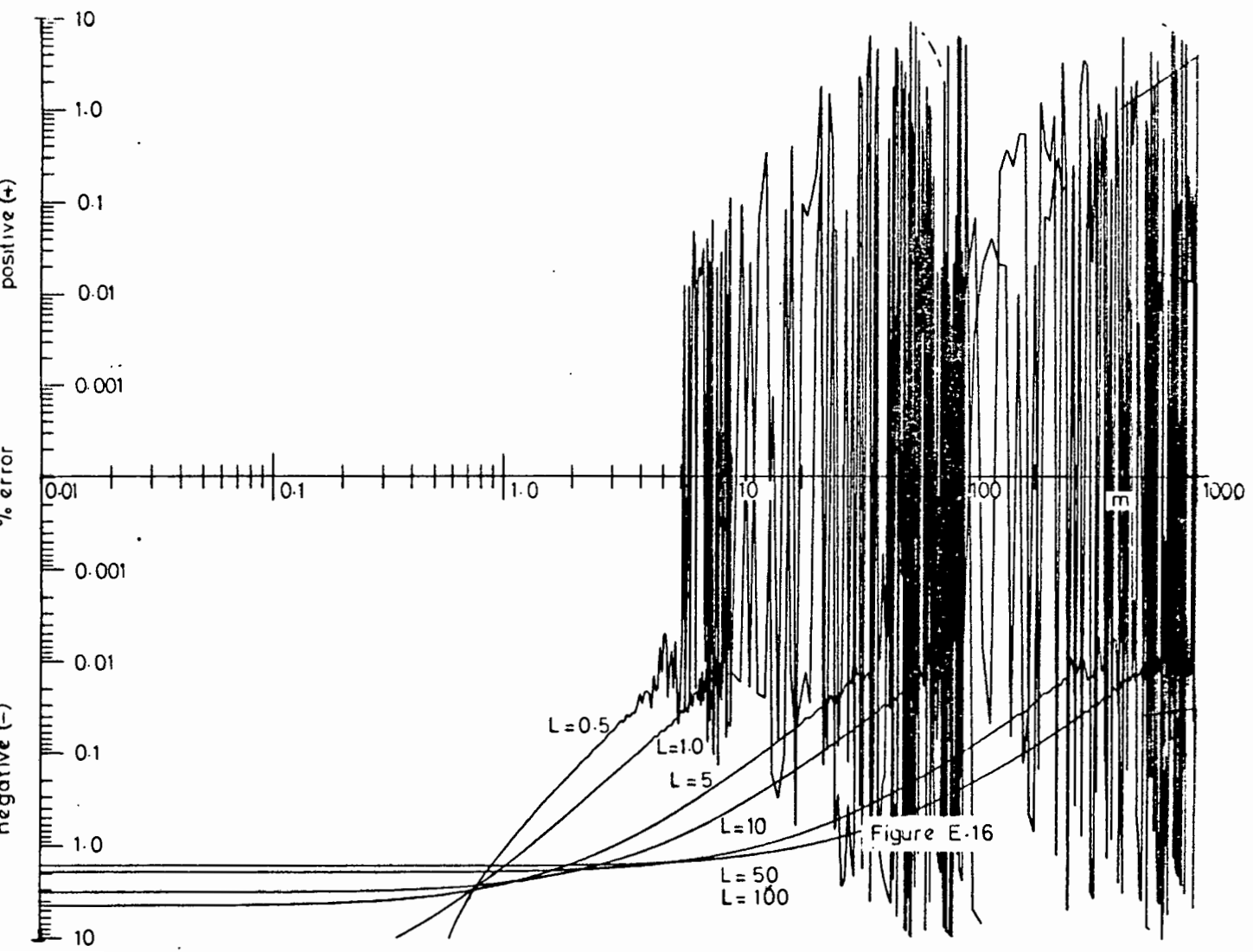

Figure E·16

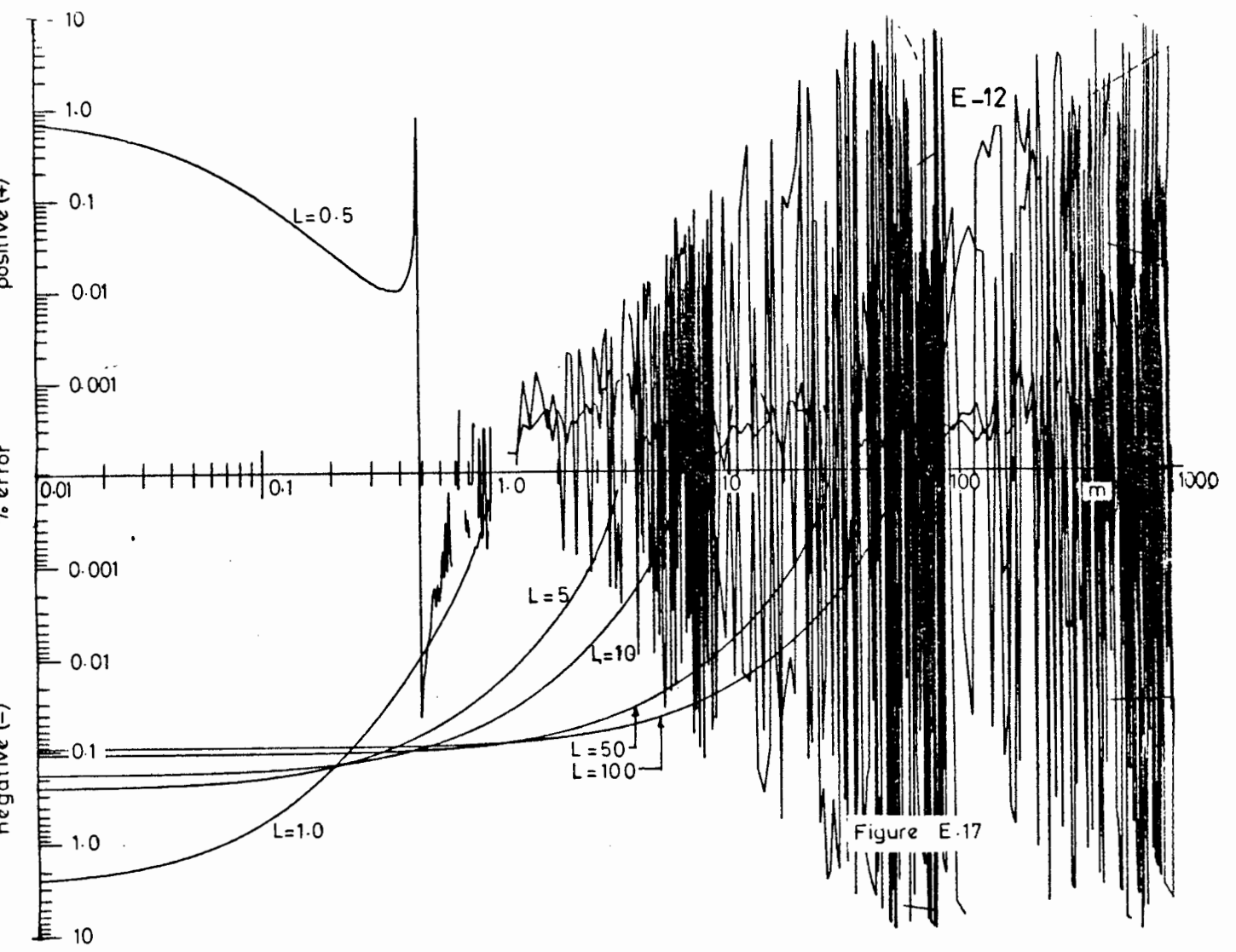

Figure E·17

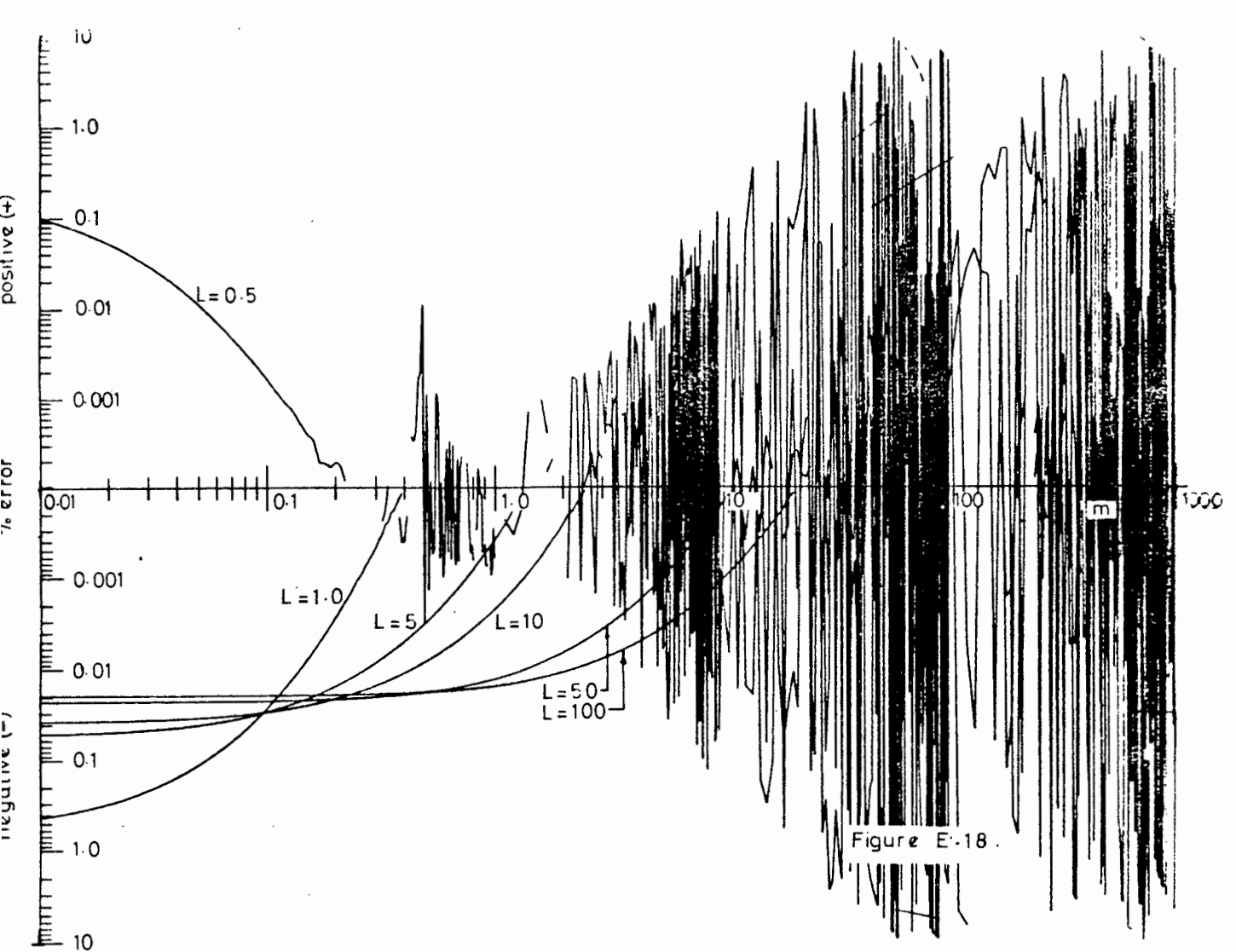

Figure E·18.

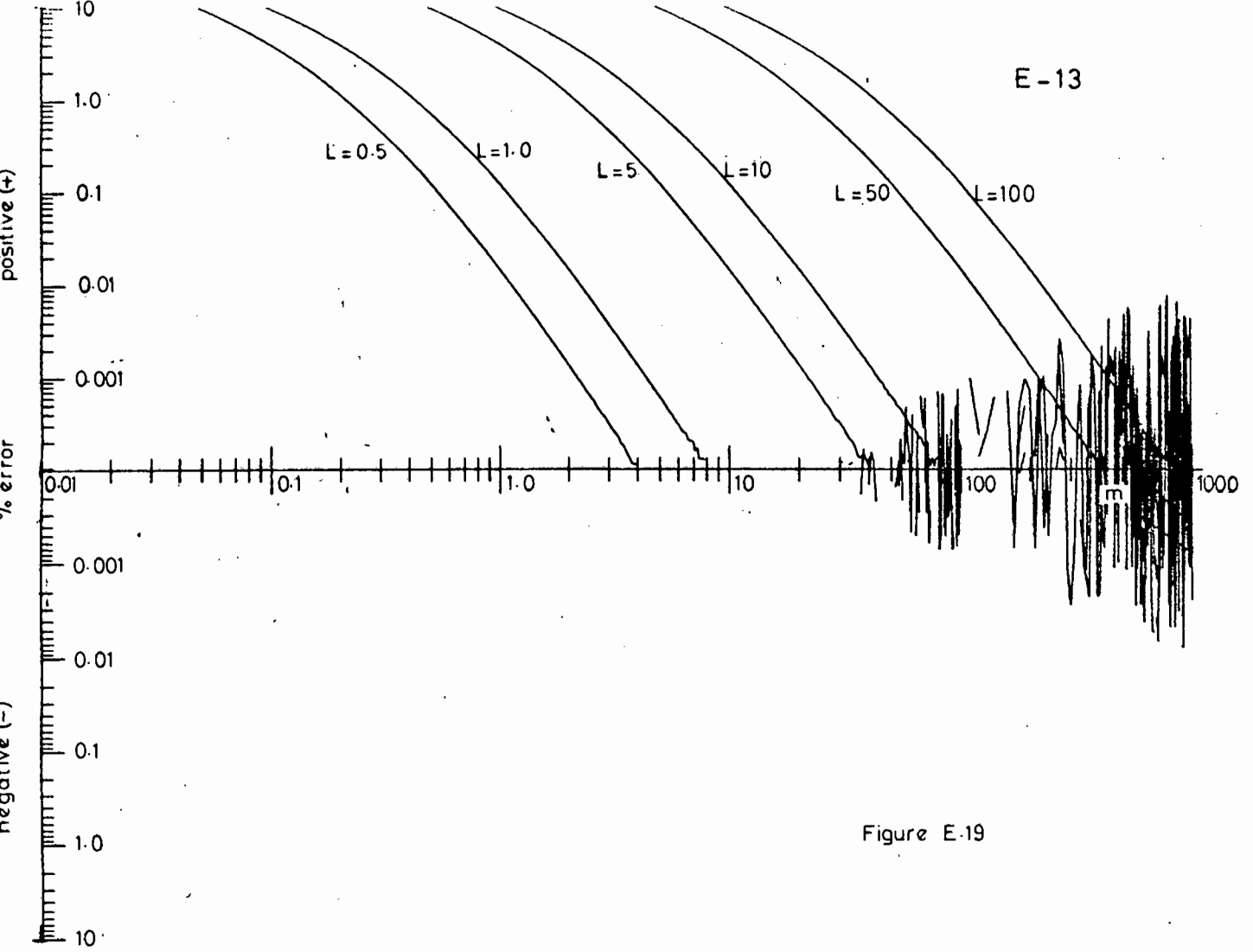

Figure E.19

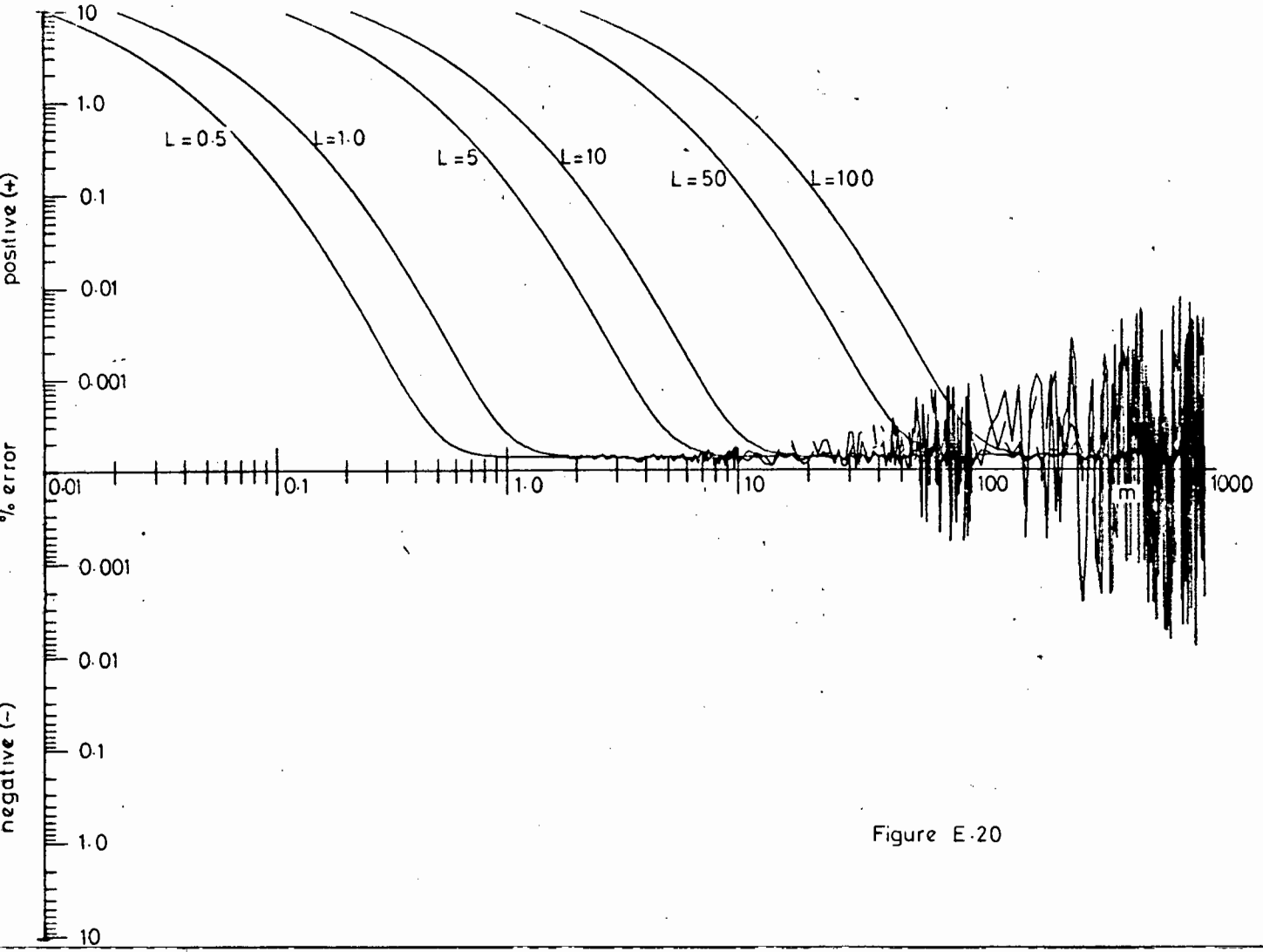

Figure E.20

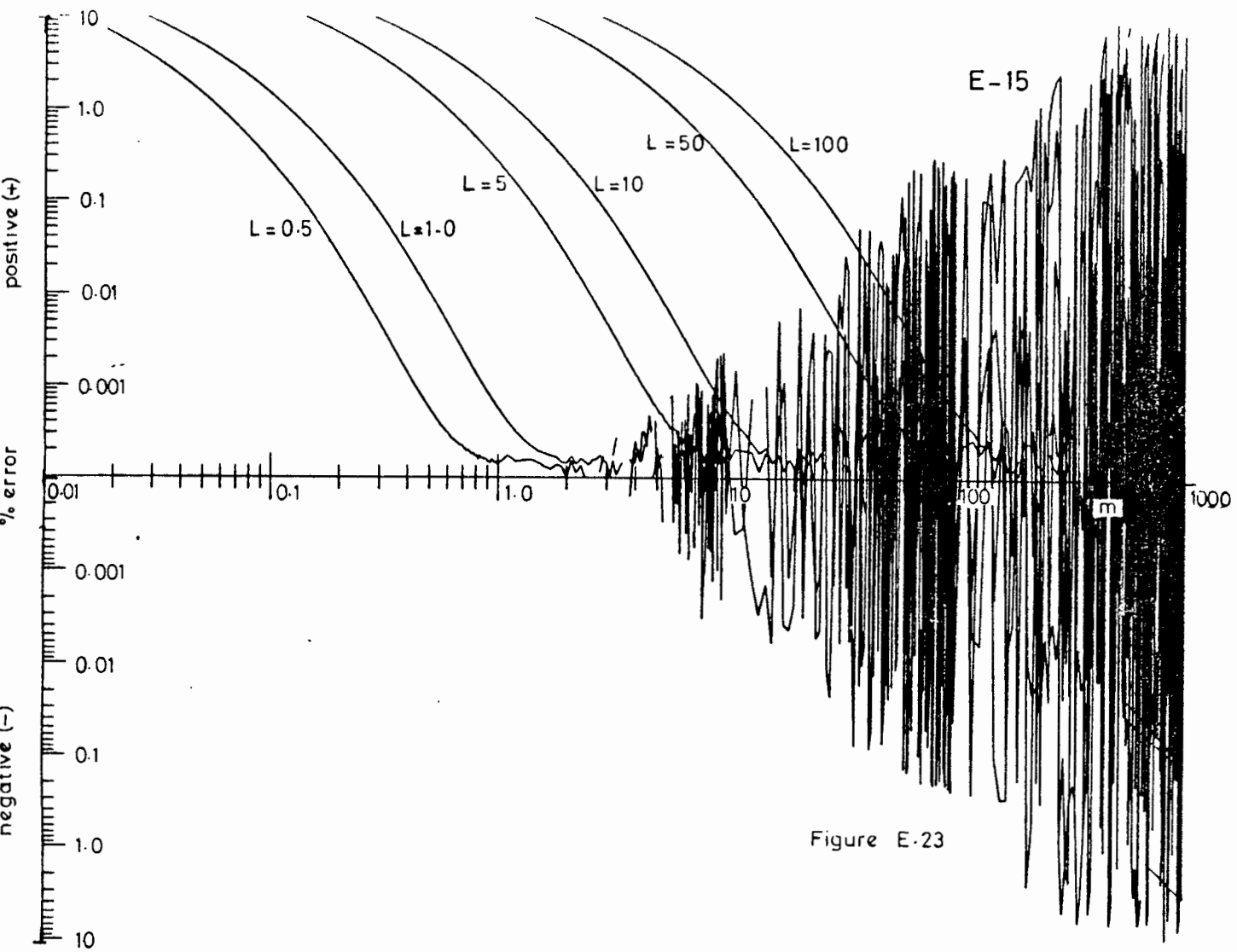

Figure E-23

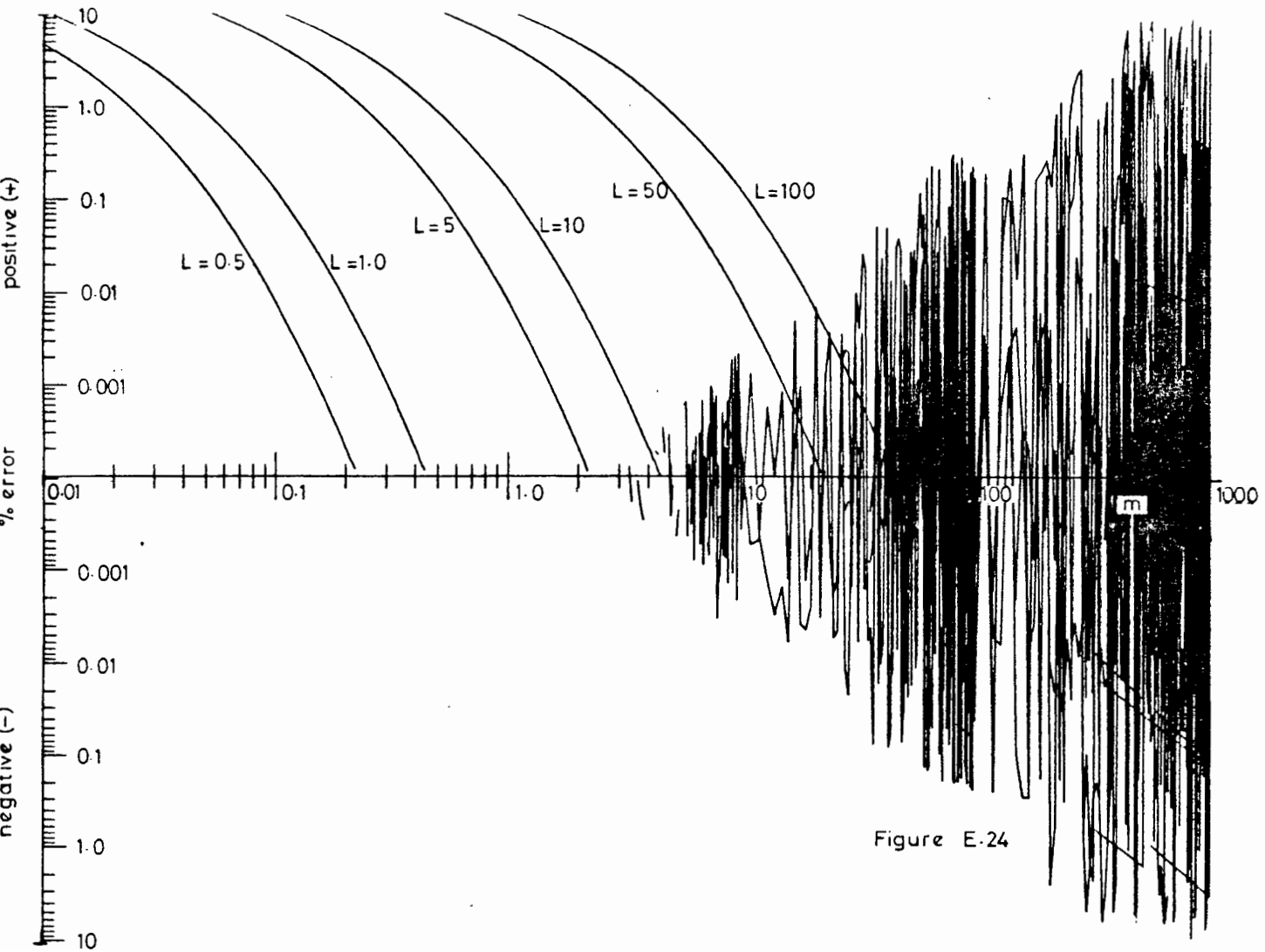

Figure E-24

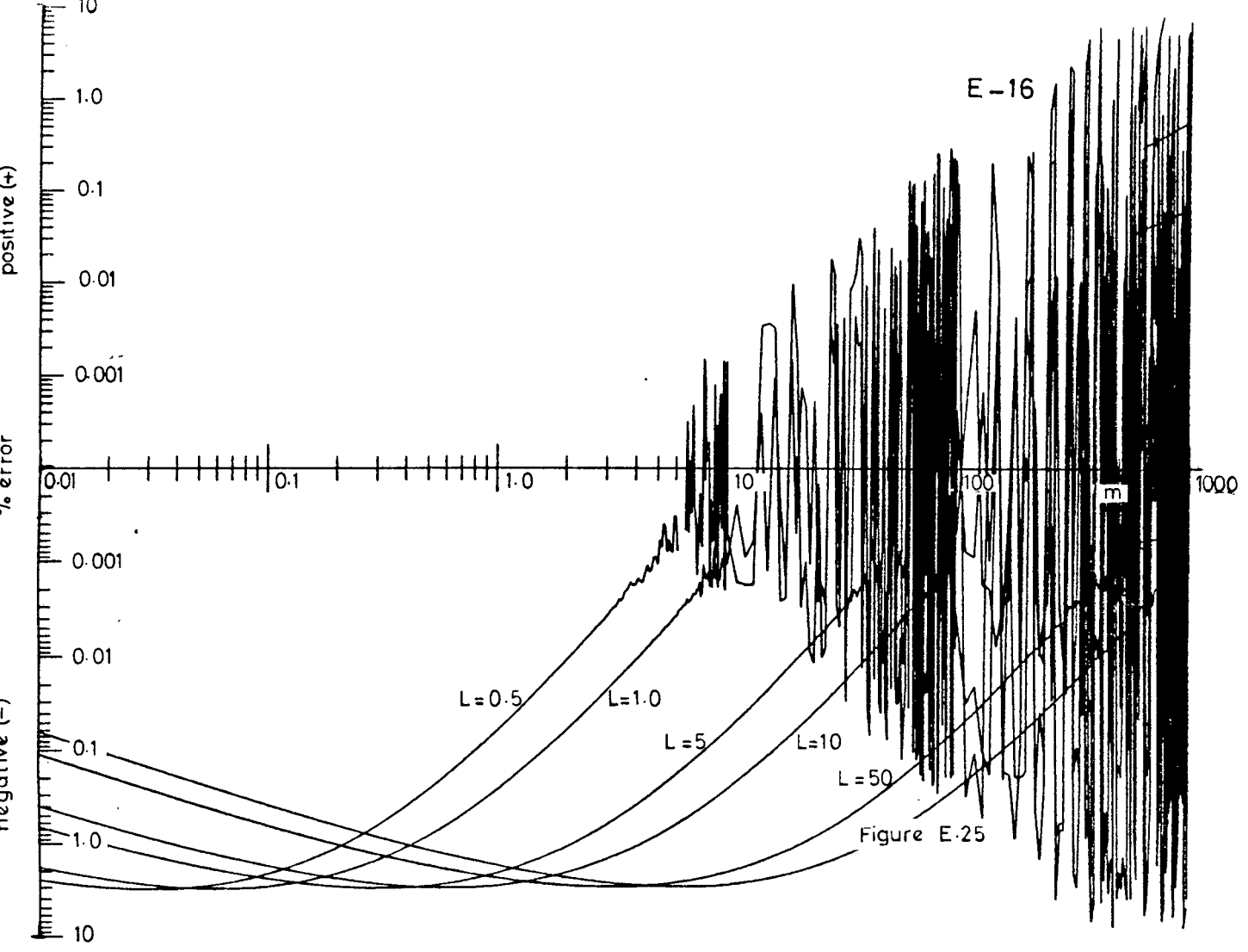

Figure E·25

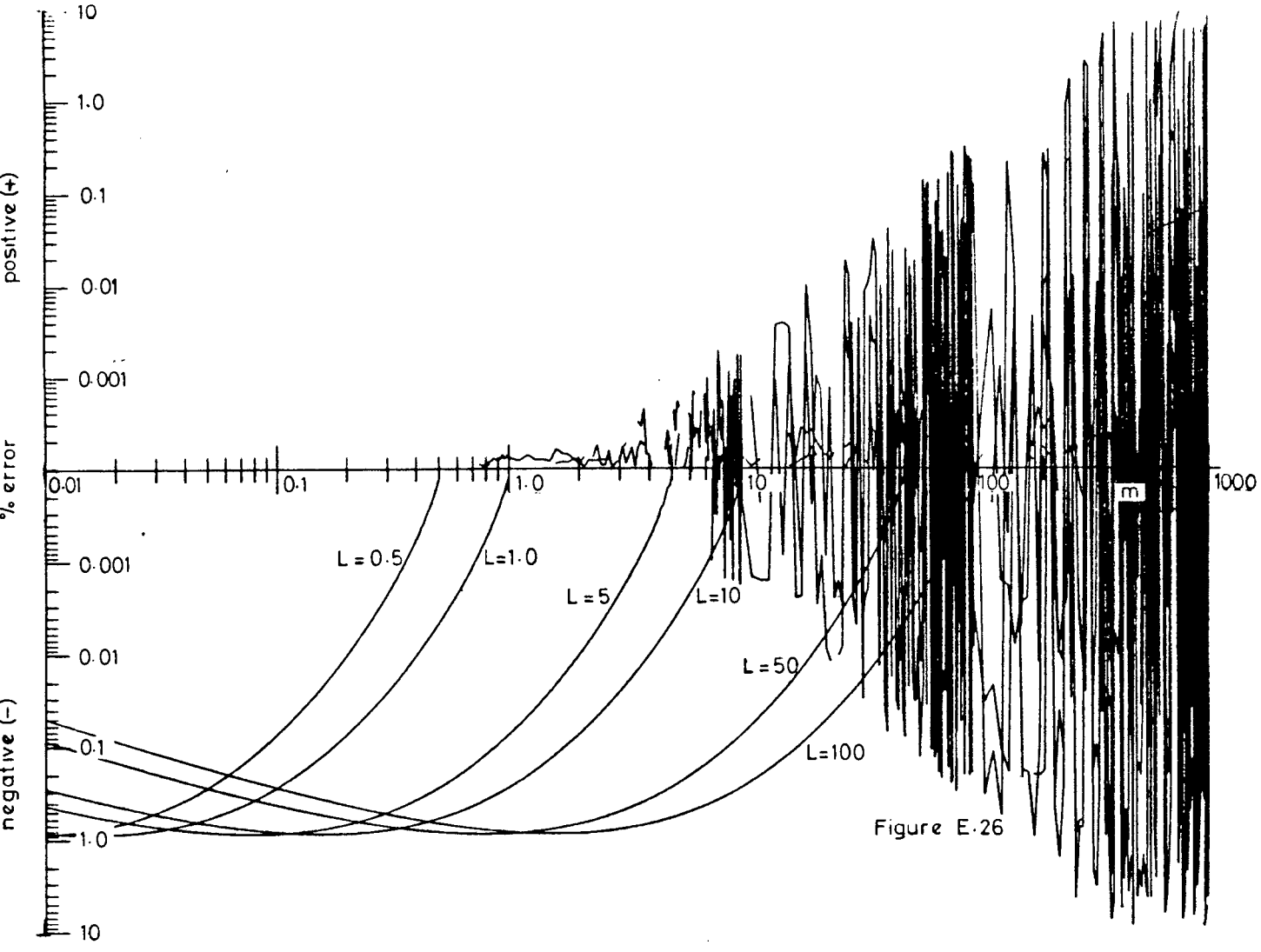

Figure E·26

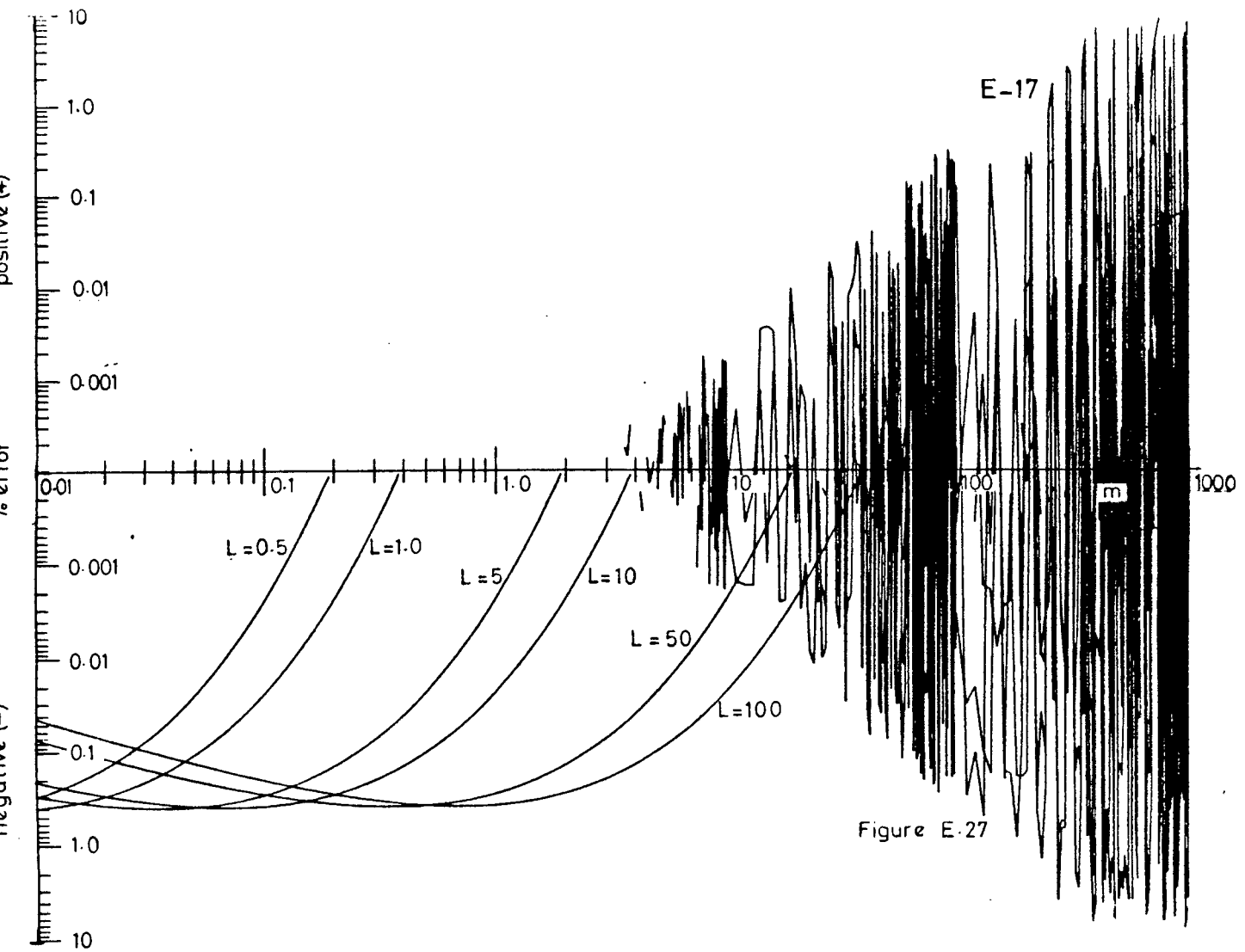

Figure E·27

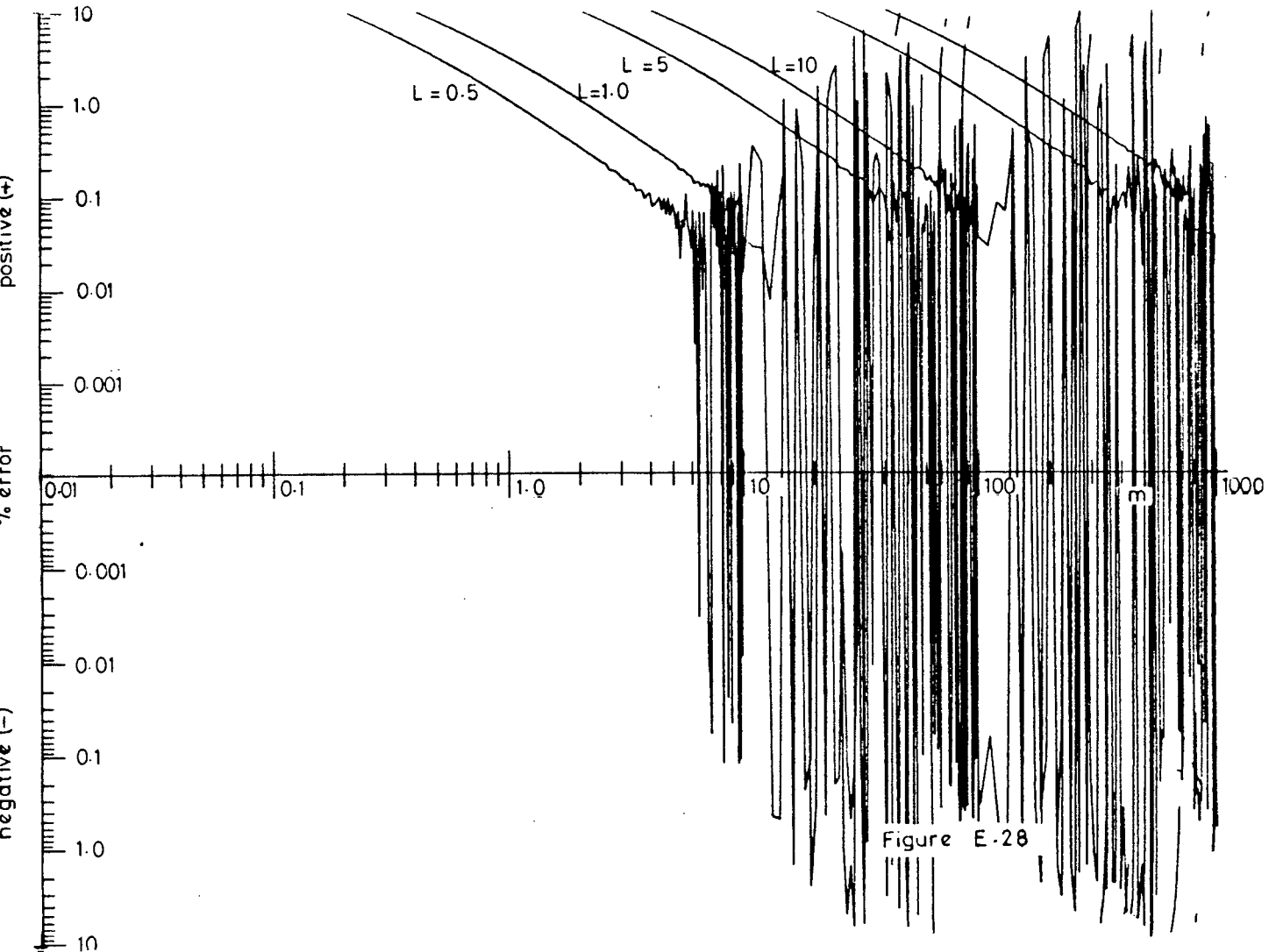

Figure E·28

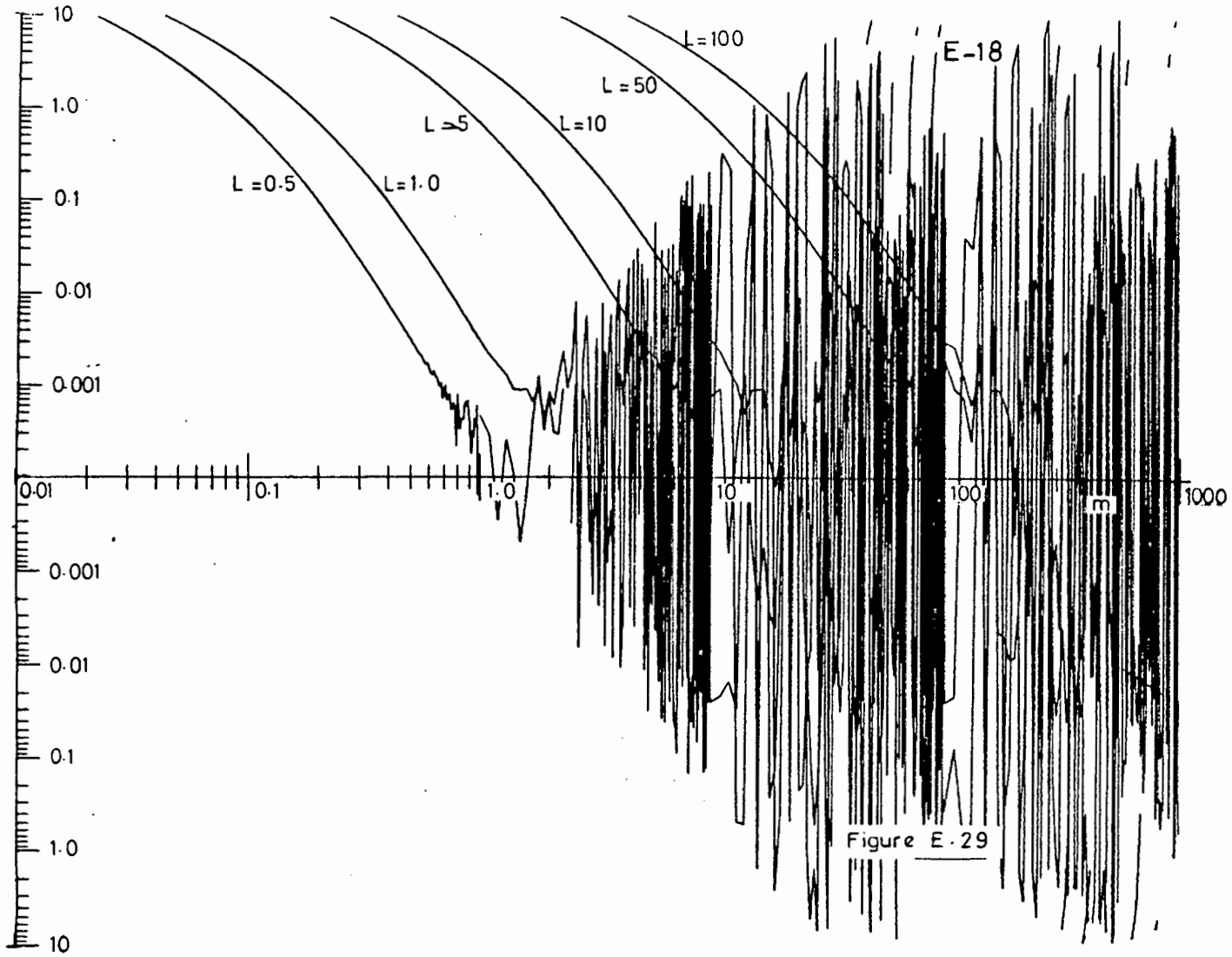

Figure E·29

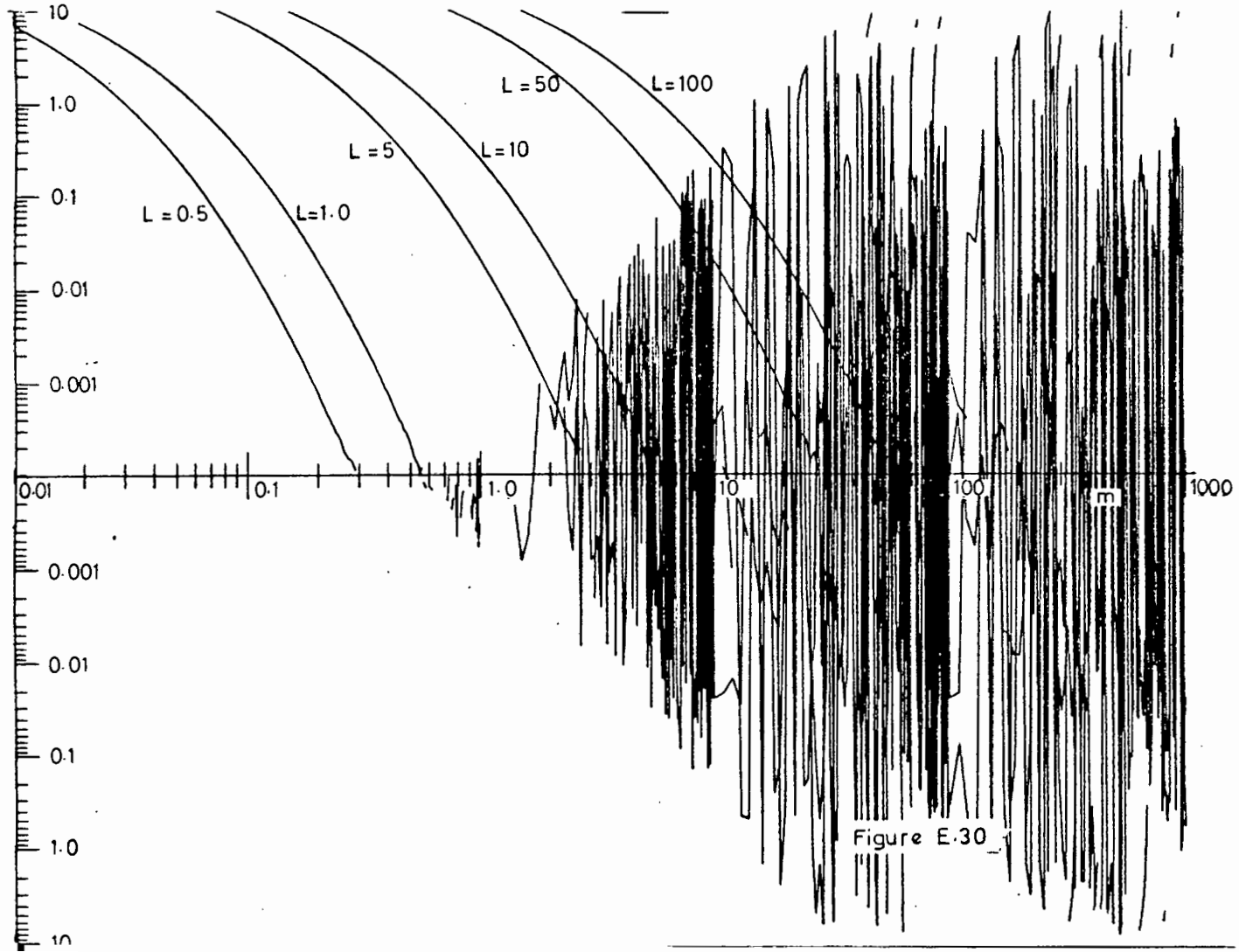

Figure E·30

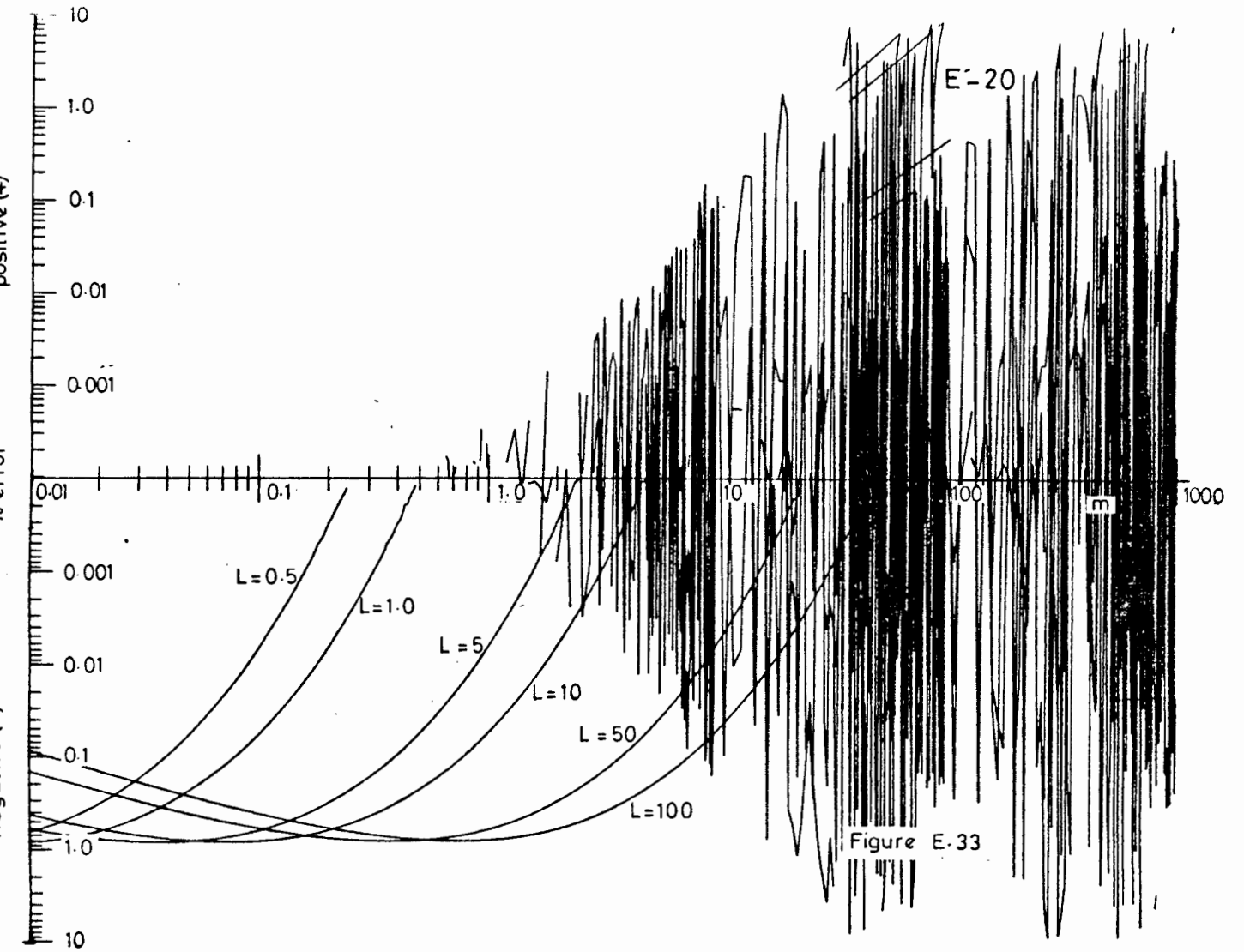

Figure E.33

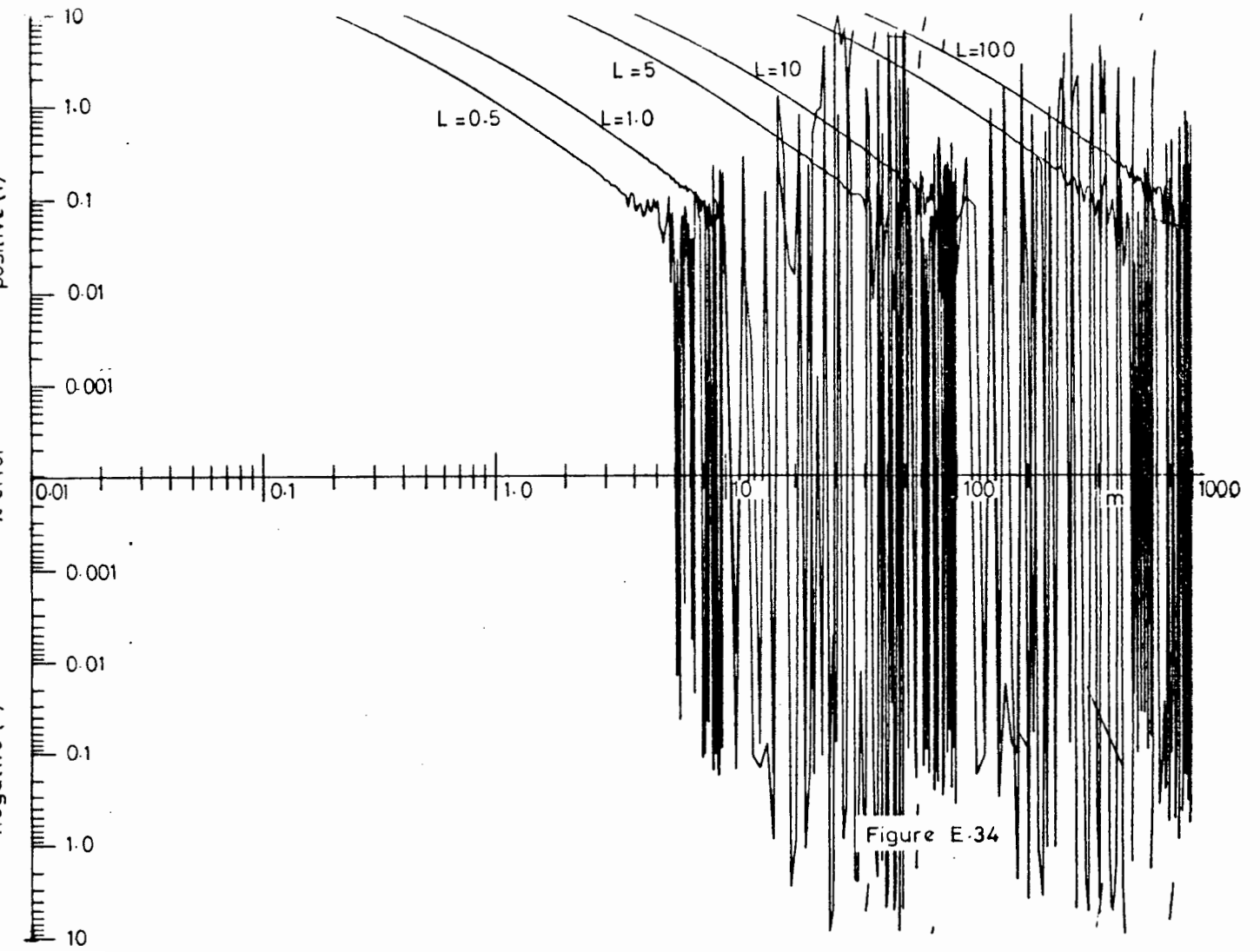

Figure E.34

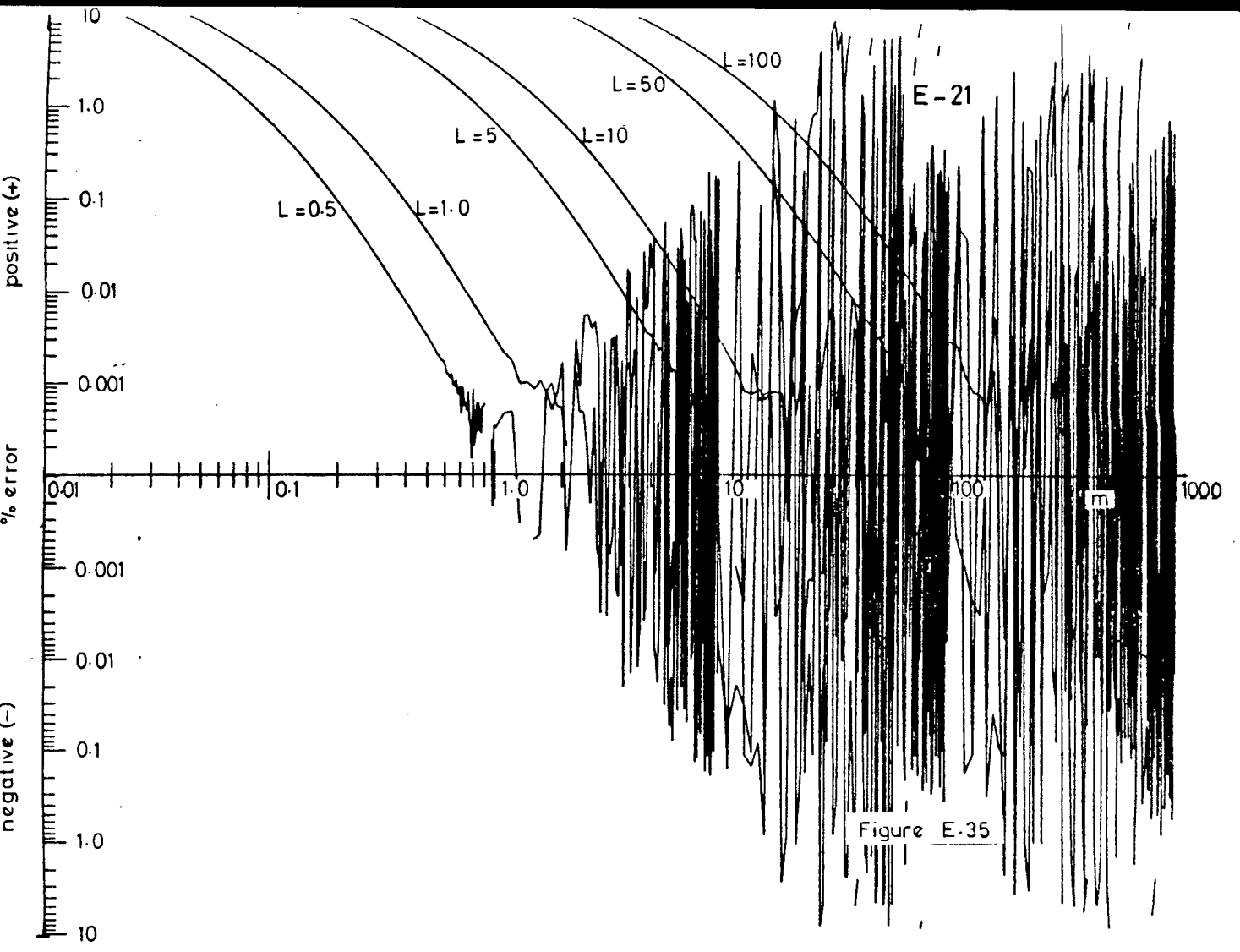

Figure E.35

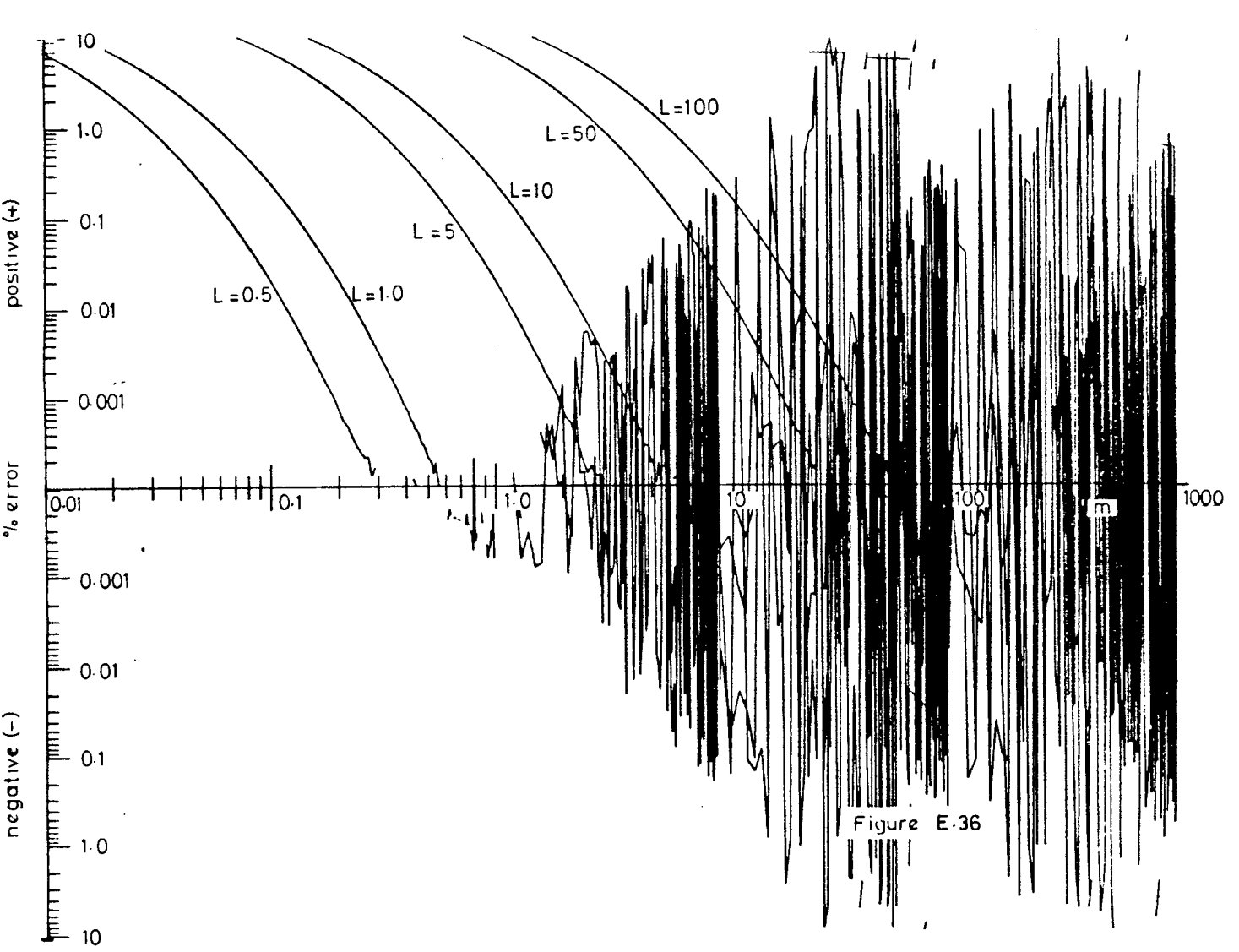

Figure E.36

APPENDIX F

The Family of Infinite Elements

F.1 TYPE 1

Linear, one way infinite Lagrangian element.

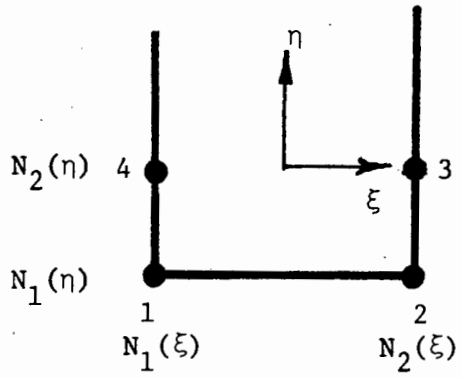

Fig. F.1-Type 1 Infinite element

One-dimensional shape functions:

(i) in ξ-direction (linear shape functions)

$$N_1(\xi) = \tfrac{1}{2}(1-\xi)$$
$$N_2(\xi) = \tfrac{1}{2}(1+\xi)$$

(ii) in η-direction (infinite shape functions)

$$N_1(\eta) = -\frac{2\eta}{(1-\eta)}$$
$$N_2(\eta) = 1 + \frac{2\eta}{(1-\eta)}$$

The 2-dimensional shape functions for the geometrical mapping follow from equation 7.15:

$$\bar{N}_1(\xi,\eta) = N_1(\xi).N_1(\eta) = \frac{-2(1-\xi)}{(1-\eta)} \qquad (F.1)$$

$$\bar{N}_2(\xi,\eta) = N_2(\xi).N_1(\eta) = \frac{-2(1+\xi)}{(1-\eta)} \qquad (F.2)$$

$$\bar{N}_3(\xi,\eta) = N_2(\xi).N_2(\eta) = \tfrac{1}{2}(1+\xi)(1 + \frac{2\eta}{1-\eta}) \qquad (F.3)$$

$$\bar{N}_4(\xi,\eta) = N_1(\xi).N_2(\eta) = \tfrac{1}{2}(1-\xi)(1 + \frac{2\eta}{1-\eta}) \qquad (F.4)$$

where for $\bar{N}_p(\xi,\eta)$, p represents the nodal point in figure F.1.

F.2 TYPE 2

Quadratic, one-way infinite Lagrangian element.

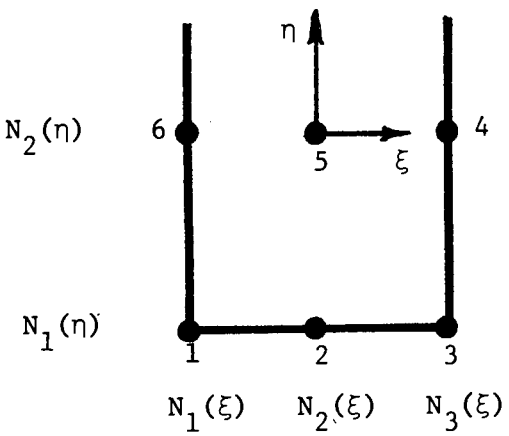

Fig. F.2 - Type 2 Infinite Element

One dimensional shape functions:

In the ξ- direction (quadratic Langrangian interpolation functions)

$$N_1(\xi) = \tfrac{1}{2}\,\xi(\xi - 1)$$

$$N_2(\xi) = (1 - \xi^2)$$

$$N_3(\xi) = \tfrac{1}{2}\,\xi\,(\xi + 1)$$

In the η-direction (infinite shape functions)

$$N_1(\eta) = \frac{-2\eta}{(1-\eta)}$$

$$N_2(\eta) = 1 + \frac{2\eta}{(1-\eta)}$$

The two-dimensional shape functions for the geometric mapping follow from equation 7.15:

$$\bar{N}_1(\xi,\eta) = N_1(\xi).N_1(\eta) = -\frac{\xi\eta(\xi-1)}{(1-\eta)} \qquad (F.5)$$

$$\bar{N}_2(\xi,\eta) = N_2(\xi).N_1(\eta) = -\frac{2\eta(1-\xi^2)}{(1-\eta)} \qquad (F.6)$$

$$\bar{N}_3(\xi,\eta) = N_3(\xi).N_1(\eta) = -\frac{\xi\eta(\xi+1)}{(1-\eta)} \qquad (F.7)$$

$$\bar{N}_4(\xi,\eta) = N_3(\xi).N_2(\eta) = \tfrac{1}{2}\,\xi(\xi+1)\left(1 + \frac{2\eta}{(1-\eta)}\right) \qquad (F.8)$$

$$\bar{N}_5(\xi,\eta) = N_2(\xi).N_2(\eta) = (1 - \xi^2)\left(1 + \frac{2\eta}{(1-\eta)}\right) \qquad (F.9)$$

$$\bar{N}_6(\xi,\eta) = N_1(\xi).N_2(\eta) = \tfrac{1}{2}\,\xi\,(\xi+1)(1+\frac{2\eta}{(1-\eta)}) \qquad (F.10)$$

where, for $\bar{N}_p(\xi,\eta)$, p represents the nodal point in figure F.2.

F.3 TYPE 3

Quadratic, two-way infinite Langranian element.

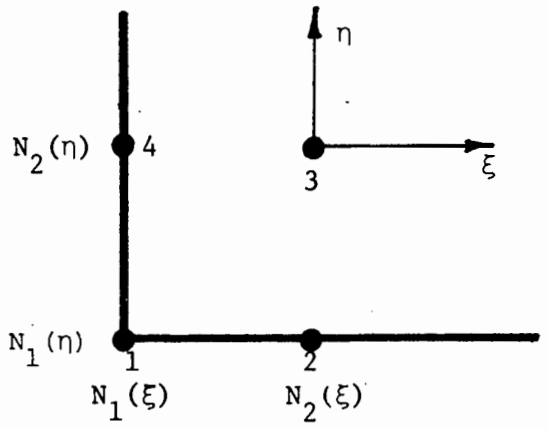

Fig. F.3 - Type 3 Infinite Element.

One-dimensional shape functions:

(i) in the ξ-direction (infinite shape functions):

$$N_1(\xi) = -\frac{2\,\xi}{(1-\xi)}$$

$$N_2(\xi) = 1 + \frac{2\xi}{(1-\xi)}$$

(ii) in the η-direction (infinite shape functions):

$$N_1(\eta) = -\frac{2\eta}{(1-\eta)}$$

$$N_2(\eta) = 1 + \frac{2\eta}{(1-\eta)}$$

The two-dimensional shape functions for the geometric mapping follow from equation 7.15:

$$\bar{N}_1(\xi,\eta) = N_1(\xi).N_1(\eta) = \frac{4\xi\eta}{(1-\xi)(1-\eta)} \qquad (F.11)$$

$$\bar{N}_2(\xi,\eta) = N_2(\xi).N_1(\eta) = (1+\frac{2\xi}{(1-\xi)})(\frac{-2\eta}{(1-\eta)}) \qquad (F.12)$$

$$\bar{N}_3(\xi,\eta) = N_2(\xi).N_2(\eta) = (1+\frac{2\xi}{(1-\xi)})(1+\frac{2\,\eta}{(1-\eta)}) \qquad (F.13)$$

$$\bar{N}_4(\xi,\eta) = N_1(\xi).N_2(\eta) = \frac{-2\xi}{(1-\xi)}\left(1 + \frac{2\eta}{(1-\eta)}\right) \qquad (F.14)$$

where, for $\bar{N}_p(\xi,\eta)$, p represents the nodal points in figure F.3.

F4 TYPE 4

Quadratic, one-way infinite Serendipity element.

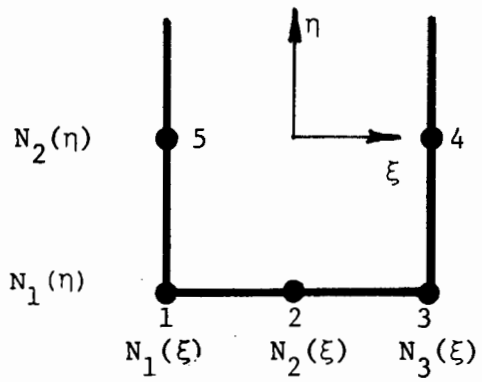

Fig. F.4 Type 4 Infinite Element

The derivation of an infinite element based on a Serendipity formulation, follows the form set out in reference [7.9], for standard 2-dimensional Serendipity elements.

One-dimensional shape functions:

(i) in the ξ-direction (finite shape functions)

$N_1(\xi) = \frac{1}{2}(1 - \xi)$ (linear)

$N_2(\xi) = (1 - \xi^2)$ (quadratic)

$N_3(\xi) = \frac{1}{2}(1 + \xi)$ (linear)

(ii) in the η-direction (infinite shape functions):

$N_1(\eta) = \frac{2}{(1-\eta)}$ (linear infinite, corresponding to $\xi = 0$)

$N_2(\eta) = 1 + \frac{2\eta}{(1-\eta)}$ (quadratic infinite, required for $\xi = \pm 1$)

The shape functions for the infinite Serendipity elements are derived, firstly, for the mid-side nodes 2, 4 and 5, from the product of a quadratic and a linear shape function in the two orthogonal directions:

$$\bar{N}_2(\xi,\eta) = N_2(\xi).N_1(\eta) = (1 - \xi^2)\frac{2}{(1-\eta)} \qquad (F.15)$$

$$\bar{N}_4(\xi,\eta) = N_3(\xi).N_2(\eta) = \tfrac{1}{2}(1 + \xi)(1 + \frac{2\eta}{(1-\eta)}) \qquad (F.16)$$

$$\bar{N}_5(\xi,\eta) = N_1(\xi).N_2(\eta) = \tfrac{1}{2}(1 - \xi)(1 + \frac{2\eta}{(1-\eta)}) \qquad (F.17)$$

and second from the shape functions for the corner nodes 1 and 3 which are now **built** up from the product of the linear shape functions in the two orthogonal directions at these point, minus a multiple of the shape functions at the mid-side nodes. Hence:

$$\bar{N}_1(\xi,\eta) = N_1(\xi).N_1(\eta) - \tfrac{1}{2}\bar{N}_2(\xi,\eta) - 2\bar{N}_5(\xi,\eta)$$

$$= -\frac{(1-\xi)}{(1-\eta)}(1 + \xi + \eta) \qquad (F.18)$$

$$\bar{N}_3(\xi,\eta) = N_3(\xi).N_1(\eta) - \tfrac{1}{2}\bar{N}_2(\xi,\eta) - 2\bar{N}_4(\xi,\eta)$$

$$= -\frac{(1+\xi)}{(1-\eta)}(1 - \xi + \eta) \qquad (F.19)$$

The check on the necessary condition of completeness of the shape functions is met since $\sum_{i=1}^{5} N_i = 1.0$

In equations (F.15) to (F.19), for $\bar{N}_p(\xi,\eta)$, p represents the nodal point in Figure F.4.

APPENDIX G

G-1 COMPUTER PROGRAM DATA INPUT MANUAL

Computer programs written for the analysis of plane stress or strain problems by the Boundary Integral Equation Method using constant, linear or quadratic segments, all have a similar modular data input scheme. Because of this, only one manual (for quadratic segments) will be given in detail here. Special emphasis is given to this modular structure because it allows flexibility in the data input and eliminates the unnecessary formatting errors that usually occur in data preparation.

Notes on data preparation:

(i) Free format is recommended for all numerical data e.g., 5 0.3 0.175 etc.

(ii) Data input is in modular form. Each module has a heading card, a set of data cards and a terminator card.

(iii) A restriction on the use of these modules is that modules falling under a specific section must follow in sequence with one another ie., sections I, II, ..., VII. However, within each section, the modules can be arranged in any order provided that the appropriate terminator word (eg., END or FINISH) is used to complete that module's data.

(iv) Manual usage:

The convention which has been adopted is:

(a) Words written in capitals are module names. If that particular module is used then the module name must be specified eg., DISPLACEMENTS so that the 'D' is in column 1 of the data card.

(b) Variable names written in capitals and surrounded by a box are for numerical data input in free format.

DATA MANUAL

(1) Organisation of Modules

Section	Function	Modules	Submodules
I	System Parameters		
II	Geometry Module	* NODES, BELINES, CURVES	
		END	
III	Material Module		
IV	Boundary Conditions Module	* DISPLACEMENTS	* POINT, LINE
			END
		LOADS	* POINT, LINE, PRESSURE
			END
		FINISH	
V	Internal Points Module	INTERNAL POINTS	
			* POINT, LINE, BLOCK, SEGMENT
			END

* denotes modules or submodules used in any order.

(2) Data Details

I System Parameters

TITLE	title of job. (80 character Alpha numeric).
NNP,NEL	NNP = no. of node points in structure (integer). NEL = no. of segments (integer).
LDIA	parameter for type of leading diagonal to be used. = 1 proportional to internal angle = 2 0.5 = 3 sum of off-diagonal H-matrix terms
NGSS	Gaussian Quadrature order NGSS = 2, 4 or 6 (default = 4).

II Geometry module

Co-ordinate data, angles of normals, lengths of segments can be specified by these modules. Any order can be used provided that END is specified as the last entry.

(1)	NODES	module name for the data of a specific node.
	NSPN	NSPN = no. of specified nodes in the structure.
	I,X,Y	I = node number X,Y = X and Y co-ordinates of the node.
	NSE	NSE = no. of segments specified by these nodes.
	J, INC(1),INC(2),INC(3),ANOR(1),ANOR(2),ANOR(3)	J = segment number INC = first, second and third node of quadratic segment J. ANOR = direction of outward normal at first, second and third node.

(2) BELINE — module name to generate a straight line of nodes and segments.

NBLS — NBLS = no. of boundary segment lines to be generated automatically.

XS,YS,XE,YE,ANA,NINT,IFN,ILN,IRAT

XS,YS = X and Y co-ordinates at start of line.

XE,YE = X and Y co-ordinates at end of line.

ANA = direction of outward normal to this line.

NINT = no. of quadratic segments on this line.

IFN,ILN = first and last node numbers on line numbering clockwise around the structure.

IRAT = 0 all segments are the same size (skip next entry).

= 1 segment lengths to be arranged in the following ratios:

RAT(1),RAT(2) ....,RAT(NINT)

RAT = ratio of length of one segment to the next.

(3) CURVE — module name to generate the segments on a circular curve.

NCS — NCS = no. of curves to be generated automatically.

XS,YS,XE,YE,RD,ANA,ALPHA,NINT,IFN,ILN

XS,YS = X and Y co-ordinates at start of curve.

XE,YE = X and Y co-ordinates at end of curve for checking purposes.

RD = radius of curvature.

+ if curve is convexed

- if curve is concaved

ANA = arc angle between XS,YS and XE,YE
ALPHA = direction of outward normal at XS,YS.
NINT = no. of quadratic segments on this curve.
IFN,ILN = first and last node numbers on this curve numbering clockwise around the structure.

(4) END — terminator of geometry module. This card must be entered on completion of all the data in the geometry module.

III Materials Module

TYPE — type of analysis i.e., STRESS or STRAIN (6 Alphanumerics).

E,PNU — Material constants.
E = Young's Modulus
PNU = Poisson's Ratio

IV Boundary Conditions Module

Boundary conditions are both support constraints (displacement boundary conditions) and loads (applied tractions). The two types of boundary conditions are specified in the DISPLACEMENTS or LOADS modules. Each module, which consists of a number of submodules is terminated by END. All boundary condition data is terminated by FINISH.

(i) Displacements Module

DISPLACEMENTS — module name.

Submodules

(1)	POINT	submodule to specify displacement boundary conditions at specified nodes.
	NDN	NDN = no. of nodes at which displacements are specified.
	NN,XDISP,YDISP	NDN cards are needed in this submodule. NN = node number. XDISP,YDISP = specified displacements in X,Y directions. If node is free in either direction then XDISP or YDISP = 999.
(ii)	LINE	submodule to specify the same displacement boundary conditions on a line of consecutively numbered nodes.
	NBCL	NBCL = no. of displacement boundary condition lines.
	IFN,ILN,XDISP,YDISP	NBCL cards are needed in this submodule. IFN,ILN = first and last node numbers in the line. XDISP,YDISP = specified displacements in X,Y directions. If one direction is free, use 999.
(iii)	END	terminator card for displacement boundary condition module.

(2) Loads Module

	LOADS	Module name.
(i)	ELEMENT	submodule to specify loads per unit length on specified segments.
	NLN	NLN = no. of segments over which loads are to be applied.

	NE,XLOAD,YLOAD	NLN cards are needed in this sub-module. NE = segment number. XLOAD,YLOAD = load/unit length in X,Y directions over segment NE.
(ii)	LINE	submodule to specify the same loads to a line of segments
	NLL	NLL = no. of line loads.
	IFE,ILE,XLOAD,YLOAD	NLL cards are needed in this sub-module. IFE,ILE = first and last segment numbers in the line. XLOAD,YLOAD = load/unit length in X,Y directions to be applied over segments IFE through ILE.
(iii)	PRESSURE	submodule to specify a normal pressure to a group of consecutively numbered segments.
	NPL	NPL = no. of sets of pressure loads.
	IFE,ILE,PRES	NPL cards are needed in this sub-module. IFE,ILE = first and last segment numbers. PRES = pressure (force/unit length) to be applied normal to segments IFE through ILE. +ve for pressure acting in direction of outward normal. -ve in direction opposite to outward normal.
(iv)	END	terminator card for loads module.
(3)	FINISH	terminator card for completion of all Boundary condition data.

XLL,YLL = X and Y co-ordinates of point at lower left hand side of block.
XUR,YUR = X and Y co-ordinates of point at upper right hand side of block.
NPX,NPY = no. of equally spaced points parallel to the X-axis and Y-axis respectively

(iv) SEGMENT — submodule to specify a circular band of equally spaced internal points.

NIPSEG — NIPSEG = no. of segments to be specified.

OX,OY,RI,RE,DIR,ANG,N1,N2

NIPSEG cards are needed in this submodule.
OX,OY = X and Y co-ordinates of central point of the band.
RI,RE = inner and outer radii of the band.
DIR = direction of first radial line of points.
ANG = angle subtending the segment measured anticlockwise from DIR.
N1 = no. of equally spaced points on the circumference of the segment.
N2 = no. of equally spaced points on the radial line.

(v) END — terminator card for the internal points module.

End of data input.

G-2 LIST OF COMPUTER PROGRAMS WRITTEN FOR THE BOUNDARY INTEGRAL ANALYSIS OF 2-DIMENSIONAL PLANE STRESS/STRAIN PROBLEMS

CONTRA*BEL.	Program using constant segment interpolation.
CONTRA*BELL.	Program using linear segment interpolation.
CONTRA*BELQ.	Program using quadratic segment interpolation.
CONTRA*BILS.	Program using linear segments and including constraint equations for the solution of problems with boundaries at infinity.
CONTRA*BELR.	Program using quadratic segment interpolation; including constraint equations and multi node concepts and the facility to solve problems with multi regions.
CONTRA*BELG.	Program using Adaptive programming techniques.
CONTRA*PLANET.	Finite Element Program including infinite elements - Adaption of program by D.R.J. Owen and E. Hinton contained in book "Finite Elements in Plasticity", Pineridge Press, Swansea, (1980).

APPENDIX H

BIBLIOGRAPHY

H.1 ADINA A Finite Element Program for Automatic Dynamic Incremental Non-linear Analysis, K-J. Bathe, Massachusetts Institute of Technology (1978).

H.2 E. ALARCON, A. MARTIN and F. PARIS, "Improved Boundary Elements in Torsion Problems", in Recent Advances in Boundary Elements, ed. C.A. BREBBIA (1978).

H.3 E. ALARCON, A. MARTIN and F. PARIS, "Boundary Elements in Potential and Elasticity Theory", Computers and Structures, Vol. 10, pp. 351-362 (1979).

H.4 N.J. ALTIERO and D.L. SIKARSKIE, "A Boundary Integral Method applied to Plates of Arbitrary Plan Form", Computers and Structures, Vol. 9, pp. 163-168 (1978).

H.5 N.J. ALTIERO and S.D. GAVAZZA, "An Effective Boundary Integral Approach for the Mixed Boundary Value Problems of Linear Elastostatics", Appl.Math.Modelling, Vol. 3, pp. 99-104 (1979).

H.6 T. ANDERSSON, B. FREDERIKSSON and B.G. ALLAN PERSSON, "The Boundary Element Method applied to Two-Dimensional Contact Problems", in New Developments in Boundary Element Methods, ed. C.A. BREBBIA (1980).

H.7 T. ANDERSSON, "The Boundary Element Method applied to Two-Dimensional Contact Problems with Friction", in Boundary Element Methods, ed. C.A. BREBBIA (1981).

H.8 J. BALAS and J. SLADEK, "Method of Boundary Integral Equations for Analysis of Three-Dimensional Crack Problems", in Boundary Element Methods, ed. C.A. BREBBIA, Proceedings of the 3rd Int. Seminar on Boundary Element Methods, July 1981.

H.9 P.K. BANERJEE, "Integral Equation Methods for analysis of Piecewise Non-Homogeneous Three Dimensional Elastic Solids of Arbitrary Shape", Int.J. Mechanical Science, Vol. 18, pp. 293-303 (1976).

H.10 P.K. BANERJEE, "The Boundary Element Method for Two-Dimensional Problems of Elastoplasticity", in Recent Advances in Boundary Element Methods, ed. C.A. BREBBIA (1978).

H.11 P.K. BANERJEE and R. BUTTERFIELD (eds), Developments in Boundary Element Methods - 1, Applied Science Publishers Ltd, London (1979).

H.12 P.K. BANERJEE, D.N. CATHIE and T.G. DAVIES, "Two- and Three-Dimensional Problems of Elastoplasticity", in Developments in Boundary Element Methods - 1, eds. P.K. BANERJEE and R. BUTTERFIELD (1979).

H.13 M.R. BARONE and A.R. ROBINSON, "Determination of Elastic Stresses at Notches and Corners by Integral Equations", Int.J. Solids Structures, Vol. 8, pp. 1319-1338 (1972).

H.14 K-J. BATHE and E.L. WILSON, Numerical Methods in Finite Element Analysis, Prentice-Hall Inc., New Jersey (1976).

H.15 K-J. BATHE, Finite Element Procedures in Engineering Analysis, Prentice-Hall, Inc., New Jersey (1982).

H.16 G. BEER, J.L. MEEK, 'A boundary finite element for underground mining applications', in New Developments in Boundary Element Methods, (ed. C.A. BREBBIA) Newnes-Butterworths, London(1980).

H.17 G. BEER, J.L. MEEK, 'Infinite domain elements', Int.J. Num. Meth. Engng, Vol. 17, pp. 43-51 (1981).

H.18 R. BENJUMEA and D.L. SIKARSKIE, "On the Solution of Plane Orthotropic Elasticity Problems by an Integral Method", JAM, Vol. 39, Series E, pp. 801-808 (1972).

H.19 P. BETTESS, 'Infinite Elements', Int.J.Num. Meth. Engng, Vol. 11, pp. 53-64 (1977).

H.20 P. BETTESS, O.C. ZIENKIEWICZ, 'Diffraction and refraction of surface waves using finite and infinite elements'. Int.J.Num. Meth. Engng, Vol. 11, pp. 1271-1290 (1977).

H.21 P. BETTESS, 'More on Infinite Elements', Int.J.Num.Meth. Engng, Vol. 15, pp. 1613-1626 (1980).

H.22 P. BETTESS, "Operation Counts for Boundary Integral and Finite Element Methods", Int.J. Num. Methods Eng., Vol. 17, pp. 300-308 (1981).

H.23 P.M. BESUNER and D.W. SNOW, "Application of the Two Dimensional Integral Equation Method to Engineering Problems", in the Boundary Integral Equation Method : Computational Applications in Applied Mechanics, (eds) T.A. CURSE and F.J. RIZZO, ASME publication, AMD - Vol. 11 (1975).

H.24 G.P. BEZINE and D.A. GAMBY, "A New Integral Equation Formulation for Plate Bending Problems", in Recent Advances in Boundary Element Methods, ed. C.A. BREBBIA (1978).

H.25 M. L. BOAS, Mathematical Methods in the Physical Sciences, John Wiley & Sons Inc., USA (1965).

H.26 C.A. BREBBIA and J. DOMINGUEZ, "Boundary Element Methods for Potential Problems", Appl.Math.Modelling, Vol. 1, pp. 372-378 (1977).

H.27 C.A. BREBBIA, The Boundary Element Method for Engineers, Pentech Press, London (1978).

H.28 C.A. BREBBIA (ed.), Recent Advances in Boundary Element Methods, Pentech Press, London (1978).

H.29 C.A. BREBBIA and S. WALKER, "Simplified Boundary Elements for Radiation Problems", Appl. Math.Modelling, Vol. 2, pp. 135-137 (1978).

H.30 C.A. BREBBIA and R. BUTTERFIELD, "Formal Equivalence of Direct and Indirect Boundary Element Methods", Appl. Math. Modelling, Vol. 2, pp. 132-134 (1978).

H.31 C.A. BREBBIA and P. GEORGIOU, "Combination of Boundary and Finite Elements in Elastostatics". Appl. Math. Modelling, Vol. 3, pp. 212-230 (1979).

H.32 C.A. BREBBIA and S. WALKER, Boundary Element Techniques in Engineering, Newnes-Butterworths, London (1980)

H.33 C.A. BREBBIA (ed.), New Developments in Boundary Element Methods, Butterworths, London (1980). Proceedings of the Second International Seminar Southampton, March 1980.

H.34 C.A. BREBBIA (ed.) Boundary Element Methods, CML Publications, Springer-Verlag Berlin, Heidelberg (1981). Proceedings of the Third International Seminar, Irvine, California, July 1981.

H.35 M. BRUNET, "Numerical Analysis of Cyclic Plasticity Using the Boundary Integral Equation Method", in Boundary Element Methods, ed. C.A. BREBBIA (1981).

H.36 H.D. BUI, "Some Remarks about the Formulation of Three-Dimensional Thermoelastoplastic Problems by Integral Equations", Int.J. Solids Structures, Vol. 14, pp.935-939 (1978).

H.37 D.N. CATHIE, "On the Implementation of Elasto-Plastic Boundary Element Analysis", in New Developments in Boundary Element Methods, ed. C.A. BREBBIA (1980), also Appl. Math.Modelling, Vol. 5, pp. 39-44 (1981).

H.38 M. CHAUDONNERET, "On the Discontinuity of the Stress Vector in the Boundary Inregral Equation Method for Elastic Analysis",in Recent Advances in Boundary Element Methods, ed. C.A. BREBBIA (1978).

H.39 D.L. CLEMENTS and F.J. RIZZO, "A Method for the Numerical Solution of Boundary Value Problems Governed by Second-Order Elliptic Systems", J.Inst.Maths.Applics, Vol. 22, pp. 197-202 (1978).

H.40 T.A. CRUSE and F.J. RIZZO, "A Direct Formulation and Numerical Solution of the General Transient Elastodynamic Problem - 1", J. Math. Anal. and Applic., Vol. 22, pp. 244-259 (1968).

H.41 T.A. CRUSE, "A Direct Formulation and Numerical Solution of the General Transient Elastodynamic Problem - II, J.Math.Anal. and Applic., Vol.22, pp.341-355(1968).

H.42 T.A. CRUSE and W. VAN BUREN, "Three-Dimensional Elastic Stress Analysis of a Fracture Specimen with an Edge Crack", Int.J. Fracture Mech., Vol. 7, pp. 1-15 (1971).

H.43 T.A. CRUSE, "Application of the Boundary Integral Equation Solution Method in Solid Mechanics", Proc.Int.Conference on Variational Methods in Engineering, September 25-29, 1972.

H.44 T.A. CRUSE, "Some Classical Elastic Sphere Problems Solved Numerically by Integral Equations", Transactions of ASME, J. of Applied Mechanics, pp. 272-274 (1972).

H.45 T.A. CRUSE, "An Improved Boundary Integral Equation Method for Three Dimensional Elastic Stress Analysis", Computers and Structures, Vol. 4, pp. 741-754 (1974).

H.46 T.A. CRUSE and F.J. RIZZO (eds), Boundary Integral Equation Method : Computational Applications in Applied Mechanics, ASME publication, AMD-Vol. 11 (1975).

H.47 T.A. CRUSE, "Boundary Integral Equation Fracture Mechanics Analysis" in Boundary Integral Equation Method : Computational Applications in Applied Mechanics, eds., T.A. CRUSE and F.J. RIZZO, ASME publication, AMD - Vol. 11 (1975).

H.48 T.A. CRUSE, D.W. SNOW and R.B. WILSON, "Numerical Solutions in Axisymmetric Elasticity", Computers and Structures, Vol. 7, pp. 445-451 (1977).

H.49 T.A. CRUSE and R.B. WILSON, "Advanced Applications of Boundary Integral Equation Methods". Nuclear Eng. and Design, Vol. 46, pp. 223-234 (1978).

H.50 T.A. CRUSE, "Two-Dimensional BIE Fracture Mechanics Analysis", Appl. Math. Modelling, Vol. 2, pp. 287-293 (1978).

H.51 T.A. CRUSE, "Two- and Three-Dimensional Problems of Fracture Mechanics", in Developments in Boundary Element Methods - 1, eds. P.K. BANERJEE and R. BUTTERFIELD (1979).

H.52 D.A.S. CURRAN, M. CROSS and B.A. LEWIS, "Solution of Parabolic Differential Equations by the Boundary Element Method Using Discretisation in Time", Appl.Math.Modelling, Vol. 4, pp. 398-400 (1980).

H.53 D.J. DANSON, 'A Boundary Element formulation of Problems in Linear Isotropic Elasticity with Body Forces', Proceedings of the 3rd International Seminar on Boundary Element Methods, Irvine, California, July 1981.

H.54 G. DE MEY, "The Use of Approximate Functions for the Numerical Solution of La Place Equation by an Integral Equation", Computers and Structures, Vol. 10, pp. 709-711 (1979).

H.55 J.A. DERUNTZ and T.L. GEERS, "Added Mass Computation by the Boundary Integral Method", Int.J.Num.Meth.Engng, Vol. 12, pp. 531-549 (1978).

H.56 R. EATOCK-TAYLOR and J.B. WAITE, "The Dynamics of Offshore Structures Evaluated by Boundary Integral Techniques", Int. J. NUM. METHODS ENG., Vol. 13, pp. 73-92 (1978).

H.57 E.B. HANSEN, "Numerical Solution of Integro-differential and Singular Integral Equations for Plate Bending Problems", J. of Elasticity, Vol. 6, pp. 39-56 (1976).

H.58 U. HEISE, "Numerical Properties of Integral Equations in which the given Boundary Values and the Sought Solutions are defined on Different Curves", Computers and Structures, Vol. 8, pp. 199-205 (1978).

H.59 U. HEISE, "The Spectra of Some Integral Operators for Plane Elastostatical Boundary Value Problems", J. Of Elasticity, Vol. 8, No. 1, pp. 47-79 (1978).

H.60 U. HEISE, "Integral Equations for the mixed Boundary Value Problem in Plane Elastostatics", Appl. Math. Modelling, Vol. 4, pp. 63-66 (1980).

H.61 I. HERRERA, "Theory of Connectivity : Systematic Formulation of Boundary Element Methods", Appl. Math. Modelling, Vol.3, pp. 151-156 (1979).

H.62 P.G. HODGE, Continuum Mechanics, McGraw-Hill (1970).

H.63 G.C. HOWELL, "Dynamic Programming and Direct Iteration for the Optimum Design of Space Structures, M.Sc.(Eng.)thesis in the Faculty of Engineering, University of Cape Town, 1978.

H.64 G.C. HOWELL and W.S. DOYLE, "A Résumé of Boundary Integral Methods in 2-dimensional Elasticity", unpublished Technical Report No. 804S, Department of Civil Engineering, UCT, 1980.

H.65 G.C. HOWELL and W.S. DOYLE, "Boundary Integrals - An Alternative to Finite Elements for Plane Elasticity Problems", Proceedings of the Symposium on Design Application of the Finite Element Method held at the University of Cape Town on 12-14 January 1981.

H.66 G.C. HOWELL and W.S. DOYLE, "Plane Stress/Strain Analysis by Boundary Integral Equation and Finite Element Methods", Proceedings of the Conference on Finite Element Methods in South Africa held at the CSIR, Pretoria, S.A. on 17-18 March 1981.

H.67 G.C. HOWELL and W.S. DOYLE, "An Assessment of the Boundary Integral Equation Method for In-Plane Elastostatic Problems", Applied Mathematical Modelling, Vol. 6, No. 4, August 1982.

H.68 G.C. HOWELL and W.S. DOYLE, "Infinite Domain Problems by Finite Elements and Boundary Integrals", Proceedings of the FEMSA/83 International Symposium on Design and the Finite Element Method, held on 11-12 January 1983 at the University of Cape Town.

H.69 G.C. HOWELL and W.S. DOYLE, "The Plane Stress/Strain Analysis of Non-Homogeneous Continua by the Boundary Integral Equation Method", Computers and Structures, Vol. 17, No. 4, pp. 603-610, 1983.

H.70 M.A. JASWON, "Integral Equation Methods in Potential Theory. I" Proc. Royal Soc. : Series A, Vol. 275, pp. 23-32 (1963).

H.71 M.A. JASWON and A.R. PONTER, "An integral equation solution of the Torsion Problem", Proc. Royal Soc. : Series A, Vol. 273, pp. 237-246 (1963).

H.72 M.A. JASWON, M. MAITI and G.T. SYMM, "Numerical Biharmonic Analysis and Some Applications", Int. J. Solids Structures, Vol. 3, pp. 309-332 (1967).

H.73 M.A. JASWON and M. MAITI, "An Integral Equation Formulation of Plate Bending Problems", J.ENG. MATHS., Vol.2, pp.83-93 (1968).

H.74 M.A. JASWON and G.T. SYMM, Integral Equation Methods in Potential Theory and Elastostatics, Academic Press, London (1977).

H.75 G. JENG and A. WEXLER, "Isoparametric, Finite Element, Variational Solution of Integral Equations for Three Dimensional fields", Int. J. NUM. METHODS ENG. Vol. 11, pp. 1455-1471 (1977).

H.76 I. KATZ, A.G. PEANO, M.P. ROSSOW, "Nodal Variables for complete conforming Finite Elements of arbitrary polynomial order", Computers and Maths, with Applic., Vol. 4, pp. 85-112 (1978).

H.77 D.W. KELLY, G.G.W. MUSTOE and O.C. ZIENKIEWICZ, "Coupling Boundary Element Methods with other Numerical Methods" in Developments in Boundary Element Methods, 1, eds., P.K. BANERJEE and R. BUTTERFIELD (1979).

H.78 T. KERMANIDIS, "A Numerical Solution for Axially Symmetric Elasticity Problems", Int. J. Solids Structures, Vol. 11, pp. 493-500 (1975).

H.79 E. KREYSIG, Advanced Engineering Mathematics, 4th Edition, John Wiley & Sons, Inc., USA (1962).

H.80 V. KUMAR and S. MUKHERJEE, "A Boundary Integral Equation Formulation for Time-Dependent Inelastic Deformation in Metals", Int. J. MECH.SCI., Vol. 19, pp. 713-724 (1977).

H.81 J.C. LACHAT and J.O. WATSON, "A Second Generation Boundary Integral Equation Program for Three Dimensional Elastic Analysis", in Boundary Integral Equation Method : Computational Applications in Applied Mechanics, (eds.) T.A. CRUSE and F.J. RIZZO, ASME publication, AMD - Vol. 11 (1975).

H.82 J.C. LACHAT and J.O. WATSON, "Effective Numerical Treatment of Boundary Integral Equations : A Formulation for Three dimensional Elastostatics", INT. J. NUM. METHODS ENG., Vol. 10, pp.991-1005 (1976).

H.83 J.A. LIGGETT and J.R. SALMON, "Cubic Spline Boundary Elements", Int. J. NUM. METHODS ENG., Vol. 17, pp. 543-556 (1981).

H.84 A.R. LLOYD, "Computer Aided Design of Axisymmetric Thin Shell Concrete Structures", Ph.D. Thesis in the Faculty of Engineering, University of Cape Town, 1982.

H.85 A.E.H. LOVE, A treatise on the mathematical theory of Elasticity, 4th edition, Cambridge University Press, (1927).

H.86 P.P. LYNN, H.A. HADID, "Infinite elements with $1/r^n$ type decay", Int.J. Num. Meth. Engng, Vol. 17, pp. 503-526 (1981).

H.87 M. MAITI and S.K. CHAKRABARTY, "Integral Equations Solutions for Simply Supported Polygonal Plates", Int.J. Eng.Sci., Vol. 12, pp. 793-806 (1974).

H.88 G.D. MANOLIS and D.E. BESKOS, "Dynamic Stress Concentration Studies by Boundary Integrals and La Place Transform", Int.J. NUM. METHODS ENG., Vol. 17, pp. 573-599 (1981).

H.89 C.E. MASSONET, "Numerical use of -ntegral procedures", in Stress Analysis, (eds.) O.C. Zienkiewicz and G.S. Holister (1965).

H.90 M. MAYR, W. DREXLER and G. KUHN, "A Semi-Analytical Boundary Integral Approach for Axisymmetric Elastic Bodies with Arbitrary Boundary Conditions", Int. J. Solids Structures, Vol. 16, pp. 863-871 (1980).

H.91 F. MEDINA, "An axisymmetric infinite element", Int.J. Num.Meth. Engng, Vol. 17, pp. 1177-1185 (1981).

H.92 A. MENDELSON and L.U. ALBERS, "Application of Boundary Integral Equations to Elastoplastic Problems", in Boundary Integral Equation Method : Computational Applications in Applied Mechanics, eds. T.A. CRUSE and F.J. RIZZO, ASME publication, AMD - Vol. 11 (1975).

H.93 M. MORJARIA and S.MUKHERJEE, "Improved Boundary Integral Equation Method for Time-Dependent Inelastic Deformation in Metals", INT. J. NUM. METHODS ENG., Vol. 15, pp. 97-111 (1980).

H.94 S. MUKHERJEE, "Corrected Boundary Integral Equations in Planar Thermoelastoplasticity", Int. J. Solids Structures Vol. 13, pp. 331-336 (1977).

H.95 S. MUKHERJEE and V. KUMAR, "Numerical Analysis of Time-Dependent Inelastic Deformation in Metallic Media Using the Boundary Integral Equation Method", J. of Applied Mech., Vol. 45, pp. 785-790 (1978).

H.96 N.I. MUSKHELISHVILI, "Some Basic Problems of the Mathematical Theory of Elasticity", 3rd edition, P. Noordhoff Ltd, Groningen, Holland (1953).

H.97 N.I. MUSKHELISHVILI, "Singular Integral Equations", Noordhoff Ltd, Groningen (1953).

H.98 D.R.J. OWEN and E. HINTON, "Finite Elements in Plasticity : Theory and Practice", Pineridge Press Ltd, Swansea, U.K. (1980).

H.99 D.R.J. OWEN, private communication, February 1982.

H.100 PAFEC 75, A Program for Automatic Finite Element Calculations, PAFEC Ltd, Nottingham, England.

H.101 A.G. PEANO, "Hierarchies of conforming Finite Elements for Plane Elasticity and Plate Bending", Computers and Maths. with Applic., Vol. 2, pp. 211-224 (1976).

H.102 A.G. PEANO, A. PASINI, R. RICCIONI, L. SARDELLA, "Self-Adaptive Finite Element Analysis", Paper presented at the 6th International Finite Element Conference, Baden-Baden, Germany, November 1977.

H.103 A.G. PEANO, M. FANELLI, R. RICCIONI, L. SARDELLA, "Self-Adaptive Convergence at the crack tip of a dam buttress", Paper presented at the International Conference on Numerical Methods in Fracture Mechanics, Swansea, January 9 - 13, 1978.

H.104 A.G. PEANO, R. RICCIONI, A. PASINI, L. SARDELLA, "Adaptive Approximation in Finite Element Structural Analysis", research publication of the Mathematical Models Dept, ISMES, Bergamo, Italy and MCS, Centre for Computational Mechanics, Polytechnico di Milano.

H.105 A.G. PEANO, R. RICCIONI, "Automated Discretization Error Control in Finite Element Analysis", research publication of the Mathematical Models Dept, ISMES, Bergamo, Italy and MCS, Centre for Computational Mechanics, Polytechnico di Milano.

H.106 G. PETRUSKA, "Finite Element convergence on a fixed grid", Computers and Maths. with Applic., Vol. 4, pp. 67-71 (1978).

H.107 H.L.G. PINA, JLM. FERNANDES and C.A. BREBBIA, "Some Numerical Integration Formulae over Triangles and Squares with a 1/R Singularity", Appl. Math. Modelling, Vol. 5, pp. 209-211 (1981).

H.108 A. PORTELLA, "Theoretical Basis of Boundary Solutions for the Linear Theory of Structures", Appl. Math. Modelling, Vol. 5, pp. 57-59 (1981).

H.109 B.D. REDDY, Course Notes on Solid Mechanics, UCT (1979).

H.110 F.J. RIZZO, "An Integral Equation Approach to Boundary Value Problems of Classical Elastostatics", Quart. Appl. Maths, Vol. 25, pp. 83-95 (1967).

H.111 F.J. RIZZO and D.J. SHIPPY, "An Advanced Boundary Integral Equation Method for Three-Dimensional Thermoelasticity", Int. J.NUM. METHODS ENG., Vol. 11, pp. 1753-1768 (1977).

H.112 F.B. SEELEY and J.O. SMITH, Advanced Mechanics of Materials, 2nd edition, John Wiley & Sons, Inc. (1952).

H.113 D.J. SHIPPY, "Application of the Boundary Integral Equation Method to Transient Phenomena in Solids", in Boundary Integral Equation Method : Computational Applications in Applied Mechanics, eds. T.A. CRUSE and F.J. RIZZO, ASME Publication, AMD-Vol. 11 (1975).

H.114 South African Standard Building Regulations (1970).

H.115 R.A. SWANN, "A Feature Survey of concrete base spine-beam Bridges", Technical Report 42.459 Cement and Concrete Association, June 1972.

H.116 J.L. SWEDLOW and T.A. CRUSE, "Formulation of Boundary Integral Equations for Three-Dimensional Elasto-Plastic Flow", Int. J. Solids Structures, Vol. 7, pp. 1673-1683 (1971).

H.117 J.L. SWEDLOW, "Singularity Computations", Int. J. NUM. METHODS ENG., Vol. 12, pp. 1779-1798 (1978).

H.118 G.T. SYMM, "Integral Equation Methods in Potential Theory II", Proc. Royal Soc. : Series A, Vol. 275, pp. 33-46 (1963).

H.119 K. TANAKA and M. TANAKA, "Time-Space Boundary Elements for Transient Heat Conduction Problems", Appl. Math. Modelling, Vol. 4, pp. 331-334 (1980).

H.120 K. TANAKA and M. TANAKA, "Time-Space Boundary Elements for Boundary-Value Problems", Appl. Math. Modelling, Vol. 4, pp. 473-476 (1980).

H.121 J.C.F. TELLES and C.A. BREBBIA, "On the Application of the Boundary Element Method to Plasticity", Appl. Math. Modelling, Vol. 3, pp. 466-470 (1979).

H. 122 J.C.F. TELLES and C.A. BREBBIA, "The Boundary Element Method in Plasticity", in New Developments in Boundary Element Methods, ed. C.A. BREBBIA (1980).

H.123 J.C.F. TELLES and C.A. BREBBIA, in "New Developments in Elasto-plastic Analysis", in Boundary Element Methods, ed. C.A.BREBBIA (1981).

H.124 S.P. TIMOSHENKO and G.N. GOODIER, Theory of Elasticity, 3rd Edition, McGraw-Hill (1970).

H.125 H. TOTTENHAM, "The Boundary Element Method for Plates and Shells", in Development in Boundary Element Methods - 1, eds. P.K. BANERJEE and R. BUTTERFIELD (1979).

H.126 S. WALKER, "Boundary elements in Fluid/Structure Interaction Problems", in New Developments in Boundary Element Methods, ed. C.A. BREBBIA (1980).

H.127 S. WALKER, "Boundary Elements in Fluid/Structure Interaction Problems Rotational Shells", Appl. Math. Modelling, Vol. 4, pp. 345-350 (1980).

H.128 S.T. WANG and G.E. BLANDFORD, "Comparison of Boundary Integral Equation and FE Methods", J. STRUCT. DIV. ASCE, ST 9, pp. 1941-1947 (1976).

H.129 L.J. WARDLE and J.M. CROTTY, "Two-dimensional Boundary Integral Equation Analysis for Non-homogeneous Mining Applications", Proceedings of the Conference on Recent Advances in Boundary Element Methods, Southampton, July 1978 (ed. C.A. Brebbia).

H.130 J.O. WATSON, "Advanced Implementation of the Boundary Element Method for Two- and Three-dimensional Elastostatics", in Developments in Boundary Element Methods - 1 (eds. P.K. Banerjee and R. Butterfield).

H.131 A. WEXLER, "Some Recent Developments in Field Calculations", Paper presented at the Joint Intermag-MMM Conference, New York, July 17 - 20, 1979.

H.132 R.B. WILSON and T.A. CRUSE, "Efficient Implementation of Anisotropic Three-Dimensional Boundary Integral Equation Stress Analysis", INT. J. NUM. METHODS ENG., Vol. 12, pp. 1383-1397 (1978).

H.133 J.P. WONG and G. AGUIRRE-RAMIREZ, "A Finite Element-Integral Equation Solution to Torsion Problems", Computers and Structures, Vol. 9, pp.53-55 (1978).

H.134 D.J. WOOD, "Determination of the Torsional Properties of a Plane Section using Boundary Integral Techniques", Appl. Math. Modelling, Vol. 4, pp. 410-416 (1980).

H.135 B.C. WU and N.J. ALTIERO, "A Boundary Integral Method Applied to Plates of Arbitrary Plan Form and Arbitrary Boundary Conditions", Computers and Structures, Vol. 10, pp. 703-707 (1979).

H.136 O.C. ZIENKIEWICZ, The Finite Element Method, 3rd edition, McGraw-Hill, New York (1977).

H.137 O.C. ZIENKIEWICZ, D.W. KELLY and P. BETTESS, "The Coupling of the Finite Element Method and Boundary Solution Procedures", INT. J. NUM. METHODS ENG., Vol. 11, pp. 355-375 (1977).

H.138 O.C. ZIENKIEWICZ, D.W. KELLY and P. BETTESS, "Marriage à la mode - The Best of Both Worlds (Finite Elements and Boundary Integrals)", Chapter 5 of Energy Methods in Finite Element Analysis, eds. R. GLOWINSKI, E.Y. RODIN and O.C. ZIENKIEWICZ.

H.139 O.C. ZIENKIEWICZ and P. BETTESS, "Fluid Structure Dynamic Interaction and wave forces, an introduction to Numerical Treatment", INT. J. NUM. METHODS ENG., Vol.13, pp. 1-16 (1978).